



Ultrafine particles in the urban environment

Thesis Submitted for the degree of
Doctor of Philosophy
at the University of Leicester

By

Sarkawt M. L. Hama

Atmospheric Chemistry Group

Department of Chemistry

The University of Leicester

2018

Ultrafine particles in the urban environment

Sarkawt M. L. Hama

Abstract

Ultrafine particles (UFP) are the smallest constituents of atmospheric particulate matter (PM). Until now, their potential adverse effects on human health are of great concern because of their specific properties and acting mechanisms. The work in this thesis focuses on the measurement of UFP and their effect and contribution to air quality in Leicester, UK and a set of cities in North West (NW) Europe. The thesis explores novel work around new particle formation (NPF) events and their association with Lung Deposited Surface Area (LDSA) in an urban environment. A final focus of this thesis was the identification sources are contribute to the PM₁₀ across NW Europe region.

Particle number size distribution were measured at two urban background locations (automatic urban and rural network (AURN), and Brookfield (BF)) in Leicester in order to quantify NPF events. Quantification of primary and secondary sources of UFP was undertaken using black carbon as a tracer for the primary UFP in urban areas. At the AURN site, which is influenced by fresh vehicle exhaust emissions, total number concentrations (TNC) was segregated into two components, $TNC = N1 + N2$. The component N1 represents components directly emitted as particles and compounds which nucleate immediately after emission. The component N2 represents the particles formed during the dilution and cooling of vehicle exhaust emissions and by in situ NPF. Furthermore, the composition of the PM₁₀ was studied at five sites across NW Europe. The samples collected at four urban background, and one industrial sites were analysed for elements, water soluble ions, organic matter, and monosaccharides, and the principal component analysis (PCA) was applied to the data set.

Overall, during the measurement period, the frequency of NPF events was 13.3%, and 22.2% at AURN and BF sites, respectively. The percentage of N2 (57%) was greater than the percentage of N1 (43%) for all days at the AURN site. The PCA yielded 5 factors which apportioned the main pollution sources to PM₁₀ concentrations across NW Europe: (1) traffic emissions, (2) secondary inorganic aerosols, (3) organic matter, (4) industrial and sea salt, (5) biomass burning.

Acknowledgments

I would like to show my very great appreciation to my supervisor, Prof Paul S. Monks for his patience, guidance and enthusiastic encouragement throughout my research degree. It has been a great privilege to pursue a PhD at the University of Leicester where I have been honoured to work with my supervisor. He has provided me with invaluable and continuous support for the past three years. His invaluable advices have greatly impacted the quality of this thesis. I would also like to thank Professor Andrew M Ellis for his guidance and encouragement.

I would like to thank the HCDP (Human Capacity Development Program), for funding my study.

Special thanks should be given to Prof Alfred Wiedensohler and Dr Nan Ma at the Leibniz Institute for Tropospheric Research (TROPOS) for their helping during a month that I spent there.

A big thanks to my colleagues and friends in the atmospheric chemistry group for their help and support and for making the last four years highly enjoyable, especially to Dr Cordell Rebecca for her help and suggestions.

My final special thanks must be reserved for my parents Lateef and Aesha, without whose love and support I would not have made it anywhere near this far.

Contents

1.	Introduction.....	1
1.1	Atmospheric aerosols.....	1
1.1.1	Definition and physical properties.....	1
1.1.2	Aerosols and climate	6
1.2	Ultrafine particles (UFPs)	8
1.2.1	Characteristics and sources.....	8
1.2.2	Mechanism and chemistry of Nucleation	10
1.2.3	State of Knowledge of NPF in Europe	11
1.2.4	Health effects of UFPs.....	15
1.3	Thesis motivation.....	18
1.3.1	The JOAQUIN project.....	18
1.3.1.1	Overview.....	18
1.3.1.2	Monitoring sites and periods.....	21
1.3.2	Thesis objectives.....	22
2.	Methodology.....	25
2.1	Study areas	25
2.2	Joaquin Measurement sites	25
2.2.1	University of Leicester Monitoring site (Leicester, UK).....	27
2.2.2	Vondelpark Monitoring site (AD, Amsterdam, the Netherlands).....	29
2.2.3	Borgerhout Monitoring site (AP, Antwerp, Belgium)	30
2.2.4	Lille-Fives Monitoring site (LL, Lille, France)	32
2.2.5	Wijk aan Zee Monitoring site (WZ, the Netherlands)	33
2.3	Instrumentation	35
2.3.1	Ultrafine particle instruments	35
2.3.1.1	SMPS (Grimm 5420/L-DMA)	37
2.3.1.2	EPC (TSI 3783)	38

2.3.1.3 UFPM (TSI 3031)	40
2.3.2 NSAM (TSI 3550)	45
2.3.3 Sampling systems	48
2.3.4 MAAP (Thermo Scientific 5012)	49
2.3.5 NO _x monitors	51
2.3.6 PM ₁₀ sampler	53
3.1 Introduction.....	57
3.2 Experimental.....	60
3.2.1 Sampling sites.....	60
3.2.2 Instrumentation	61
3.2.3 Data processing and analysis.....	63
3.2.4 New particle formation event characteristics.....	64
3.3 Results and Discussion.....	67
3.3.1 Overview of the particle number concentrations.....	67
3.3.2 Particle number size distributions.....	71
3.3.2.1 Easter holiday	72
3.3.2.2 Temporal Variations.....	74
3.3.3 Dependency on wind speed and direction.....	81
3.3.4 Observation of new particle formation	85
3.3.5 Nucleation event characterisation.....	89
3.4 Conclusions	92
4.1 Introduction.....	94
4.2 Methods.....	96
4.2.1 Measurement site.....	96
4.2.2 Instrumentation	98
4.2.3 Data processing and analysis.....	99
4.3 Results and discussion.....	100
4.3.1 Annual Variation.....	100

4.3.2 Weekly and Daily variations.....	102
4.3.3 Exploring the Relationship between total particle number and black carbon concentrations	108
4.3.4 Segregating the components contributing to UFPs.....	111
4.3.5 Dependency on wind speed and direction.....	115
4.4 Conclusions	118
5.1 Introduction.....	120
5.2 Experimental.....	122
5.2.1 Monitoring site	122
5.2.2 Instrumentation	124
5.3 Results and Discussion.....	126
5.3.1 The annual behaviour of LDSA, eBC and NO _x concentrations.....	126
5.3.2 Diurnal and Weekly variations of LDSA, eBC, and NO _x	130
5.3.3 Correlation between LDSA and other pollutants (eBC, NO _x and N _{TOTAL})...	132
5.3.4 Variation with wind speed and direction.....	136
5.3.5 Contribution of new particle formation on LDSA: a case study.....	138
5.4 Conclusions	141
6.1 Introduction.....	143
6.2 Experimental.....	145
6.2.1 Sampling sites.....	145
6.2.2 PM ₁₀ sampling.....	146
6.2.3 Chemical analysis and Analytical techniques.....	147
6.2.4 The coefficients of divergence.....	148
6.2.5 Reconstruction of PM ₁₀	148
6.2.6 Principal component analysis.....	150
6.3 Results and Discussion.....	151
6.3.1 PM ₁₀ Mass concentrations and spatial comparison.....	151
6.3.2 Characteristic of chemical species in PM ₁₀	153

6.3.2.1 The water soluble ions (WSIs) analysis.....	153
6.3.2.2 Carbonaceous material analysis.....	156
6.3.2.3 Minerals and trace elements analysis	158
6.3.2.4 Monosaccharide anhydrides (MAs) analysis.....	160
6.3.3 Chemical Mass closure of PM10.....	161
6.3.4 Identification of emission source by PCA.....	167
6.4 Conclusions	172
7. Conclusions and Future work.....	173
7.1 Conclusions.....	173
7.2 Limitations Future work.....	178
Appendix.....	180
Bibliography.....	195

List of Tables

Table 1.1: The five main chemical components of atmospheric aerosols adapted from (Wilson and Suh, 1997).....	3
Table 1.2: Previous NPF studies in diverse atmospheric environments of Europe.....	13
Table 2.1: Joaquin monitoring sites.....	27
Table 2.2: Summarises relevant specifications of the ultrafine particle monitors used in this study.....	36
Table 2.3: Overview of PM ₁₀ filter sampling in this study.....	55
Table 3.1: Summary of the results from previous PNSD studies at various sites in UK...59	
Table 3.2: Overview of instrument types per sampling site (March-June 2014).....	62
Table 3.3: Mean, Median, and Max of the Metrological parameters at AURN and BF sites.....	63
Table 3.4: Summary statistics of size-segregated particle number concentrations (# cm ⁻³), and eBC (µgm ⁻³).....	67
Table 3.5: Comparisons of size-resolved particle number concentrations (cm ⁻³) between this study and other European studies. (Size range: nm).....	69
Table 3.6: Pearson correlation coefficients between PNSD (# cm ⁻³), and the metrological parameters (WS (m s ⁻¹), WD (knot), T (OC), RH (%)) at AURN and BF sites.....	70
Table 3.7: Mean, and Median, of the NO _x (µg m ⁻³), eBC (µg m ⁻³), PNSD (# cm ⁻³), and Traffic (vehicles h ⁻¹) at BF site Week before, Easter and Week after Easter holiday 2014.....	73
Table 3.8: Statistics of particle number concentrations measured during NPF and non-NPF event days.....	88
Table 3.9: Summary of N _{total} (# cm ⁻³), and N _{nuc} (# cm ⁻³), O ₃ (µg m ⁻³), NO _x (µg m ⁻³), and NPF event characteristics (GR (nm h ⁻¹), J ₁₀₋₂₅ (cm ⁻³ s ⁻¹), CS (10 ⁻³ s ⁻¹), Q (10 ⁵ cm ⁻³ s ⁻¹)) during the NPF event days.	91
Table 4.1: Air quality instrumentation at Leicester AURN site during the sampling period.	98

Table 4.2: Values of the slopes S1 and S2 found at AURN site. S1 and S2 are expressed as 10^6 particles/ng eBC	109
Table 4.3: Summary of S1 and S2 values found during rush hours in previous studies and this study.....	110
Table 4.4: Total mean percentage of N1 and N2 for daily and midday-afternoon at the AURN site (2014-2015).	113
Table 5.1: Instruments and monitors used in this study	124
Table 5.2: Statistics of LDSA ($\mu\text{m}^2 \text{cm}^{-3}$), eBC ($\mu\text{g m}^{-3}$), and NO_x ($\mu\text{g m}^{-3}$) measured at AURN site from November 2013 to May 2015.....	126
Table 5.3: Summary of average and standard deviations of LDSA (Alveolar region) concentrations measured in previous studies and this study in urban area.....	127
Table 6.1: Location and characteristics of the five PM_{10} sampling sites.....	146
Table 6.2: PM_{10} mass concentration ($\mu\text{g m}^{-3}$) at the five sites.....	152
Table 6.3: COD of the daily PM_{10} ($\mu\text{g m}^{-3}$) between the monitoring sites.....	153
Table 6.4: The ratios of $\text{NO}_3^-/\text{PM}_{10}$, $\text{SO}_4^{2-}/\text{PM}_{10}$, and $\text{SO}_4^{2-}/\text{NO}_3^-$ in PM_{10} at five sampling sites during different periods.....	155
Table 6.5: PM_{10} mass closure results ($\mu\text{g m}^{-3}$) at sampling sites.....	162
Table 6.6: Factor loadings for PM_{10} at AD, AP, LL, WZ, and LE sites.....	169

List of Figures

Figure 1.1: Atmospheric cycling of atmospheric aerosols and effects on the climate system and human health adapted from (Fuzzi et al., 2006).	2
Figure 1.2: Average aerosol mass concentrations with associated chemical compositions at multiple locations in the northern hemisphere adapted from (Zhang et al., 2007).....	4
Figure 1.3: Typical number and volume size distributions of atmospheric particles adapted from (Seinfeld and Pandis, 2006).....	5
Figure 1.4: Particle size distribution of different modes of aerosol particles adapted from (González, 2012).....	6
Figure 1.5: Global average radiative forcing (RF) with respect to the industrial revolution (1750) for GHG and aerosols. The net anthropogenic radiative forcing is positive and equal to 1.6 W m^{-2} adapted from (IPCC, 2007). GHG, CO ₂ , N ₂ O concentrations, emissions and other important components and atmospheric processes are well recognised by their high level of scientific understanding (LOSU) and small error bars...	7
Figure 1.6: The potential toxicity mechanisms of UFPs in air pollution adapted from (Chen et al., 2016).....	17
Figure 1.7: Trailer of ECN used for mobile air quality monitoring and public awareness raising (in Leicester).....	20
Figure 2.1: Map of the Joaquin sampling sites in NW Europe.....	26
Figure 2.2: Detail of the locations of AURN and BF sites in Leicester.....	28
Figure 2.3: Detail of the location of AD site in Amsterdam.	30
Figure 2.4: Detail of the location of AP site in Antwerp.....	31
Figure 2.5: Detail of the location of LL site in Lille.....	32
Figure 2.6: Detail of the location of WZ site in Wijk aan Zee.....	34
Figure 2.7: Grimm SMPS+C 5420 with L-DMA.....	38
Figure 2.8: Model 3783 Environmental Particle Counter.....	39
Figure 2.9: Model 3783 Environmental Particle Counter™ Monitor Flow System Schematic.....	40
Figure 2.10: Model 3031 Ultrafine Particle Monitor.....	41

Figure 2.11: Typical Field Operation of UFP monitor TSI 3031	42
Figure 2.12: Flow schematic of UFP monitor TSI 3031	43
Figure 2.13: Flow Schematic of the Differential Mobility Analyser (DMA)	45
Figure 2.14: Nanoparticle surface area monitor TSI 3550	46
Figure 2.15: Flow schematic of NSAM TSI 3550	47
Figure 2.16: Curves for tracheobronchial and alveolar lung deposition for a reference worker	48
Figure 2.17: Schematic of the Environmental Sampling System (TSI 3031200),	49
Figure 2.18: MAAP Thermo Scientific 5012	50
Figure 2.19: Principle of operation of the MAAP Monitoring Instrument	51
Figure 2.20: Model 42i NO-NO ₂ -NO _x monitor	52
Figure 2.21: Model 42i Flow Schematic	53
Figure 2.22: Leckel SEQ47/50 (a) and Derenda PNS 16 (b)	54
Figure 2.23: The sampling inlet of the sequential sampler SEQ47/50 according to CEN EN 12341	54
Figure 3.1: Map of Leicester and locations of the sampling sites	61
Figure 3.2: Particle number size distribution at AURN and BF sites	71
Figure 3.3: Particle number size distribution at Brookfield site. During week before Easter (Red line), Easter break (green line) and week after Easter (black line). Easter Holidays in Leicester: Mon 14th April – Fri 25th April 2014	72
Figure 3.4: Particle number size distribution at a) AURN and b) BF sites under day time (7:00-19:00), and night (22:00-4:00) conditions	74
Figure 3.5: Particle number size distribution during weekends and weekdays at a) AURN and b) BF sites	75
Figure 3.6: Mean diurnal variations of particle number concentration for a) AURN and b) BF sites. During workdays and weekends	76
Figure 3.7: Weekly variation of particle number concentrations at a) AURN and b) BF sites	78
Figure 3.8: Diurnal variation of N _{nuc} , N _{total} , NO _x , and eBC for a) NPF event days (n =14), and b) Non-NPF event days (n =72)	80

Figure 3.9: At AURN site a) CPF plot of TNC for concentrations >50th percentile ($7728.7 \text{ \# cm}^{-3}$), (b) Bivariate polar plot of TNC, (c) CPF plot of eBC for concentrations >50th percentile (1.3 \mu g m^{-3}), (d) Bivariate polar plot of eBC concentrations. The radial axis is wind speed in m s^{-1}	82
Figure 3.10: At BF site a) CPF plot of TNC for concentrations >50th percentile ($7031.6 \text{ \# cm}^{-3}$), (b) Bivariate polar plot of TNC, (c) CPF plot of eBC for concentrations >50th percentile (0.9 \mu g m^{-3}), (d) Bivariate polar plot of eBC concentrations. The radial axis is wind speed in m s^{-1}	83
Figure 3.11: Correlation of the a) Nnuc, b) NAitken, c) Nacu, and d) Ntotal and wind speed for March 2014 at AURN site.	84
Figure 3.12: Correlation of the a) Nnuc, b) NAitken, c)Nacu, and d)Ntotal and wind speed for April and May 2014 at BF site.....	85
Figure 3.13: The NPF events measured on a) 3rd May 2014, and b) 27th April 2014. From bottom to top, the parameters are: (i) Average PNSD, (ii) N_{TOTAL} , and eBC mass concentrations, (iii) temperature, and relative humidity.....	87
Figure 4.1: Leicester and location of the sampling site (denoted AURN).....	97
Figure 4.2: Monthly variations in the median, 25/75th and 5/95th quantile values for PNC size classes, and TNC for 2014 at AURN site.....	101
Figure 4.3: Daily variations in the median, 25/75th and 5/95th quantile values for PNC size classes, and TNC for 2014 at the AURN site.....	103
Figure 4.4: Diurnal variations of eBC, and TNC concentrations for each month in 2015.98	
Figure 4.5: Diurnal variations of different size channel of PNC for each month in 2014	107
Figure 4.6: Half-hourly mean values of TNC versus eBC concentrations at different times of the day in Leicester. $S1$ (10^6 particles per ng eBC).....	109
Figure 4.7: Half-hourly mean values of N1, N2, the gaseous pollutants (NO_x , O_3 , mg m^{-3}) concentrations and the wind speed (m s^{-1}) for every day of the week.....	112
Figure 4.8: Half-hourly mean values of N2 (cm^{-3}), the temperature (T, $^{\circ}\text{C}$) and the relative humidity (RH, %) for every day of the week.....	114
Figure 4.9: Bivariate polar plots of a) TNC, c) eBC, and e) NO_x concentrations, respectively at the AURN site. The centre of each plot represents a wind speed of zero,	

which increases radially outward. The concentrations are shown by the colour scale. Polar annulus plots of b) TNC, d) eBC, and f) NO_x concentrations, respectively at the AURN site. Inside of circle is 00:00-01:00 h running through the day to 23:00-24:00.....116

Figure 4.10: Bivariate polar plots of a) N1, and c) N2, concentrations, respectively at the AURN site. The centre of each plot represents a wind speed of zero, which increases radially outward. The concentrations are shown by the colour scale. Polar annulus plots of b) N1, and d) N2, concentrations, respectively at the AURN site. Inside of circle is 00:00-01:00 h running through the day to 23:00-24:00.117

Figure 5.1: AURN and Brookfield sites at Leicester University campus, sampling locations.....123

Figure 5.2: Monthly variations of LDSA, eBC, and NO_x concentrations (error bars represent the standard deviation).....129

Figure 5.3: The diurnal and weekly variations of LDSA, eBC, and NO_x concentrations.....131

Figure 5.4: : Correlations between LDSA concentrations and (a) Black Carbon (eBC), (b) NO_x, (c) Total Particle Number concentration (N_{TOTAL}) at AURN monitoring site from Nov-2013 to Apr-2015.....132

Figure 5.5: Seasonal correlations between LDSA concentrations and (a) Black Carbon (eBC), (b) NO_x, (c) Total Particle Number concentration (N_{TOTAL}) at AURN monitoring site from Nov-2013 to Apr-2015.....133

Figure 5.6: : Linear relationship between direct LDSA (from NSAM) and calculated LDSA (from PNSD) concentrations for different particle size ranges, a) 10-30 nm b) 20-100 nm, c) 20-400 nm, d) 400-1000 nm size ranges.....134

Figure 5.7: Linear relationships between the calculated LDSA and eBC: (a) scatterplots for weekdays and weekends, (b) diurnal variation of the calculated LDSA and eBC....135

Figure 5.8: Wind speed and direction dependence map of a) LDSA ($\mu\text{g}^2/\text{cm}^3$), b) eBC ($\mu\text{g}/\text{m}^3$), c) NO_x ($\mu\text{g}/\text{m}^3$) at AURN site, d) wind frequency rose for the whole period. In each figure, the shaded contour indicates the average of variables for varying wind speeds (radial direction) and wind direction (transverse direction). The dash-dot lines stand for the relative mean values for each wind direction.....137

Figure 5.9: Contour plot of particle size distribution observed on 3rd May 2014. From bottom to top, the parameters are: (i) total Particle number and volume concentrations,

(ii) contour plot of particle size distributions, (iii) LDSA and eBC concentrations (iv) wind speed and relative humidity.....	139
Figure 5.10: Diurnal variation of PNSD, LDSA, and NO _x for a) NPF event days (n=14), and b) Non-NPF event days (n= 72). N _{nuc} is the particle number concentrations when diameter 10 -25 nm and N _{total} = Particle number concentrations with diameter =10 -1000 nm.	140
Figure 6.1: Map of the locations of all monitoring sites.....	145
Figure 6.2: Monthly variations of PM ₁₀ concentrations at the sampling sites.....	151
Figure 6.3: Correlations between OC and EC during different seasons at all sampling sites.....	155
Figure 6.4: Crustal enrichment factor (EF) for the different elements in all cities.....	159
Figure 6.5: Average annual mass closure of PM ₁₀ for a) AD, b) AP, c) LE, d) LL, and e) WZ sites.....	163
Figure 6.6: Chemical mass closure of PM ₁₀ at different season at five sampling sites..	165
Figure 6.7: Correlation between the calculated and the gravimetric measured PM ₁₀ mass concentrations at a) AD, b) AP, c) LE, d) LL, and e) WZ sites.....	166

List of Acronyms and symbols

AURN	Automatic Urban and Rural Network
BF	Brookfield
DEFRA	Department for Environment, Food and Rural Affairs
ECN	Energy research Centre of the Netherlands
PCA	Principal Component Analysis
NO	Nitrogen oxide
NO ₂	Nitrogen dioxide
NO _x	Nitrogen oxides
NH ₄ ⁺	Ammonium
NO ₃ ⁻	Nitrate
NO _x	Nitrogen oxides
SO ₄ ²⁻	Sulphate
CO	Carbon monoxide
PNSD	Particle number size distribution
MAAP	Multiangle absorption photometer (MAAP Thermo Scientific model 5012)
SMPS	Scanning Mobility Particle Sizer
NSAM	Nanoparticle surface area monitor; TSI model 3550
D _p	Particle mobility diameter
O ₃	Ozone
OC	Organic carbon
OM	Organic Matter
N1	Components directly emitted as particles and compounds which nucleate immediately after emission.
N2	The particles formed during the dilution and cooling of vehicle exhaust emissions and by in situ NPF.
N _{nuc}	Nucleation mode particles (d<25nm)
N _{Aitken}	Aitken Mode particles (25≤d<100nm)
N _{total}	Total number of particle (10≤d≤1000nm)
NPF	New Particle Formation

PM	Particulate matter
PM ₁₀	Particles smaller than 10 µm. PM ₁₀ are the particles that pass a size-selective inlet with an efficiency limit of 50% for an aerodynamic diameter of 10 µm
PM _{2.5}	Particles smaller than 2.5 µm. PM _{2.5} are the particles that pass a size-selective inlet with an efficiency limit of 50% for an aerodynamic diameter of 2.5 µm
TNC	Total number concentration of particles
UFP	Ultrafine particles, or particles smaller than 100 nm
VOC	Volatile organic compound
WD	Wind Direction
WS	Wind speed
WHO	World Health Organisation
IPCC	Intergovernmental Panel on Climate Change

Scientific contributions

Sarkawt M.L Hama, Nan Ma, Rebecca L. Cordell, Gerard P.A. Kos, Alfred Wiedensohler, and Paul S. Monks, **2017**. Lung deposited surface area in Leicester urban background site/UK: Sources and contribution of new particle formation. *Atmospheric Environment*, 151, 94-107.

Author contributions

Sarkawt Hama performed aerosol measurements, analysed and interpreted the data, and wrote the manuscript. **Nan Ma** helped with interpretation of results and reviewed of the manuscript. **Rebecca Cordell** assisted with the aerosol measurements and review manuscript. **Gerard Kos** assisted with the aerosol measurements and provided data from the SMPS Monitor. **Alfred Wiedensohler** reviewed the manuscript. **Paul Monks** (supervisor) assisted with the interpretation of the data and preparation of the manuscript.

Sarkawt M.L Hama, Rebecca L. Cordell, Gerard P.A. Kos, E.P. Weijers, and Paul S. Monks, **2017**. Sub-micron particle number size distribution characteristics at two urban locations in Leicester. *Atmospheric Research*, 194, 1-16.

Author contributions

Sarkawt Hama performed aerosol measurements, analysed and interpreted the data, and wrote the manuscript. **Rebecca Cordell** assisted with the aerosol measurements and review manuscript. **Gerard Kos** assisted with the aerosol measurements and provided data from the SMPS Monitor. **E.P. Weijers** assisted with the aerosol measurements and provided data from the SMPS Monitor. **Paul Monks** (supervisor) assisted with the interpretation of the data and preparation of the manuscript.

Sarkawt M.L Hama, Rebecca L. Cordell, and Paul S. Monks, **2017**. Quantifying primary and secondary source contributions to ultrafine particles in the UK urban background. *Atmospheric Environment*, 166, 62-78.

Author contributions

Sarkawt Hama performed aerosol measurements, analysed and interpreted the data, and wrote the manuscript. **Rebecca Cordell** assisted with the aerosol measurements and reviewed the manuscript. **Paul Monks** (supervisor) assisted with the interpretation of the data and preparation of the manuscript.

Sarkawt M.L Hama, Rebecca L. Cordell, Jeroen. Staelens, Dennis Mooibroek and Paul S. Monks, 2017. Chemical composition and source identification of PM10 in Five North Western European Cities. Atmospheric Research (under review).

Author contributions

Sarkawt Hama performed aerosol measurements, analysed and interpreted the data, and wrote the manuscript. **Rebecca Cordell** assisted with the aerosol measurements and reviewed the manuscript. **Jeroen. Staelens** assisted with reviewed the manuscript. **Dennis Mooibroek** assisted with reviewed the manuscript. **Paul Monks** (supervisor) assisted with the interpretation of the data and preparation of the manuscript.

J. Hofman, J. Staelens, R. Cordell, C. Stroobants, N, Zikova, **Sarkawt M.L. Hama**, K.P. Wyche, G.P.A. Kos, S. Van Der Zee, K.L. Smallbone, E.P. Weijers, P.S. Monks, E. Roekens, 2016. Ultrafine particles in four European urban environments: first results of a continuous long-term monitoring network. Atmospheric Environment, 136, 68-81.

R. L. Cordell, M. Mazet, C. Dechoux, **Sarkawt M.L. Hama**, J. Staelens, J. Hoffman, C. Stroobants, E. Roekens, G.P.A. Kos, E. Weijers, K.F.A. Frumau, P. Panteliadis, T. Delaunay, K. P. Wyche and P. S. Monks, 2016. Evaluation of Biomass Burning across North West Europe and Its Impact on Air Quality. Atmospheric Environment, 141, 276-286.

Conference and meeting contributions

Tackling tomorrow's Air Pollution Today: a solution oriented approach, Leicester, UK, 21-22 May 2014. (attended)

Sarkawt M.L. Hama, Rebecca L. Cordell, and Paul S. Monks, (2014): Ultrafine particles measurement in Leicester city. Joaquin group meeting (CGM), Haarlem, The Netherlands, 1-3 October 2014. (Presented)

Sarkawt M.L. Hama, Rebecca L. Cordell, and Paul S. Monks, (2015): Ultrafine particles results in Leicester city. Joaquin group meeting (CGM), Paris, France, 11-13 March 2014. (Presented)

Sarkawt M.L. Hama, Rebecca L. Cordell, Iain R. White, and Paul S. Monks, (2014): Ultrafine particles measured in Leicester as part of Joaquin project. Final UFIREG Conference Ultrafine Particles and Health, Dresden, Germany, 28th November 2014. (Poster)

Sarkawt M.L. Hama, Paul S. Monks, Rebecca L. Cordell and Iain R. White (2015): Sources and distribution of ultrafine particles measured at one urban background site in Leicester. EFCA Ultrafine Particles Symposium, Brussels, Belgium, May 4-5, 2015. (Poster)

Staelens, J. Hofman, **Sarkawt M.L. Hama**, K.P. Wyche, G. Kos, C. Matheussen, R. Cordell, J. van der Laan, J. Meydam, K.L. Smallbone, A. Frumau, E. Weijers, P.S. Monks, E. Roekens (2015): Monitoring of UFP concentration and size distribution at four urban background sites in NW-Europe. EFCA Ultrafine Particles Symposium, Brussels, Belgium, May 4-5, 2015.

Sarkawt M.L. Hama, Rebecca L. Cordell and Paul S. Monks, (2015): Sources and distribution of ultrafine particles (UFP) measured at one urban background site in Leicester (UK). EFCA Ultrafine Particles Symposium, Brussels, Belgium, May 4-5, 2015. (Poster)

Sarkawt M.L. Hama, Rebecca L. Cordell and Paul S. Monks, (2015): Temporal variation of ultrafine particles (UFP) in Leicester (UK). Cleaner Air, Better Health conference, Amsterdam, The Netherlands, 11th June, 2015. (Poster)

Jelle Hofman, Jeroen Staelens, Christophe Stroobants, **Sarkawt M.L. Hama**, Kevin Wyche, Gerard Kos, Christina Matheussen, Rebecca Cordell, Jorrit van der Laan, Jennes Meydam, Kirsty Smallbone, Arnoud Frumau, Ernie Weijers, Paul Monks, Edward Roekens (2015): Ultrafine particles in Joaquin cities. Cleaner Air, Better Health conference, Amsterdam, The Netherlands, 11th June, 2015.

Sarkawt M.L. Hama, Paul S. Monks, and Rebecca L. Cordell (2015): Monitoring of particle number concentration and other traffic- related air pollutants at one urban background site in Leicester, over The Course of a Year. 19th ETH Conference on Combustion Generated Nanoparticles, Zurich, Switzerland, June 28th –July 1st, 2015. (Poster)

Sarkawt M.L. Hama, Rebecca L. Cordell, and Paul S. Monks, (2015): Seasonal and temporal variations of ultrafine particle number concentrations in urban Leicester. European Aerosol Conference, Milan, Italy, September 6-11, 2015. (Poster)

J. Hofman, J. Staelens, C. Stroobants, **Sarkawt M.L. Hama**, K.P. Wyche, G.P.A. Kos, C. Matheussen, R. Cordell, J. van der Laan, J. Meydam, K.L. Smallbone, A. Frumau, E. Weijers, P.S. Monks, E. Roekens (2015): The added value of UFP monitoring in urban environments: number concentration and size distribution assessments in Amsterdam (NL), Antwerp (BE), Leicester (UK) and London (UK), European Aerosol Conference, Milan, Italy, September 6-11, 2015.

Sarkawt M.L. Hama, Rebecca L. Cordell, and Paul S. Monks (2016): Chemical Composition of PM10 a background site in Leicester, UK: Correlation between Levoglucosan and PNSD. IGAC Conference, Breckenridge, USA, September 26-30, 2016. (Poster)

Chapter one

1. Introduction

1.1 Atmospheric aerosols

1.1.1 Definition and physical properties

Atmospheric aerosols (including so-called particulate matter (PM)), are defined as solid or liquid or both suspended in the atmosphere with diameters between about 0.002 μm to about 100 μm . The source of these aerosols has an impact on both the chemical composition and the physical properties (e.g. mass, size, number-density) of atmospheric particles. The lifetime of aerosols in the atmosphere ranges from days to weeks, and therefore their impacts range from local to regional. Atmospheric particles can be classified in various ways according to their origin, formation mechanism, chemical composition or size among other properties.

- i. Origin of aerosols: Atmospheric aerosol particles originate from a wide variety of natural and anthropogenic sources. Natural atmospheric aerosols are present in the absence of human activity, and form from primary materials such as sea salt, mineral dust emitted from disturbed soils by the action of winds, volcanic ash, forest fires and biological materials (micro-organisms, plant fragments, pollen, etc.), and secondary species for example, sulphate formed by natural emissions of SO_2 (volcanoes or conversion of marine dimethyl sulphide) or secondary organic materials (such as biogenic emissions of isoprene and monoterpenes). Anthropogenic primary sources include carbonaceous materials related to combustion (elemental, black and organic), demolition dust and road dust (abrasion of brakes, tires and pavement). Anthropogenic secondary particle sources includes nitrate, sulphate, ammonium and carbonaceous compounds mostly linked to urban, industrial, and agriculture-farming emissions of gaseous precursors (Monks et al., 2009; von Schneidemesser et al., 2015).
- ii. Formation mechanism of aerosols: Primary aerosol particles are directly emitted into the atmosphere e.g. from incomplete combustion of fossil fuels, volcanic eruptions, biomass burning, wind-driven, industrial and traffic-

related road suspensions. Secondary particles, on the other hand, are produced as a result of gas-to-particle conversion processes in the atmosphere: homogenous nucleation (only involving only gaseous precursors) or heterogeneous nucleation (reaction of gases with solid or liquid phases) (Monks et al., 2009; Pöschl, 2005). Aerosol particles undergo different physical and chemical interactions and transformations, such as changes in structure, particle size and chemical composition via chemical reactions, coagulation, restructuring, phase transitions and gas uptake (Pöschl et al., 2007)) as shown in Figure 1.1.

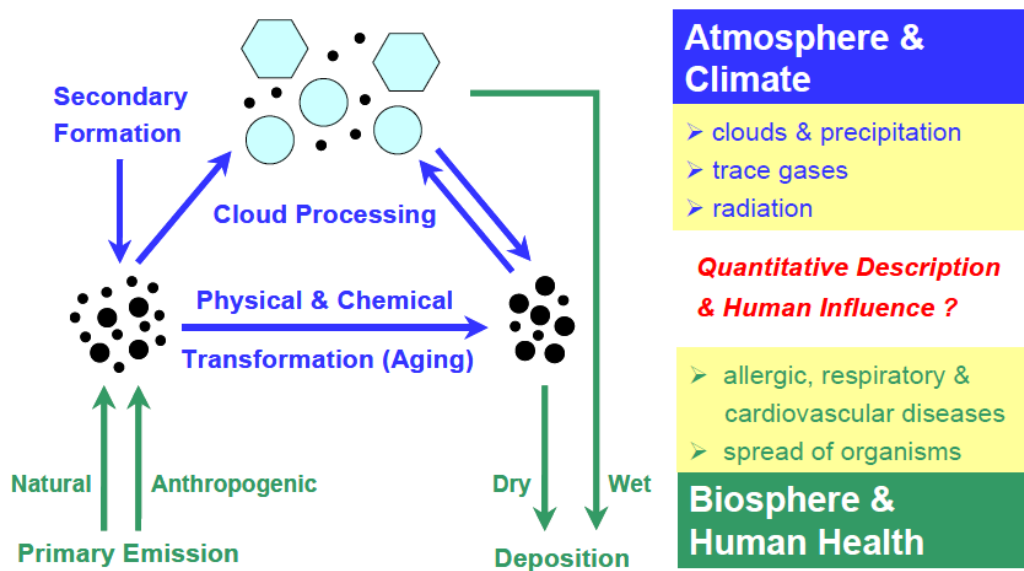


Figure 1.1: Atmospheric cycling of atmospheric aerosols and effects on the climate system and human health adapted from (Fuzzi et al., 2006).

- iii. **Chemical composition of aerosols:** atmospheric aerosols are usually composed of variable amounts of sulphate, nitrate, ammonium, sodium, chloride, carbonaceous species, crustal elements, trace metals and water. The major chemical component of atmospheric aerosols are sulphate, nitrate, ammonium, sea salt, mineral dust, and carbonaceous species (see Table 1.1). The average aerosol concentrations and their chemical compositions vary significantly across the Earth owing to various sources and meteorological conditions as shown in Figure 1.2.

Table 1.1: The five main chemical components of atmospheric aerosols adapted from (Wilson and Suh, 1997).

Chemical composition	Composition	Sources
Mineral dust	Al, Ca, Si, Fe, Ti, K, Mg, Co, Ba Mineral composition: SiO ₂ , CaCO ₃ , CaMg(CO ₃) ₂ , clays, Fe ₂ O ₃ , CaSO ₄ .2H ₂ O	Resuspension of soils and long range transport from arid regions
Carbonaceous materials	Elemental, and organic carbon	Fuel combustion
Nitrogen compounds	NO ₃ ⁻ , NH ₄ ⁺ , NH ₄ NO ₃	The result of the nitric acid (HNO ₃) and ammonia (NH ₃) reaction
Sea salt	NaCl (85%) + sulphates Species: Cl ⁻ , Na ⁺ , SO ₄ ²⁻ , Br ⁻ , HCO ₃ ³⁻ , Mg ²⁺ , Ca ²⁺ , K ⁺ , MgCl ₂ , MgSO ₄ , Na ₂ SO ₄ , Al, Co, Cu, Fe, Mn, Pb, V, Zn	Generated by bubble processes on the ocean surface
Sulphate aerosols	(NH ₄) ₂ SO ₄	SO ₂ , DMS, transport, industry, and combustion

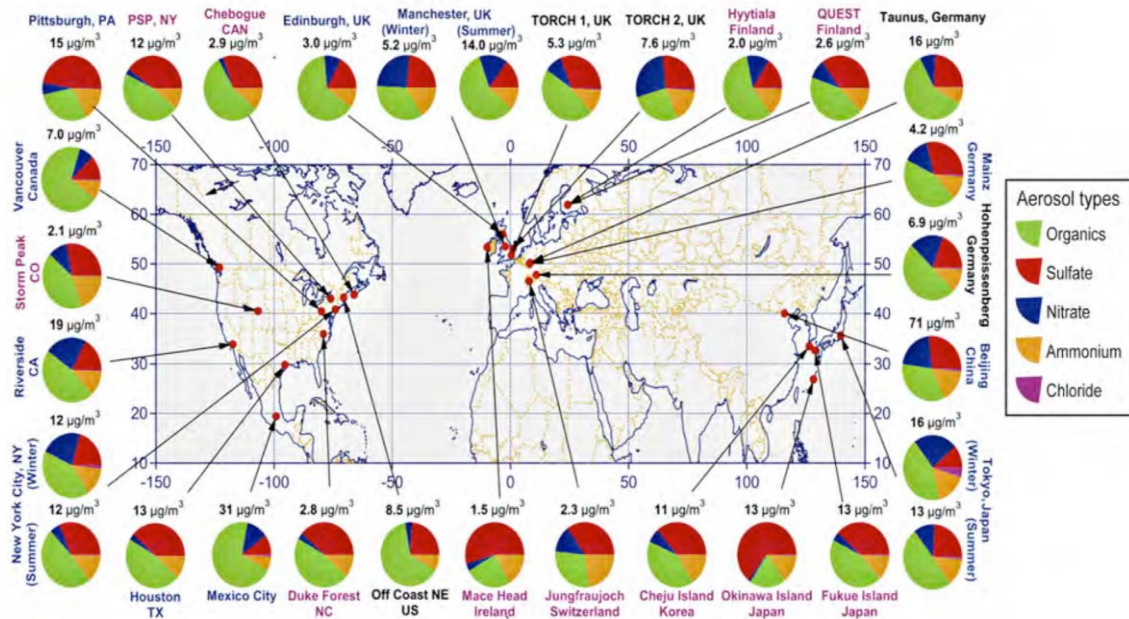


Figure 1.2: Average aerosol mass concentrations with associated chemical compositions at multiple locations in the northern hemisphere adapted from (Zhang et al., 2007).

- iv. Size distribution of aerosols: the diameter of aerosol particles span over four orders of magnitude, and may range from a few nanometres (e.g. for nucleated particles or some fresh emission sources) to $100 \mu\text{m}$. Atmospheric aerosol particles can be categorised by their diameter (D_p): nanoparticles ($D_p < 50\text{nm}$), ultrafine ($D_p < 100\text{nm}$), fine ($D_p < 2.5\mu\text{m}$) and coarse particles ($2.5\mu\text{m} < D_p < 100\mu\text{m}$). Typical aerosol size distributions are characterized by a multi-modal structure (see Figure 1.3 and Figure 1.4A) and different particle formation processes (see Figure 1.4B and C) for each mode: nucleation mode (1-30 nm), Aitken mode (30-100nm), accumulation mode (100 nm to 1000 nm) and coarse mode ($D_p > 1000 \text{ nm}$) (Harrison et al., 2000; Hussein et al., 2005; Kulmala et al., 2004). Nucleation mode particles are mainly formed by homogeneous nucleation involving gas-to-particle conversion. These type of particles have a relatively short lifetime and tend to show high number concentrations close to their sources shortly after formation (Kulkarni et al., 2011). Aitken mode may originate from primary combustion emissions and from particle growth processes. The nucleation and Aitken modes often make dominant contribution to the total particle number concentration in urban areas (Hama et al., 2017b; Seinfeld and Pandis, 2006; von Bismarck-Osten et

al., 2013; Vu et al., 2015). Accumulation mode particles are mainly generated from combustion of fuel and lubricant oil, and are formed through coagulation of nucleation mode particles and condensational growth of Aitken mode particles. Ultrafine particles can also be directly emitted into the ambient air by combustion sources (e.g. vehicle exhausts), as this process involves only condensation without chemical reaction. Fine particles are mostly emitted by combustion processes (e.g. fossil fuel, biomass burning, coal combustion), and can also be formed by secondary formation processes involving sulphur and nitrogen oxides to produce ammonium nitrate and sulphate in the aerosol particle phase and oxidation processes involving organic gaseous precursors. Coarse mode particles are generally formed by mechanical processes and include wind-blown soil, sea spray, volcanic and other natural emissions (see Figure 1.4C). The number concentration peaks in the nucleation and Aitken modes, while the volumetric size distribution is more relevant for the other modes is shown in Figure 1.3.

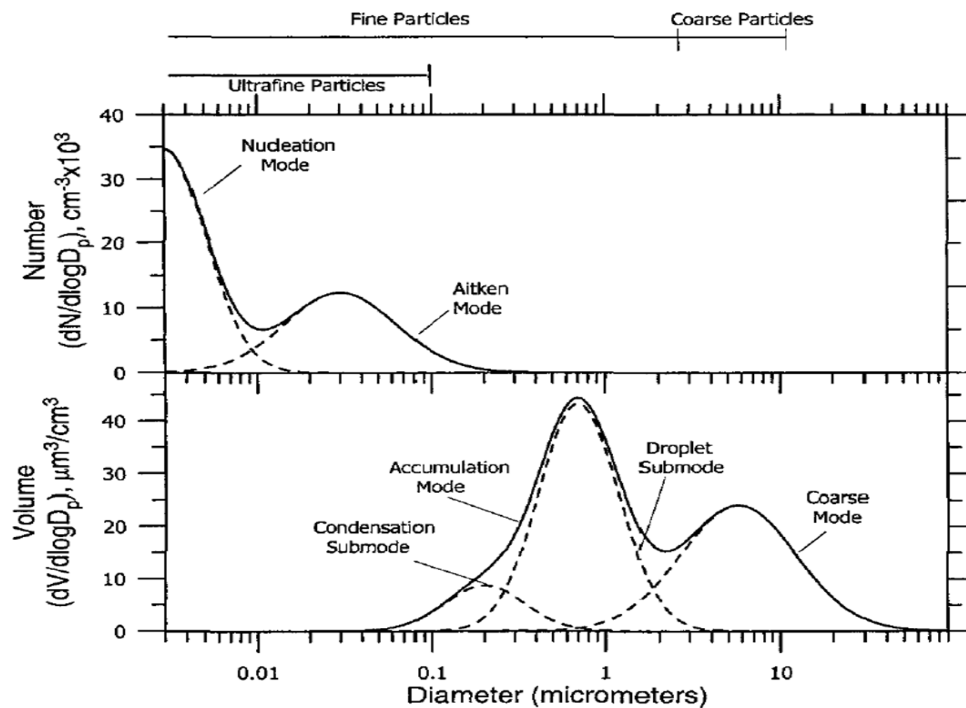


Figure 1.3: Typical number and volume size distributions of atmospheric particles adapted from (Seinfeld and Pandis, 2006).

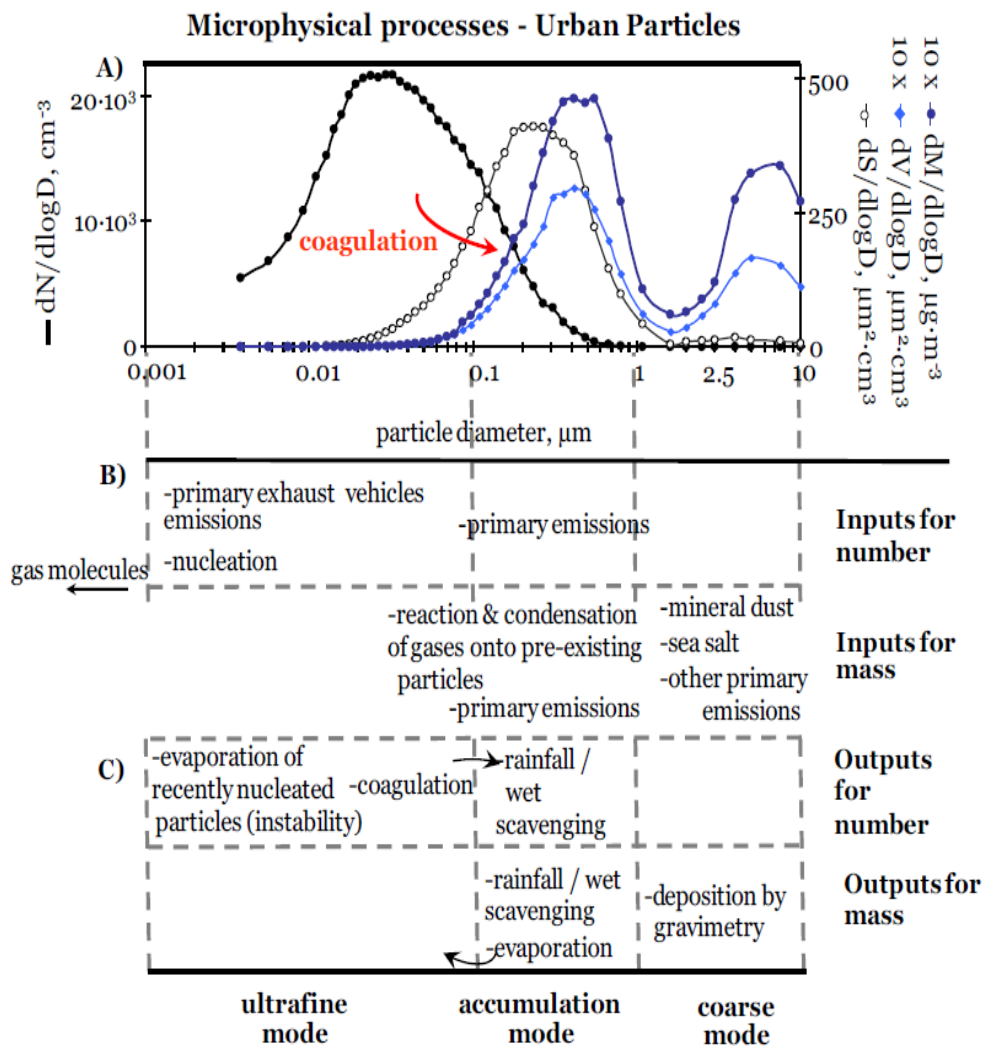


Figure 1.4: Particle size distribution of different modes of aerosol particles adapted from (González, 2012).

1.1.2 Aerosols and climate

Atmospheric aerosols have an impact on the climate by interactions with the Earth's radiative balance. This includes both a direct effect on solar radiation, and also their impact on cloud formation and albedo. The effects of atmospheric aerosols on climate has been found by the fourth Intergovernmental Panel on Climate Change (IPCC) as shown in Figure 1.5 (IPCC, 2007). Figure 1.5 illustrates the radiative forcing ($W m^{-2}$) species (positive and negative components) acting on the Earth's radiative balance (incoming vs. outgoing radiation). Positive radiative forcing leads to increase the surface

temperature, while negative radiative forcing acts in the opposite way. Greenhouse gases (GHG) (such as carbon dioxide (CO₂), methane (CH₄), nitrous oxide (N₂O), water vapour (H₂O), ozone (O₃) and halocarbons) change the incoming solar (short wavelength) radiation and absorb and re-emit the long wavelength radiation which released from the Earth's surface increasing the Earth's temperature. The observed levels of GHG have continuously increased in the atmosphere, which is the major reason for global warming (IPCC, 2007).

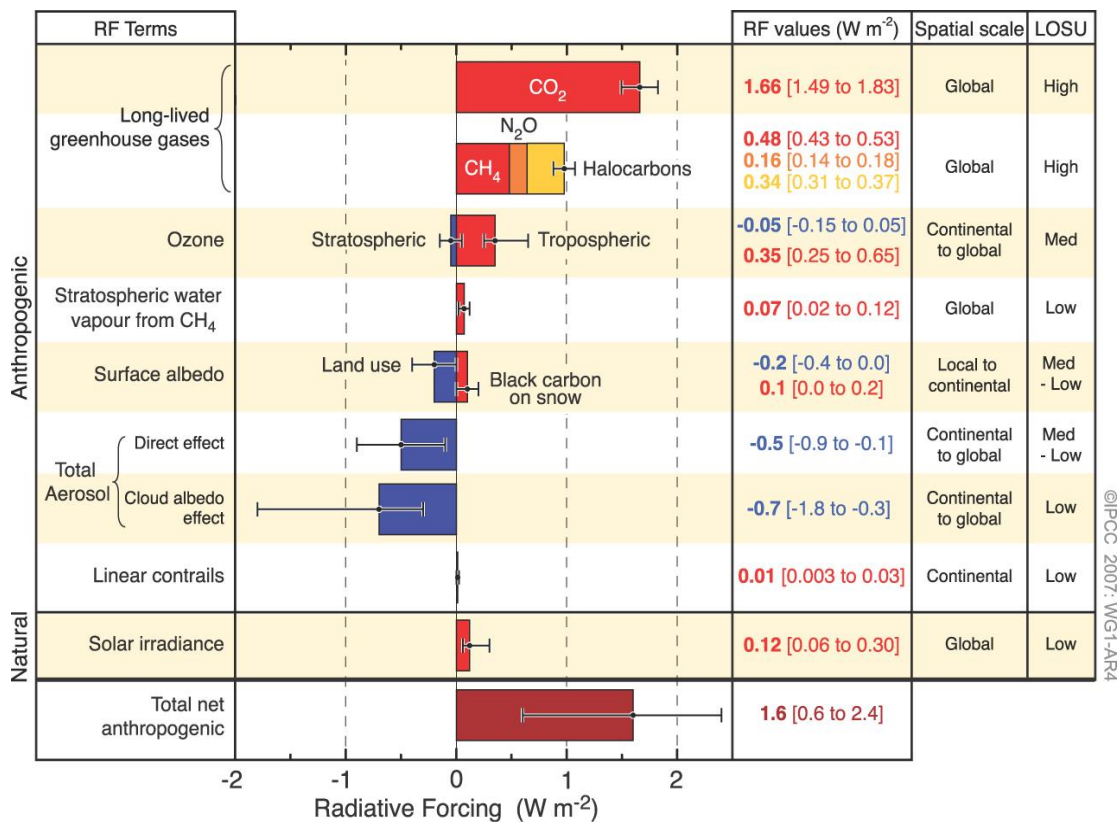


Figure 1.5: Global average radiative forcing (RF) with respect to the industrial revolution (1750) for GHG and aerosols. The net anthropogenic radiative forcing is positive and equal to 1.6 W m⁻² adapted from (IPCC, 2007). GHG, CO₂, N₂O concentrations, emissions and other important components and atmospheric processes are well recognised by their high level of scientific understanding (LOSU) and small error bars.

Figure 1.5 shows that atmospheric aerosols act as a negative constituent of the radiative forcing and scientific understanding is poorly characterised (low-medium LOSU and large error bars). Atmospheric aerosols have also impact on climate such as cloud lifetime and precipitation. Aerosols directly absorb and scatter short and long wavelength radiation depending on their concentrations, chemical composition, size distribution, and other physical properties (Schwartz, 1996). Anthropogenic source contributions to aerosols (mainly sulphate, nitrate, organic and black carbon, and dust) have a cooling effect, with a total direct radiative forcing of -0.5 (-0.9 to -0.1) W m^{-2} and an indirect cloud albedo forcing of -0.7 (-1.8 to -0.3) W m^{-2} . These radiative forcing are now better understood owing to improved in-situ, ground-based and satellite measurements and modelling, but still the main uncertainty in radiative forcing is unknown (IPCC, 2007). Higher uncertainties are related with the aerosol indirect impacts on climate through their effects on cloud formation processes, lifetime and structure (Lohmann and Feichter, 2005).

1.2 Ultrafine particles (UFPs)

1.2.1 Characteristics and sources

Ultrafine particles (UFPs; diameter < 100 nm) are ubiquitous in urban environment, and an acknowledged risk to human health. Generally, UFPs can be classified as primary (Aitken and accumulation modes) or secondary (nucleation mode). Primary natural sources of UFPs are marine aerosols and volcanic particles, which both have a small UFP constituent, and also pyrogenic processes such as forest fires (Heal et al., 2012). In addition, secondary sources of UFPs are new particle formation (NPF) via atmospheric photochemistry reactions and condensation of semi-volatile vapours (Holmes, 2007; Kumar et al., 2009). NPF events usually happen during high global radiation, low relative humidity, and low wind speed (Brines et al., 2015; Řimnáčová et al., 2011). The most popular atmospheric nucleation mechanism involves sulphuric acid nucleation, followed by condensational growth (oxidised organic materials play a major role in this process) (Alam et al., 2003). Oxidation of terpenes or other organic materials released from trees and iodine oxides are two other nucleation mechanism existing in natural urban environments (Kulmala et al., 2012; O'Dowd et al., 2002).

The dominant anthropogenic source of UFP concentrations is traffic emission (vehicle exhaust) in urban areas, contributing as much as 90% of total particle number concentrations (PNC) (Kumar et al., 2010). For instance, Charron and Harrison (2003) observed 71 to 95% of total PNC in London in the size range 11-100 nm. In addition, other anthropogenic sources of UFPs are combustion by-products from industry such as power plants, construction, waste incineration, agriculture processes, biomass burning, ship emissions and cooking. Contribution to UFPs from the other sources are likely to be modest compared with road vehicle exhaust emissions in urban areas. For example, Harrison et al. (2011) found in London about 65, 2, 5, and 18% of total PNC from road vehicles, brake dust, resuspension dust, and urban background sources, respectively. UFPs have high spatial variability in urban environments with the spatial inhomogeneity of UFPs remaining a key challenge for the control and assessment of these particles in urban areas.

The current European legislation for air quality set limit values for the outdoor air levels of aerosol particles in terms of mass concentrations of particles (PM_{10} , $PM_{2.5}$, aerodynamic diameter $< 10 \mu m$ and $< 2.5 \mu m$, respectively) (EC Directive, 2008). However, there are no ambient air quality limit values for UFP in Europe or anywhere else in the world. The PM working group of the European commission have discussed on these two metrics should be complement with other air quality important parameters such as UFPs and/or black carbon (BC) (COST 633 Report, 2009). In addition, Europe has PNC emission limits for the new road vehicles. This is currently the only such legislation in the world. The Euro 5 and Euro 6 standards specify a particle number emission limit (6.0×10^{11} particles/km) for compression ignition (diesel) road vehicles exhaust (EC Directive, 2008). Euro 6 standard also places a similar standard (6.0×10^{11} particles/km) for direct injection gasoline road vehicles, exempted to 6.0×10^{12} particles/km for the first three years of its implementation date in September 2014 (EC Directive, 2008).

1.2.2 Mechanism and Chemistry of Nucleation

New particle formation (NPF; also known as nucleation) events have been observed in different places, including rural, urban, the free troposphere, coastal, and forested areas (Cheung et al., 2011; Hama et al., 2017b; Hofman et al., 2016; Kulmala et al., 2007; Lee et al., 2008; Salma et al., 2011; Vehkamäki et al., 2004; Weber et al., 2001; Woo et al., 2001), and these events are one of the main sources of UFPs in addition to combustion-emitted particles in urban areas (Brines et al., 2015; Hama et al., 2017c). Atmospheric particles usually form during the late morning and then grow throughout the day, reaching growth rates of 1 to 20 nm hour⁻¹ (Kulmala, 2003). Ambient particles can be formed by four main nucleation mechanisms (Kulmala, 2003; Kulmala et al., 2004), such as homogenous binary nucleation (involving H₂O and H₂SO₄), homogenous ternary nucleation (involving H₂O, H₂SO₄, and NH₃), ion-induced nucleation of binary, ternary, or organic vapours, depending on the environmental conditions, and homogenous nucleation involving iodide species. Moreover, NPF events could be initiated through photochemical reactions enhanced by gaseous precursors in ambient air such as H₂SO₄, NH₃ and volatile organic compounds (VOCs) (Kulmala et al., 2000). Low volatility vapours nucleate into neutral molecular clusters that are stabilized by amines, ammonia and organic vapours, and are activated by condensation of low VOCs (Kulmala et al., 2013). Low relative humidity, existing SO₂ and low pre-existing particle surface area, high insolation and wind speed are common features that enhance NPF events (Kulmala and Kerminen, 2008), considered by a great increase in PNC in the nucleation mode and subsequent particle growth, if conditions are favourable in urban areas. In addition, urban NPF can interact with and can be influenced by regional NPF events, at least under some environmental conditions, and can become part of a phenomenon with a much larger horizontal extension than the city (Salma et al., 2016). At the same time, UFP concentrations in urban areas are strongly affected by high-temperature emission sources from different sectors (Paasonen et al., 2016) such as household and domestic heating (Butt et al., 2016), power production and industrial processes (Xiao et al., 2015), and vehicular road emissions (Morawska et al., 2008). Their diurnal variation often displays daily time-activity patterns of citizens (Dall'Osto et al., 2013a). Finally, up to approximately 40-50 % of all cloud condensation nuclei can initiate from NPF and growth of particles (Merikanto et al., 2009; Spracklen et al., 2008), which relates the

process to the climate system and shows its global importance (Carslaw et al., 2013; Kerminen et al., 2012; Shen et al., 2017).

1.2.3 State of Knowledge of NPF in Europe

In the global troposphere aerosol particles are assumed to contribute to air quality and climate change profiles (Ramanathan et al., 2001; Stott et al., 2000). Understanding these effects needs detailed information on how particles enter the atmosphere and how they are changed and transformed before being removed by dry or wet deposition mechanism. Key processes in this respect are the formation of new particles and their subsequent growth to larger sizes in the ambient air (Kulmala et al., 2004b). Over the past years, the traditional understanding of the NPF has evolved in light of the recent breakthroughs in this field. The key outcomes leading to the current understanding of NPF events were observations and theoretical prediction of molecular clusters and their size-dependent growth via nano-Kohler-type processes (Kulmala et al., 2007; 2013; 2004b). NPF events of regional origin have also been detected in urban areas (Hama et al., 2017b; Kulmala et al., 2004; Wehner et al., 2007). This is in contrast to what was assumed in the past, which is that NPF events only occur in background and regional environments (O'Dowd et al., 2010; Vakkari et al., 2011). This is generally attributed to the fact that such natural environments are characterised by a low condensations sink, thus assisting nucleation processes. By contrast, urban areas are often characterised by high condensations sink, so that a lower frequency of NPF events is expected. Nevertheless, there many studies showing that NPF events in fact can be found in urban areas (see Table 1.2). Previous studies regarding NPF events in diverse environments within Europe are tabulated in Table 1.2. Within northern Europe, NPF events in many urban areas are not very often observed. However, Reche et al. (2011) found that a different behaviour was observed in southern European cities, where NPF events at midday occurred with higher frequency than in northern European cities. The reason for this difference is likely due to the higher intensity of solar radiation and presences of different gaseous precursors in the southern European cities (see Table 1.2). The nucleation of aerosol particles from gaseous precursors in one of the most significant sources of atmospheric particle number in urban environments. The formation of new atmospheric particles in the atmosphere has been observed in many studies at various environment within Europe (see Table 1.2).

However, there are some important open questions remain: for example, the relevance of ion-induced formation and growth or the involvement of organic vapour molecules in the nucleation mechanism. Several studies strongly recommended looking at the NPF process from a micrometeorological perspective, including the role of turbulent fluctuations (Nilsson et al., 2001 and references therein). Those ideas have not substantiated in the form of generally applicable model. Based on global aerosol model studies, it is estimated that 30–50% of global tropospheric cloud condensation nuclei concentrations might be formed by atmospheric NPF events (Luo and Yu, 2011; Merikanto et al., 2009; Spracklen et al., 2008). Because NPF is a global phenomenon with climate implications, it is vital to increase our understanding of the processes that manage the formation of new particles and their growth in the atmosphere. Future research needs field observations including vertical resolution, as conditions at the ground are not always capable of predicting new particle formation aloft. Continuous field observations obtained at different environments will deliver insight into the features of new particle formation such as strength, frequency and related meteorology. Gaseous phase measurement of compounds that are likely to be participating in new particle formation and growth are also necessary. Other suggestions include the development of instrumentation to allow for measurement of clusters below 3 nm as well as the chemical composition of newly formed particles (Kulmala and Kerminen, 2008). This information will be important in creating appropriate predictive models that will be able to adapt to changing future scenarios.

Table 1.2: Previous NPF studies in diverse atmospheric environments of Europe.

Region	Site location: City (country)	Representative	Size range (nm)	References
Northern Europe (relatively clean area)	Birmingham (UK)	Urban background		Alam et al. (2003)
	Tahkuse (Estonia)	Rural	3-1000	Vana (2004)
			3-500	Kulmala et al. (2001)
	Hyttiala (Finland)	Boreal Forest	8-460	Dal Maso et al. (2005)
			3-1000	Hussein et al. (2009);
			3-1000	O'Dowd et al. (2009)
	Aspvreten (Sweden)	Coastal	8-460	Dal Maso et al. (2007)
	Rotterdam (Netherlands)	Urban background	3-1000	Crumeyrolle et al. (2010)
	Vavihil (Sweden)	Urban background	21.5-857	Kristensson et al. (2017)
	Pallas region (Finland)	Boreal forest	7-500	Asmi et al. (2011)
	Ferrand(France)	Rural	10-400	Boulon et al. (2011)
	Harwell (UK)	Rural	11-450	Charron et al. (2007)
	Amsterdam (Netherlands, Antwerp (Belgium), Leicester and London (UK).	Urban background	10-1100	Hofman et al. (2016)
Leicester (UK)	Urban background	10-1100	Hama et al. (2017b)	

Table 1.2: continued.

Region	Site location: City (country)	Representative	Size range (nm)	References
Southern Europe (highly polluted areas)	Barcelona (Spain), Madrid	Urban, and Regional	15-600	Pey et al. (2008)
			13-800	Brines et al. (2015);
	Rome (Italy)	Regional background	11.3-	Brines et al. (2014);
			358.79	Dall'Osto et al.
	Po Valley (Italy)	Industrial, and agricultural	17.5-572.9	(2013a); Gómez-
			10.2-615.3	Moreno et al. (2011)
Bologna (Italy)	Rural	3-20	Hamed et al. (2007)	
Central Europe (moderately polluted areas)	Melpitz (Germany)	Urban, and Regional background	3-20	Joutsensaari et al.
			15-600	(2018)
	Leipzig (Germany)	Urban background	3-11	Birmili and Wiedensohler
			3-800	(2000)
	Dresden (Germany)	Urban background	3-800	Größ et al. (2018)
			5-800	Wehner et al. (2007)
	Budapest (Hungary), Vienna (Austria), and Prague (Czech Republic)	Urban, and suburban background	6-1000	Ma and Birmili (2015)
			10-487	Birmili et al. (2013)
	Budapest (Hungary)	Urban background	10-505	Borsos et al. (2012)
			7-540	Németh and Salma
		10-600	(2014) Wonaschütz et al. (2015) Salma et al. (2016) de España et al. (2017); Németh et al. (2018)	
		6-1000	Salma et al. (2011)	

1.2.4 Health effects of UFPs

Epidemiological studies on UFPs are still rare, whereas many studies investigated adverse effects of particles (PM₁₀, and PM_{2.5}) on mortality and morbidity (Atkinson et al., 2014; R ckerl et al., 2011). Owing to their small size and small mass, the deposition and clearance of UFPs in the respiratory system differ from larger aerosol particles (Kreyling et al., 2006). Since the deposition in the respiratory system of inhaled UFPs is governed by diffusional mechanism, it is assumed that UFP translocation within the human body is dependent on the size of particles. Hence, the smallest UFPs mainly deposit in the nasopharyngeal region, larger size (>20 nm) UFPs generally reach the alveoli and enter the bloodstream (ICRP, 1994; Oberd rster et al., 2004; Peters et al., 1997). Up to date, experimental studies do not provide enough evidence to confirm this assumption. Additional, there is suggestive, but not consistent epidemiological indications on the link between short-term exposures to UFP and cardiorespiratory health problems (HEI, 2013; WHO, 2013a). Several studies have shown that exposure to UFPs results in harmful effects on human health (Chen et al., 2016; HEI, 2013; Ostro et al., 2015). After inhalation of UFPs, a very small fraction of UFPs penetrate deep into the respiratory system, allowing interaction between particles and lung tissue. Recent studies have showed that human alveolar macrophages are unable to remove particles less than 70 nm, and they can be potentially translocated into the blood stream (Bakand et al., 2012; R ckerl et al., 2011). Translocation of inhaled UFPs from the lungs to the liver and accumulation in the liver has been documented as happening in a matter of a few hours (Oberdorster et al., 2002). The UFPs from the air pollution might cause negative effects on human health either through direct damage to the respiratory system from deposition of particles or indirect effects resulting from sequential lung inflammation (see Figure 1.6).

The few epidemiological studies on UFPs and mortality have reported inconsistent results (HEI, 2013). For example, a study has reported that one day delayed increases in respiratory mortality and four-days delayed increases in cardiovascular mortality in association with UFPs in urban areas (Wichmann et al., 2000). Moreover, other studies have found that increases in cardiorespiratory mortality with a delay of at least two days in association with UFPs increases (Breitner et al., 2011; Breitner et al., 2009; St lzel et al., 2007). In UK, a recent report has found that an average loss of ~ 6 months in life

expectancy occurs to the residents due to $PM_{2.5}$ exposure, while such estimates are non-existent to the UFPs exposure (COMEAP, 2010).

It remains an open question as to which metric is best for demonstrating the toxicity of UFPs in the atmosphere because both general properties such as shape, particle number concentrations, size distribution, and surface area, and more specific characteristics (e.g. chemical composition, surface chemistry, agglomeration state, crystal structure, surface charge or porosity) may impact the toxicity of UFPs in the ambient air. While some epidemiological studies have indicated that particle surface area might be a suitable metric to quantify human exposure, other studies favour particle number concentration (Heal et al., 2012). The former is suggested because the larger surface area to mass ratio of UFPs, compared with larger particles, allows greater contact area for adsorbed materials to interact with biological surfaces (Maynarda and Maynard, 2002). The majority of toxicological studies have confirmed that the number and surface area of UFPs have great effect on human health rather than their mass (Lighty et al., 2000; Stoeger et al., 2009). On the other hand, some studies have showed that *in vitro* toxicity per unit mass is mostly independent of particle size fraction (Godri et al., 2011; Stoeger et al., 2007).

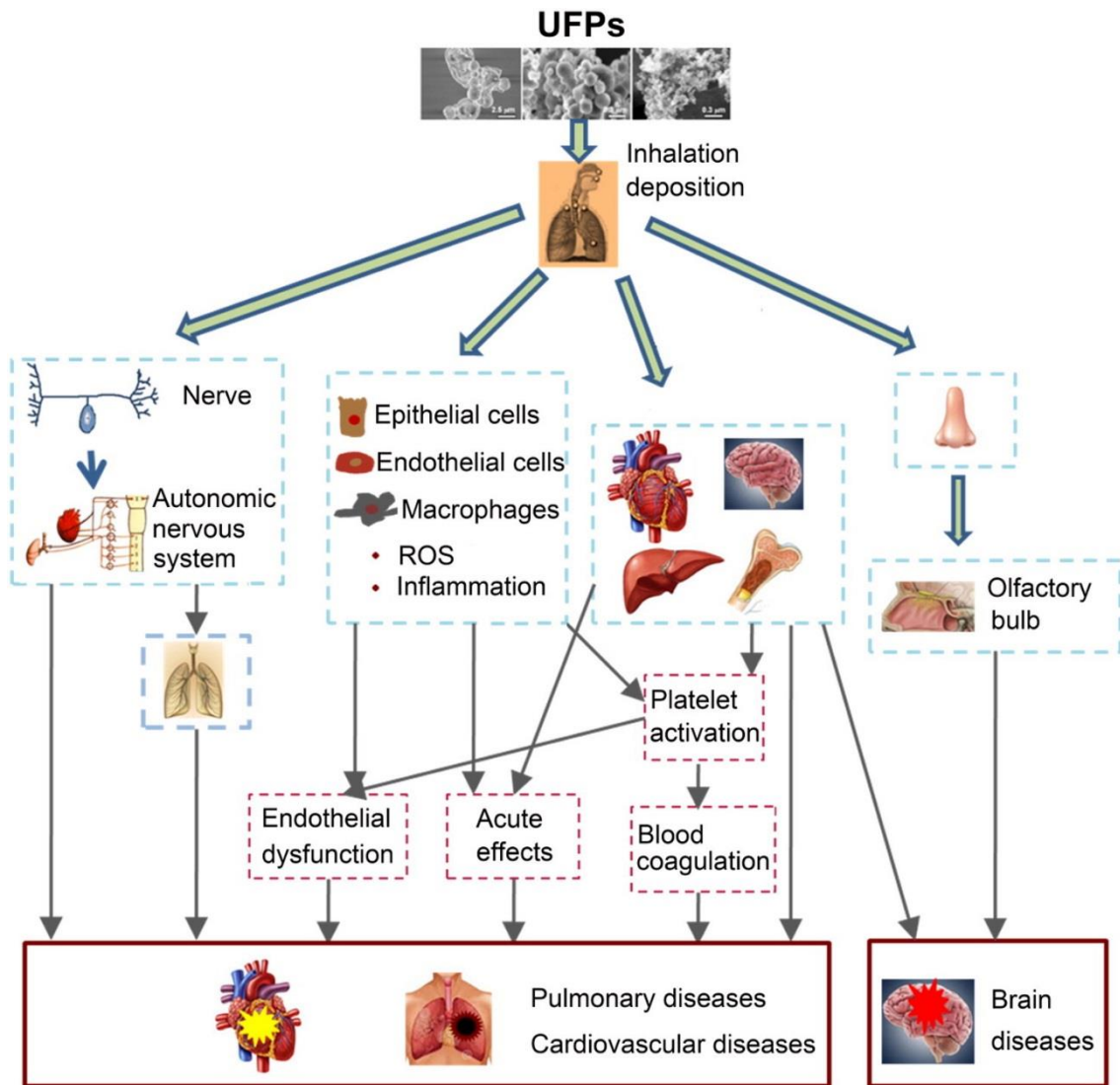


Figure 1.6: The potential toxicity mechanisms of UFPs in air pollution adapted from (Chen et al., 2016).

1.3 Thesis motivation

1.3.1 The JOAQUIN project

JOAQUIN (JOint Air QUality INitiative) was an EU cooperation project (1 January 2010 – 30 September 2015) supported by the INTERREG IVB North-West (NW) Europe programme (www.nweurope.eu). The project focused on air quality monitoring in the NW Europe region, the related health effects and possibilities for improvement. The project comprised the measurement of some air pollutants (such as UFPs, composition of particulate matter), demonstrating clearer evidence of the relationship between adverse health effects and the currently measured PM₁₀ and PM_{2.5} parameters. The aim of the project was to support health oriented air quality policies in Europe. To obtain this, the project provided policy makers with the necessary evidence on the current local and/or regional situation by measuring emerging health related parameters (such as NO_x, PNC, eBC, UFPs, and LDSA), and provided them with best-practice measures that can be taken and motivate them to adapt and strengthen their current air quality policies.

1.3.1.1 Overview

The project partnership undertook three work packages, each of which is specifically tailored to target the aims identified above.

- **Work package 1: Capacity building**

The project aimed to explain the science of new and emerging health-relevant air pollutants, to collect data and information on the current local and/or regional conditions and to improve the collective understanding of air pollution and its effect on residents' health. This result aimed to improve health related information available, to air quality experts, authorities and public health professionals in order to facilitate and deliver the motivation for better air quality policies.

The overall aim of JOAQUIN work package 1 was novel knowledge gathering of emerging health-pertinent pollutants for the future protection of human health and sustainable progress. Previously information on the number, size and distribution of such emerging pollutants in NW Europe was limited and air quality experts unable to identify UFP pollution sources, adapt their current policies and re-define appropriate mitigation measures to protect resident's health. Before action can be taken to mitigate against those

pollutants that have the greatest impact on public health, the problem must first be understood.

This work package aimed to enhance the understanding of novel, health-relevant air pollution and its sources within the NW Europe hotspot zone, with specific focus on emerging health-related pollutants.

Work package 1 consisted of four actions:

- Setting up a transnational next-generation "Watchdog network" for health related pollutants.
- Health-relevant source characterisation of PM: identifying air pollution sources and composition of PM₁₀ and revealing the links between air pollution and human health.
- Using a mobile air pollutants monitoring station to validate, expand and publicise the NW Europe Watchdog Network Infrastructure.
- Design the NW European air pollution observatory and information centre.

Together, these actions aimed to result in the acquisition and dissemination of health-relevant information and tools needed for air quality experts (authorities/public health professionals) for development and implementation of future policies and pollution reduction measures.

Action 3 of work package 1 was entitled: "Validation and expansion of the NW Europe "Watchdog Network" for health-pertinent pollution parameters with mobile monitoring". A mobile station (ECN trailer, Figure 1.7) was equipped with identical instruments and acted as a (fifth) reference site in each of the four cities contributing in the UFP measurements of the JOAQUIN project (Antwerp, Amsterdam, Leicester, London). In this JOAQUIN monitoring network, cutting edge instrumentation is applied to measure airborne concentrations of BC and the number concentration and size distribution of UFP. Dedicated monitoring campaigns were carried out at the fixed sites to ensure the quality and comparability of the experimental data collected in this project. Moreover, the trailer was placed at a second urban background site in three of the UFP monitoring cities (Amsterdam, Antwerp and Leicester). Finally, the action also contributed to support raising public awareness. The trailer was emblazoned with JOAQUIN corporate colours in order to raise awareness of the project and the air quality problem. This took place

during several public events in each of the JOAQUIN cities, synchronized with the mobile monitoring campaigns.



Figure 1.7: Trailer of ECN used for mobile air quality monitoring and public awareness raising (in Leicester).

- **Work package 2: Measures**

The project also wanted to support decision makers to find particular key points within this adapted framework by identifying, piloting and evaluating the most efficient and cost-effective measures to reduce exposure to health-relevant air pollutants. This will lead to a ranking of measures which will assist decision makers at different levels to adapt their current policies and/or action plans.

- **Work package 3: Dissemination and communication**

Finally, the project looked to further progress the support base for policy changes by involving an extended stakeholder consultation procedure during the lifetime of the project and by raising the awareness of the general public on the adverse health effects of air pollution. The aim being to result in an enhanced relationship between the involved

policy levels, stakeholder groups and the general public on the necessity of health relevant policies and clean air in day-to-day life.

1.3.1.2 Monitoring sites and periods

In the JOAQUIN project, air quality parameters were measured in six cities in NW Europe region as follow:

- Leicester and London (United Kingdom);
- Amsterdam and Wijk aan Zee (The Netherlands);
- Antwerp (Belgium);
- Lille (France).

In each city continuous air quality measurements were carried out in long-term air quality monitoring stations. In Amsterdam, Antwerp and Leicester there were additional measurements at a second site (mobile monitoring). This resulted in a total of nine JOAQUIN air pollutants monitoring sites.

Measurements of UFPs, TNC, PNSD, BC and NO_x were carried out in Amsterdam, Antwerp, Leicester and London. Data collection started in April 2013 (Amsterdam, Antwerp), November 2013 (Leicester) and April 2014 (London).

Particulate matter (PM₁₀) was collected (daily) on filters at eight sites located in five cities (Amsterdam, Antwerp, Leicester, Lille, and Wijk ann Zee). In each city PM₁₀ was sampled in an air quality monitoring station.

PM₁₀ sampling were measured during 14 months (426 days) from 1st April 2013 to 31st May 2014, except for the site in Lille where measurements started two months later (5th June 2013 to 31st May 2014; 361 days), and Leicester where the measurements were continued until 31st May 2015(791 days). More details about the monitoring sites and periods can be found in the final JOAQUIN reports (Joaquin, 2015a, 2015b).

1.3.2 Thesis objectives

Clean air is crucial for human health and the environment. However, since the industrial revolution air quality has deteriorated considerably. Air quality has been shown to be an important environmental issue that impacts most of the world's population. Factors such as rising industrial activity and energy production, burning of fossil fuels and increases in road vehicles have all contributed to making air pollution become one of the most significant environmental problems in the densely populated and vastly industrialized NW Europe region. Compared to other European areas, the very 'economically successful' NW Europe region seems to be more exposed when it comes to air quality and its impacts, with poor air quality imposing serious effects on the human health and climate.

On top of serious human health impacts produced by air pollution, damage to the cultural heritage and ecosystems and the economic costs of poor air pollution are creating a serious problem that needs to be tackled. Mitigation strategies have been shown to be less successful than expected in recent years, with air pollutants level being measured above legal standards at over 40% of roadside air pollutant monitoring stations in 2010 in Europe (EEA, 2013). Despite recent actions to reduce particulate matter (PM) concentrations, 50% and 85% of the European population was exposed to levels exceeding the WHO guidelines for PM₁₀, and PM_{2.5}, respectively in 2014 (EEA, 2016).

The aim of this project is to tackle the problem of air quality in NW Europe areas and more specifically the issue of UFPs and air quality and health in a comprehensive and transnationally coordinated manner. This project aims to result in a long-lasting, transnational air quality infrastructure to ensure: (i) a permanent follow-up of the evolution of risks and improvements, (ii) reduced air pollution concentrations, (iii) reduced future hospital admissions, (iii) increased awareness and (iv) an up-to-date policy ensuring more effective actions can be taken on local, regional and Europe level in the future.

In the City of Leicester, 80% of nitrogen dioxides (NO₂), and most of UFPs are produced by road vehicle exhausts (DEFRA, 2011a; Hama et al., 2017b; Hama et al., 2017c). Leicester, along with many other cities in the UK, still fails to meet its European regulatory limits for urban environment air pollution (Evan, 2011). In this work, the focus is on the city of Leicester with the aim to better characterise and understand the UFPs pollutant emissions sources of this urban city. To accomplish this task, long term

campaigns (UFPs monitoring at AURN site) were performed during October 2013 to December 2015 as a part of JOAQUIN project. Comprehensive measurements of PM, eBC and gaseous pollutants were also performed, but here we will mainly focus on the submicron particle number concentrations measured by UFP and CPC monitors. In addition, three month mobile monitoring campaigns were performed to measure UFPs, and particle number size distribution (PNSD), eBC at two urban background sites within Leicester. The mobile monitoring campaigns were carried out at the AURN and BF sites to ensure the quality and comparability of the experimental data gathered in this study.

The objective of this thesis is to study the origin and sources of UFPs and their relationship with trace gases in the urban environment in Leicester and across the JOAQUIN cities. This study is the first to examine UFPs in an urban background location in the East Midlands area of the UK. The specific objectives are:

- To determine the typical concentrations of UFPs in Leicester and to identify the sources and processes that contribute to the UFPs, as well as to characterise NPF events in the Leicester urban environment.
- To quantify the contributions of primary and secondary sources to UFPs in Leicester. Particular attention is paid to the contribution of secondary sources (non-vehicle road emissions).
- To identify the sources of LDSA in Leicester, and its impact on NPF events in the urban area.
- To identify and characterise PM₁₀ chemical composition across NW Europe.

The structure of the thesis is as follow:

- Chapter 2. Methodology. In this chapter a brief description of the location of the monitoring sites as well as the experimental techniques used in this study are described.
- Chapter 3. Sub-micron particle number size distribution characteristics at two urban locations in Leicester. In this chapter, the characterisation of the NPF events and their impact on PNSD by taking measurements at two sites within the urban area of Leicester are identified. The investigation of the effect of the Easter school holiday on PNSD are also presented. The influence of traffic emissions and meteorological conditions on PNSD are also investigated.
- Chapter 4. Quantifying primary and secondary source contributions to ultrafine particles in the UK urban background. The factors responsible for the variability of the total particle number concentrations (TNC), eBC, and the gaseous pollutants at the Automatic Urban Rural Network (AURN) site in Leicester are studied. A specific focus on exploring the relative contributions of primary and secondary sources to TNC is made.
- Chapter 5. Lung deposited surface area at the Leicester urban background site is examined and the contribution of urban new particle formation to LDSA. The exploration of extra-annual cycles of LDSA in a mid-size urban environment are studied. The association of the calculated LDSA with eBC is also investigated to assess the effect of LDSA on human health.
- Chapter 6. Chemical composition and source identification of PM₁₀ in Five North Western European Cities. The comparison of chemical composition, seasonal and spatial variability, chemical characteristics of ambient PM₁₀ concentrations at four urban background sites, and one industrial site located in NW Europe, using a harmonized approach for aerosol sampling and laboratory analyses are studied. A mass closure model is applied to PM₁₀ daily samples to test whether the gravimetrically determined mass can be reconstructed by the chemically determined components at the five sampling sites.
- Chapter 7. Conclusions. The most relevant findings of this work are presented.

Chapter Two

2. Methodology

2.1 Study areas

The study areas of this project was the north-west of Europe. The NW Europe region includes Ireland, the United Kingdom, Belgium, Luxembourg, Switzerland, and parts of France, Germany and the Netherlands. It has an area of 845 000 km² and is home to 180 000 000 inhabitants. Considered as one of the most vibrant and prosperous areas of Europe, it also faces a number of environmental and air pollution challenges.

The main study area for this work was the city of Leicester. Leicester is a city which located in the East Midlands region of the UK (latitude of 52.63°, longitude of -1.13°). It situates on the River Soar and at the edge of the National Forest. In 2011, the Population of Leicester was 329,000 making it the tenth biggest city in the UK. Leicester fails to meet its European guidelines for city air pollution concentrations (Evan, 2011).

2.2 Joaquin Measurement sites

All Joaquin monitoring sites are summarised in Table 2.1. In this study long-term continuous air quality measurements were collected from a network of air quality monitoring stations. In Leicester there was additional measurements at a second site. (see Figure 2.1).



Figure 2.1: Map of the Joaquin sampling sites in NW Europe.

Table 2.1: Joaquin monitoring sites.

City	Site	Site name	Near street	Latitude	Longitude
Amsterdam	AD	Vondelpark	Overtoom	52°21'35"N	4°51'59" E
Antwerp	AP	Borgerhout	Plantin en Moretuslei	51°12'35"N	4°25'55" E
Leicester	AURN	University of Leicester	Welford and University Road	52°37'12"N	1°07'38" W
	BF		Brookfield	London Road	52°37'15"N
Lille	LL	Lille-Fives	rue du Vieux Moulin	50°37'41"N	3°05'25" E
London	LO	Eltham	Bexley Road	51°27'09"N	0°04'14" E
Wijk aan Zee	WZ	Wijk aan Zee	Burgemeester Rothestraat	52°49'40"N	4°60'23" E

2.2.1 University of Leicester Monitoring site (Leicester, UK)

2.2.1.1 AURN site

The Joaquin sampling site in Leicester is an urban background station of the Automatic Urban and Rural Network (AURN). The station was located at the University of Leicester campus (http://uk-air.defra.gov.uk/networks/site-info?uka_id=UKA00573), as shown in Figure 2.2. The nearest road is the University Road (20 m NW). The nearest main road is Welford Road (140 m SSW) with 2x1 lanes. According to traffic counts by the Department for Transport, the traffic intensity on the Welford Road was about 22 100 vehicles/day in 2016 (<http://www.dft.gov.uk/traffic-counts>, count point 36 549). The majority of the vehicles were cars and taxis (84%), followed by light goods vehicles (12.8%), heavy goods vehicles (1.11%), buses and coaches (0.93%) and motorcycles (0.9%).

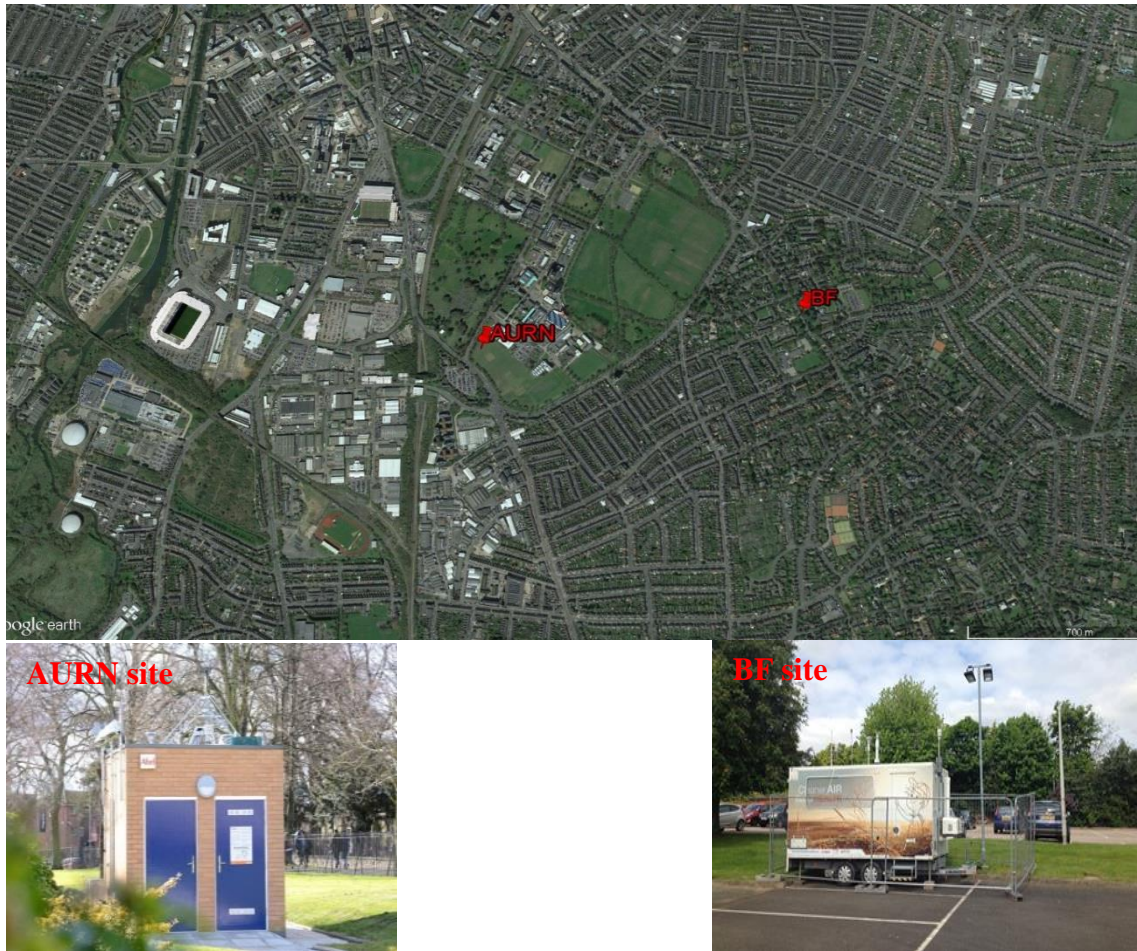


Figure 2.2: Detail of the locations of AURN and BF sites in Leicester.

By wind direction:

- N: university buildings
- E: two-storey building (sports centre)
- S: grass, Welford Road (140 m)
- W: park area.

East Midlands airport is at a distance of 27 km north-northwest of AURN site. There are also several power stations in the region:

- Ratcliffe-on-Soar power station (EON), the biggest one in the region (29 km N-NW of AURN)
- Corby power station (33 km E-SE of AURN)
- Stamford power plant (46 km E-NE of AURN)
- Spalding power station (70 miles E-NE of AURN).

2.2.1.2 Brookfield site

The temporary Joaquin site in Leicester is an urban background site in Brookfield (BF), at a distance of about 1.2 km east from AURN site (Figure 2.2). The trailer was located on a large and frequently-used parking lot (Figure 2.2). The nearest roads are Ashfield Road (90 m in the north) and Holmfield Road (90 m south). The nearest main road is London Road, at 190 m west of BF site. According to traffic counts by the Department for Transport, the traffic intensity on London Road was about 21500 vehicles/day in 2016 (<http://www.dft.gov.uk/traffic-counts>, count point 56147). The majority of the vehicles were cars and taxis (88.7%), followed by light goods vehicles (8.4%), buses and coaches (1.5%), heavy goods vehicles (0.94%) and motorcycles (0.4%).

By wind direction:

- N: residences, Ashfield Road at 90 m
- E: residential gardens
- S: Holmfield Road at 90 m
- W: London Road at 190 m.

2.2.2 Vondelpark Monitoring site (AD, Amsterdam, the Netherlands)

The Joaquin sampling site in Amsterdam is an urban background station of the air quality monitoring network of GGD Amsterdam, located at the northern edge of the public park Vondelpark (Figure 2.3). Website information: <http://www.luchtmetingen.amsterdam.nl/DetailPage.aspx?SID=014>. At a distance of 64 m to the north there is a main road (Overtoom) with a mean traffic intensity of about 17 000 vehicles/day (<http://www.verkeersprognoses.amsterdam.nl> for 2015). The Overtoom road has two lanes, one in each direction plus two bus/tram lanes in the centre of the road and has relatively high buildings on both sides resulting in a ‘street canyon’ effect. Between the site and the Overtoom there is a six-storey building. A small passage connects the Overtoom with the site. The measuring station is located in the courtyard of a revalidation centre. The site is close to tennis courts and a public park (in the south). The gravel tennis court can be a source of coarse dust particles. In the Vondelpark, barbecue activities are allowed at specific locations, except during dry periods.



Figure 2.3: Detail of the location of AD site in Amsterdam.

By wind direction:

- N: main road (Overtoom at 64 m)
- E: private parking and green area
- S: tennis court and public park (Vondelpark)
- W: six-storey building

The harbour of Amsterdam is located north-northwest of AD. Typical activities in the harbour are road and shipping traffic, storage and transshipment of petrochemical products, ore and coal. In the harbour, there is a coal-fuelled electricity plant (Hemwegcentrale) 5.2 km north of AD. Schiphol airport is located about 8.7 km southwest of AD.

2.2.3 Borgerhout Monitoring site (AP, Antwerp, Belgium)

The Joaquin sampling site in Antwerp is an urban background station that is part of the VMM air quality monitoring network. The station is located in Borgerhout (VMM station code 42R801). Website information:

<http://luchtkwaliteit.vmm.be/details.php?station=42R801>. Site AP is located 30 m from

a major access road (Plantin en Moretuslei) (Figure 2.4). The station is set on a terrain of a primary school, next to the playground. The Plantin en Moretuslei connects the inner city with a major highway eastwards (E313). The road is east-west orientated and has four lanes (two in each direction). There is a bus stop in front of the entrance to AP.



Figure 2.4: Detail of the location of AP site in Antwerp.

In February 2010, daily traffic volume on the Plantin en Moretuslei was 37000 vehicles on weekdays and 25000 vehicles in the weekend ((Mishra et al., 2012); based on video counting), or a time-weighted average of 33500 vehicles/ day. The reported fraction of heavy duty vehicles was 7% (week) and 3% (weekend) (Mishra et al., 2012). In February and October 2013, the mean traffic intensity was 32000 vehicles on week days and 23500 vehicles in the weekend (VMM, 2014; based on counting loops), or a time-weighted average of 29500 vehicles/day.

By wind direction:

- N: school area (grass and trees)
- E: first a small parking area, then a 6-storey office, then a smaller street
- S: main road (Plantin and Moretuslei) with a bus stop in front of the entrance to the station
- W: playground of the school (pavement and artificial grass mat).

At the regional scale, a potential source of air pollution is the harbour of Antwerp (N-NW, >4 km distance), with power plants and important (petro) chemical and other industrial activities. In the SW direction at about 8 km from the station, there is an industrial site (Umicore) with metal processing (e.g. As, Cd, and Pb).

Antwerp airport is located 3 km SE of site AP. In 2014 there were about 44000 flight movements (= departures and arrivals) at this airport (http://www.antwerp-airport.be/contentpage_en.php).

2.2.4 Lille-Fives Monitoring site (LL, Lille, France)

The Joaquin sampling site in Lille is an urban background site that is part of the air quality monitoring network of atmo Nord-Pas-de-Calais. The station is located in Lille-Fives (Figure 2.5). Website information: <http://www.atmo-npdc.fr/mesures-et-previsions/mesures-en-direct/carte-d-identite-des-stations.html>. Site LL is set on the campus of a school (Groupe Scolaire Lakanal). The nearest road is at 35 m (rue du Vieux Moulin). This is a local street with 2x1 lanes that is located east, south-east and south of the site. No traffic data is available for this street.



Figure 2.5: Detail of the location of LL site in Lille.

By wind direction:

- N and E: one-storey building
- E, SE and S: nearest street
- S and W: grass.

Site LL is located ~230 m from a large number of railroads.

Power plants:

- Centrale thermique du Mont de Terre-Resonor (~750 m S)
- Chaufferie de Lille-Hellemmes (~1.5 km E)
- Chaufferie des Beaux-Arts (~1.9 km W)
- Mons Energie (~2.7 km NW).
-

The Centrale thermique du Mont de Terre-Resonor is a power plant that uses gas and, from time to time, also coal. In 2013 no wood has been used as fuel, there is no declaration for wood burning.

Other industrial sites are:

- Brasserie Heineken de Mons / G Goossens (~ 3 km NE): brewery
- H2D (~1.1 km E-SE): "surface treatment, mechanics"
- Haghebaert et Fremaux (~2.5 km E-SE): chemicals
- Technicentre SNCF D'Hellemmes (~1.3 km SE), main activity: surface treatment, mechanics
- ECL - Electrification Charpente Levage (~2.3 km S)
- LFB Biomédicaments (~1.1 km SW).

2.2.5 Wijk aan Zee Monitoring site (WZ, the Netherlands)

The Joaquin sampling site in Wijk aan Zee is an industrial monitoring site of Province North Holland. Site WZ is located approximately 30 km west from Amsterdam (Figure 2.6). Website information: <http://www.luchtmetingen.noord-holland.nl/DetailPage.aspx?SID=553>. Site WZ is located at the north side of a parking lot used by visitors of a camping site (Banjaert). Residences of Wijk aan Zee inhabitants are present at a distance of approximately 40 m. The nearest road (Burgemeester

Rothestraat) is at a distance of 70-80 m to the south and west. The nearest main road (Verlengde Voorstraat) is at 175 m.



Figure 2.6: Detail of the location of WZ site in Wijk aan Zee.

By wind direction:

- N and E: camping area (Banjaert);
- S and W: parking lot and residences (40 m), local road (70-80 m).

The industrial zone of IJmond is located east (750 m) and south (1-2 km) of site WZ. The main activities in the industrial zone are the production of steel (Tata Steel, south of WZ) and energy (NUON).

2.3 Instrumentation

This section describes the main instruments used in this study for measuring particle number concentration, size distribution, lung deposited surface area (LDSA), equivalent black carbon (eBC), Nitrogen oxides (NO-NO₂-NO_x), and PM₁₀.

2.3.1 Ultrafine particle instruments

Increasing our understanding of the physical and chemical properties of ultrafine particles in ambient air is vital for properly assessing their impacts on various problems such as human health, air quality and global climate, and ultimately establishing effective control strategies. However, the identities and concentrations of many ultrafine atmospheric species, particularly organic components, are still unknown. To characterise the chemical composition of aerosols in the atmosphere, a complementary collection of different analytical methodologies is typically used. Numerous factors need to be taken into consideration when instruments are being developed for the measurements of UFPs. Further consideration might include the weight and portability of the developed instrumentation. The physical and chemical measurements of UFPs in the atmosphere have been recently reviewed in a number of publications (Hama et al., 2017cc; Hofman et al., 2016; Kumar et al., 2014). This section discusses instrumentation in the field of atmospheric aerosols measurements with a particular focus on measurements of ultrafine particles in ambient air within Joaquin project across north-west Europe. A summary of the UFP instruments used in this study at the monitoring sites are tabulated in Table 2.2.

Table 2.2: Summarises relevant specifications of the ultrafine particle monitors used in this study.

	EPC	UFPM	SMPS	NSAM
	TSI 3783	TSI 3031	Grimm5420/ L-DMA	TSI 3550
Size range				
Lower size (nm)	7	20	10	10
Upper size (nm)	1000	~800 with TSI 3031200 system	1084	1000 (by cyclone)
Size classes				
Number	1	6	45	1
Range per class	7 nm - < 3 µm	20-30, 30-50, 50-70, 70-100, 100-200, >200 nm		Alveolar
Accuracy (according to manufacturer)	±10% at 10 ⁶ particles/cm ³	Not given	Not given Systematic error of CPC is <5%	± 20% for 20-200 nm range
Sample time	1 min	10 min	10 min	1 min
Inlet flow rate (L/min)	3.0	5.0	0.3	2.5
Sample flow rate (L/min)	0.12	4.0	0.3	1.5
Radioactive source	-	-	⁸⁵ Kr (185 MBq)	-
Working fluid	Water	-	Butanol	-

2.3.1.1 SMPS (Grimm 5420/L-DMA)

The particle number size distributions were measured by a scanning mobility particle sizer spectrometer (Grimm SMPS+C 5420 with L-DMA, see Figure 2.7) in Amsterdam and Antwerp (AD, AP) and in the trailer. An SMPS is actually a cylindrical capacitor: two flows enter the differential mobility analyser (DMA), the particle-free sheath air and the aerosol flow containing charged particles. By knowing the dimensions of the DMA, one can calculate the voltage between the electrodes to transport particles with a certain electrical mobility to a small slit in the centre rod of the capacitor. A flow carrying particles with nearly the same electrical mobility is then sucked through this small slit. The number concentration of this sample aerosol (particles with the same electrical mobility) is finally counted in a CPC (Figure 2.7).

The main components of the Grimm SMPS are:

- Neutralizer: ^{85}Kr source, 185 MBq, obtained from Eckert & Ziegler (Grimm normally uses ^{241}Am);
- DMA: Vienna type L-DMA (~50 cm long), with up to 255 size channels per scan;
- CPC: butanol-based condensation particle counter.

The flow rate of the CPC is 0.3 L/min. To measure a 10-1100 nm range, the sheath air flow rate is 3 L/min. A complete particle sizing scan for 32 channels can be done in 5 min. In the Joaquin project a scan time of 10 min was used to measure the particle concentration in 45 size classes by stepping the voltage downwards. The software corrects for internal diffusion losses and multiple charging (Wiedensohler, 1988). For comparability between data sets, the ambient aerosol is kept at low relative humidity (RH) by a Nafion dryer in the inlet system (see section 2.3.3 for more information on the sampling and drying systems). However such a drying system leads also to extra losses of the smallest particles (starting at sizes of below approximately 70 nm). Although in JOAQUIN project these losses were calculated and corrected for, the losses might have been higher, as can be derived from field tests (Joaquin, 2015a; Wiedensohler et al., 2012).

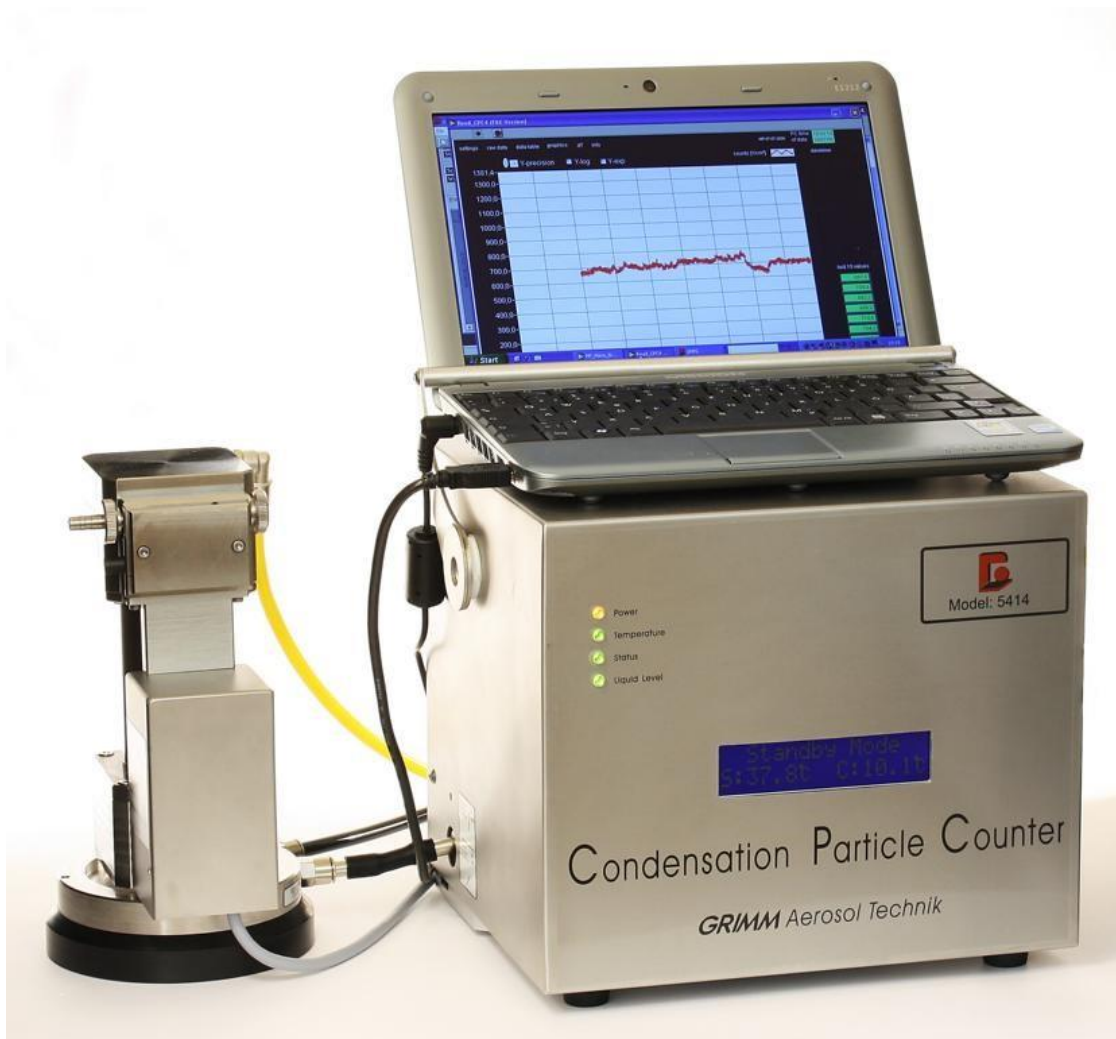


Figure 2.7: Grimm SMPS+C 5420 with L-DMA.

2.3.1.2 EPC (TSI 3783)

The total particle number concentration (N_{TOTAL}) was measured by a Water-Based Condensation Particle Counter (W-CPC, TSI Environmental Particle Counter (EPC) model 3783 (see Figure 2.8), <http://www.tsi.com/environmental-particle-counter-3783>) in Amsterdam, Antwerp, Leicester and in the mobile trailer.



Figure 2.8: Model 3783 Environmental Particle Counter.

Its operation principle is illustrated in Figure 2.9. The aerosol sample is pulled through a conditioner that is saturated with water vapour and then passes to a warmer growth section with thermodynamic ‘supersaturation’ conditions. As a result, the small particles act as condensation nuclei and grow into micron size droplets, which are detected individually by a light pulse when passing through a laser beam. As the EPC uses water as condensation liquid, this mode of operation differs slightly from the more common butanol-based CPCs. When an alcohol is used as condensation liquid, after the conditioning phase particles pass through a condenser region (10°C). In a water-based CPC, in contrast, after conditioning the particles pass through a warmer “growth tube” (60°C). The EPC can be used with a high-flow (3 L/min) or low-flow (0.6 L/min) inlet. The aerosol flow rate is 0.12 L/min. Based on the initial tests, we used the high-flow mode to minimize particle losses during the sampling. The response time (95%) is < 3 s (high-flow) or <5 s (low-flow). The averaging interval can be set from 1 to 60 s. Most partners recorded the particle number at 1-min resolution.

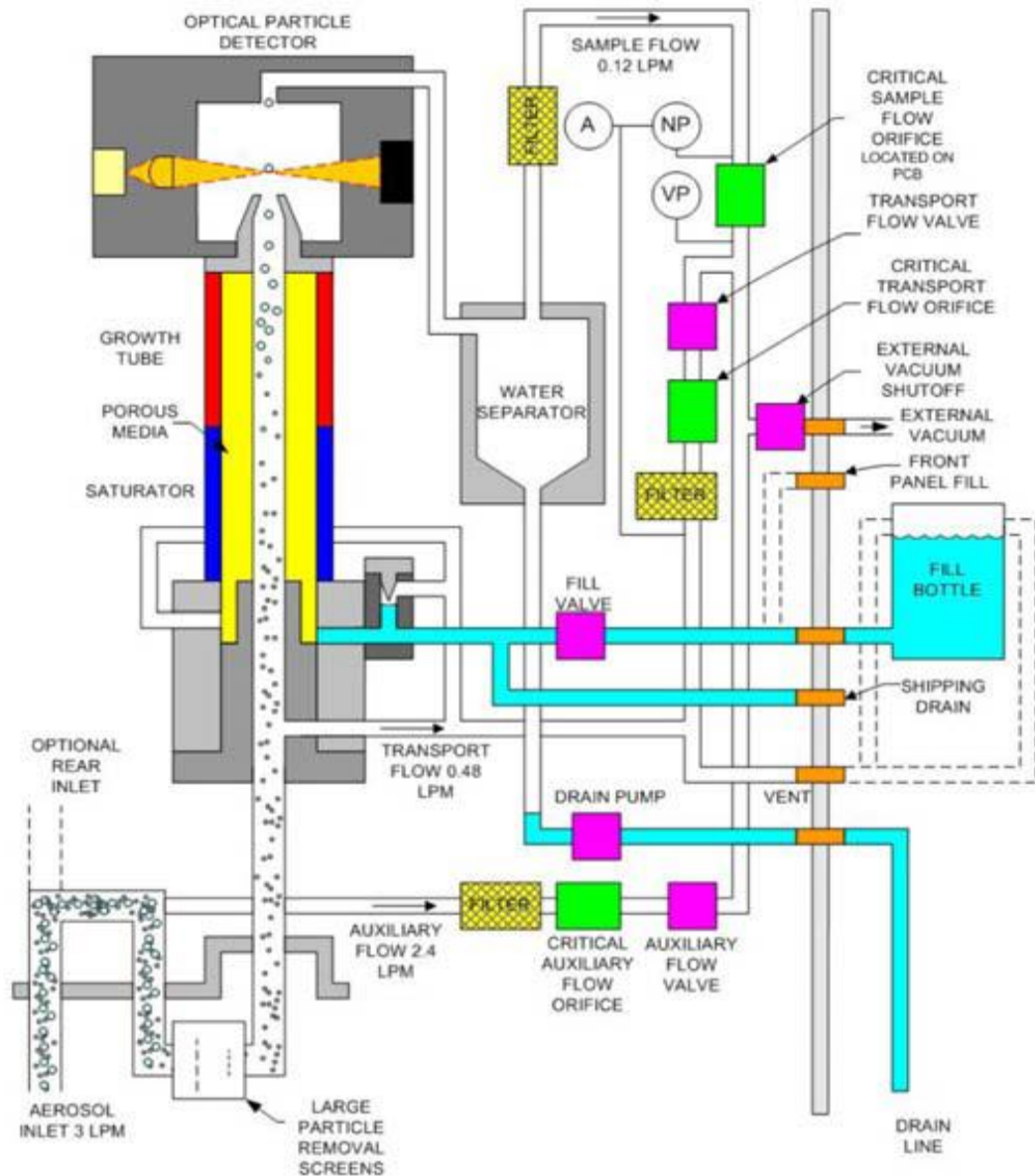


Figure 2.9: Model 3783 Environmental Particle Counter™ Monitor Flow System Schematic

2.3.1.3 UFPM (TSI 3031)

The particle number size distribution was measured by UFP monitor TSI model 3031 (Figure 2.10) in Leicester and in the trailer.



Figure 2.10: Model 3031 Ultrafine Particle Monitor

The operational principle is based on diffusion charging of particles, followed by size segregation within a differential mobility analyser (DMA) and detection of the aerosol via a sensitive electrometer. A typical field setup in a monitoring station is shown in Figure 2.11. The flow schematic is shown in Figure 2.12. An aerosol sample is drawn into the instrument continuously at a rate of 5.0 L/min. Within the instrument, the aerosol sample mixes in an equalization tank to smooth out short-term fluctuations in the aerosol sample and then passes on to the diffusion charger, a "Corona-Jet" charger. The TSI 3031 UFPM needs no working fluid or radioactive source (Joaquin, 2015a).

The main components of the UFP monitor are:

- **Diffusion Charger**

The charging device in the UFP is a "Corona-Jet" charger (Medved et al., 2000; Stommel and Riebel, 2004). Inside the charger, the total flow of 5.0 L/min is divided into 1.0 L/min

passing through two filters (a HEPA and a carbon) and an ioniser and 4.0 L/min of aerosol residual as air sample flow. The flow streams are combined in a mixing chamber where particles in the sample aerosol flow mix with the ions carried by the filtered air. This patented counter-flow diffusion charging transports the air particles into a well-defined, charged state. The separation of aerosol particles makes the charging method more effective and reproducible. The charged aerosol samples then transfer onto the DMA for size separation.

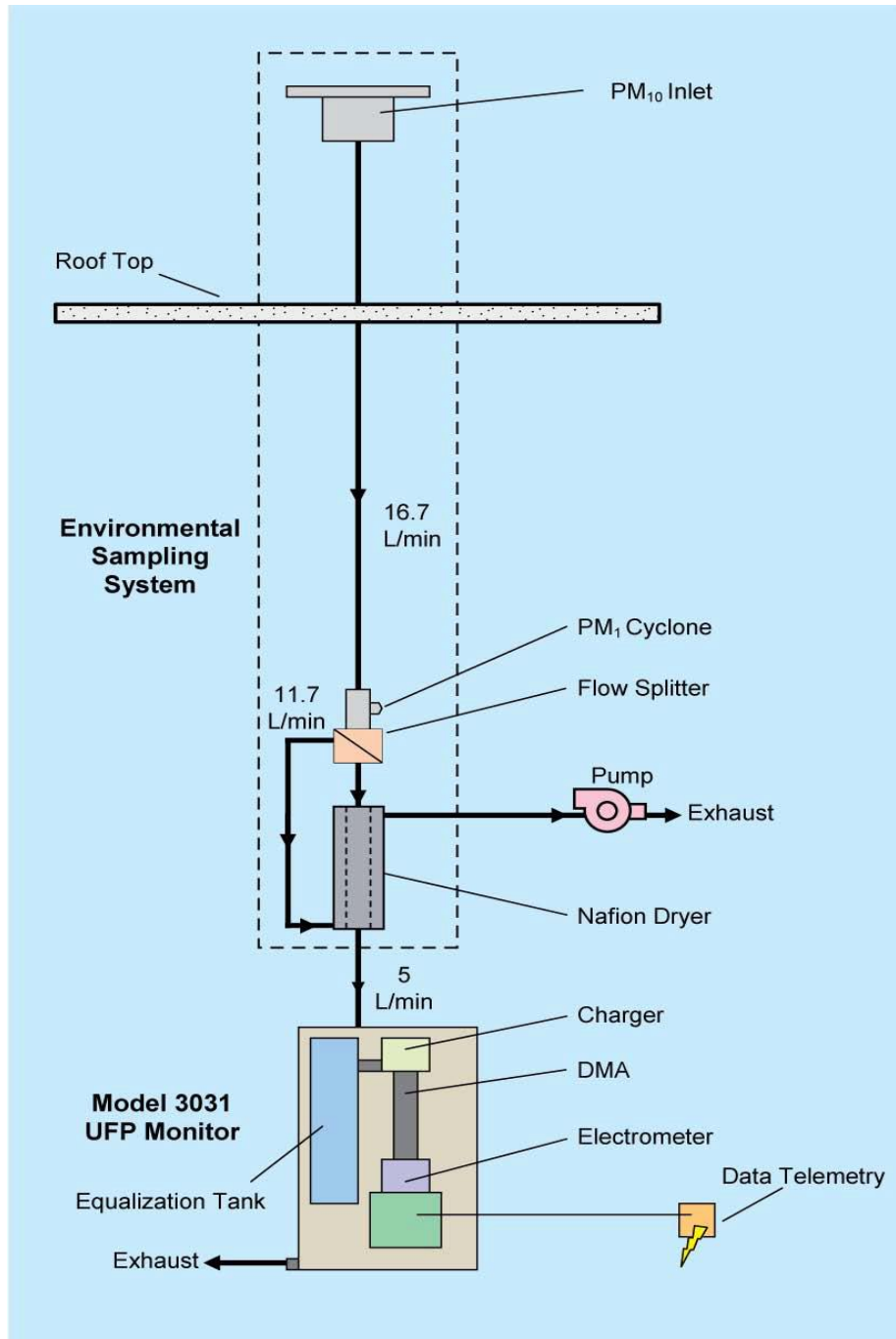


Figure 2.11: Typical Field Operation of UFP monitor TSI 3031.

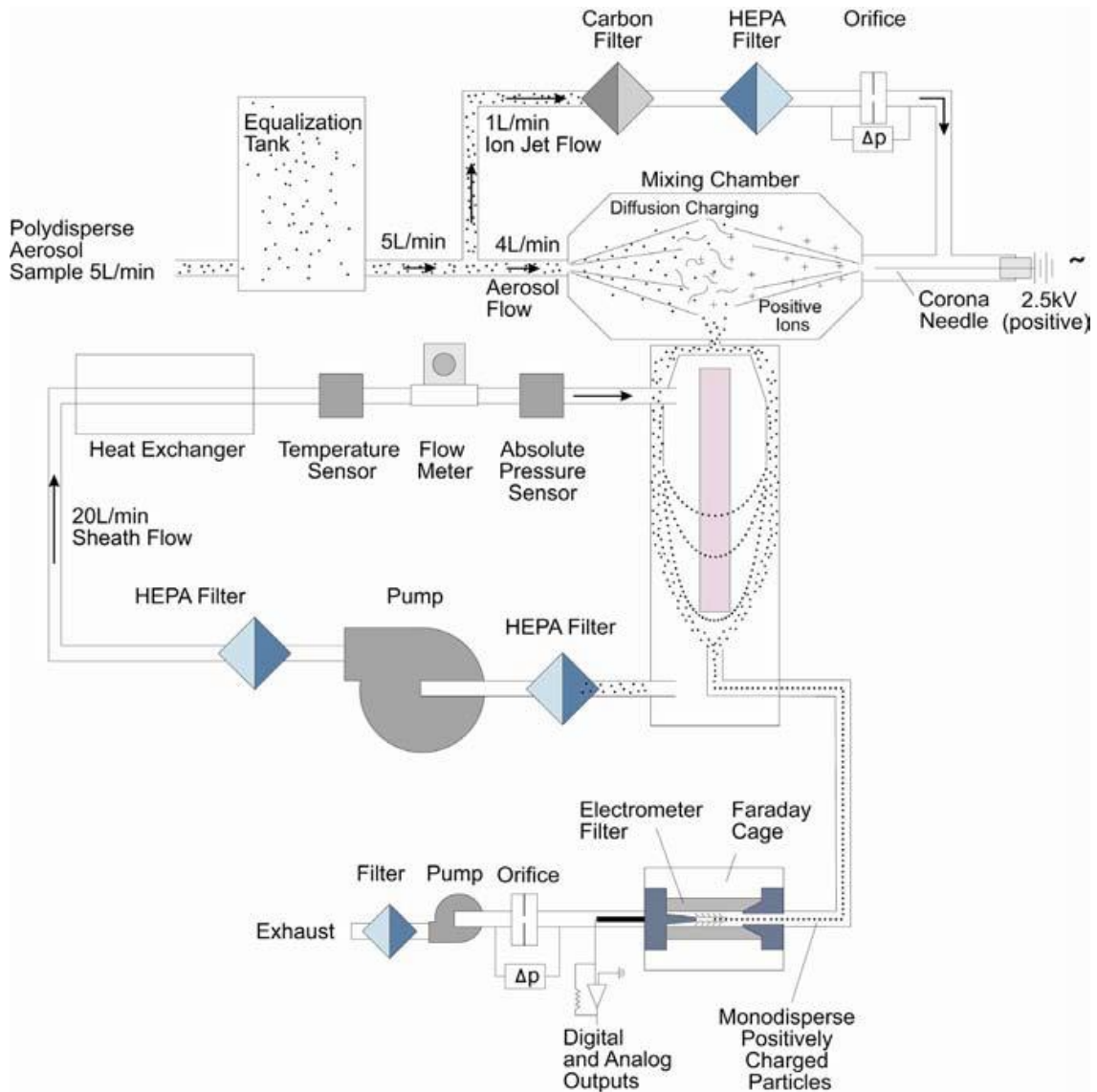


Figure 2.12: Flow schematic of UFP monitor TSI 3031.

- **Differential Mobility Analyser**

The DMA (Figure 2.13) consists of a hollow, earthed cylinder, and an outer cylinder and the inner high voltage cylindrical rod. The polydisperse aerosol (contains more than one size of particles) and sheath air are introduced at the top of the DMA column and flow down the annular space between two cylinders. The aerosol sample circles the internal core of sheath air, and both flows pass down the annulus with no mixing of the two laminar flows. The internal cylinder, the collector rod, is kept at a negative voltage, while the external cylinder is electrically grounded. This generates an electric field between the two cylinders. The electric field creates positively charged aerosol particles to be

involved through the sheath air to the negatively charged collector bar. Aerosol particles are collected on the collector rod (see Figure 2.13). The position of the precipitating particles depends on the particle electrical movement, the DMA flow rate, and the DMA geometry. Particles with a high electrical mobility are collected along the upper part of the rod; particles with a low electrical mobility are precipitated on the lower part of the rod. Particles inside a narrow range of electrical mobility exit with the monodisperse air stream through a small slit situated at the bottom of the rod. These particles are moved to the electrometer to determine the concentration of particles. The remaining particles are removed from the sheath flow with a high efficiency filter which is moved to the top of the column as a re-circulating flow.

- **Electrometer**

After departure the DMA, the aerosol arrives at a faraday cage where the particles, and their charge, are collected on the particle filter. The filter is conductive, and is electrically joined to the input of a sensitive electrometer amplifier. By successively stepping the DMA voltage and measuring the current at each step with the electrometer, an on-board computer determines and reports the number concentration of particles for each of the six size bins. One measurement cycle takes 10 minutes (approximately) with an extra 1 minute zeroing time between measurement cycles.

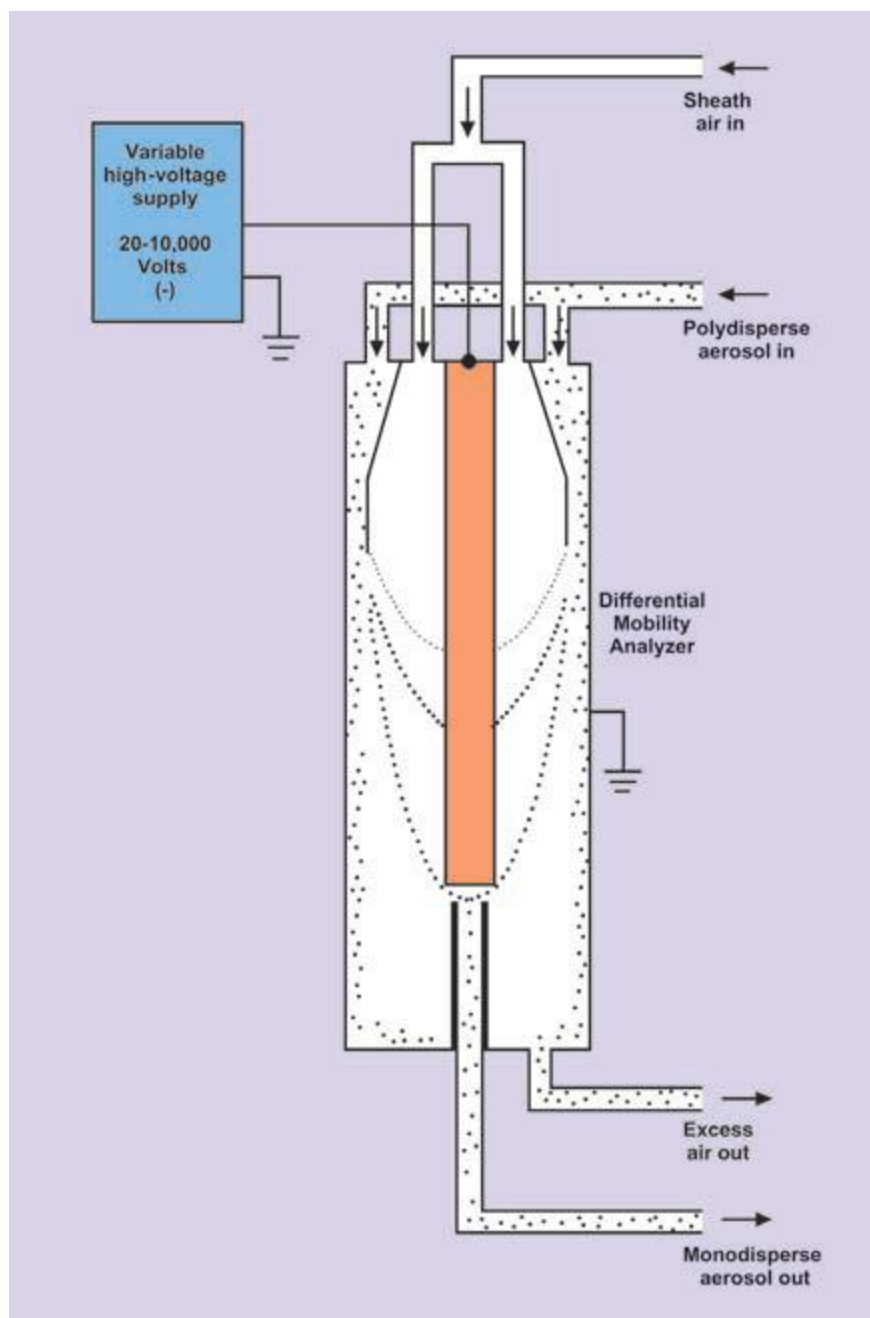


Figure 2.13: Flow Schematic of the Differential Mobility Analyser (DMA).

2.3.2 NSAM (TSI 3550)

In the AURN station in Leicester, lung deposited surface area (LDSA) was measured by a Nanoparticle Surface Area Monitors (NSAM, TSI model 3550, Figure 2.14) originally developed by Fissan et al. (2007). The NSAM operational principle is based on diffusion charging of particles, followed by detection of the charged aerosol using an electrometer (Figure 2.15). The instrument can be switched between sampling for the tracheobronchial

(TB) and alveolar (A) fractions of the total aerosol by changing the ion trap voltage. The ion trap essentially acts as a size-selective sampler for the electrometer. The inlet flow rate is 2.5 L/min, of which 1.5 L/min is used as aerosol flow rate. The NSAM does not measure the total surface area of airborne particles. The instrument was designed to report the surface area of particles (reported as $\mu\text{m}^2/\text{cm}^3$) deposited in the tracheobronchial (TB) or alveolar (A) regions of the lung. The calculations are made for a reference worker as predicted by human lung deposition models published by the International Commission on Radiological Protection (ICRP, 1994) (Figure 2.16). In Leicester the NSAM was set to measure the alveolar LDSA at a 1-min time resolution. The NSAM detects particles ranging in size from 20 to 1000 nm, however, it measures only up to 400 nm with high precision (Asbach et al., 2009). According to Asbach et al. (2009), particle hygroscopicity may cause the lung deposition curves to change significantly, a factor which is not taken into account by this monitor



Figure 2.14: Nanoparticle surface area monitor TSI 3550.

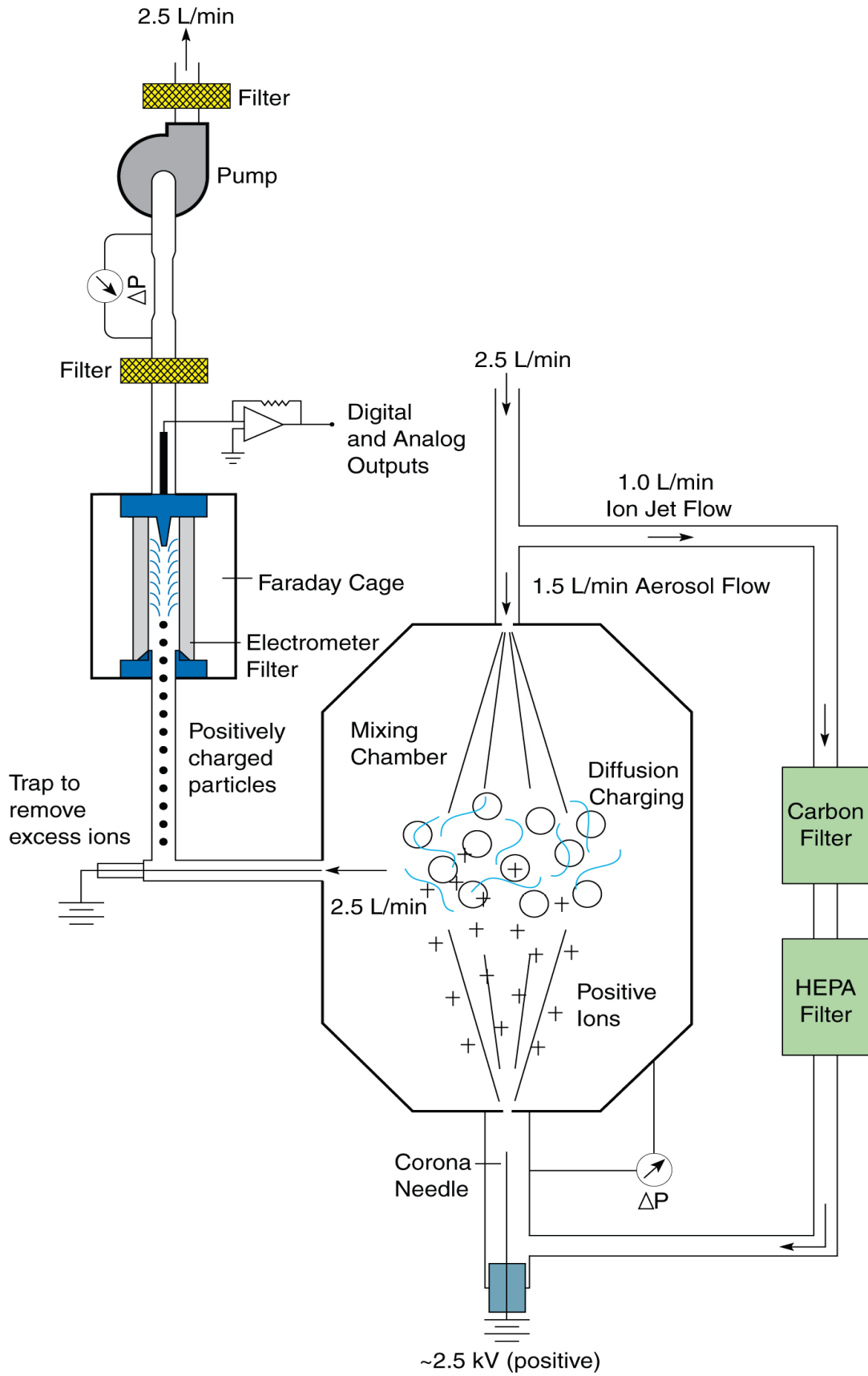


Figure 2.15: Flow schematic of NSAM TSI 3550.

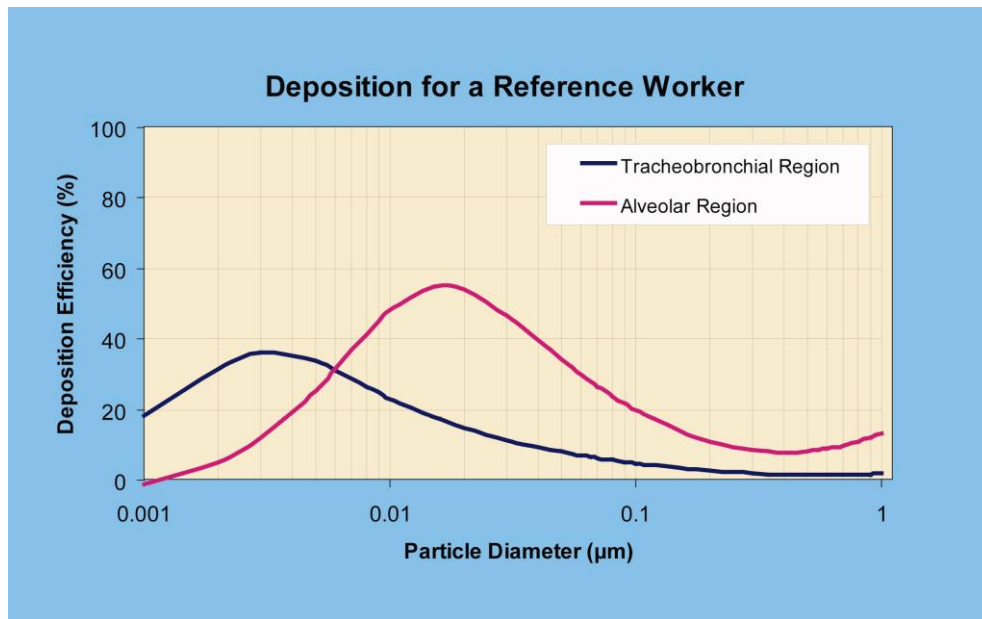


Figure 2.16: Curves for tracheobronchial and alveolar lung deposition for a reference worker.

2.3.3 Sampling systems

The TSI monitors (W-CPC, UFP and NSAM) were connected to an Environmental Sampling System (TSI 3031200; Figure 2.17) to provide the monitor with dry ambient aerosol. It consists of a standard PM₁₀ inlet and a sharp-cut PM₁ cyclone to remove large particles that may contaminate the monitor. Essential is also the Nafion dryer (reduces humidity to less than 50% RH), which conditions the sample to lower RH to avoid humidity effects on the particle size and behaviour. It has also a disadvantage: it removes a certain amount of nano-sized particles due to diffusion losses in the PermaPure system. In recent studies by ECN and other organizations dealing with UFP number measurements losses up to 40% were noted (unpublished results). Further research is necessary to assess the implications. The recommended flow rate is 16.7 L/min at the PM₁₀ inlet and up to 5 L/min sampling flow. According to TSI, the particle transmission efficiency (with the given flow rates) is 82% at 25 nm, 87% at 40 nm, 93% at 60 nm, 97% at 150 nm and 100% at 300 nm.

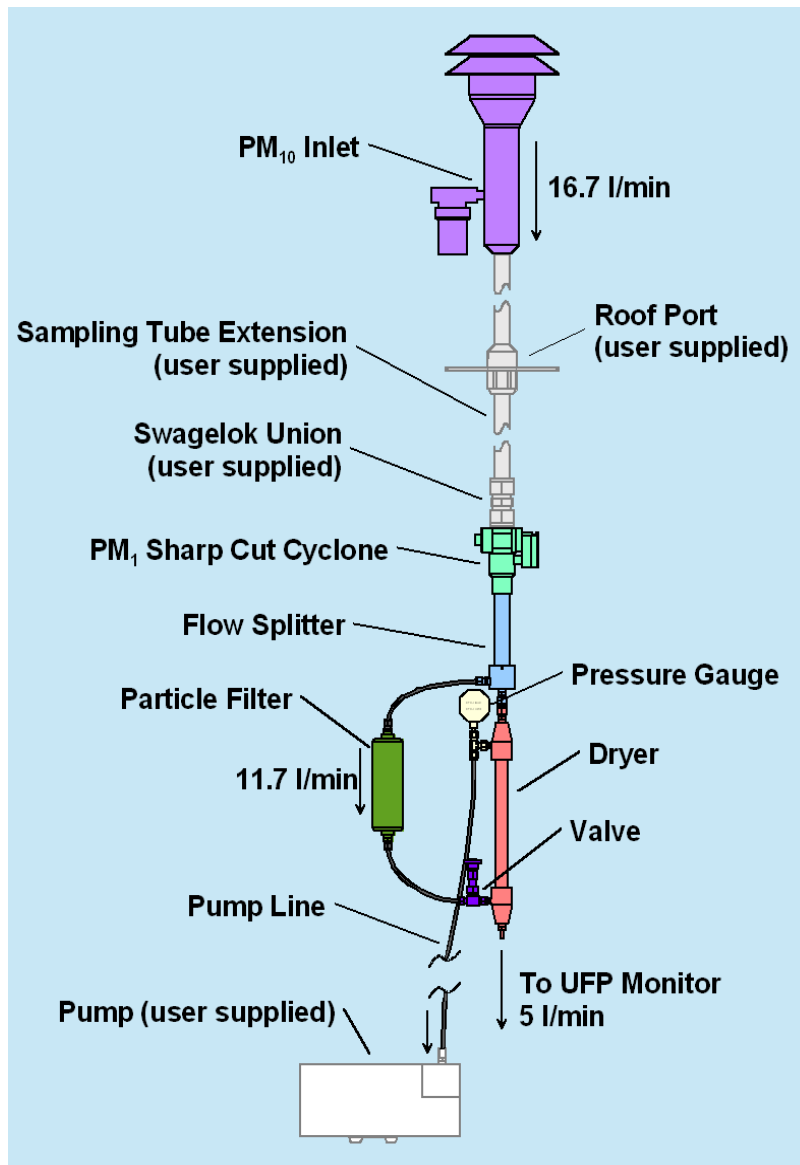


Figure 2.17: Schematic of the Environmental Sampling System (TSI 3031200),

2.3.4 MAAP (Thermo Scientific 5012)

The equivalent black carbon (eBC) mass concentration was measured with a multiangle absorption photometer (MAAP Thermo Scientific model 5012; Figure 2.18) (Petzold et al., 2013). The MAAP determines the eBC content of aerosols by simultaneous measurement of optical absorption and scattering of light by the particles collected on the filter tape (glass fibre type GF10). Within the detection chamber a 670 nm visible light source is aimed towards the deposited aerosol and filter tape matrix (Figure 2.19). The light transmitted into the forward hemisphere and reflected into the back hemisphere is measured by a series of photo-detectors. During sample accumulation the light beam is

attenuated from an initial reference reading from a clean filter spot. More information on the principle of the MAAP is given by Petzold et al. (2002). The following equations are used by the MAAP instrument to calculate black carbon mass loading:

$$MBC = \frac{(1 - \omega_0) * X1 * Area}{\sigma_{BC}} \dots \dots \dots (2.1)$$

where MBC is the mass of black carbon deposited on the filter, ω_0 is the single scattering albedo, X1 is the ln (transmittance), AREA is the area of the dust collection spot (2.0 cm²), and σ_{BC} is the scattering cross section of black carbon (6.6m²/g).

$$CBC = \frac{\Delta MBC}{Vol} \dots \dots \dots (2.2)$$

where CBC is the concentration of black carbon (mass per unit volume of air), ΔMBC is the variance of MBC, and Vol is the volume of air sampled.

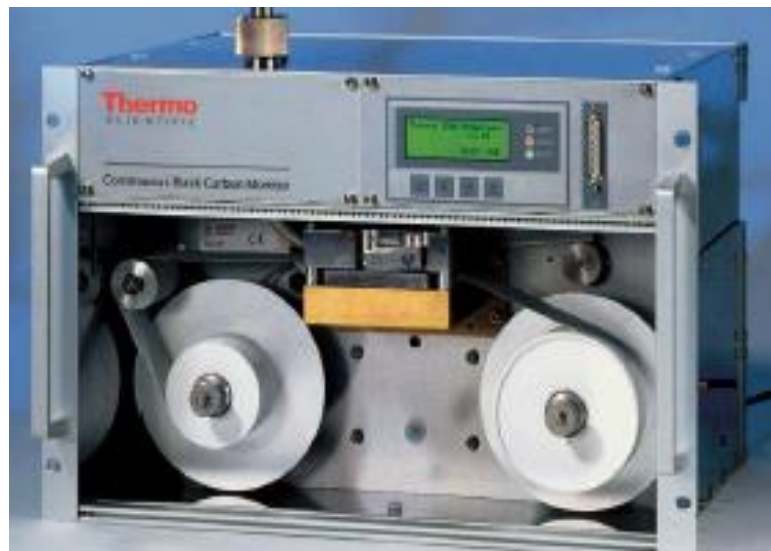


Figure 2.18: MAAP Thermo Scientific 5012.

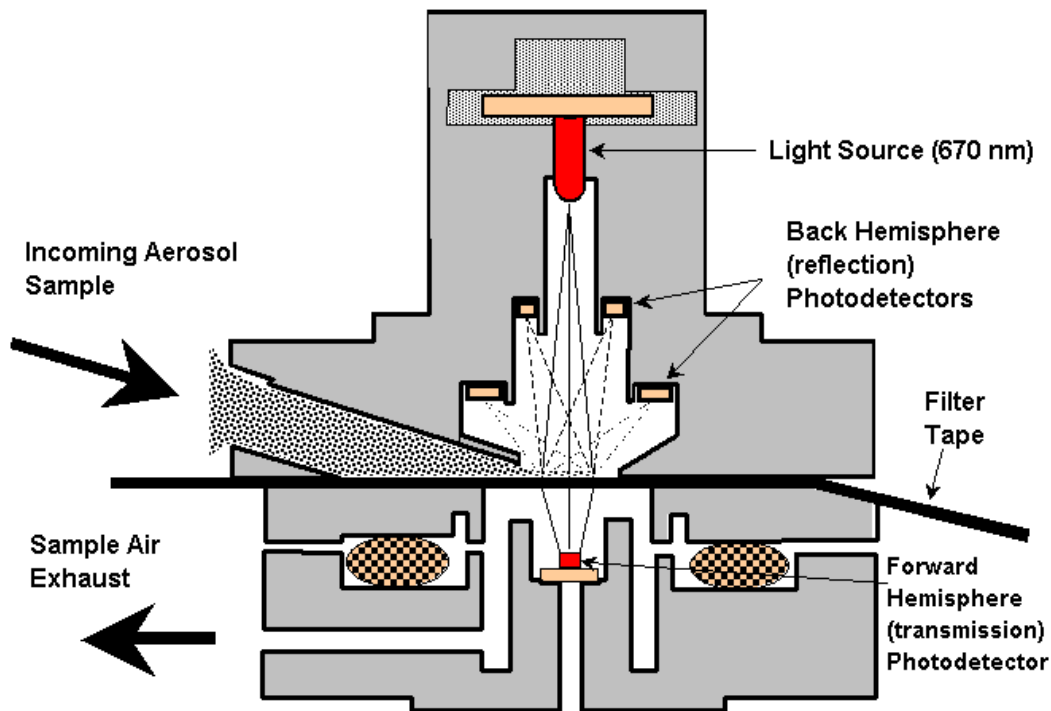
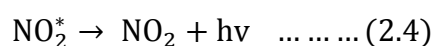
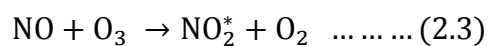


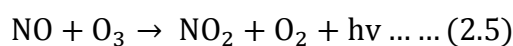
Figure 2.19: Principle of operation the MAAP Monitoring Instrument.

2.3.5 NO_x monitors

Nitrogen oxides were also measured by a Thermo 42i NO-NO₂-NO_x monitor (Figure 2.20). This monitor uses chemiluminescence technology to measure the concentration of nitrogen oxides in the ambient air. It operates that nitric oxide (NO) and ozone (O₃) react to produce a characteristic luminescence with an intensity linearly proportional to the NO concentrations. This reaction occurs in two steps: first, one molecule of NO and one molecule of O₃ react to produce O₂ and excited nitrogen dioxide (NO₂^{*}). Infrared light emission results when electronically excited NO₂^{*} molecules decay to lower energy states.



The net reaction is:



NO₂ must first be converted into NO before it can be measured using the chemiluminescent reaction. NO₂ is transformed to NO by a molybdenum NO₂-to-NO converter heated to 325°C (the stainless steel converter is heated to about 625°C). The air sample is drawn into the NO_x monitor through the sample bulkhead, as shown in Figure 2.21. The air sample flows through a tube, and then to the mode solenoid valve. The solenoid valve passes the air sample either straight to the chamber (NO mode) or through the NO₂ to NO converter and then to the chamber (NO_x mode). A flow sensor to the reaction chamber measures the air sample stream. Dry air arrives the monitor through the dry air bulkhead, passes through a flow switch, and then through a discharge ozonator. The ozonator produces the ozone required for the chemiluminescent reaction. At the chamber, the ozone reacts with the NO in the air sample to form excited NO₂ molecules. A photomultiplier tube (PMT) contained in a thermoelectric cooler detects the luminescence produced during this chemical reaction. From the chamber, the exhaust travels through the ozone converter to the pump, and is released through the vent. The concentrations of NO and NO_x calculated from the NO and NO_x modes, and they are stored in memory. The variance between the concentrations of the NO and NO_x is used to determine the NO₂ concentration.

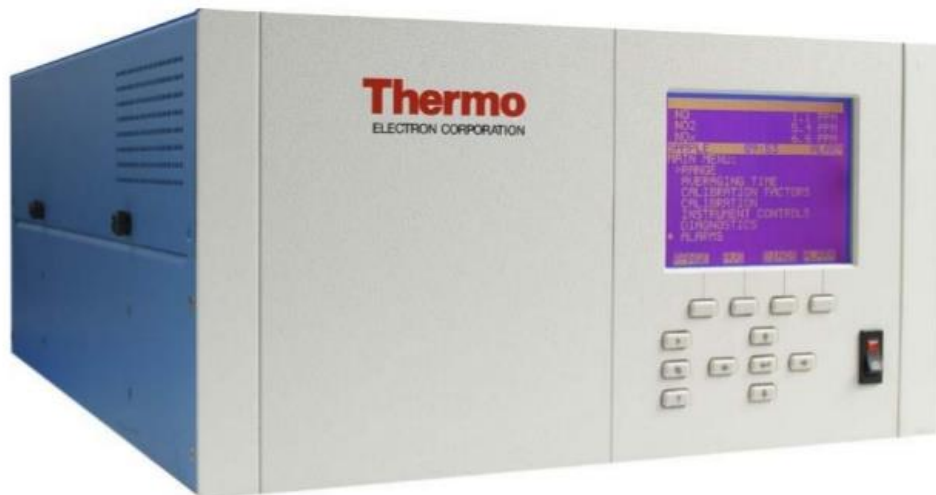


Figure 2.20: Model 42i NO-NO₂-NO_x monitor.

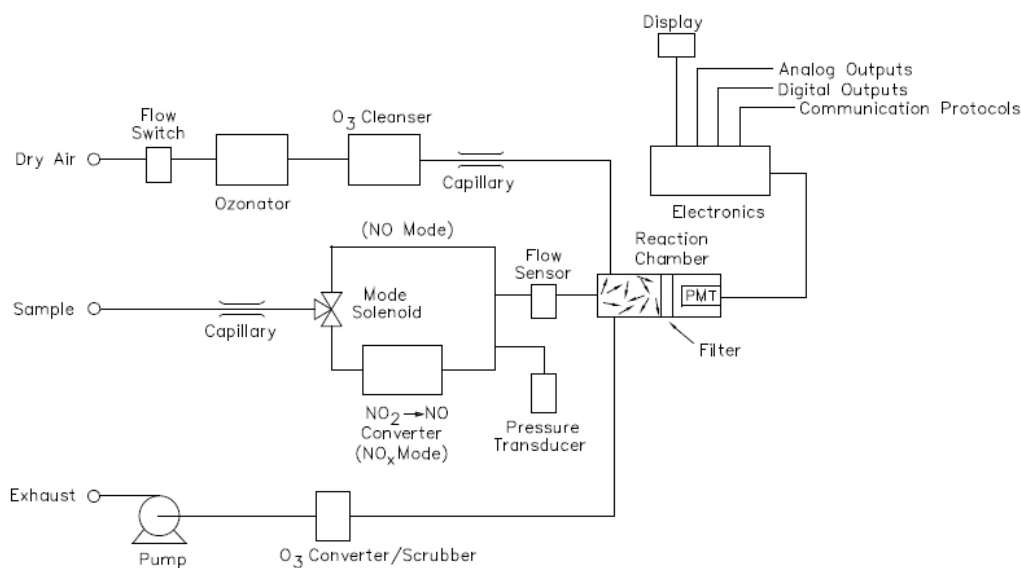


Figure 2.21: Model 42i Flow Schematic.

2.3.6 PM₁₀ sampler

PM₁₀ was sampled on filters with two types of low-volume samplers with PM₁₀ inlet: Leckel SEQ 47/50 (Germany) and Derenda PNS16 (Comde-Derenda GmbH, Germany), except for site LL where initially a third type of sampler was used. At sites AP, LE and LL, a sequential Leckel sampler with cooling device (<23°C) (Leckel SEQ47/50 CD) was used (Figure 2.22). At LL, initially a sequential PM162 sampler (Environment, France) was used, but this device was replaced because of too frequent sampling problems leading to unusable filters. At the sites AD and WZ cooled sequential Derenda PNS16 samplers were used. In the trailer, a non-cooled Leckel SEQ47/50 was used, but since it was installed inside the trailer it was also in a temperature-controlled environment. All these instruments gravimetrically sample PM₁₀ during 24h periods according to the reference method EN12341. In both samplers the exposed filters were automatically changed to non-sampled ones at midnight. The sampling methodology is summarized in Table 2.3. More information about the gravimetric analysis and filter punching can be found in the final Joaquin report (Joaquin, 2015b). The size classification inlet followed the designing criteria of the EN 12341 and is shown in Figure 2.23. By switching the jets inside, the inlet can be used for PM₁₀ and PM_{2.5} measurements. The sampler is equipped with a heater to keep the temperature above the dew point to avoid sample filters from freezing in low temperature in winter. In addition, cooled sample tube

by sheath flow and enclosed sample filters within the filter cartridge prevent the volatilization of semi-volatilized compounds such as nitrate, sulphate, and ammonia.

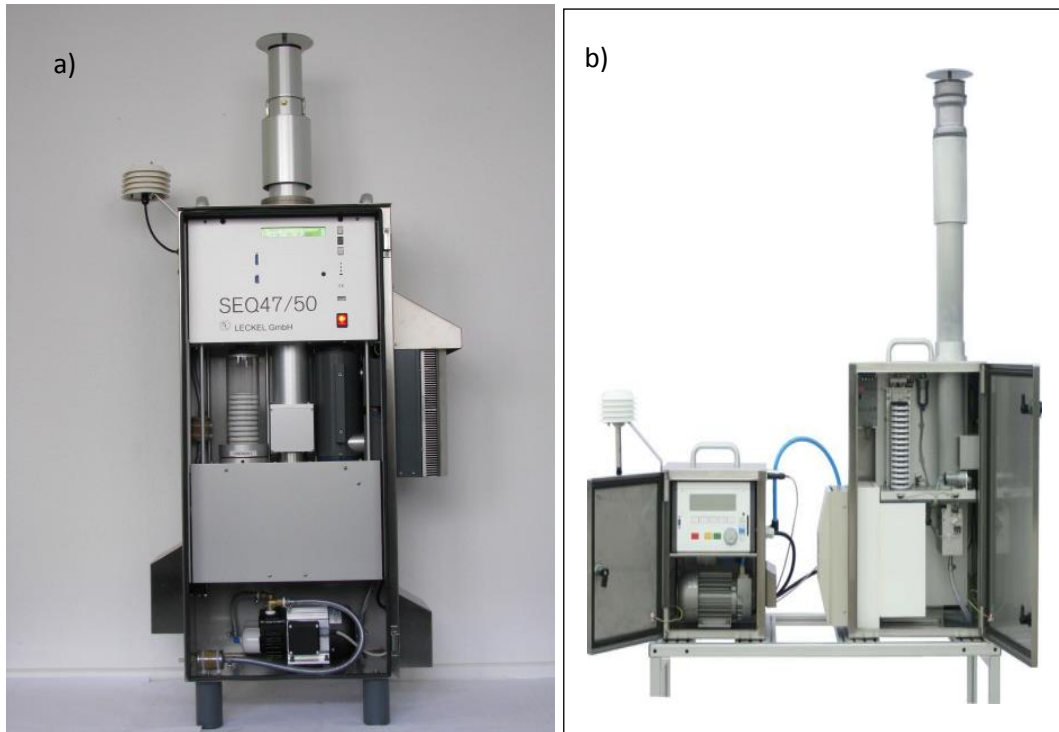


Figure 2.22: Leckel SEQ47/50 (a) and Derenda PNS 16 (b).



Figure 2.23: The sampling inlet of the sequential sampler SEQ47/50 according to CEN EN 12341

Table 2.3: Overview of PM₁₀ filter sampling in this study.

	Description
Locations	One site in Amsterdam, Antwerp, Leicester, Lille and Wijk aan Zee Trailer: measurements at an extra site in Amsterdam, Antwerp and Leicester
Method	24-h collection of PM ₁₀ on a filter sampled by a sequential sampler with PM ₁₀ inlet
Sampler	Derenda (AD and WZ) Cooled Leckel (AP, LE and LL) Uncooled Leckel in trailer
Filter	Quartz filters (Pall Tissuquartz 2500 QAT-UP; 47 mm diameter) All filters (same batch) and slides were purchased and distributed by VMM
Air volume	55 m ³ day ⁻¹ in ambient conditions (2.3 m ³ h ⁻¹) Flow check every 14 days (when changing filter compartments)
Period	1 April 2013 to 31 May 2014 (except for Lille, started 5 June 2013)
Sampling for characterisation	Every 6 th day sampling for chemical analysis. On other days the same filters were used for gravimetric analysis but not chemically analysed.

Chapter Three

Sub-micron particle number size distribution characteristics at two urban locations in Leicester

This Chapter has been published in Atmospheric Research (Hama et al., 2017b).

What is the status of PNSD in Leicester urban area? What are the characterisations the NPF events and its impact on PNSD in the urban area of Leicester?

The particle number size distribution (PNSD) of atmospheric particles not only provides information about sources and atmospheric processing of particles, but also plays an important role in determining regional lung dose. Owing to the importance of PNSD in understanding particulate pollution two short-term campaigns measurements of sub-micron PNSD were conducted at two urban background locations in Leicester, In spite of its importance, aerosol size distributions at urban and road sites in UK have been reported at relatively few sites. Those studied summarised in Table 3.1. To our knowledge, there are no studies regarding particle number size distribution measurements and analysis of NPF events in detail in a UK urban area such as Leicester. Information on the behaviour of particle number size distributions is still sparse. There is also a lack of knowledge about particle number size distributions generally in the UK. The objective of this study is to characterize the NPF events and its impact on PNSD by taking measurements at two sites within the urban area of Leicester. This study also investigates the effect of Easter school holiday on PNSD. Daily and weekly variations of PNSD, and the difference between daily patterns of weekday and weekends of PNSD are explored. The influence of traffic emissions and metrological conditions on PNSD are also investigated

3.1 Introduction

Atmospheric aerosol particles are ubiquitous and have negative impacts on human health, air quality and global climate change (Lohmann and Feichter, 2005; Pope and Dockery, 2006; Stevens and Feingold, 2009). Epidemiological studies have revealed that the existence of a relationship between fine particle concentration and respiratory and cardiovascular diseases (Pope, 2000). Numerous studies have since proposed that ultrafine particles (UFP – particles <100 nm) are more toxic compared to larger particles of same composition and the adverse health effects caused by UFP number concentrations have been indicated to be stronger than those by the fine particle mass concentrations (Li et al., 2002; Nel, 2005; Penttinen et al., 2001; Peters et al., 1997). Nevertheless, current air quality standards are based on the particle mass concentrations. The mass concentrations of the particles less than 100 nm, which really govern the total particle number concentrations in urban areas are insignificant (Seinfeld and Pandis, 1998). Thus, current air quality measurements might be insufficient to permit assumptions to be drawn concerning the association between particle number and the detrimental health effects. It is, therefore, vital to measure the particle number size distributions in order to fully understand the environmental effects of atmospheric ultrafine particles (Penttinen et al., 2001; Peters et al., 1997). Air quality at many urban background sites is influenced by road traffic emissions with diurnal patterns found to be strongly influenced by the primary traffic exhaust emissions in the urban areas (Hussein et al., 2004; Pérez et al., 2010; Rodríguez and Cuevas, 2007; Stanier et al., 2004; Tuch et al., 2003; Wehner and Wiedensohler, 2003). Traffic emissions are considered to be one of the most significant sources of UFP number concentrations in the urban atmosphere, with the other significant source originating from particle formation (NPF) (Brines et al., 2015; Shi et al., 2001; Stanier et al., 2004). In addition, NPF events can occur widely under various meteorological and atmospheric conditions (Dal Maso et al., 2005; Kulmala et al., 2004). NPF can be a second source of UFPs in urban areas (Brines et al., 2015). Several NPF studies in rural and urban areas have revealed that NPF is generally favoured under high insolation and wind speed, low relative humidity, and low pre-existing particle surface area (Kulmala and Kerminen, 2008; Kulmala et al., 2004). As

such, the increased background concentration of UFPs in polluted areas seems to decrease the NPF. Nevertheless, NPF events are still observed in many polluted urban areas and some of the studies have revealed that strong correlation between the NPF and the levels of vapour-phase H_2SO_4 which is mainly produced by the chemical oxidation of SO_2 with the hydroxyl radical during daytime (Jeong et al., 2004; Kulmala et al., 2012; Wang et al., 2014; Zhu et al., 2013).

eBC is typically formed by incomplete combustion of fossil fuels, biofuel and biomass, and is emitted from traffic. Several studies have shown that a strong relationship between black carbon and road traffic emissions (Boogaard et al., 2011; Butterfield et al., 2015; Fruin et al., 2008; Invernizzi et al., 2011; Pérez et al., 2010; Reche et al., 2011) and biomass burning emissions (Butterfield et al., 2015; Ingrid Sundvor, 2012). Moreover, numerous studies have revealed that exposure to road traffic emissions is best assessed by combining measurements of particle number and eBC concentrations (Harrison et al., 2004; Rodríguez and Cuevas, 2007; Smargiassi et al., 2005), since these parameters need to be controlled by air quality limit values.

In spite of its importance, aerosol size distributions at urban and road sites in UK have been reported at relatively few sites. Those studied summarised in Table 3.1. To our knowledge, there are no studies regarding particle number size distribution measurements and analysis of NPF events in detail in a UK urban area such as Leicester. Information on the behaviour of particle number size distributions is still sparse. There is also a lack of knowledge about particle number size distributions generally in the UK. The objective of the present study is to characterise the NPF events and its impact on PNSD by taking measurements at two sites within the urban area of Leicester.

This study also investigates the effect of Easter school holiday on PNSD. Daily and weekly variations of PNSD, and the difference between daily patterns of weekday and weekends of PNSD are explored. The influence of traffic emissions and meteorological conditions on PNSD are also investigated.

Table 3.1: Summary of the results from previous PNSD studies at various sites in UK.

Site	Size range (nm)	Study
Urban background site (London)	10-415	Rodríguez et al. (2007)
Road site (London)	14.6-661.2	Dall'Osto et al. (2011)
Urban background site (London)	8-700	von Bismarck-Osten et al. (2013)
Road site (London)	19.2-600	von Bismarck-Osten et al. (2013)
Urban background site (Birmingham)	10-1000	Harrison et al. (1999)
Road site (Birmingham)	9.47-359	Shi et al. (2001)
Road site (Manchester)	4-160	Longley et al. (2003)
Rural site (Harwell)	11-450	Charron et al. (2007)
Urban background site (Cambridge)	10-2500	Kumar et al. (2008)
Road site (Leicester)	5-1000	(Agus et al., 2007)
AURN urban background (Leicester)	10-1093	This study
BF urban background (Leicester)	10-1093	This study

The study was carried out between March 2014 and June 2014 over which time particle number size distributions (PNSD) were measured concurrently with black carbon mass concentration (eBC), total particle number (TNC), and NO_x at two sites in Leicester. This study reports on the first results of PNSD measurements which were taken as part of the air quality monitoring network established across North West Europe as part of the JOint Air QUality INitiative (JOAQUIN, www.joaquin.eu), an INTERREG IVB funded European project, which aims at supporting health-oriented air quality policies in North-

West Europe. More information can be found in the Joaquin report and publications (Cordell et al., 2016; Hama et al., 2017a; Hofman et al., 2016; Joaquin, 2015a).

3.2 Experimental

3.2.1 Sampling sites

The measurements were a part of the JOAQUIN project (www.joaquin.eu). Sampling was conducted during the spring (March-June 2014) at two sites located at the University of Leicester (Figure 3.1). More detailing about the characteristics and locations of the sampling sites can be found in Hama et al. (2017a). In this study hourly traffic density data was provided by Leicester City Council was used. For a detailed overview of the monitoring sites and the JOAQUIN project, the reader is referred to the final report (Joaquin, 2015a).



Figure 3.1: Map of Leicester and locations of the sampling sites

3.2.2 Instrumentation

Table 3.2 summarizes the availability of monitors for PNSD, eBC, TNC, NO_x and O₃ per site. Measurements at the AURN and BF sites were carried out with the devices in the mobile measurement trailer.

In this study the particle size distribution was measured by a Scanning Mobility Particle Spectrometer (Grimm SMPS+C 5420 with L-DMA). TNC was measured with a TSI model 3783 water-based condensation Particle counter (CPC).

Table 3.2: Overview of instrument types per sampling site (March-June 2014).

Station	Location	Meteorological Parameters	W-CPC	SMPS	NO _x	O ₃	MAAP
AURN	UoL	-	x	-	x	x	x
Trailer (Mobile Campaign)	UoL and BF	x	x	x	-	-	x

This instrument measures the number of particles in the size range of ~7 to 1000 nm. To measure the eBC (Petzold et al., 2013) mass concentration a MAAP (model 5012, Thermo-Scientific) was used. NO_x were measured by a Thermo 42i NO-NO₂-NO_x monitor. The concentrations of O₃ were measured by UV absorption at AURN site. The reference method for the determination of concentrations of O₃ are described in European Standard EN14625, more information can be found in this website (<https://uk-air.defra.gov.uk/networks/monitoring-methods?view=eu-standards>). For a detailed overview of the instruments and monitors that were used in this study and also about data quality assurance in the JOAQUIN project, the reader is referred to Hama et al. (2017a).

Meteorological data were obtained from a mobile laboratory van during this study. Moreover, Meteorological data were also provided by the Air Quality Group from the Leicester City Council, located 4.9 km northwest the AURN site. The mean, median, and max values of wind speed (WS), wind direction (WD), temperature (T), and the relative humidity (RH) from March to May 2014 at both sites are shown in Table 3.3.

Table 3.3: Mean, Median, and Max of the Meteorological parameters at AURN and BF sites.

Site	WS (m s ⁻¹)			WD (°)			T(°C)		
AURN	Mean	Median	Max	Mean	Median	Max	Mean	Median	Max
March	1.44	1.21	9.44	176	186	329	8.8	8.84	18.5
BF									
April	1.3	1.24	4.85	175	189	313	10.76	10.8	19.1
May	0.99	1.15	3.91	192	205	305	11.7	12.45	23.75
AURN	RH (%)								
March	73.9	76.6	93.95						
BF									
April	71.4	74.41	92.44						
May	71.55	70	92.11						

3.2.3 Data processing and analysis

Particle number concentrations for different size ranges were calculated by the particle size distribution from the Grimm SMPS measurement. The particle number concentrations were categorised into $10 \leq d \leq 1093$ nm (N_{total}), $100 \leq d \leq 1093$ nm (N_{acu}), $25 \leq d < 100$ nm (N_{Aitken}) and $d < 25$ nm (N_{nuc}), for total, accumulation mode, Aitken mode and nucleation mode, respectively. Data analyses have been carried out using the Openair software package (Carslaw, 2015; Carslaw and Ropkins, 2012) using R software (R Core Team, 2014) and sometimes Igor software. The Openair is freely available as an R package.

All data were screened for irregularities. Continuous air quality data collected during instrument errors or maintenance were removed from the analysis. For PNSD, particle

losses to the surface of the sampling system and the measuring device can occur via diffusion. Therefore, sampling pipes were kept as short as possible and laminar flow conditions used. Nevertheless, meaningful diffusional losses during sampling and measurement occur for particles $<100 \mu\text{m}$, so that diffusion correction factors should be applied. For the results of the Grimm SMPS, the diffusion correction factors used were manufacturer factors integrated into the instruments algorithms, after which an additional correction was done using factors based on the simplified expression formula for cylindrical pipes (Hinds, 1999). No other instrument corrections were applied, more detail can be found in the final JOAQUIN report (Joaquin, 2015a).

3.2.4 New particle formation event characteristics

The particle formation rate (J) is defined as the flux of the nucleated particles into the observed nucleation mode particle size range (for example, 10-25 nm, in this study) (Kulmala et al., 2004). The experiential particle formation rate was found by simplified calculation of the general dynamic equation (GDE), describing the evolution of particle size distribution (Seinfeld and Pandis, 2006). The nucleation rate formation (J_{10-25}) was calculated according to Dal Maso et al. (2005), as follows:

$$J_{10-25} = \frac{dN_{10-25}}{dt} + F_{\text{coag}} + F_{\text{growth}} \quad (3.1)$$

where F_{coag} is the flux due to coagulation losses, and F_{growth} is the flux of particles growing out of the nucleation mode size range. dN_{10-25}/dt is the rate of change of nucleation mode particles with time, t . It should be noted that particles grew out of the freshly nucleated size range of 10-25 nm, as a result F_{growth} term in Eq. (1) cannot be neglected and was calculated by Dal Maso et al. (2005) method as follow:

$$F_{\text{growth}} = \frac{1}{\Delta D_p} \cdot GR_{10-25} \cdot N_{10-25} \quad (3.2)$$

where, $\Delta D_p = (25-10) = 15\text{nm}$

Here, GR_{10-25} was obtained from the SMPS data in the size range 10-25 nm, and N_{10-25} is the number concentration of nucleation mode particles. The coagulation loss for the size range 10-25, F_{coag} , was calculated as:

$$F_{coag} = N_{10-25} \cdot \sum_j K_{ij} \cdot N_j \quad (3.3)$$

where $\sum K_{ij} \cdot N_j$ is the coagulation sink. N_j is the particle number concentration of size bin j . K_{ij} is the coagulation coefficient between size bin i and j , and is given as (Seinfeld and Pandis, 2006):

$$K_{ij} = 2\pi \cdot (d_i + d_j) \cdot (D_i + D_j) \cdot \beta_{Fij} \quad (3.4)$$

where d is the diameter of a size bin, D and β_F are the size dependent diffusion coefficient and Fuchs correction factor of particles, respectively (Seinfeld and Pandis, 2006).

The growth rate (GR) of NPF events is defined as the rate of change in the diameter. The GR was calculated according to Kulmala et al. (2012):

$$GR = \frac{\Delta D_p}{dt} = \frac{D_{p2} - D_{p1}}{t_2 - t_1} \quad (3.5)$$

where d_{p1} and d_{p2} are the geometric mean diameter of nuclei mode particles and dt is the time interval. The units of GR are $nm \ h^{-1}$.

The condensation sink (CS) is a measure of how rapidly vapour molecules will condense onto pre-existing particles and depends mainly on the shape of particle size distribution (Dal Maso et al., 2002; Kulmala et al., 2001; Lehtinen et al., 2003).

An expression for the CS, with unit of s^{-1} , the CS can be calculated as follows (Kulmala et al., 2001):

$$CS = 2\pi \cdot D \cdot \sum_i \beta_{Mi} \cdot d_{pi} \cdot N_i \quad (3.6)$$

$$\beta_M = \frac{1 + K_n}{1 + 0.337 K_n + \frac{4K_n}{3\alpha} + \frac{4K_n^2}{3\alpha}} \quad (3.7)$$

where D is the diffusion coefficient for H_2SO_4 ($0.104 \text{ cm}^2 \text{ s}^{-1}$), β_M is the size-dependent transition correction factor, d_{pi} is the aerosol particle diameter, N_i is the particle number concentration, α is mass accommodation coefficient ($\alpha=1$), and K_n is the Knudsen number can be expressed in terms of particle diameter and the mean free path vapor molecules (λ_v) as (Pirjola et al., 1999):

$$K_n = \frac{2\lambda_v}{d_p} \quad (3.8)$$

The pressure and temperature dependant mean free path of vapour molecule (λ_v) can be calculated by the following equation from Willeke (1976):

$$\lambda_v = \lambda_r \cdot \left(\frac{101}{P}\right) \cdot \left(\frac{T}{293}\right) \cdot \left(\frac{1 + 110/293}{1 + 110/T}\right) \quad (3.9)$$

where P is in kPa and T in K. at 293 K and 1 kPa atmospheric pressure, the λ_r (mean free path) is $0.039 \mu\text{m}$ for H_2SO_4 . By using this reference value of λ_r , λ_v can be calculated for measured pressures and temperatures during NPF event days at the sampling sites. By using these above equations and measured PNSD at AURN and BF sites, the CS were computed for the NPF event days.

The condensable vapour source rate (Q , $\text{cm}^{-3} \text{ s}^{-1}$) can be calculated according to Kulmala et al. (2001):

$$Q = CS \cdot C \quad (3.10)$$

where C is the condensable vapour concentration (cm^{-3}), can be calculated as follows:

$$C = A \cdot \frac{dD_p}{dt} \quad (3.11)$$

where A is a constant, ($1.37 \times 10^7 \text{ h cm}^{-3} \text{ nm}^{-1}$).

3.3 Results and Discussion

3.3.1 Overview of the particle number concentrations

Table 3.4 summarizes the statistical parameters for size segregated particle number concentrations and eBC covering the entire measurement period at both sites. The particle number concentrations for the N_{nuc} , N_{Aitken} , and N_{acu} are 2002, 3528, and 1576 # cm^{-3} , at AURN site, 1455, 2407, and 874 # cm^{-3} at BF site, respectively. The particle number concentration of the Aitken mode generally dominates at both sites. This might be related to the strong impact of vehicle emissions and meteorological factors on the particle number concentration of the N_{Aitken} in urban areas. Generally, the vehicles in urban area of Leicester are dominated by petrol cars and diesel buses according to the newest data of registered vehicles in Leicester City (Department of Transport of UK government, <http://www.dft.gov.uk/traffic-counts>, and count point 36549).

Table 3.4: Summary statistics of size-segregated particle number concentrations (# cm^{-3}), and eBC ($\mu\text{g m}^{-3}$).

Site	Mode	Mean	50th percentile	75th percentile	Standard deviation	Validated data
AURN	N_{nuc}	2002	1522	2612	1828	4345
	N_{Aitken}	3258	2553	3897	2646	4345
	N_{acu}	1576	1174	2073	1403	4345
	N_{total}	6837	5680	8446	4549	4345
	eBC	1.7	1.27	1.97	1.67	4308
BF	N_{nuc}	1455	1131	1878	1313	6714
	N_{Aitken}	2407	2021	3124	1513	6714
	N_{acu}	874	742	1178	548	6714
	N_{total}	4737	4250	5899	2514	6714
	eBC	0.77	0.67	0.96	0.51	7344

Laboratory studies have demonstrated that the average diameters of particles emitted by gasoline engine vehicles range from 40 nm to 80 nm (Harris and Maricq, 2001; Ristovski et al., 1998). Those studies suggest that the particles measured within this size range are most likely associated with traffic emissions. In addition, some studies have shown that particle diameter on urban road measurements were smaller (probably smaller than 30 nm) than those observed under laboratory conditions (Kittelson et al., 2004; Wehner et al., 2002). The average size-segregated particle number concentrations in this study are compared with other European studies (Table 3.5). The average concentrations of N_{nuc} and N_{Aitken} are lower than that in Leipzig, Helsinki, and London. However, they are higher than that in Copenhagen and Harwell. The average concentrations of N_{acu} are higher than those studies at AURN site, whereas they are lower than those studies except in Harwell at BF site. It should be noted that the differences might be related to the instrumentation (different size range of diameter), and also the sampling locations and weather conditions at each cities. The mean and median values of the meteorological parameters are shown in Table 3.3. From these values it can be suggested that the weather conditions are similar during the measurements at both sites (from March to May 2014). However, temperature is lower in March, when compared with April, and May, for instance average T are 8.84, 10.8, and 12.45 °C for March, April, and May 2014, respectively. It is clearly showed that little change in temperature ($\sim \pm 2\text{-}3$ °C). It should be noted that the PNSD might also be influenced by meteorological conditions during our measurements. Table 3.6 presents Pearson's correlation coefficients between PNSD and meteorological parameters at both sites. PNSD showed no relation with all meteorological parameters. The very low correlation coefficients can be explained as a results of the local sources (such as traffic emissions) that dominate the sources of PNSD and also indicated that traffic emissions have higher impact on PNSD than meteorological conditions at both sites. From these results it can be concluded that PNSD at both sites are influenced more by vehicle exhaust emissions rather than meteorological conditions during our campaign.

Table 3.5: Comparisons of size-resolved particle number concentrations (cm^{-3}) between this study and other European studies. (Size range: nm).

Location	N_{nuc}	N_{Aitken}	N_{acu}	N_{total}	Study
Leipzig	9850 (3-20)	9413 (20-100)	2107 (100-1000)	21377 (3-2500)	Wehner and Wiedensohler (2003)
Leipzig	4495 (8-30)	3287 (30-100)	1632 (100-700)	9398 (8-700)	von Bismarck- Osten et al. (2013)
Helsinki	7100 (8-30)	6320 (20-100)	960 (90-400)	14500 (8-400)	Hussein et al. (2004)
Helsinki	3080 (8-30)	3099 (30-100)	1053 (100-700)	7231 (8-700)	von Bismarck- Osten et al. (2013)
London	1632 (19-30)	3825 (30-100)	1437 (100-600)	6680 (19-600)	von Bismarck- Osten et al. (2013)
Copenhagen	1294 (8-30)	2994 (30-100)	984 (100-700)	5287 (8-700)	(von Bismarck- Osten et al., 2013)
Harwell	944 (11-30)	1770 (30-100)	628 (100-450)	3342 (11-450)	Charron et al. (2007)
Leicester (AURN site)	2002 (10-25)	3258 (25-100)	1756 (100-1093)	6837 (10-1093)	This study
Leicester (BF site)	1455 (10-25)	2407 (25-100)	874 (100-1093)	4737 (10-1093)	This study

Table 3.6: Pearson correlation coefficients between PNSD ($\# \text{ cm}^{-3}$), and the meteorological parameters (WS (m s^{-1}), WD (knot), T ($^{\circ}\text{C}$), RH (%)) at AURN and BF sites.

site	Parameters	N_{nuc}	N_{Aitken}	N_{accu}	N_{total}
AURN	WS	-0.13	-0.182	-0.187	-0.216
	T	-0.055	-0.182	-0.0423	-0.141
	RH	-0.0786	0.179	0.183	0.129
BF	WS	-0.0685	-0.458	-0.340	-0.392
	T	-0.0311	-0.201	0.152	-0.105
	RH	-0.249	-0.029	-0.055	-0.015

In addition, Figure 3.2 shows the variability of the atmospheric particle number size distribution at two urban background sites within Leicester. The AURN site shows considerably higher particle number concentrations than the BF site. Proximity to roads is the primary driver: the distance between AURN site and the major and minor roads were 140 m and 20 m, respectively, and also to the effect of numbers of vehicles that passing by the major and busy road (see section 2.1). For particle diameters smaller than 100 nm an obvious difference in the concentrations is observed between the both sites. The small particles dominate the total particle number concentration (N_{total}) (Table 3.4) at both sites. This observation is indicative of on-road traffic exhaust emissions as the main source of particles and particularly of the small particles as observed in previous studies in an urban areas (Bukowiecki et al., 2003; Putaud et al., 2004; Wehner and Wiedensohler, 2003). The number size distribution for particles greater than 200 nm is fairly similar at both sites. This size range belongs to the long-lived particles in accumulation mode. From the data in Figure 3.2 and Table 3.4 it can be suggested that sources of larger particles ($> 200 \text{ nm}$) differ from sources of the smaller particles ($< 100 \text{ nm}$); these larger particles are most likely dominated by regional

background sources (Birmili et al., 2013). Moreover, the size distribution at the AURN site shows bimodal distribution at ~ 22 nm with a minor peak at ~ 70 nm (Figure 3.2), which is consistent with a previous study in an urban area (Jeong et al., 2010). The size distribution at BF site, however, exhibits unimodal distribution at ~ 35 nm (Figure 3.2), and was similar to previous studies that have observed unimodal size distribution in urban areas (Harrison et al., 1999; Krudysz et al., 2009). This difference might be indicative of the impact of vehicle exhaust particles with high instability, which might undergo rapid changes in size distribution of particles through evaporation or condensation process.

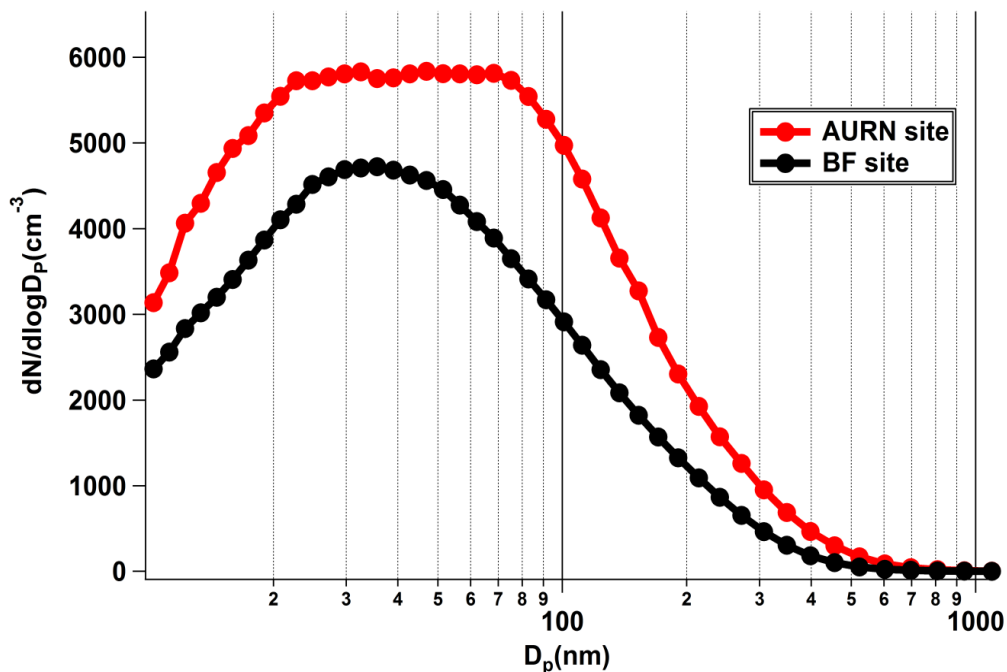


Figure 3.2: Particle number size distribution at AURN and BF sites.

3.3.2 Particle number size distributions

The following sections will focus on the discussion of the measured average particle number size distribution at both sites and also its dependence on the time of the day. In addition, the impact of school holidays (Easter) on particle number at the BF site, along with weekday and weekend variations at both sites will be discussed.

3.3.2.1 Easter holiday

Figure 3.3 shows particle size distribution for three weeks (before Easter, Easter Week, and after Easter) at the BF site. To show the impact of vehicle emissions at this site three weeks data have been selected around the school holidays. Several primary, preparatory schools and day nurseries are located near the BF site. The impact of the Easter holiday period on UFP number concentration can clearly be observed, with much lower UFP concentrations during the Easter holidays. Generally, the UFP number concentrations observed during Easter holiday week were lower when compared with the week before and after the holiday. This was because of lower traffic density during Easter holiday and also because the schools are closed during Easter in Leicester.

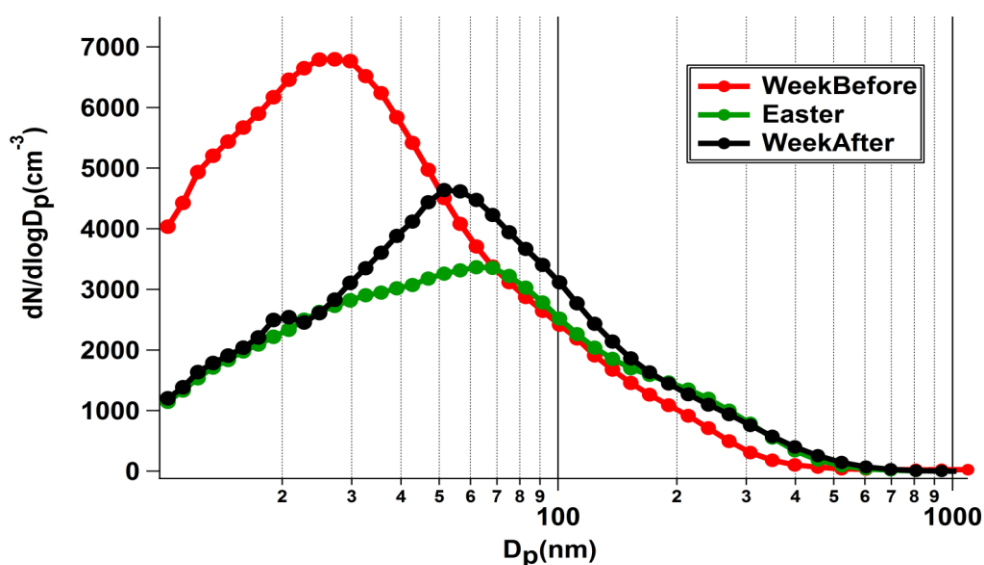


Figure 3.3: Particle number size distribution at Brookfield site. During week before Easter (Red line), Easter break (green line) and week after Easter (black line). Easter Holidays in Leicester: Mon 14th April – Fri 25th April 2014.

Moreover, Table 3.7 shows mean and median levels of the PNSD, traffic-related pollutants, and the traffic intensity to reveal the impact of traffic on PNSD in detail during Easter school holiday (14th-25th April 2014) in Leicester. It can be seen the levels of traffic-related pollutants such as NO_x , and eBC during a week (Monday-Friday) before

and after are higher than the levels during the Easter holiday weeks. The average concentrations of NO_x are a 42.98, 43.91, and 31 $\mu\text{g m}^{-3}$, and eBC are 1.52, 1.45, 0.91 $\mu\text{g m}^{-3}$ for week before, after, and Easter period, respectively. In addition, the traffic intensity (number of vehicles per hour) are also shown in Table 3.7. The lower traffic density during Easter holiday was observed when compared with the week before and after, the traffic intensity are 539, 518, and 373 vehicles h^{-1} for week before, after, and Easter period, respectively. This result showed that during Easter holiday was observed lower traffic intensity, the traffic-related pollutants, and the PNSD. This might be linked to the impact of holiday of the schools in Leicester during the Easter holiday since people have not used their cars as much as normal school days. It can be concluded that Easter holidays can impact on PNSD in Leicester.

Table 3.7: Mean, and Median, of the NO_x ($\mu\text{g m}^{-3}$), eBC ($\mu\text{g m}^{-3}$), PNSD ($\# \text{cm}^{-3}$), and Traffic (vehicles h^{-1}) at BF site Week before, Easter and Week after Easter holiday 2014.

	Mean					
	NO_x	eBC	N_{nuc}	N_{Aitken}	N_{acu}	Traffic
Week before	42.98	1.52	2376	2796	592	539
Easter	31	0.91	821	1856	805	373
Week after	43.91	1.45	2147	2339	668	518
	Median					
Week before	39.7	1.3	2269	2386	502	651
Easter	27.7	0.86	969	1605	752	460
Week after	38.61	1.25	1956	2182	627	669

3.3.2.2 Temporal Variations

Diurnal and nocturnal variations of the particle size distribution at both sites shown in Figure 3.4. At both sites higher concentrations were found in the nucleation mode (diameters less than 25 nm) during daytime (7:00-19:00), caused by the new particle formation events that are observed at both sites. Lower concentration of particle diameter in the size range ~30-100nm are observed during the daytime at both sites. This is probably as a result of the higher mixing layer and higher wind speed leading to better mixing of particles, which occurs mostly in spring and summer in urban background areas (Ketzel et al., 2004; Wu et al., 2008). Previous studies conducted in different areas in Sweden and Copenhagen have found similar results during daytime (Ketzel et al., 2004).

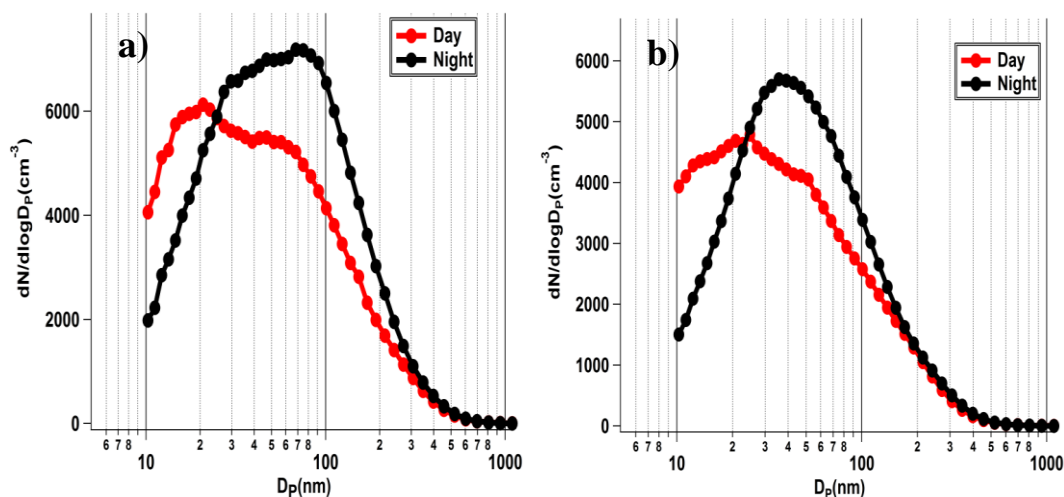


Figure 3.4: Particle number size distribution at a) AURN and b) BF sites under day time (7:00-19:00), and night (22:00-4:00) conditions.

Particle number size distribution showed higher concentrations during weekdays than weekends, which is related to the influence of vehicle emissions and number of vehicles in urban areas (Morawska et al., 2002). Variations of particle size distribution between weekdays (Monday to Friday, excluding holidays) and weekends at both sites are shown in Figure 3.5. Generally, during weekday's higher ultrafine particle number

concentrations were observed at both sites. On weekends, ultrafine particle number concentrations were lower due to lower traffic intensity.

Similar results have been found in previous studies in urban areas (Hussein et al., 2004; Morawska et al., 2002). Particles greater than 100 nm in diameter did not show differences during weekdays and weekends: this suggests that these particles might be partially associated to other sources rather than vehicle exhaust emissions.

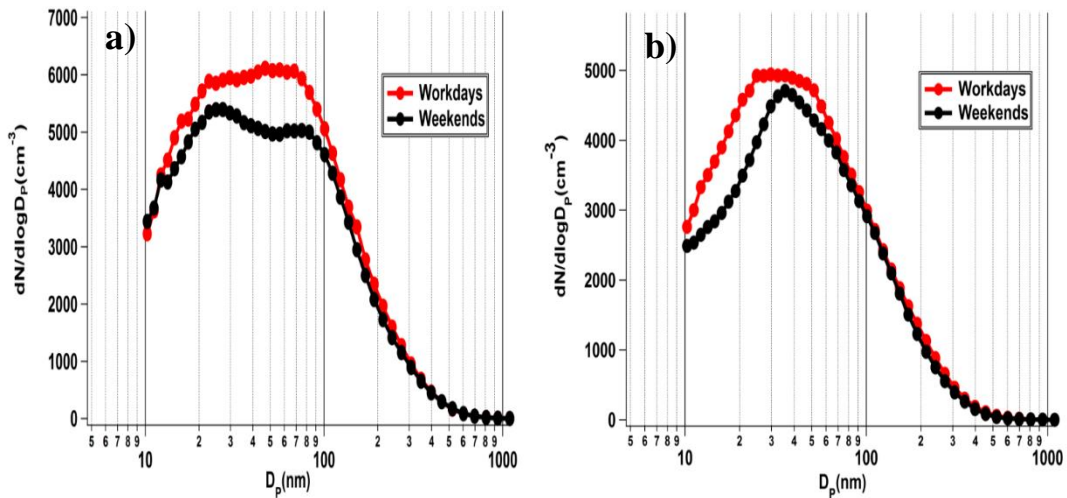


Figure 3.5: Particle number size distribution during weekends and weekdays at a) AURN and b) BF sites.

Average diurnal variations of the N_{nuc} , N_{Aitken} , N_{acu} , and N_{total} concentrations for both the sites averaged separately for weekdays and weekends are shown in Figure 3.6a and 6b. Statistical parameters for the four modes over the entire measurement period were calculated and tabulated in Table 3.4. For both sites the mean diurnal variation of N_{nuc} , N_{Aitken} , and N_{total} concentrations for weekdays clearly resemble the usual activity pattern of people in cities, particularly that of traffic activity. Figure 3.6a and 6b show clear peaks for two modes (N_{nuc} and N_{Aitken}) in the morning between 6-8 am on weekdays, which coincide with morning traffic rush hours combined with a lower mixing layer height and lower ambient temperature. The second clear peak on working days and even on weekends, however, occurs at about 7-9pm, thus significantly later than the evening

traffic rush hours, which typically occur in Leicester around 4-6pm. The late afternoon peak is more influenced by local meteorology conditions than by vehicular exhaust emissions.

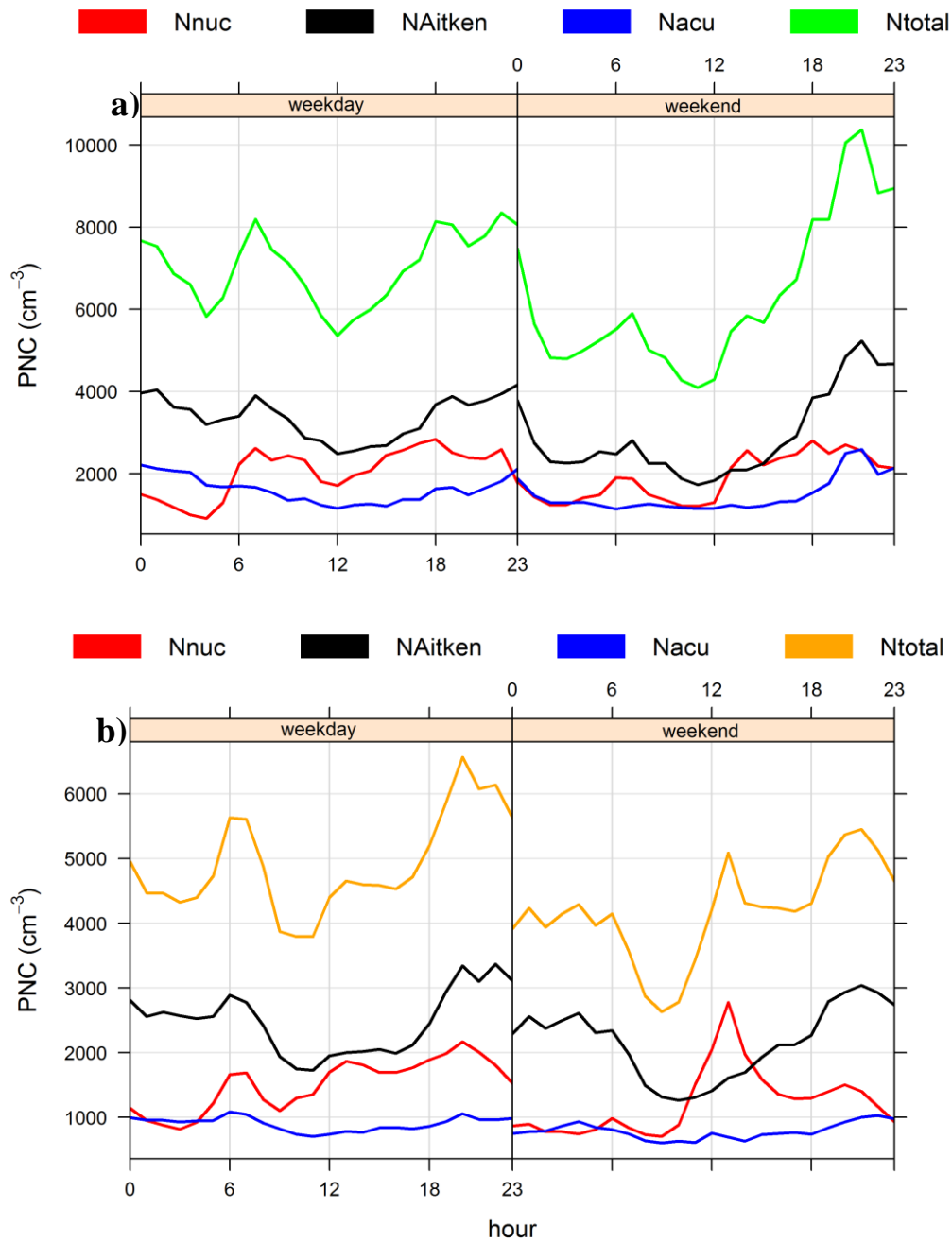


Figure 3.6: Mean diurnal variations of particle number concentration for a) AURN and b) BF sites. During workdays and weekends.

The influence of combustion activities and domestic heating at evenings can also play a crucial role on increasing particle number concentration in urban areas (Allan et al., 2010). The observed diurnal behaviour in the Leicester urban background is consistent with the previous studies that have been made in many other European cities at similarly located sites (Aalto et al., 2005; Avino et al., 2011; Borsos et al., 2012; Dall'Osto et al., 2013; Hussein et al., 2004; Moore et al., 2007). Interestingly, another clear peak was observed at midday or early afternoon and which N_{Aitken} peak which did not track as shown in Figure 3.6a and 6b for N_{nuc} on weekdays and even more clearly on weekends. This peak might be related to the new particle formation which typically occurs at midday when traffic intensity is quite low, and most strongly during spring or summer (Brines et al., 2015; Reche et al., 2011). The lowest concentration was observed for accumulation mode particles in the afternoon, which was mainly affected by the higher mixing layer. At the weekends, it can be seen that the morning peak occurs later compared to weekdays, associated with the tendency for people to go out later in the morning at weekends. Another high peak was also observed during evening; this is probably due to intense leisure traffic at the weekend evening.

The weekly variations of the different modes of particle number concentration at both sites are shown in Figure 3.7a and 7b. In general, all particle modes concentrations (except Naccu) had a weekly cycle with higher number concentrations from Monday to Saturday and lower on Sunday, because there are less traffic emissions on Sunday in Leicester. The urban traffic emissions have large impact on weekly cycle of particle number concentrations and this is one possibility to separate traffic vehicle emissions from other emission sources within the city (Harrison and Jones, 2005; Hussein et al., 2004; Massling et al., 2005).

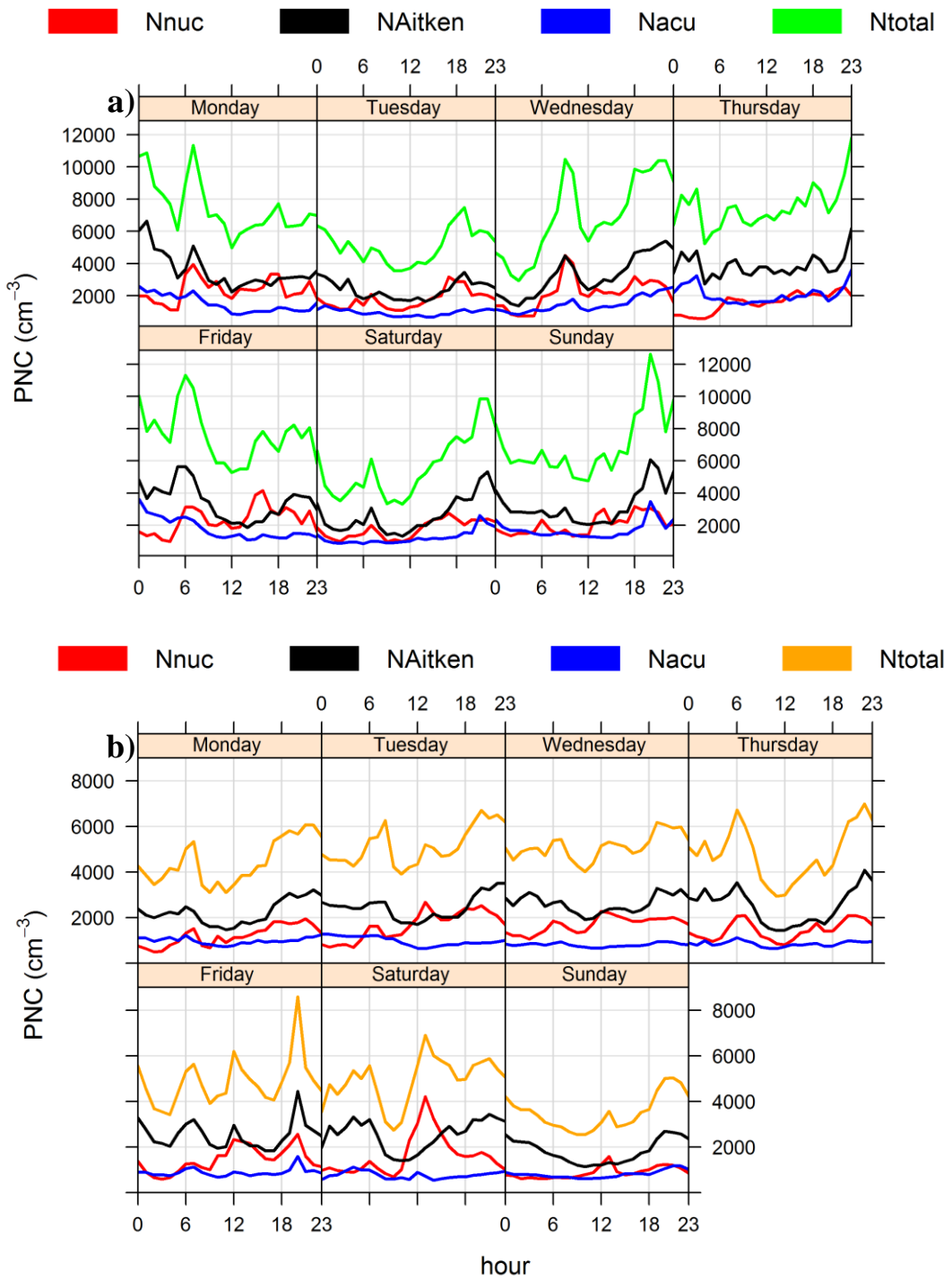


Figure 3.7: Weekly variation of particle number concentrations at a) AURN and b) BF sites.

To confirm the role or otherwise of NPF in the observed afternoon peaks (Figure 3.6a and 6b) diurnal variations of N_{nuc} , N_{total} , NO_x , and eBC for the NPF and non-NPF event days were averaged (Figure 3.8a and 8b). Figure 3.8a clearly shows a peak for N_{nuc} , and N_{total} , at noon during NPF event days that confirm NPF occur at urban background sites in Leicester. It should be noted that NO_x and eBC were only observed in the morning and afternoon rush hour peaks, but do not show peaks at noon; confirmation that the peak at noon belongs to NPF rather than local sources (such as traffic emissions). However, during non-NPF event days the diurnal variations of N_{nuc} , N_{total} , NO_x , and eBC clearly showed two peaks during morning and afternoon traffic rush hours in Leicester which belongs to the local sources and N_{nuc} follows NO_x and eBC profile as presented in Figure 3.8b. It can be concluded that the peaks were found at noon in Figure 3.6a and b can be related to NPF events and more clearly appeared at BF site (Figure 3.6b) since NPF event days at BF site happen more than AURN site in this study (Figure 3.6a).

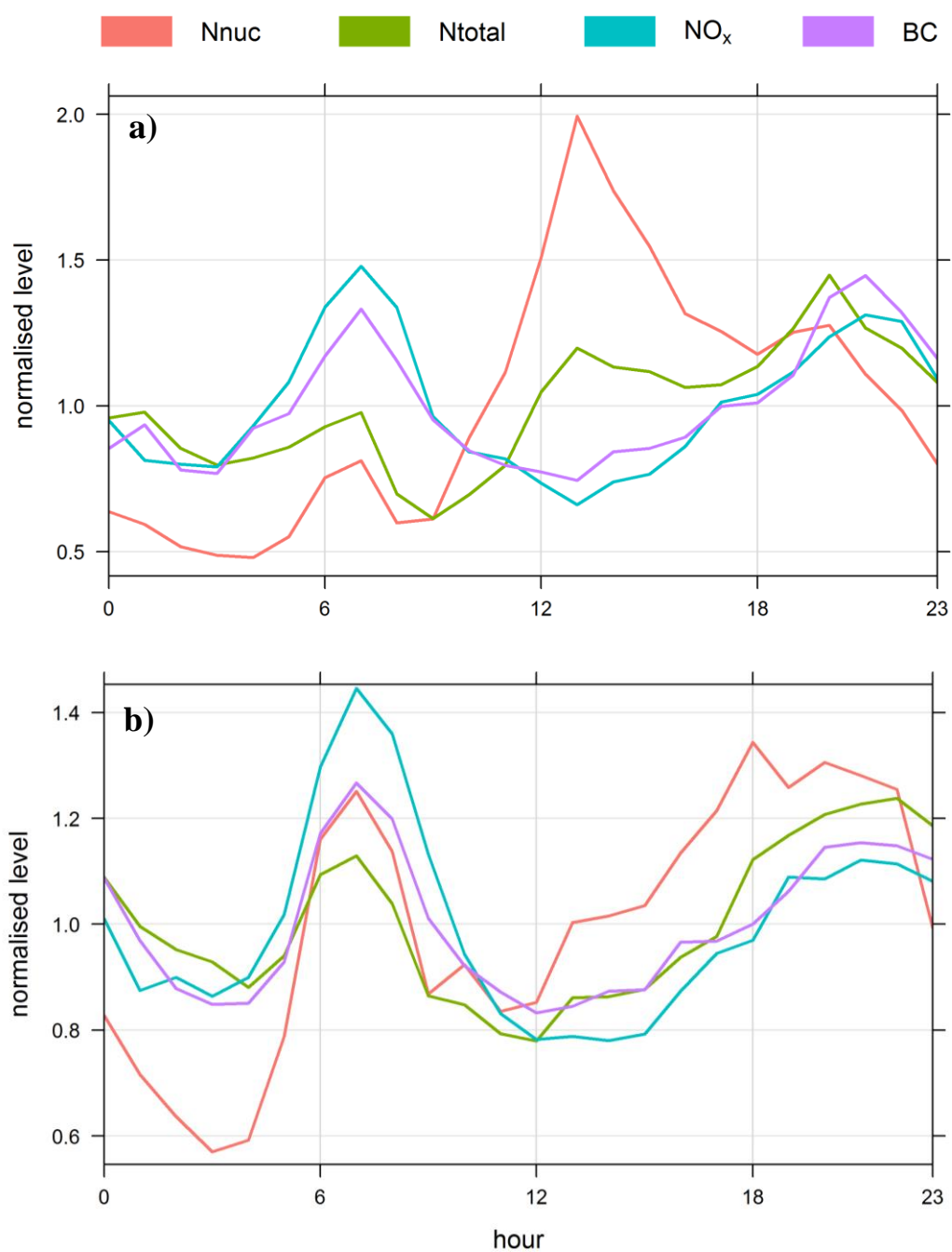


Figure 3.8: Diurnal variation of N_{nuc} , N_{total} , NO_x , and eBC for a) NPF event days ($n=14$), and b) Non-NPF event days ($n=72$) at AURN and BF site.

3.3.3 Dependency on wind speed and direction

A technique that has been used with previous success for identifying emission sources is the Conditional Probability Function (CPF). The CPF is a simple, fast and effective technique for providing directional information about main pollutant sources (Carslaw, 2015; Uria-Tellaetxe and Carslaw, 2014). In addition, bivariate polar plots have been shown to be particularly valuable for recognising and understanding sources of air pollutants (Carslaw et al., 2006; Westmoreland et al., 2007). CPF plots display how a pollutant concentration varies by wind speed and direction at a receptor (Carslaw and Ropkins, 2012). Figure 3.9a shows a CPF plot for TNC at AURN site, representing TNC sources where the total particle number concentration (30 min averaged) is $>50^{\text{th}}$ percentile TNC equal to 7728 \# cm^{-3} . In Figure 3.9a there is a clear implication that there is a higher probability of these particle concentrations originating from the north-west and south-west, corresponding to the direction of University and Welford Roads (see sampling sites in section 2.1). By comparison, Figure 3.9b shows a bivariate polar plot for the same TNC data period. In this plot also the most obvious feature are the higher particle concentrations of total number particles can be found at low WS (less than 2 ms^{-1}) from the same directions of the CPF plot. This behaviour would typically be expected at urban background sites where high particle number concentrations are observed in stable atmospheric environment conditions and when non-buoyant ground-level sources such as road traffic emissions and domestic heating are important sources. Figure 3.9c and 9d illustrate CPF and bivariate plot for eBC at the AURN site, highlighting eBC sources where the eBC concentration is $>50^{\text{th}}$ percentile eBC equals 1.3 \mu g m^{-3} . Figure 3.9c shows there that could be more than two major sources of eBC, when compared with the TNC plots. The maxima to the north-east indicative of residential sources (domestic heating, and wood burning sources). Moreover, Figure 3.9d shows a similar feature with observed high concentration of eBC at low WS.

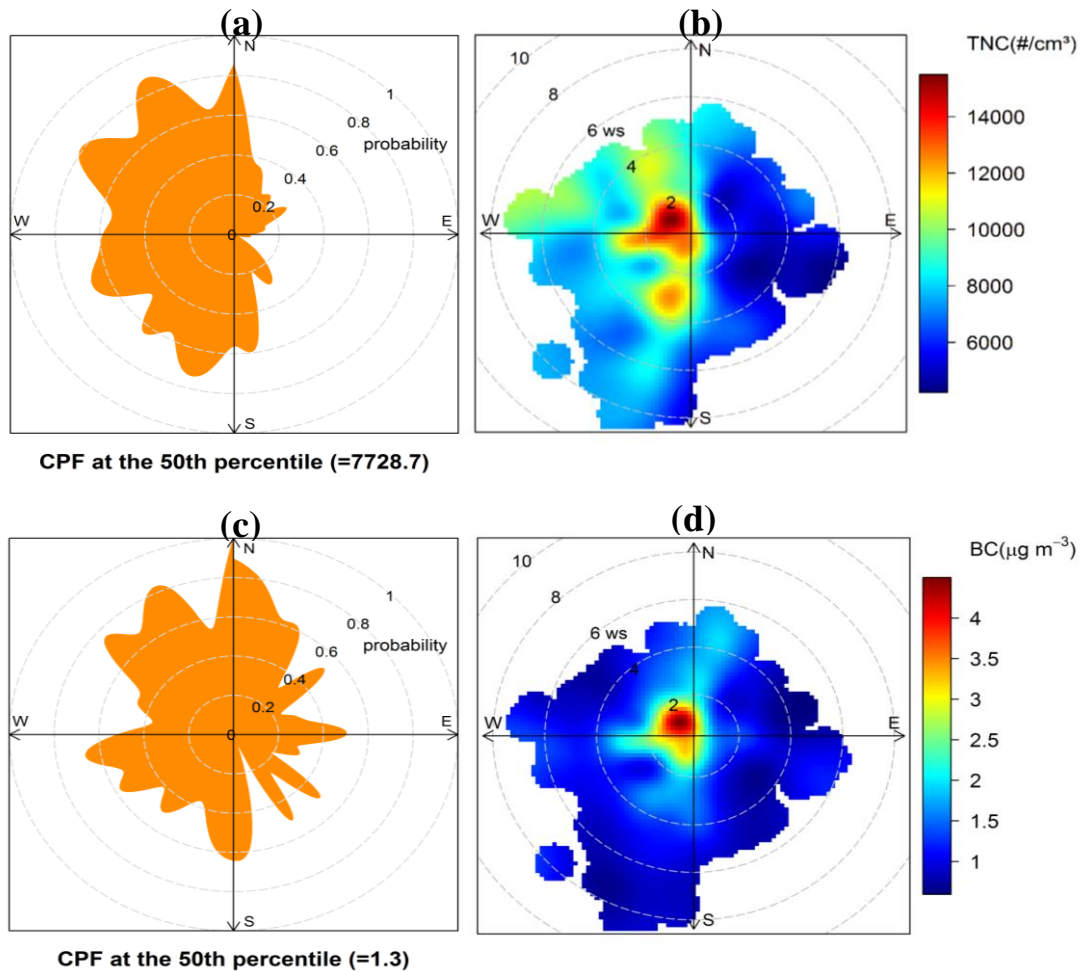


Figure 3.9: At AURN site a) CPF plot of TNC for concentrations >50 th percentile (7728.7 # cm^{-3}), (b) Bivariate polar plot of TNC, (c) CPF plot of eBC for concentrations >50 th percentile ($1.3 \mu\text{g m}^{-3}$), (d) Bivariate polar plot of eBC concentrations. The radial axis is wind speed in m s^{-1} .

In the case of the BF site (Figure 3.10a and 10c), it can be seen high concentrations of TNC and eBC are dominated by north and south west wind directions, corresponding to minor and major roads (Ashfield and London Roads, for more detail see sampling sites in section 2.1) near this temporary station as well as domestic heating emissions including wood burning and cooking. Figure 3.10b and 10d provides the same features as Figure 3.9b and 9d, showing that low concentrations are observed for 30 min averaged TNC and

eBC at low WS (lower than 2 ms^{-1}). In addition, in Figure 3.10b and d indicate the same directions as that found in the CPF plots, showing that high concentration of TNC and eBC are originating from the major road (London Road) which lies in a north and south-west direction. Both the CPF and bivariate polar plots are useful in highlighting the dominant wind direction and source types affecting the monitoring sites.

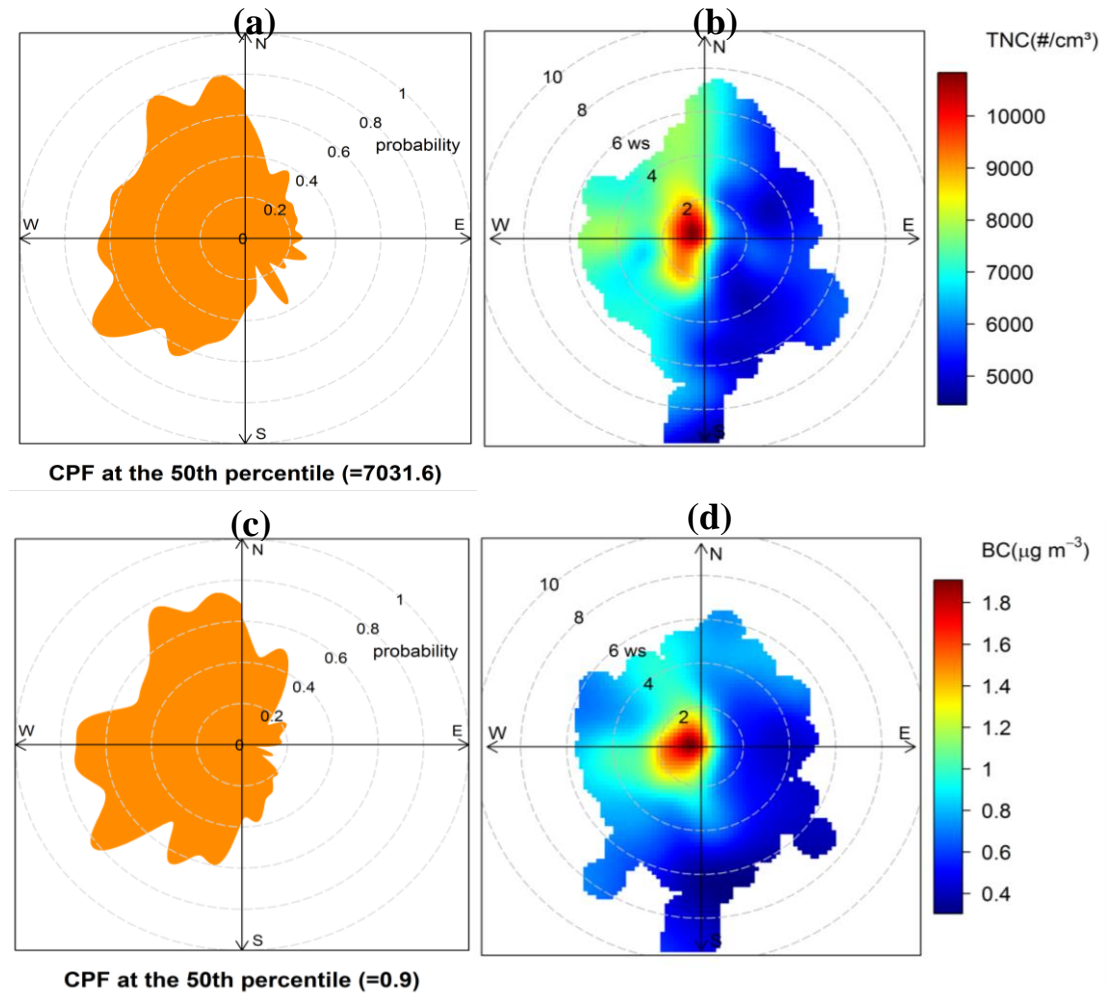


Figure 3.10: At BF site a) CPF plot of TNC for concentrations >50th percentile (7031.6 # cm^{-3}), (b) Bivariate polar plot of TNC, (c) CPF plot of eBC for concentrations >50th percentile (0.9 µg m^{-3}), (d) Bivariate polar plot of eBC concentrations. The radial axis is wind speed in m s^{-1} .

In addition, inverse relationships between different modes of PNSD and WS are observed (Figure 3.11a-d and Figure 3.12a-d). Figure 3.11 shows the relationships between different modes of PNSD and WS at the AURN site. It should be noted that high concentrations of PNSD were observed at low WS ($< 2 \text{ m s}^{-1}$). This might be related to the dilution effect. The dilution effects are affected by meteorological conditions, for example the mixing layer height, which controls the vertical dilution, and wind direction and speed, which control horizontal dilution. This is a typical behaviour of an urban background site. This association with lower wind speeds probably relates to the balance between lower dilution at low wind speeds and the longer transport times at these lower wind speeds, which allow more time for dispersion and deposition. Similar patterns were observed at the BF site when high PNSD levels were measured during low WS as presented in Figure 3.12a-d. It can be concluded that the PNSD being dominated by local sources, rather than regional sources in Leicester urban areas.

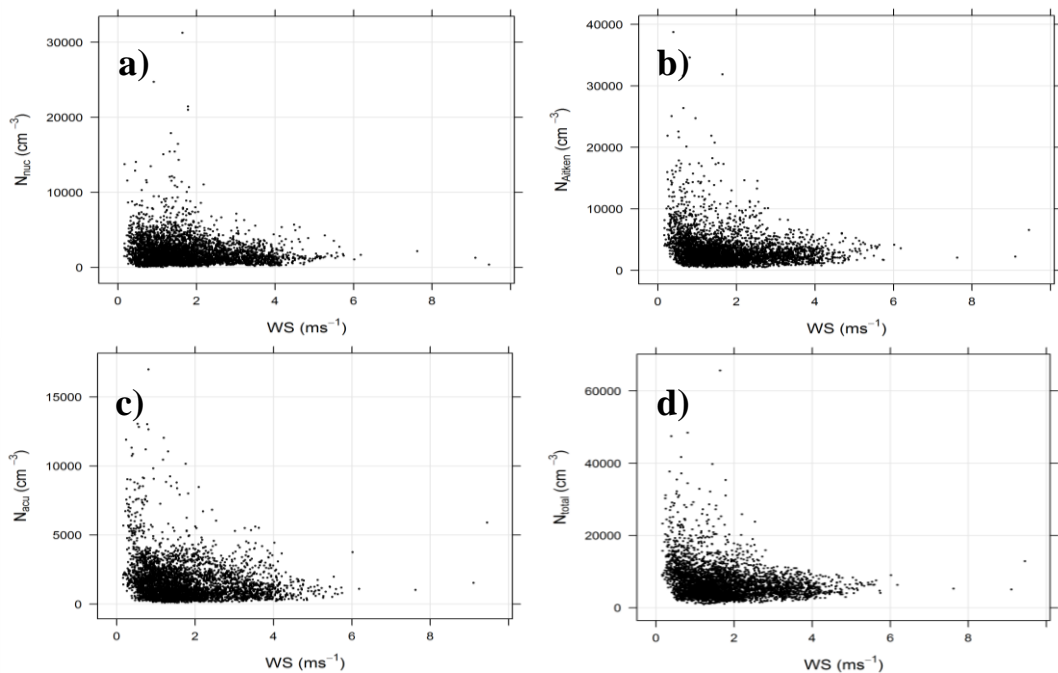


Figure 3.11: Correlation of the a) N_{nuc} , b) N_{Aitken} , c) N_{acu} , and d) N_{total} and wind speed for March 2014 at AURN site.

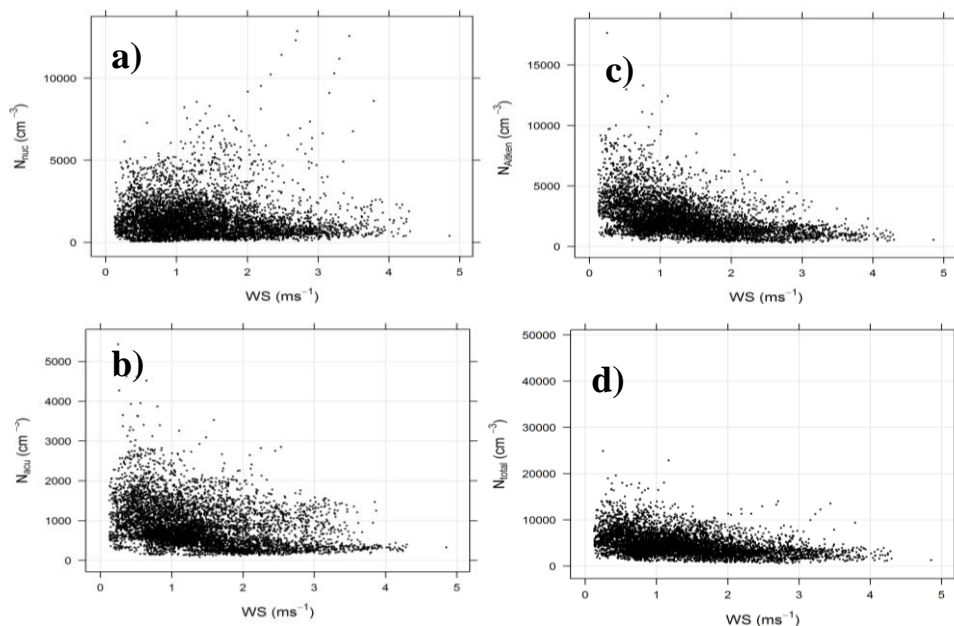


Figure 3.12: Correlation of the a) N_{nuc} , b) N_{Aitken} , c) N_{acu} , and d) N_{total} and wind speed for April and May 2014 at BF site.

3.3.4 Observation of new particle formation

The general definition of a nucleation event is a period when an increase in the number concentration of nucleation mode particles occurs, and those particles begin to grow into Aitken or accumulation mode particles, typically over a few hours until they disappear into the atmosphere by condensation/coagulation sinks (Dal Maso et al., 2005; Kulmala et al., 2004). The second major source of ultrafine particles in the urban atmosphere of developed urban areas is secondary aerosol formation (Brines et al., 2015). Previous studies using measurements in Birmingham (approximately 55 km from Leicester) have shown that there are three main sources of such particles: emissions from road traffic, emissions within the plumes from stationary point sources, and secondary particle formation within urban air (Alam et al., 2003; Shi et al., 2001). Recently, Hoffman et al (2016) simply described NPF events only at the AURN site (31 days). In this study NPF events were observed on 86 days (including the AURN site data) and focused on NPF

events at the BF site. During the study period in Leicester a total of 14 days of NPF events (four days at the AURN site, and ten days at the BF site) were observed during the morning (after morning rush hours) and afternoon hours (before evening rush hour). This emphasises the importance of this mechanism during the spring season. This is consistent with the previous study conducted in Helsinki (Northern Europe) urban atmosphere that observed maximum photochemical particle formation during spring (Hussein et al., 2008). Figure 3.13a and 13b show two NPF events on two different days that were observed at the BF site. In the first case (Figure 3.13a) three peaks were observed for TNC during the day: the first of which occurred from around 06:00 to 08:00, possibly due to traffic exhaust emissions during the morning peak hours in Leicester; the second peak was observed from around 10:30 to 15:00, probably owing to the formation of new particles; and the third one was also most likely caused by traffic exhausts emissions during the evening peak hours. The NPF event was observed clearly at around 10:30-15:00 when traffic emissions were low due to a decrease in traffic volume, but TNC was found to be high (12289 \# cm^{-3}) and eBC (known as a traffic emission marker) concentrations were low ($0.45 \text{ \mu g m}^{-3}$). The highest temperature was about $13.8 \text{ }^\circ\text{C}$ and relative humidity was around 30-40 % at around 10:30-15:00. In the second case (Figure 3.13b), NPF occurred at around 12:00-13:50, in similar conditions to the previous example: TNC was found high (15516 \# cm^{-3}) and eBC was low (0.33 \# cm^{-3}). The temperature was similar at $14.4 \text{ }^\circ\text{C}$ with a low relative humidity (40-50%). Conditions observed during these NPF events, of higher temperature and lower relative humidity, are typical as they produce the stable atmospheric condition which are the most favourable for the formation of new particles (Boy and Kulmala, 2002; Holmes, 2007; Kulmala and Kerminen, 2008). Higher mean N_{total} and N_{nuc} were found for NPF event days at 2664 \# cm^{-3} and 7296 \# cm^{-3} , compared to that for non-event days (1901 \# cm^{-3} and 6766 \# cm^{-3}) at the AURN and BF sites (Table 3.8). These results suggested that the burst of nucleation mode particles encouraged by the NPF had a significant influence on the increasing particle number concentration during the campaign period at both sites.

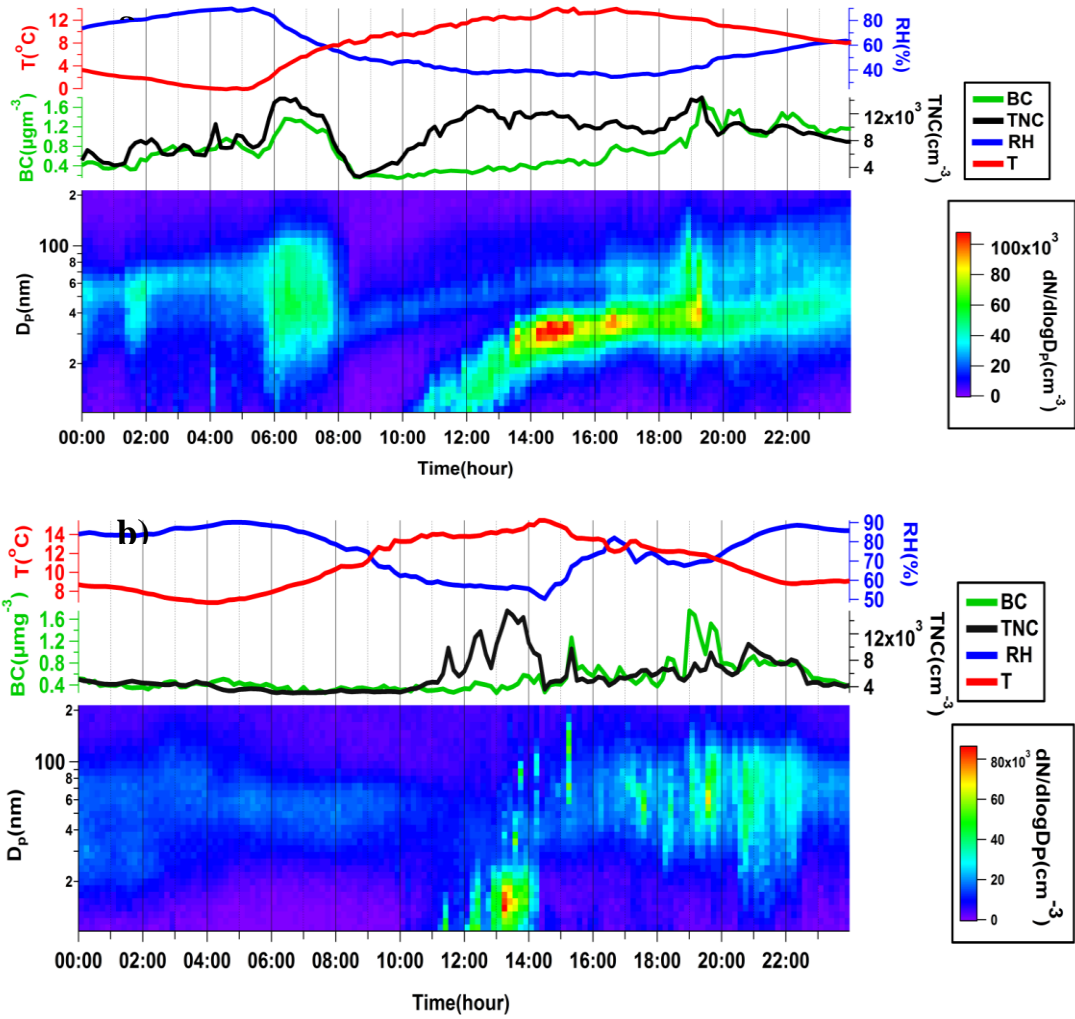


Figure 3.13: The NPF events measured on a) 3rd May 2014 (BF site), and b) 27th April 2014 (AURN site). From bottom to top, the parameters are: (i) Average PNSD, (ii) N_{TOTAL} , and eBC mass concentrations, (iii) temperature, and relative humidity.

Table 3.8: Statistics of particle number concentrations measured during NPF and non-NPF event days.

	Particle Modes (# cm ⁻³)	Avg	Median	95 th percentile	S.D	No. of data
AURN Site						
	N_{total}	2664.5	2015.8	6854.40	2049.3	576
NPF event days	N_{acu}	3475.5	2941.8	8062.99	2378.4	576
	N_{Aitken}	1156.9	855.26	3078.42	932.75	576
	N_{nuc}	7296.9	6422.4	14884.28	3956.6	576
Non-event days	N_{total}	1901.3	1450.2	4638.22	1770.9	3769
	N_{acu}	3225.2	2499.5	7763.36	2683.3	3769
	N_{Aitken}	1640.1	1279.2	3885.43	1451.4	3769
	N_{nuc}	6766.6	5554.7	14856.55	4629.3	3769
BF Site						
	N_{total}	1994.7	1593.2	4923.37	1550.0	1565
NPF event days	N_{acu}	2630.3	2094.6	6363.31	1841.1	1565
	N_{Aitken}	727.84	567.77	1782.82	542.16	1565
	N_{nuc}	5352.9	4808.5	10831.69	2855.6	1565
Non-event days	N_{total}	1259.4	993.71	3128.39	1185.4	4862
	N_{acu}	2382.5	2046.6	4670.57	1396.4	4862
	N_{Aitken}	948.67	824.24	1919.25	537.58	4862
	N_{nuc}	4590.6	4169.0	8766.80	2385.9	4862

3.3.5 Nucleation event characterisation

Table 3.9 summarises the GR, J_{10-25} , CS, Q, and relevant measurements for respective nucleation events observed in this study. The parameters (GR, J_{10-25} , CS, and Q) were calculated as described earlier. At the AURN site, the GR values varied in the range from 6.6 to 8.33 nm h⁻¹ (average 7.42 nm h⁻¹), the J_{10-25} values between 0.89 and 1.82 cm⁻³ s⁻¹ (average 1.3 cm⁻³ s⁻¹). At BF site, the GR values varied in the range from 1.74 to 8.77 nm h⁻¹ (average 5.3 nm h⁻¹), the J_{10-25} values between 0.41 and 1.70 cm⁻³ s⁻¹ (average 1.17 cm⁻³ s⁻¹). The average values of GR, and J_{10-25} at AURN site were higher than BF site, which can be explained by impact of meteorological conditions From March to May at both sites. In addition, the average of GR found in this study in line with the range of typical growth rate of 1-20 nm h⁻¹ (Kulmala et al., 2004). The variations in GR values were related to the meteorological condition (T, and RH), and the production of condensable vapours (Yli-Juuti et al., 2011). The J_{10-25} values observed at both sites were lower than observed at other urban areas such as Helsinki (2.4 cm⁻³ s⁻¹, (Hussein et al., 2008)), Marseille (3-5.3 cm⁻³ s⁻¹, (Petäjä et al., 2007), and Budapest (4.2 cm⁻³ s⁻¹, (Salma et al., 2011)). However, the values at both sites were higher than the observations in clean environments such as Hyytiälä (0.8 cm⁻³ s⁻¹, (Dal Maso et al., 2005)), and Hohenpeissenberg (1 cm⁻³ s⁻¹, (Birmili et al., 2003)). The formation rate of nucleation mode particles is known to be influenced by the chemical and physical condition of the atmosphere. Nucleation mode particles related to traffic emissions are produced behind the exhaust tailpipe as the exhaust gases are cooled and diluted in ambient air. These particles are secondary, whereas since they are formed close to the source, it can be called as primary. In this study, the J_{10-25} was impacted by the primary and secondary sources in Leicester urban areas. It should be noted that the low values of J_{10-25} in this study, might be associated to the relatively high concentration of pre-existing particles in Leicester environment.

The CS average values were 5.7, and 4.53×10^{-3} s⁻¹, the average Q values were 5.9, and 4.23×10^5 cm⁻³ s⁻¹, at AURN, and BF sites, respectively (Table 3.9). The CS average values observed in this study were comparable with the other studies in European cities such as Athens (0.006 s⁻¹, (Kulmala et al., 2005)), and Helsinki (0.006 s⁻¹, (Hussein et al.,

2008)). Kulmala et al. (2005) observed CS values between 1.3×10^{-2} and $0.6 \times 10^{-4} \text{ s}^{-1}$ in different locations. The CS was normally higher in more polluted areas such as New Delhi and Nanjing ($2.4\text{-}7 \times 10^{-2} \text{ s}^{-1}$, (Herrmann et al., 2014; Kulmala et al., 2005)), while the CS values in European cities (such as Athens and Marseille) were 5-10 times lower (Kulmala et al., 2005). The CS in the rural areas is approximately two to three times lower than urban environments due to the variance in number concentrations and size distributions. The Q average values found in this study were similar with other European urban background sites ($2.6 \times 10^5 - 1.6 \times 10^6 \text{ cm}^{-3} \text{ s}^{-1}$, (Kulmala et al., 2005)). It can be seen that more vapours should be involved in the particle growth processes to prevent the new particle formation in a polluted urban areas as a result the high vapour source rate obtained. For example, the high source rate of condensable vapour observed in New Delhi ($0.9\text{-}1.4 \times 10^7 \text{ cm}^{-3} \text{ s}^{-1}$, (Kulmala et al., 2005), and North Plain China ($0.6\text{-}2.5 \times 10^6 \text{ cm}^{-3} \text{ s}^{-1}$, (Wang et al., 2013)). It can be seen that high hourly average O_3 levels observed during NPF events at both site (Table 3.9). The mass concentrations of O_3 were higher than $60 \mu\text{g m}^{-3}$ in all days during NPF events, and reached maximum $89.98 \mu\text{g m}^{-3}$ on 3rd May 2014 (Table 3.9), proposing that O_3 and NPF has similar sources or formation processes and most likely the photochemical among the precursors (such as VOCs, NO_x , and SO_2) of O_3 and NPF. As such, O_3 can be a significant indicator for NPF event occurrence. In addition, O_3 can also be the precursor of NPF as it is responsible for the production of condensable compounds through direct reactions (with VOCs), and indirect formation of other oxidants (such as OH and HO_2). However, NO_x as the precursor gas in photochemistry, did not show significant correlation with NPF. The average concentrations of NO_x were found low (lower than $\sim 22 \mu\text{g m}^{-3}$) during NPF event days, and reached minimum ($\sim 9 \mu\text{g m}^{-3}$). It might be related to the increase of solar radiation during NPF which would enhance the decline of NO_x via the complex photochemical reactions.

Table 3.9: Summary of N_{total} ($\# \text{ cm}^{-3}$), and N_{nuc} ($\# \text{ cm}^{-3}$), O_3 ($\mu\text{g m}^{-3}$), NO_x ($\mu\text{g m}^{-3}$), and NPF event characteristics (GR (nm h^{-1}), J_{10-25} ($\text{cm}^{-3} \text{ s}^{-1}$), CS (10^{-3} s^{-1}), Q ($10^{-5} \text{ cm}^{-3} \text{ s}^{-1}$)) during the NPF event days.

Site	Event date	Start	End	GR	J_{10-25}	CS	Q	N_{total}	N_{nuc}	O_3	NO_x
AUR N	07/03/2 014	11:20	14:00	8.3	1.10	5	5.8	8582	5922	68.	22
	15/03/2 014	11:40	13:00	8.1	1.40	5.4	6.1	5246	3567	67	18
	16/03/2 014	12:30	14:20	6.6	1.82	5.7	5.2	8264	6147	68	17
	24/03/2 014	09:50	11:20	6.6	0.89	7	6.5	8720	6193	61	18
BF	08/04/2 014	12:20	13:40	5.4	1.27	1.8	1.3	5418	4108	69	22
	11/04/2 014	10:00	12:30	4.9	1.46	3.1	2.8	6525	4934	70	21
	27/04/2 014	12:00	13:50	4.7	1.40	3.4	3	5456	4322	73	9
	02/05/2 014	10:00	12:30	1.7	0.70	7.8	6.5	5742	9303	74	18
	03/05/2 014	10:30	15:00	5.6	0.41	6.3	7.3	6685	4468	89	9
	07/05/2 014	11:30	13:50	4.2	0.83	4.5	3.7	8222	6008	64	21
	09/05/2 014	12:00	13:10	5.8	0.89	2.5	2.1	5155	3898	62	20
	10/05/2 014	12:20	13:50	7.2	1.70	2.7	2.7	1092	9783	65	21
	14/05/2 014	10:40	12:10	8.7	1.45	5.4	6.6	6802	4060	69	22
	17/05/2 014	10:10	12:20	4.1	1.62	7.7	6.3	6037	4816	79	22

3.4 Conclusions

A SMPS was utilized for the real-time measurement of particles in the size range of 10 nm to 1093 nm, to characterize the evolution of particle number size distribution and new particle formation (NPF) events in Leicester, UK. The diurnal and weekly variations of size-segregated particle number and eBC mass concentrations were characterised. At the AURN site the N_{nuc} , N_{Aitken} , N_{accu} , N_{total} , and eBC mass concentrations were 2002, 3258, 1576, 6837 # cm³, and 1.7 µg m⁻³, and at the BF site 1455, 2407, 874, 4737 # cm³, and 0.77 µg m⁻³, respectively. N_{total} seem to be dominated mostly by the N_{nuc} , and N_{Aitken} particles at both sites, demonstrating that particles at both sites are predominantly influenced by traffic emissions. The highest N_{nuc} and N_{Aitken} were observed during workdays, and the lowest concentrations observed during weekends, especially Sundays. The temporal variation of N_{accu} was not significant. The diurnal variation of the N_{total} , eBC, and NO_x concentrations demonstrated very similar behaviour at both sites, with the maximum concentrations occurring during morning and late evening hours and the lowest variation during the afternoon hours. This behaviour could be attributed to primary emissions of ultrafine particles (e.g. traffic) and the temporal evolution of mixing layer. According to wind polar plots it can be observed that more particles come from the directions that the busy roads and residential areas in the vicinity, suggesting that aerosol particles originate mainly from traffic and domestic heating emissions. Finally, this short-term study has shown that ultrafine particles are increased by NPF events at both sites; however, not enough to conclude that new particle formation is a major source of atmospheric particles in Leicester. In order to be able to reveal the impact of NPF on ultrafine particles longer term measurements of PNSD in Leicester would be necessary

Chapter Four

Quantifying primary and secondary source contributions to ultrafine particles in the UK urban background

This Chapter has been published in Atmospheric Environment (Hama et al., 2017c)

What are the major primary and secondary sources of UFPs in the urban area of Leicester?

A number of studies have reported quantifying the sources and processes that contribute to UFP in urban areas (Fernández-Camacho et al., 2010; González and Rodríguez, 2013; González et al., 2011; Kulmala et al., 2016; Reche et al., 2011; Rodríguez and Cuevas, 2007). However, no studies to date report on quantifying the sources and processes that contribute to UFP in UK cities. In this context, the aim of this paper is to study the factors responsible for the variability of TNC, equivalent black carbon mass concentration (eBC), and the gaseous pollutants at the AURN site representative the urban background site in Leicester, with focus on the process of formation of secondary UFPs with high impact on the variability of TNC. To our knowledge, the study reported here represents the first that reveals variability of TNC and identifies the main sources of TNC in the city of Leicester, UK.

4.1 Introduction

Ultrafine particles (UFPs, $D_p < 100$ nm) are ubiquitous in the urban environment (Kumar et al., 2014), and are of concern owing to their adverse effects on human health (Araujo et al., 2008; Atkinson et al., 2010). UFPs vary from larger sized ambient particles in their potential for lung deposition and translocation to other parts of the body (HEI, 2013). Previous studies have shown that UFPs easily penetrate the respiratory system and transfer to the extra-pulmonary organs such as the central nervous system (Elder et al., 2006; Elder and Oberdörster, 2006; Oberdorster et al., 2004).

Sources of UFPs in the urban atmosphere include primary emissions sources - from motor vehicles, coal-fired power plants, gas-fired facilities, and biomass burning in winter (Kumar et al., 2014; Morawska et al., 2008; Wehner et al., 2009; Zhu et al., 2002), and those formed as new particles via nucleation (Brock et al., 2002; Holmes, 2007; Kulmala and Kerminen, 2008). The major source of primary UFPs in urban areas is combustion, with previous studies demonstrating that UFP numbers correlate with the local traffic activity, in particular in the morning and afternoon rush hours (Alam et al., 2003; Harrison and Jones, 2005). These particles can be produced in the engine or in the ambient air after emission from the vehicle tailpipe (Charron and Harrison, 2003; Shi et al., 1999). Primary UFPs associated to traffic are released during the dilution and cooling of vehicle exhaust (Charron and Harrison, 2003; Kittelson et al., 2006) or formed by fuel combustion such as carbonaceous soot (Kittelson, 1998; Shi et al., 2000).

Previous studies found that total particle number consists of 80-90% UFPs (Mejia et al., 2008; Rodríguez et al., 2007; Wehner and Wiedensohler, 2003). Reche et al. (2011) have shown from the characterisation of total particle number concentrations in various European urban background sites that total particle number is a good representation of the UFPs in urban area.

Previous studies measuring UFPs in urban areas have been measured particles larger than 7 nm (Harrison and Jones, 2005; Shi et al., 2001), and 3 nm (Shi et al., 1999). Many studies have indicated that the two main sources of UFPs in urban areas (Brines et al., 2015; Dunn et al., 2004; Morawska et al., 2008; Reche et al., 2011; Rodríguez and Cuevas, 2007) are:

- *Vehicle exhausts emissions.* These particles tend to exhibit bimodal size distribution, with a nucleation (<20 nm) and a carbonaceous mode (50-200 nm).

The nucleation mode (<20 nm) particles are not produced directly from vehicle exhaust emissions, but are created through nucleation (gas-to-particle conversion). In urban areas this occurs after rapid cooling and dilution of exhaust emissions when the saturation ratio of gaseous mixtures of low volatility (i.e. sulphuric acid) reaches a maximum (Arnold et al., 2006; Burtscher, 2005; Charron and Harrison, 2003; Kittelson et al., 2006). The carbonaceous mode (50-200 nm) is mainly composed of soot (Casati et al., 2007; Rose et al., 2006).

New particle formation in ambient air. This process may be caused by the photochemical reactions of naturally emitted gaseous precursors in ambient air by “*in-situ* nucleation” happening after emission. This mechanism includes two main steps, with nucleation of an initial cluster (<1 nm) and the initiation of such cluster resulting in particle growth (Kulmala et al., 2004). It is considered that the nucleation of sulfuric acid gas molecules play a significant role in the formation of such stable clusters, and may also contribute in particle growth by condensation (Kulmala et al., 2006). Recent studies have shown that ammonium and highly oxidised organic molecules may also play an important role in nucleation (Ehn et al., 2014; Kirkby et al., 2011).

A number of studies have reported quantifying the sources and processes that contribute to UFP in urban areas (Fernández-Camacho et al., 2010; González and Rodríguez, 2013; González et al., 2011; Kulmala et al., 2016; Reche et al., 2011; Rodríguez and Cuevas, 2007). However, no studies to date have reported the quantification of the sources and processes that contribute to UFP in UK cities. In this context, the main aim of this paper is to study the factors responsible for the variability of TNC, eBC, and the gaseous pollutants at the Automatic Urban Rural Network (AURN) site representative of the urban background site in Leicester. A specific focus on exploring the relative contributions of primary and secondary sources to the total particle number concentrations in Leicester is made. To our knowledge, this study represents the first that explores the variability of TNC and its sources in the UK urban background.

The study was carried out between January 2014 and December 2015 over which time TNC was measured concurrently with eBC, nitrogen oxides concentration (NO_x), and particle number size distributions (PNSD) at the AURN site in the Leicester (UK). This study was carried out as part of the JOint Air QUality INitiative (JOAQUIN, www.joaquin.eu), an INTERREG IVB funded European project, aimed at supporting

health-oriented air quality policies in Europe (Cordell et al., 2016; Hama et al., 2017b; Hama et al., 2017a; Hofman et al., 2016).

4.2 Methods

4.2.1 Measurement site

Measurements were carried out at the University of Leicester urban background site (lat 52°37'11.36" N, long 1°07'38.32" W) a permanent site which is part of both JOAQUIN UFP NWE observatory system and the national Defra Automatic Urban Rural Network (AURN). The site is located on the University of Leicester campus (http://uk.air.defra.gov.uk/networks/site-info?uka_id=UKA00573) and is shown in Figure 4.1. The nearest road is University Road (20 m north-west) and the nearest main road is Welford Road (140 m south-south west). According to traffic counts by the Department for Transport, the traffic intensity on the Welford Road was about 22600 vehicles/day in 2014 (<http://www.dft.gov.uk/traffic-counts>, count point 36549). For a detailed overview of the monitoring sites and the JOAQUIN project, the reader is referred to the final report (Joaquin, 2015a).

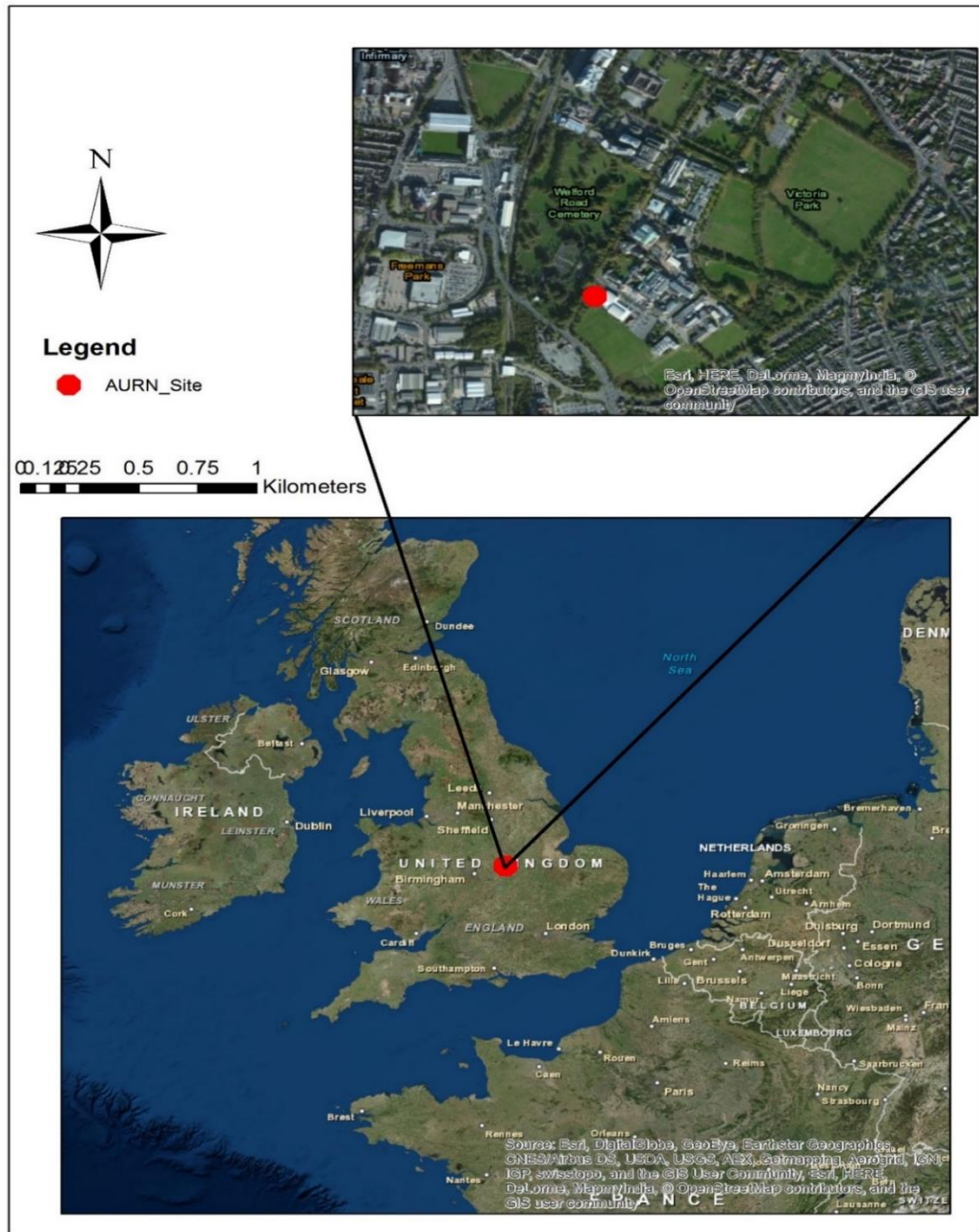


Figure 4.1: Leicester and location of the sampling site (denoted AURN).

4.2.2 Instrumentation

Table 4.1 summarizes the availability of monitors for PNC, TNC, eBC, PM_{2.5} and the gaseous pollutants at the AURN site. Size-resolved particle number concentrations (PNC; # cm⁻³) were obtained using an UFP Monitor (UFPM, TSI 3031). PNC were quantified in six size classes (20-30, 30-50, 50-70, 70-100, 100-200 and > 200 nm), using an UFPM (Table 4.1). For this study five channels (20-30, 30-50, 50-70, 70-100, 100-200 nm) were used and the size class (>200 nm) was ignored owing to low number concentrations (Joaquin, 2015a). The UFP monitor's operation is based on electrical diffusion charging of the particles, size segregation by means of a DMA, followed by aerosol detection using a Faraday cup electrometer (Hofman et al., 2016; Joaquin, 2015a). The performance of this instrument has been explored against other UFP measurement system in Hofman et al. (2016). The TNC was measured by a Water-Based Condensation Particle Counter (WCPC, TSI Environmental Particle Counter (EPC) model 3783 <http://www.tsi.com/environmental-particle-counter-3783>).

Table 4.1: Air quality instrumentation at Leicester AURN site during the sampling period.

Air quality parameters	Monitors
PNC (six size bins)	UFP Monitor TSI 3031 (~20-200nm)
TNC	WCPC TSI Model 3783 (7-1000nm)
NO, NO ₂ , NO _x	Teledyne API Model T200 Chemiluminescence NO/NO ₂ /NO _x Analyzer
eBC	MAAP (Thermo Scientific 5012) with PM _{2.5} inlet
PM _{2.5}	TEOM-FDMS
CO	Teledyne API Model T300U Trace-level Gas Filter Correlation CO Analyzer (IR Absorption)
O ₃	UV absorption

The TSI instruments (UFP monitor and W-CPC) were connected to an environmental sampling system (TSI 3031200). The components of the TSI 3031200 are a PM₁₀ inlet, sharp cut PM₁ cyclone, flow splitter and Nafion dryer (reduces humidity to less than 50% RH).

The mass concentration of equivalent black carbon (eBC) was measured by a Multi-angle Absorption Photometer (MAAP Thermo Scientific model 5012) for the whole period (Petzold et al., 2013). The MAAP determines particle light absorption due to the light transmission and backscattering at two angles of particles collected on the filter tape (glass fibre type GF10). The eBC mass concentration is calculated using a constant mass absorption cross section of 6.6 g/m².

Nitrogen oxides were also measured by a Thermo 42i NO-NO₂-NO_x monitor. This monitor uses chemiluminescence technology to measure the concentration of nitrogen oxides in the air. It has a single chamber, single photomultiplier tube design that cycles between the NO and NO_x mode.

Meteorological data (temperature, relative humidity, solar radiation and wind speed and direction) were provided for the 2014 by the Air Quality Group from the Leicester City Council. The station is located 4.9 km away from the AURN urban background monitoring site, and the meteorological data for 2015 were measured at AURN site.

4.2.3 Data processing and analysis

The raw 10 min-data were validated by screening for irregularities and removing data collected during instrument errors and maintenance periods. All validated data were subsequently aggregated to 30 min intervals. Data analyses have been carried out using the Open-air software package (Carslaw, 2015; Carslaw and Ropkins, 2012) using R software (R Core Team, 2015).

4.3 Results and discussion

4.3.1 Annual Variation

Monthly particle TNC and PNC (five size classes), and other air quality parameters, such as eBC, NO_x, PM_{2.5}, O₃, and CO are shown in Figure 4.2 and Figure S4.1. Figure 4.2 shows that higher values of TNC and PNC (except small sizes, 20-30 nm) were found in the cooler months. TNC profile shows a peak in winter (November to January), which might be associated with factors such as an increase in wood burning for domestic heating in Leicester (Cordell et al., 2016), reduced dispersion of local sources and a low mixing height in winter. In addition, TNC shows two peaks, one in March and the other in June (Figure 4.2). This could be related to NPF since previous studies have demonstrated that NPF occurs in spring and summer at this site (Hama et al., 2017b; Hofman et al., 2016). However, therefore, PNC (100-200nm) concentrations were observed highest in winter and lowest in summer. This can be linked to the above reasons, and also meteorological factors (dilution effect, (see Hama et al., 2017a)) that have a significant impact in seasonal variations. For example UFP will be influenced by the temperature dependent volatility of the traffic-generated particles which produces high particle number concentrations during the cold period (Bigi and Harrison, 2010; Charron and Harrison, 2003; Hofman et al., 2016; Mishra et al., 2012) coupled to cold period boundary layer stability. Interestingly, high concentrations of PNC (small sizes, 20-30 nm) were found during the spring and summer months. In particular, this is clear for the small particles (20-30 nm) (Figure 4.2). The observed increase in spring may be related to NPF which has been observed at this site (Hama et al., 2017b; Hama et al., 2017a; Hofman et al., 2016).

A summary of the pollutant concentrations at AURN site are given in Table S4.1. TNC and eBC concentrations observed were comparable to levels found in other European urban background sites (Hofman et al., 2016; Keuken et al., 2015; Reche et al., 2011). The mean annual TNC and eBC concentration were 8022 # cm⁻³ and 1.45 µg m⁻³, with a standard deviation of 5514 # cm⁻³ and 1.39 µg m⁻³, respectively. The annual average PNC for the five size classes were: i) 1457 # cm⁻³ (20-30 nm), ii) 1704 # cm⁻³ (30-50 nm), iii) 1193 # cm⁻³ (50-70 nm), iv) 1059 # cm⁻³ (70-100 nm), v) 980 # cm⁻³ (100-200 nm). According to these results it can be concluded that ultrafine particles (particles < 100 nm) were the dominant particle size range.

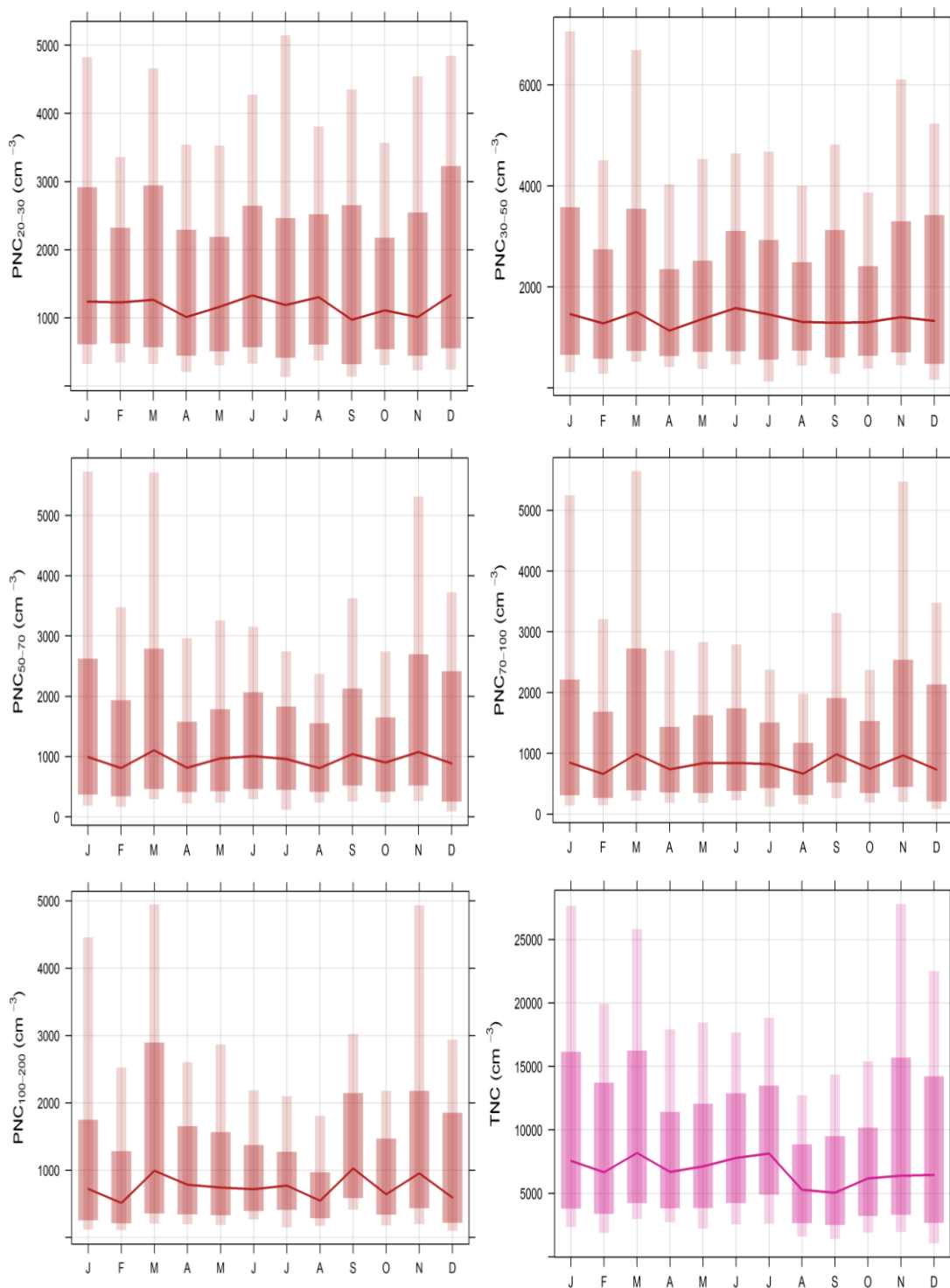


Figure 4.2: Monthly variations in the median, 25/75th and 5/95th quantile values for PNC size classes, and TNC for 2014 at AURN site.

The annual average levels of the other pollutants as shown in Table S4.1 are comparable to concentrations reported in other European urban areas (Hofman et al., 2016; Pérez et al., 2010 and references therein; Reche et al., 2011). The annual patterns of NO_x, CO, eBC, and PM_{2.5} are comparable to one another, with the highest levels occurring in the cold season and the lowest in summer (Figure S4.1). The cold period average concentrations were larger by a factor of 1.5, 1.3, 1.35, and 1.3 with respect to the warm mean value for NO_x, CO, eBC, and PM_{2.5}, respectively. The highest levels of these constituents in cold season are attributable to emissions from a variety of sources including traffic and an increase in domestic heating, for example from wood burning as reported in recent study at this site (Cordell et al., 2016), coupled to reduced dispersion (Harrison et al., 2012). The annual variations are also modulated by the annual variations in meteorological, dynamic and synoptic conditions (Barnpadimos et al., 2012; Bigi and Harrison, 2010; Reche et al., 2011; Ripoll et al., 2014). As would be expected, the O₃ annual variation shows a minimum in October and November and a maximum in spring, especially in May (Monks, 2000). The low O₃ levels in autumn and winter are related to lower temperatures, less solar radiation, and also the chemical titration reaction with NO from the higher emissions of NO_x associated with domestic heating in autumn and winter months leading to a decrease in O₃, as observed in other studies (Lin et al., 2011; Lin et al., 2008).

Finally, it is clear that the measured TNC and PNC (particularly small particles, 20-30nm) in cold period were similar to warm period which factor 1.1 and 1.01 for TNC, and PNC_{20-30nm}, respectively. It can be concluded that domestic heating and meteorological conditions in cold months, and NPF in warm period have great impact on seasonal variations on particle number concentrations in Leicester.

4.3.2 Weekly and Daily variations

The weekly cycle of TNC and PNC for 2014 at the AURN site are shown in Figure 4.3, and TNC for 2015 is shown in Figure S4.2. TNC average concentrations were slightly lower at the weekend (7500 # cm⁻³), than working days (8400 # cm⁻³) (Figure 4.3), indicating that the pollutant levels were influenced not only by anthropogenic emissions (such as traffic emissions), but also could be associated with local or regional non-anthropogenic origin sources. Moreover, PNC size range concentrations showed a

weekly cycle (Figure 4.3), with the lowest average levels occurring during weekends and the highest on weekdays, especially on Mondays. The average concentrations of PNC_{20-30} , PNC_{30-50} , PNC_{50-70} , PNC_{70-100} , and $PNC_{100-200}$ for working days are 1516, 1738, 1206, 1068, and 986 # cm^{-3} and for weekends are 1363, 1664, 1143, 1017, 922 # cm^{-3} , respectively.

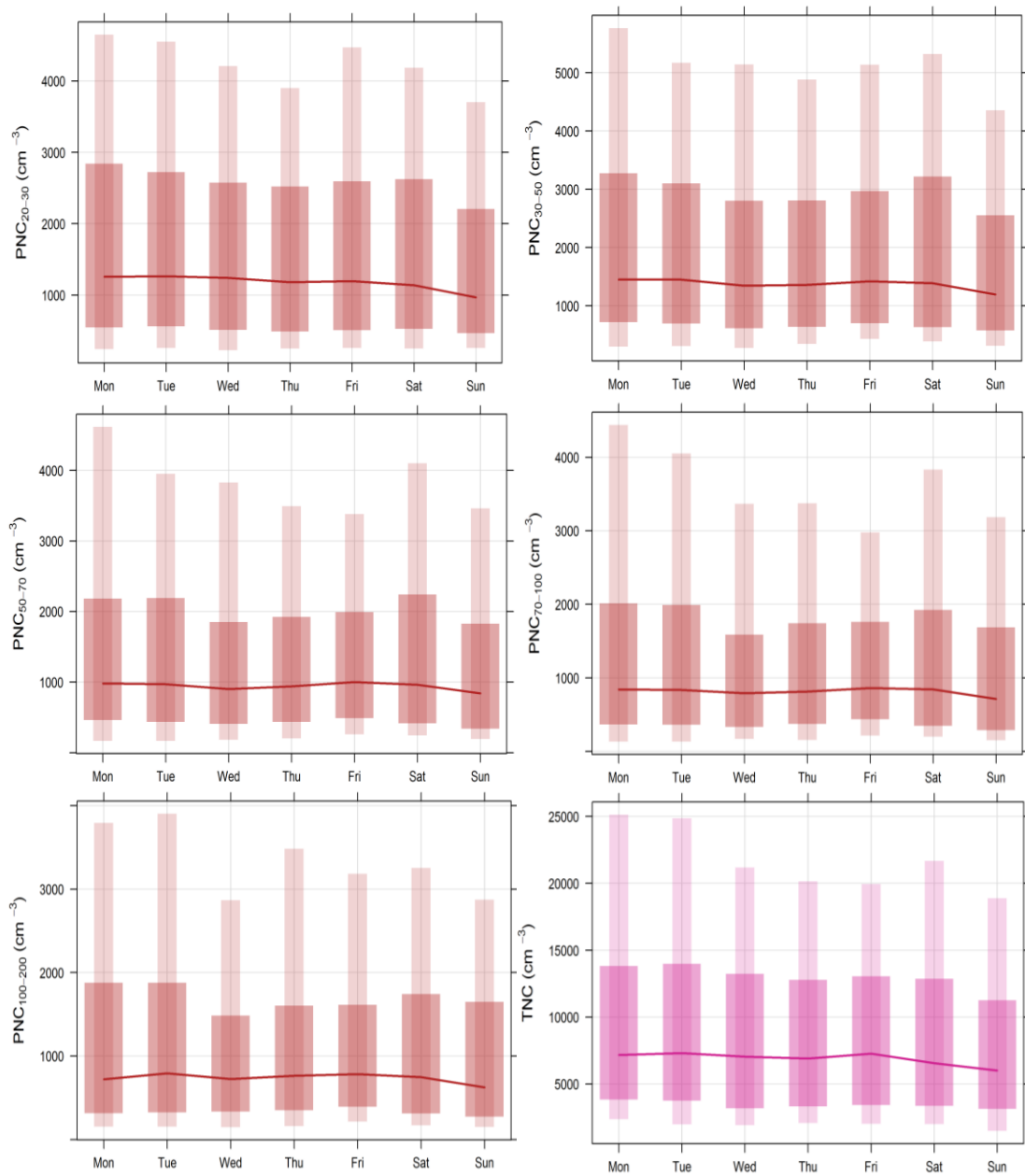


Figure 4.3: Daily variations in the median, 25/75th and 5/95th quantile values for PNC size classes, and TNC for 2014 at the AURN site.

eBC also showed the highest mean values ($1.41 \mu\text{g m}^{-3}$) on working days (Figure S4.2), and lower concentrations ($1.1 \mu\text{g m}^{-3}$) during weekends. This is probably related to decreased traffic emissions during weekends. The weekly cycle of gaseous pollutants (NO, NO₂, NO_x, CO, O₃), and PM_{2.5}, concentrations at AURN site are shown in Figure S4.2. All pollutants, except ozone, showed a similar pattern with a minimum at weekends, especially on Sundays. However, on Sundays O₃ concentrations peaked, due to the so-called O₃ weekend effect (Larsen et al., 2003). The observed behaviour is consistent with the previous studies (Bigi and Harrison, 2010; Pérez et al., 2010; Ripoll et al., 2014; Yoo et al., 2015). The eBC diurnal patterns are shown in Figure 4.4. eBC shows the same profile as the traffic-related gaseous pollutants in the morning owing to the morning rush hour (high traffic, low wind speed), but conversely to the gaseous pattern, the eBC concentrations decreased sharply after the morning rush hour until increasing again during evening rush hour. This might be associated to decreased traffic volume, increased wind speed (high dilution at midday), and increased mixing height. Similar results were found in other European urban background sites (Annual Report for the UK Black Carbon Network, 2014; Dall'Osto et al., 2013; Hofman et al., 2016; Pérez et al., 2010; Reche et al., 2011; Rodríguez et al., 2008). The variation of the eBC in warmer months (May-Sep), however, shows a weaker diurnal pattern, with a stronger diurnal variation being observed during the cold period most likely caused by the synoptic condition, and may relate to the larger domestic heating emissions during the evening (Allan et al., 2010; Cordell et al., 2016) coupled to greater atmospheric stability.

The daily variation of TNC was similar to that of eBC, suggesting it is also highly influenced by traffic emissions. The profiles matched well during the cold period, however, during summer season the TNC peaks, especially the second peak (corresponding to the evening rush hour), which became less obvious or later in the colder months. This can be explained by similar reasons to the patterns observed in eBC concentration: during the night the TNC decreased owing to the low traffic volumes, which when combined with the decrease of the boundary layer height, favours lower ultrafine particles numbers owing to the condensation and coagulation processes (Minoura and Takekawa, 2005; Pérez et al., 2010). Interestingly, during the warm period another peak of the TNC at noon was seen, as shown in Figure 4.4, which did not follow the eBC peaks. It can be concluded that the TNC peak cannot be from primary particle emissions from traffic. This extra TNC peak can be attributed to NPF resulting from

photochemical nucleation reactions from gaseous precursors (Hama et al., 2017b; Hofman et al., 2016). This midday peak coincides with the higher solar radiation, an increase in wind speed (not shown) and the growth of the mixing layer (Rodríguez et al., 2007). The detail of primary and secondary sources of TNC will be discussed in the section 3.3 and 3.4.

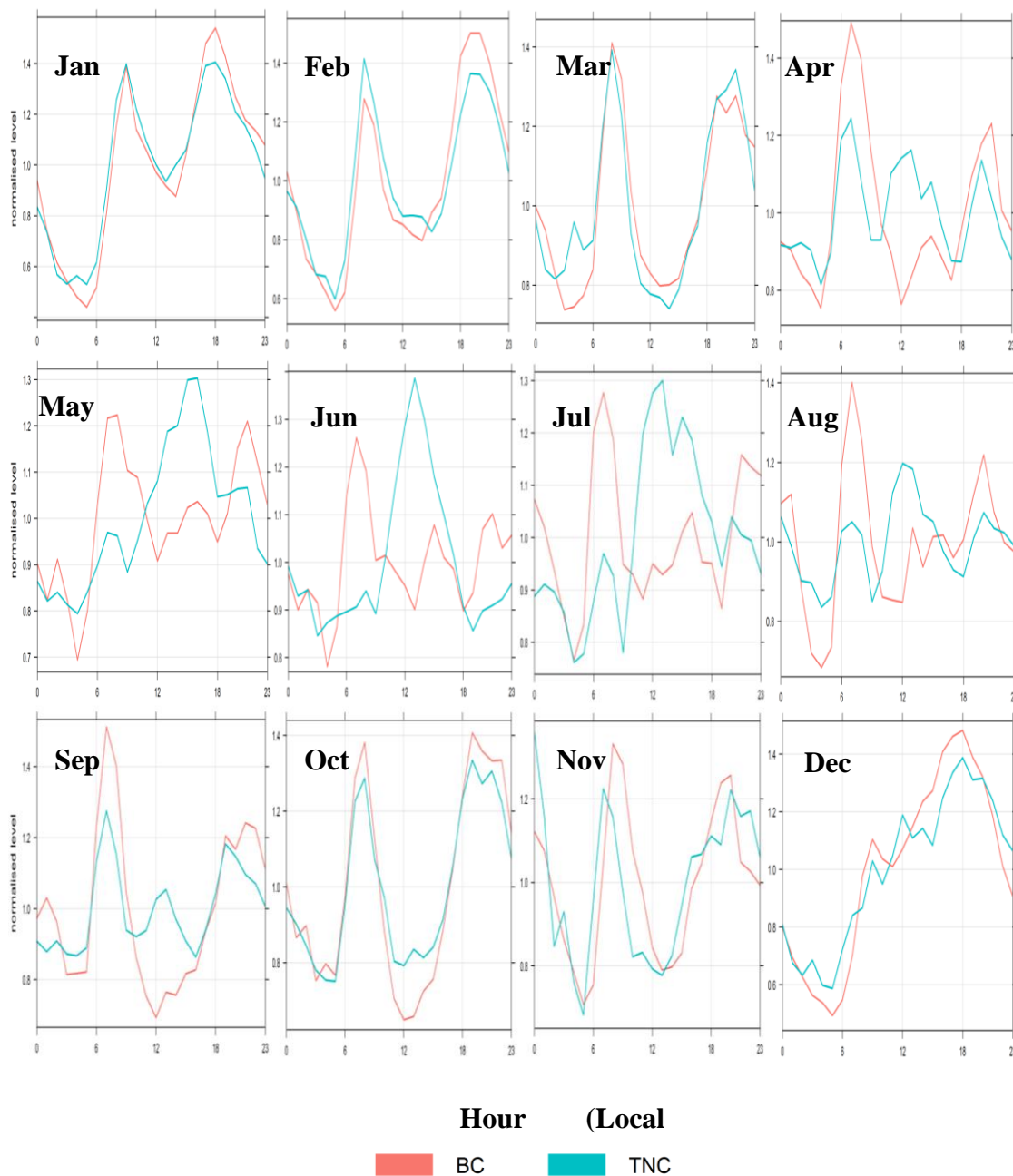


Figure 4.4: Diurnal variations of eBC, and TNC concentrations for each month in 2015 at AURN site.

The daily cycle of PNC (five size bins) showed a similar variation to the traffic related pollutants such as eBC and TNC as shown in Figure 4.5. During the cold period, the diurnal variation of PNC (mostly UFPs) clearly demonstrated two peaks which followed morning and afternoon traffic rush hours. However, like the other parameters measured during warm period the daily cycle was weaker, and the evening peak was not clearly observed. There is a notable difference in the diurnal cycles of PNC₂₀₋₃₀ (red line) during the warm season. PNC₂₀₋₃₀ shows another peak at midday, as recorded for the TNC. Those particles can be attributed as the small particles from NPF (Hama et al., 2017b).

Levels of the gaseous pollutants (NO, NO₂, NO_x, O₃), monitored at the AURN site was predominantly influenced by vehicle traffic emission, evolution of the mixing layer, and meteorological conditions. Figure S4.3 shows the diurnal patterns of the atmospheric gaseous pollutants (NO, NO₂, NO_x, and O₃) for the year 2015. It can be seen all the gaseous pollutant peaks (except O₃) followed the diurnal variation of vehicular traffic emissions, with increasing levels of the gaseous pollutants measured in the morning rush hour (high traffic intensity, poor dispersion), which then decreased during the day, due to atmospheric dilution effects, before increasing once more in the evening rush hour. Finally, it can be concluded that particle number concentrations are influenced by primary and secondary sources in Leicester (see Section 3.3 for more detail).

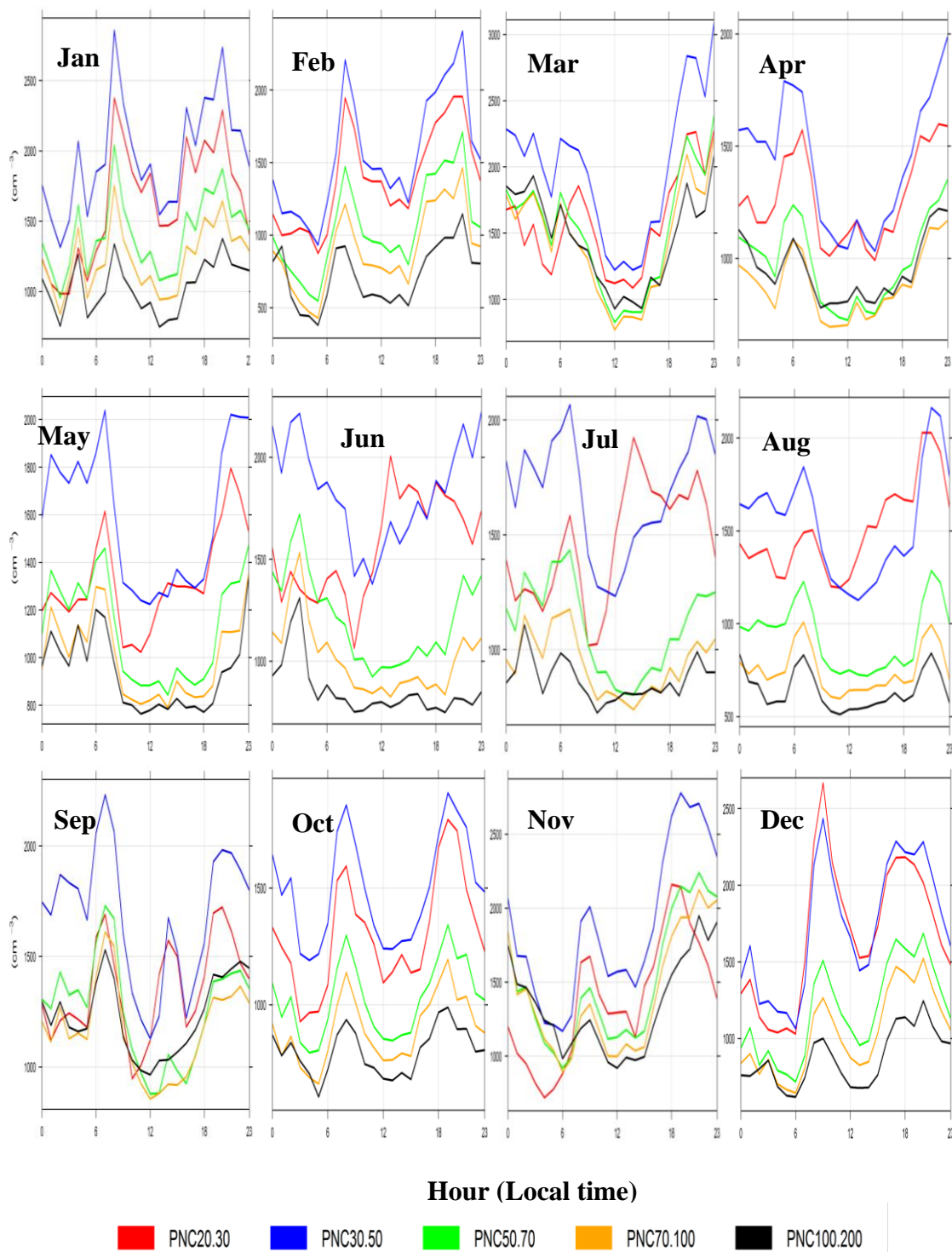


Figure 4.5: Diurnal variations of different size channel of PNC for each month in 2014 at the AURN site.

4.3.3 Exploring the Relationship between total particle number and black carbon concentrations

Traffic emissions in the urban environment in Europe tend to drive the correlation between TNC and eBC (Fernández-Camacho et al., 2010; Pérez et al., 2010; Reche et al., 2011; Rodríguez and Cuevas, 2007; Rodríguez et al., 2007). The correlation between TNC and eBC has been analysed at the Leicester AURN site using the methodology described by Rodríguez and Cuevas (2007). The correlation between TNC and eBC for four different time periods of the day (07:00-09:00, 11:00-14:00, 17:00-20:00, and 00:00-04:00) is shown in Figure 4.6. The selection of these time ranges is based upon the diurnal variations of TNC and eBC, which are mostly governed by traffic emissions and atmospheric dynamics in the Leicester urban environment. At any time of the day, the TNC versus eBC scatter plots clearly showed two defined linear lines with slopes S1 and S2, representing the minimum and maximum TNC/eBC ratios, respectively (Figure 4.6). S1 represents the minimum TNC/eBC ratio, which is interpreted as representative of the primary particles, mostly from vehicle exhaust emissions. S2 is the maximum TNC/eBC ratio (Figure S4.4), which is interpreted as arising predominately from secondary particles, mainly from NPF during the dilution and cooling of the vehicle exhaust emissions in the urban environment (Rodríguez and Cuevas, 2007). Table 4.2 shows the values of slopes S1 and S2 found at different times of the day. During the morning rush hours (07:00-09:00), when the NO_x peaks, owing to vehicle exhaust emissions, values of S1= 2.53×10^6 particles /ng eBC, and S2= 2.85×10^6 particles /ng eBC were obtained. The S1 value found at the AURN site (Table 4.3) was higher than values found in Hyytiälä and Nanjing. It is comparable to values found in some cities (London, Lugano, and Bern). However, the S1 value is lower than values obtained in Milan, Huelva, Santa Cruz de Tenerife, and Barcelona (Table 4.3). It should be noted that the greater values of S1 in earlier studies were influenced by the selection of the CPC model used, as the higher the cut size of the CPC monitor the lower the N/BC ratio (Reche et al., 2011). Another variable is the distance of the sites from fresh traffic emissions. In addition, the size of the eBC cores might be smaller than that from regular from traffic emissions. This behaviour is observed when points occur below the line S1 as shown in Figure 4.6.

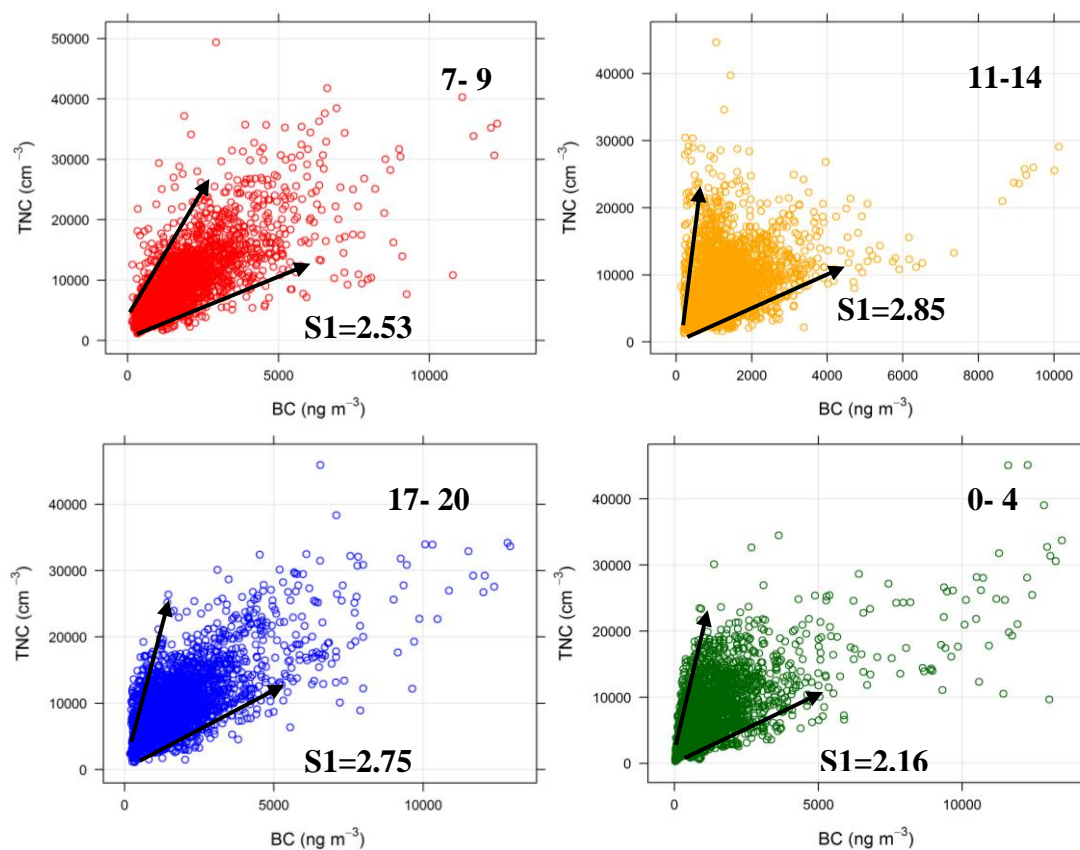


Figure 4.6: Half-hourly mean values of TNC versus eBC concentrations at different times of the day in Leicester. S1 (10^6 particles per ng eBC) at the AURN site.

Table 4.2: Values of the slopes S1 and S2 found at AURN site. S1 and S2 are expressed as 10^6 particles/ng eBC (for definitions see text).

Time of the day		S1	S2
All day	00.00-23:00 h	2.25	28.60
Night	00:00-04:00 h	2.16	32.05
Morning	07:00-09:00 h	2.53	18.15
Midday	11:00-14:00 h	2.85	36.4
Evening	17:00-20:00 h	2.75	24.35

Table 4.3: Summary of S1 and S2 values found during rush hours in previous studies and this study.

Location	S1 ($\times 10^6$) (particles /ng eBC)	S2 ($\times 10^6$) (particles /ng eBC)	Study
Milan	4.75	47	Rodriguez and Cuevas, 2007
Huelva	6.9	148	Fernández-Camacho et al., 2010
Santa Cruse de Tenerife	7.9	30.3	González et al., 2011
London	2.9	6.3	Reche et al., 2011
Lugano	3.1	20.9	Reche et al., 2011
Bern	3.6	18.9	Reche et al., 2011
Barcelona	5.1	24.5	Reche et al., 2011
Hyytiälä	1.28	-	Kulmala et al., 2016
Nanjing	1.67	-	Kulmala et al., 2016
Leicester	2.53	18.15	This study

The size of eBC is generally smaller from fresh traffic emissions compared with that from other primary particle sources (Bond et al., 2013). A small size of the eBC core in primary particle sources is likely to increase the S1 value (Kulmala et al., 2016). The diameter of eBC core can be found by application of Eq.1 assuming that the core is spherical:

$$D_P = \left[6 / (\pi S_1 \rho) \right]^{1/3} \quad (4.1)$$

Where ρ is the core density. The density of non-volatile components of diesel soot is about 1.7-1.8 gcm⁻³ (Lin et al., 2008; Oberdorster et al., 2004). By using the core density and the value of S1 (07:00-09:00) in Table 4.2, the diameter of the eBC core was found to be in the range of 75-96 nm at the AURN site. This result indicates that eBC and UFP are co-emitted by the vehicle fleet and they show a high degree of correlation. This shows that eBC and UFP are externally well mixed at this site in Leicester. This result is consistent with the general knowledge regarding eBC particle size at urban background sites (Schwarz et al., 2008). Finally, it can be concluded that the value of S1 may depend on the size of the eBC emitted by vehicular exhaust during this study at AURN site.

4.3.4 Segregating the components contributing to UFPs

By using the methodology described by Rodríguez and Cuevas (2007), the TNC measured at AURN site was segregated into two components, in order to identify the sources and processes influencing the particle number concentrations.

$$N1 = S1 \cdot eBC \quad (4.2)$$

$$N2 = TNC - N1 \quad (4.3)$$

Where, $S1 = 2.53 \times 10^6$ particles/ng eBC (Table 4.2). N1 is the minimum primary emission of vehicle exhaust which includes “those components directly emitted in the particle phase” and “those compounds nucleating immediately after the vehicle exhaust emission” (Rodríguez and Cuevas, 2007). Component N2 represents the secondary particles formed in ambient air by nucleation, impact of atmosphere conditions on the ultrafine particle formation during the dilution and cooling of the vehicle exhaust emissions, and other sources different from vehicle exhaust which contribute to TNC.

These interpretations of source function are supported by the data as shown in Figure 4.7 and Figure 4.8. Figure 4.7 shows half-hourly average values of N1 and N2 with NO_x, O₃ and wind speed for every day of the week. The weekly evolution of N1 and N2 present two different patterns (Figure 4.7a). The N1 profile follows the NO_x profile, with the

maximum percentage of N1 during morning and evening rush hours on working days, when ultrafine particles are mainly associated with vehicle exhaust emissions, 49%, and 46%, respectively (Figure 4.7b and Table 4.4). However, the N2 pattern follows the O₃ daily evolution and wind speed (Figure 4.7c, with the maximum at midday (N2= 62%, Table 4.4). The daily pattern of N2 is significantly different from that of N1, as shown in Figure 4.7a, and also from the PM_{2.5} diurnal variation (Figure S4.5). This behaviour of N2 might be linked to the NPF events at midday at AURN site (Hama et al., 2017b; Hofman et al., 2016).

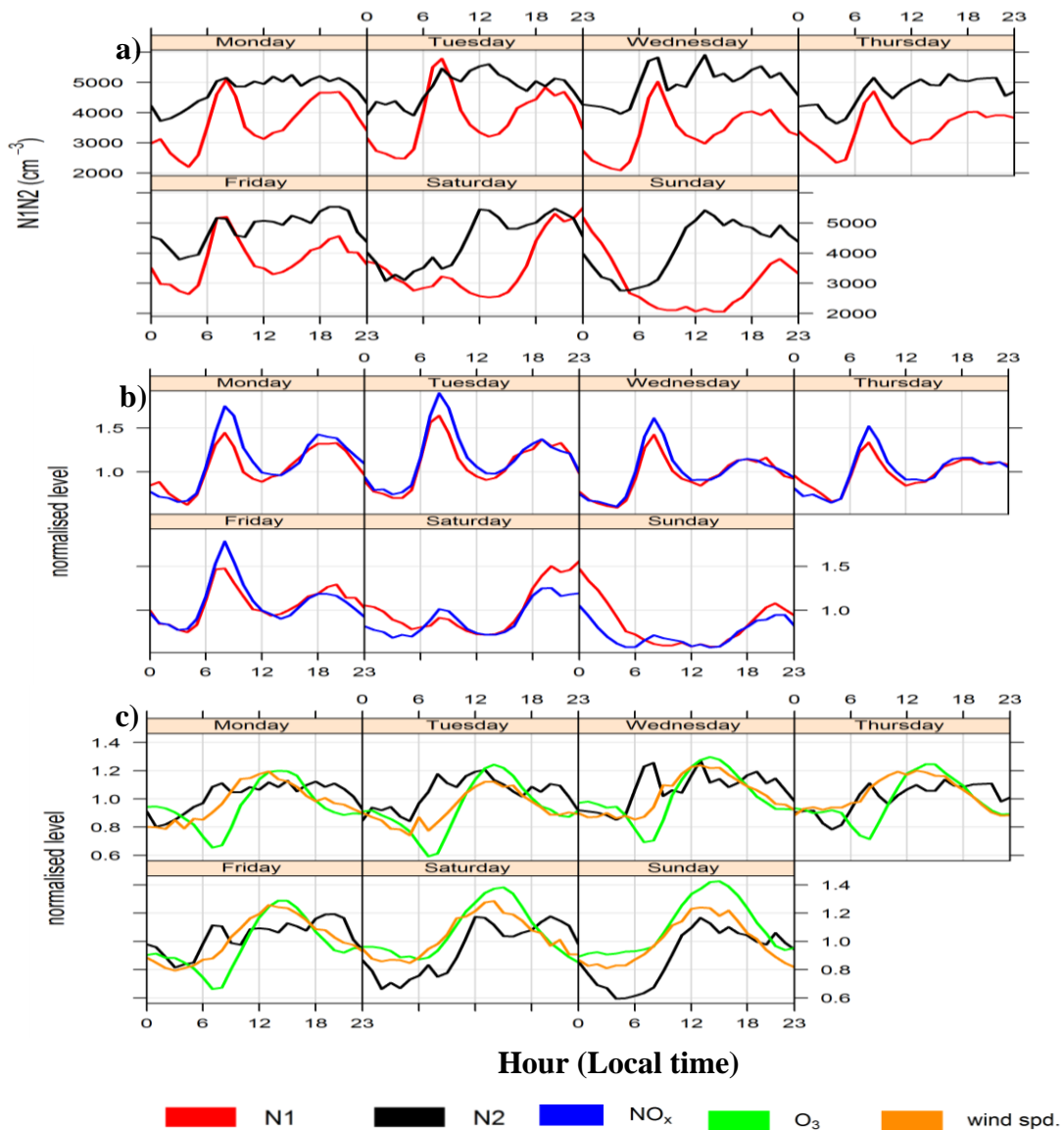


Figure 4.7: Half-hourly mean values of N1, N2, the gaseous pollutants (NO_x, O₃, mg m⁻³) concentrations and the wind speed (m s⁻¹) for every day of the week at the AURN site.

Table 4.4: Total mean percentage of N1 and N2 for daily and midday-afternoon at the AURN site (2014-2015).

Time of the day		N1%	N2%
All day	00:00-23:00 h	43	57
Night	00:00-04:00 h	39	61
Morning	07:00-09:00 h	49	51
Midday	11:00-14:00 h	38	62
Evening	17:00-20:00 h	46	54

Moreover, the similar pattern of N2 and temperature (Figure 4.8a) may suggest an active role for the oxidation products of any VOCs. Furthermore, Figure 4.8b shows an inverse correlation between N2 and RH which supports that the NPF processes at midday occur at a lower RH. Generally, the percentage of N2 (57%) was greater than the percentage of N1 (43%) for all days at the AURN site for the whole study. The high percentage of N2 could be related to the primary sources from non-traffic emissions such as domestic heating (Cordell et al., 2016), and resuspension and biogenic and VOCs emissions in Leicester. Previous studies have reported that the high N2 is caused by the combination of high solar radiation, and dilution of pollutants when the boundary layer increases, as well as SO₂ concentrations (not measured at AURN site) (Reche et al., 2011). Overall this study demonstrated that secondary particle formation is the main contributor to particle number concentration in Leicester.

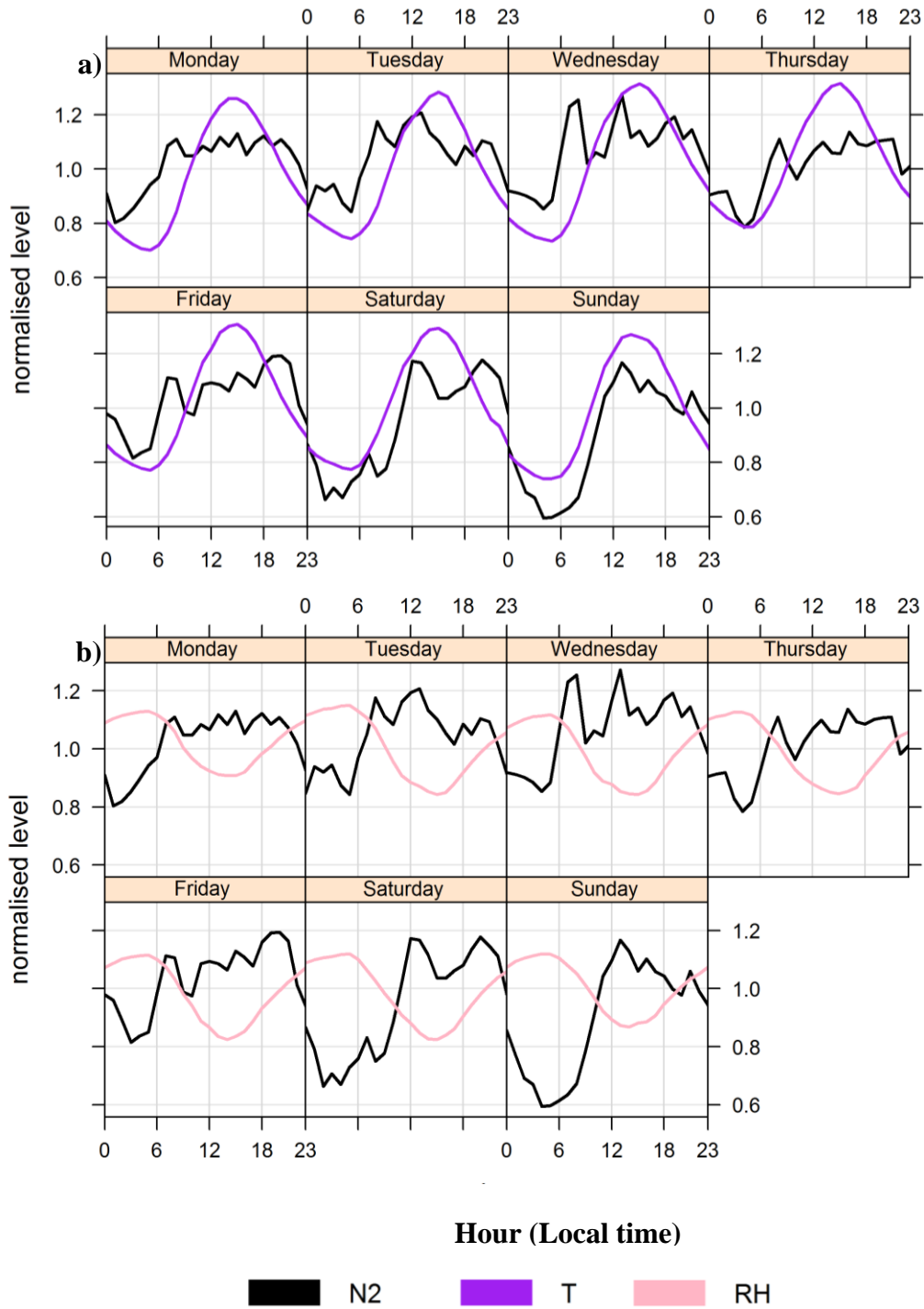


Figure 4.8: Half-hourly mean values of N₂ (cm⁻³), the temperature (T,°C) and the relative humidity (RH, %) for every day of the week at the AURN site.

4.3.5 Dependency on wind speed and direction

The relationship between traffic-related pollutants (TNC, eBC, NO_x) and wind conditions are shown in Figure 4.9 (a-f). The plots show that concentrations of the three parameters were dominated by north and south-westerly winds. The bivariate polar plots (Figure 4.9a, c, and e) show how the parameters varied by wind direction and speed at AURN site. These plots are very useful for identifying and determining sources and direction of the pollutants (Carslaw and Ropkins, 2012). For TNC, Figure 4.9a shows that there is evidence of increasing TNC when the wind speed increases from the west, north-west, and south-west. Higher TNC is found at low wind speed ($<2 \text{ m s}^{-1}$) owing to local sources, mainly traffic emissions. In addition, at high wind speed ($5\text{-}10 \text{ m s}^{-1}$) high TNC also found mostly from the north-west which indicates a potential contributor to TNC may be East Midlands Airport, which is located at about 27 km north-west of AURN site. This behaviour has been observed in other European studies (Hofman et al., 2016; Keuken et al., 2015). In the case of eBC, Figure 4.9c shows a similar pattern to TNC. The prevailing wind directions were from the north and north-west. The major eBC contribution came from these N-NW directions independent of wind speed. In addition, high eBC concentrations were categorised at high wind speed ($10\text{-}12 \text{ m s}^{-1}$) when the wind was blowing from the north-east. In case of NO_x, Figure 4.9e exhibits the highest concentrations associated with winds from north-west and south-west, at lower speeds ($<2 \text{ m s}^{-1}$) and also at higher wind speeds ($4\text{-}8 \text{ m s}^{-1}$). The most probable source of NO_x is the vehicle exhaust emissions at this site. The highest concentrations of TNC, eBC, and NO_x were observed with north and south-westerly winds and were mostly associated with the lower wind speeds ($< 10 \text{ m s}^{-1}$). These observations support the outlook that the urban background of these pollutant concentrations is dominated by local sources, rather than regional sources. The polar annulus plots for TNC, eBC, and NO_x are presented in Figure 4.9b, d and f, respectively. The patterns for the three parameters are consistent with a main traffic contribution from the nearby roads (University Road and Welford Road), with the maximum concentrations occurring during morning and evening rush hours. These roads are located at around 50-140 m of the north and south west of AURN site (see section 2.1). Moreover, it is interesting that in Figure 4.9b (for TNC) the highest concentrations occurred around noon linked to the NPF at AURN site (described in detail in section 3.1).

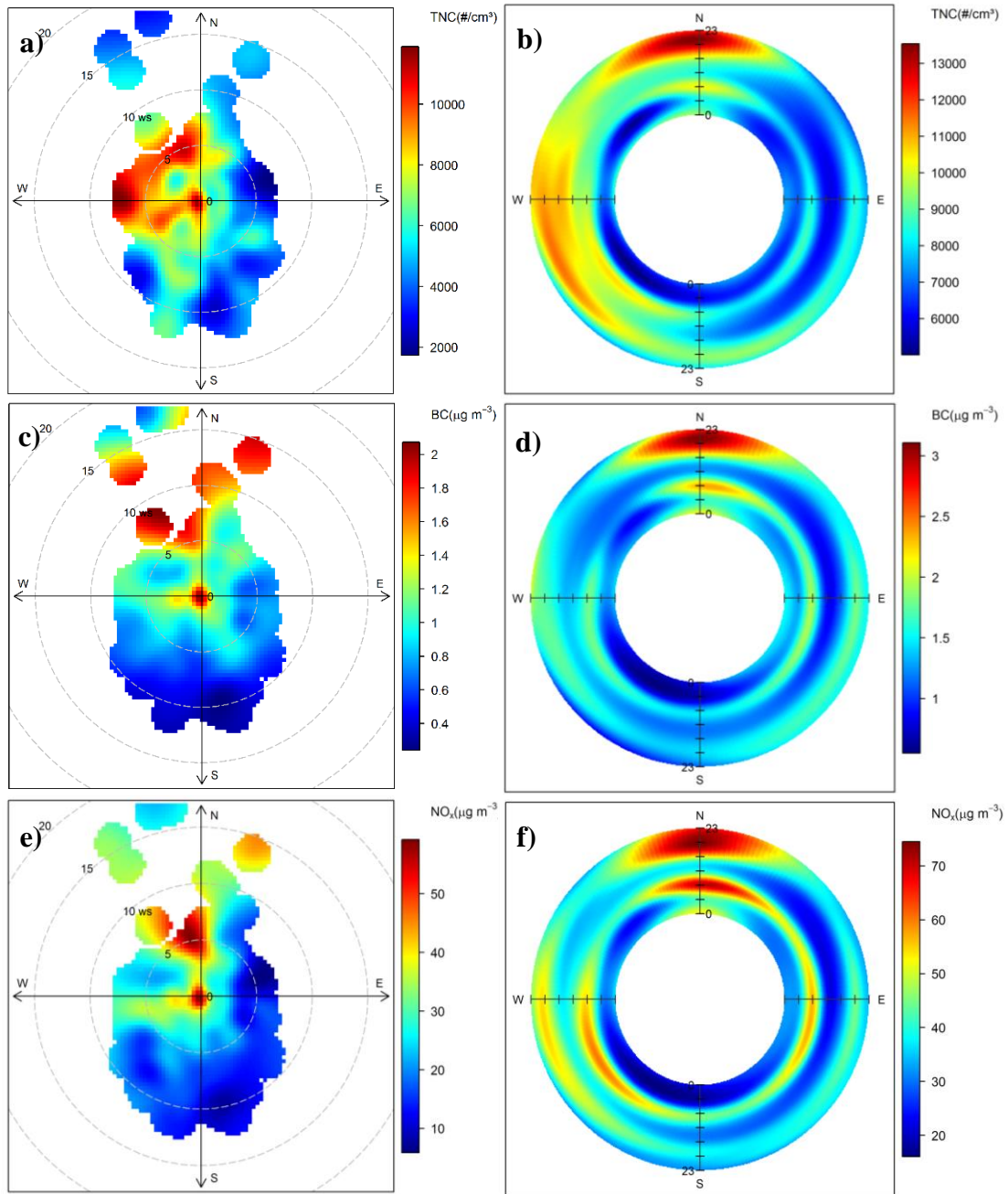


Figure 4.9: Bivariate polar plots of a) TNC, c) eBC, and e) NO_x concentrations, respectively at the AURN site. The centre of each plot represents a wind speed of zero, which increases radially outward. The concentrations are shown by the colour scale. Polar annulus plots of b) TNC, d) eBC, and f) NO_x concentrations, respectively at the AURN site. Inside of circle is 00:00-01:00 h running through the day to 23:00-24:00.

To confirm this behaviour, the relationship between N1 and N2 and wind conditions are presented in Figure 4.10 (a-b). Figure 4.10a shows the highest N1 concentrations occur with winds from north-west. In addition, it can be seen high N2 concentrations of N1 are observed during morning and evening rush hours (Figure 4.10b). This behaviour indicated that N1 is affected by primary sources such as traffic emissions. In the case of N2 (Figure 4.10c and d) a different pattern in terms of wind direction and time of the day is observed: high N2 concentrations were found with the wind blowing from the south-west (Figure 4.10c). Interestingly, Figure 4.10d shows high N2 concentrations occurring around noon, correlating with the behaviour of TNC (Figure 4.9b) and could be related to NPF events at the AURN site. Lastly, it can be concluded that wind conditions have a significant impact on N1, and N2 at the AURN site. Furthermore, the effect of differing wind conditions on N1 and N2 also revealed that they are influenced by different sources in Leicester urban areas.

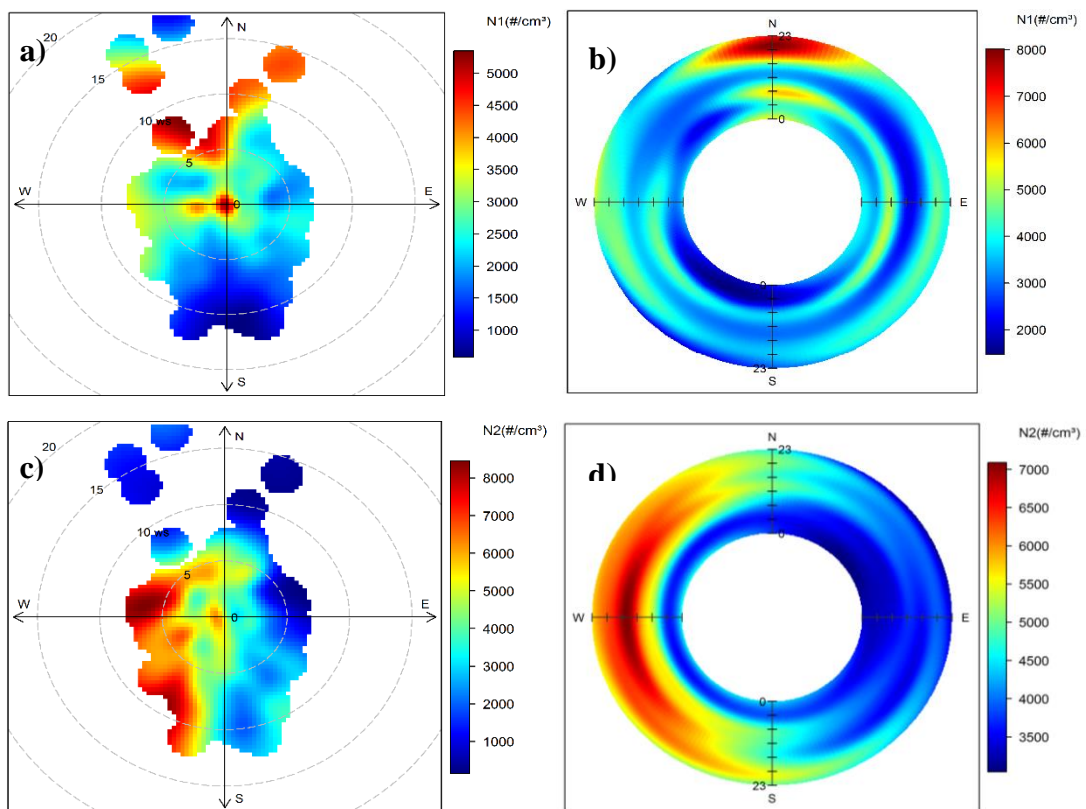


Figure 4.10: : Bivariate polar plots of a) N1, and c) N2, concentrations, respectively at the AURN site. The centre of each plot represents a wind speed of zero, which increases radially outward. The concentrations are shown by the colour scale. Polar annulus plots of b) N1, and d) N2, concentrations, respectively at the AURN site. Inside of circle is 00:00-01:00 h running through the day to 23:00-24:00.

The relationships between the TNC, eBC, and NO_x with wind speed have also been analysed (not shown) and show that the highest concentrations of the parameters observed at low wind speed ($< 5 \text{ m s}^{-1}$). This is a typical behaviour of urban background site, and is comparable with other European studies (Charron and Harrison, 2003; Pérez et al., 2010; Voigtländer et al., 2006; von Bismarck-Osten et al., 2013; Weber et al., 2013; Wehner and Wiedensohler, 2003).

4.4 Conclusions

This study shows the results of long-term measurements (2014-2015) and interpretation of the variability of TNC, PNC, PM_{2.5}, eBC, and the gaseous pollutants at the AURN urban background site in Leicester. The results demonstrate that the temporal variations of TNC are not always solely caused by road traffic emissions, whereas eBC concentrations closely follow other road traffic related pollutants, such as NO_x. The contributions of primary and secondary particle sources to the TNC were identified using the eBC concentration as a tracer for primary particles. By using the minimum slope found in the TNC versus eBC plot (2.53×10^6 particles/ng eBC), TNC was segregated into two components, $\text{TNC} = \text{N1} + \text{N2}$. The highest N1 (49%) were recorded during the morning rush hours (07:00-09:00 h), when maximum NO_x levels were recorded. Component N2 shows a profile well differentiated from that of N1 and is associated to those processes leading to increase the TNC/eBC ratio, i.e. enhancement in NPF rates owing to increased nucleation and/or growth rates to limit sizes ($\geq 7 \text{ nm}$ in our case). The maximum contribution of N2 to TNC was found around midday (11:00-14:00), where it was about 62%, when low eBC and high O₃ levels were recorded. Moreover, the majority of particles were expected to be of secondary origin. The impact of wind speed and direction also show different sources of N1 and N2. According to the bivariate polar plots, high N2 concentrations were found around noon. Finally, this long-term study has shown that primary and secondary sources of UFPs at one urban background site in UK.

Chapter Five

Lung Deposited Surface Area in Leicester Urban Background Site/UK: Contribution of urban New Particle Formation to LDSA

This Chapter has been published in Atmospheric Environment (Hama et al., 2017a)

What are the temporal and seasonal variations of LDSA in Leicester urban area? What is the impact of NPF on LDSA in urban area?

LDSA has been identified as a potential metric for the correlation of a physical aerosol particle property with health outcomes. Currently, there is little urban LDSA data. As a case study, we investigated long-term measurements of LDSA (alveolar) concentrations in a mid-size European city. The LDSA concentrations have been reported globally at several urban background sites (Buonanno et al., 2012; Buonanno et al., 2010; Geiss et al., 2016; Spinazzè et al., 2015; Albuquerque et al., 2012; Gomes et al., 2012; Moshhammer and Neuberger, 2003; Eeftens et al., 2015; Fierz et al., 2011; Reche et al., 2015; Kuuluvainen et al., 2016). However, the concentrations of LDSA in UK cities have not been reported in any previous studies and it is important to know the levels of the LDSA in UK as a reference for future studies. The aim of this study is to explore extra-annual cycles of LDSA in a mid-size urban environment. In addition, the association of the calculated LDSA with eBC was investigated to assess the effect of LDSA on human health. To our knowledge, the study reported here represents the first that reveals variability of LDSA and the impact of NPF on LDSA in the UK.

5.1 Introduction

The surface area concentration is an important property of atmospheric aerosol particles which links aerosol loading to its health effects. Over recent years a number of epidemiological studies have shown that atmospheric particle surface area concentration may have a stronger correlation with negative health effects than particle mass or number concentration (Brown et al., 2001; Brown et al., 2000; LeBlanc et al., 2010; Nel et al., 2006; Nurkiewicz et al., 2009; Nygaard et al., 2004; Oberdörster et al., 2005; Sager and Castranova, 2009; Singh et al., 2007; Stoeger et al., 2005). Toxicological studies have found that ultrafine particles may have an increased toxicity compared to larger particles with the same composition (Johnston et al., 2000; Karlsson et al., 2009), and that the surface area concentration might be the most relevant physical measurement of ultrafine particle exposure (Maynard and Maynard, 2002; Moshhammer and Neuberger, 2003; Oberdörster, 2000). All these studies reveal that the surface area concentration of atmospheric particles in various environments is a suitable property to represent the negative human health effects of aerosol exposure.

Instruments based on unipolar diffusion charging of particles or lung-deposited surface area concentrations (NSAM model 3550 and AeroTrak TM 9000, TSI Inc), (Bau et al., 2012) can measure a value related to particle surface area concentration and are more sensitive to ultrafine particles than gravimetric methods (e.g., Gravimetric Filter Method and Mass PM Analyser, (Mohr et al., 2005). Such instruments may offer the ability to explore source-related ultrafine particle exposure as they deliver high temporal and spatial variability measurements, which addresses the requirements around the ability of ultrafine particles to coagulate quickly and create concentration gradients (Imhof et al., 2005; Peters et al., 2009). In these instruments a corona discharge produces unipolar ions, which can diffuse towards the particles and an electrometer is used to measure the total charge that transfers from the ions to the particles; the amount of charge is related to the active surface area concentration (Asbach et al., 2009; Baltensperger et al., 2001).

The LDSA concentrations have been reported at urban background sites in Upper Austria (Moshhammer and Neuberger, 2003), Minneapolis (Wilson et al., 2007), Los Angeles (Ntziachristos et al., 2007), Lisbon (Albuquerque et al., 2012; Gomes et al., 2012), Italy (Buonanno et al., 2012; Buonanno et al., 2010; Geiss et al., 2016; Spinazzè et al., 2015), Switzerland (Eeftens et al., 2015; Fierz et al., 2011), Barcelona (Reche et al., 2015), Helsinki (Kuuluvainen et al., 2016). However, the concentrations of LDSA in UK cities have not been reported in any previous studies and it is important to know the levels of the LDSA in UK as a reference for future studies. The aim of the present study is to explore extra-annual cycles of LDSA in a mid-size urban environment. In addition, the association of the calculated LDSA with eBC was investigated to assess the effect of LDSA on human health. To our knowledge, the study reported here represents the first that reveals variability of LDSA and the impact of NPF on LDSA in the UK.

The study was carried out between November 2013 and May 2015 over which time aerosol lung deposited surface area (LDSA) concentrations in the alveolar region were measured concurrently with equivalent black carbon mass concentration (eBC), nitrogen oxides concentration (NO_x), and particle number size distributions (PNSD) at Automatic Urban Rural Network (AURN) site in the Leicester city (UK), where air quality is mainly influenced by traffic emissions owing to the high vehicle density across the city. This study reports on the first results of a novel LDSA measuring which is a part of air quality monitoring network, established in Amsterdam (Netherlands), Antwerp (Belgium), Leicester (UK) and London (UK) and was carried out as part of the JOint Air Quality INitiative (JOAQUIN, www.joaquin.eu), an INTERREG IVB funded European project, which aims at supporting health-oriented air quality policies in Europe (Cordell et al., 2016).

5.2 Experimental

The study was carried out between November 2013 and May 2015 over which time aerosol LDSA concentrations in the alveolar region were measured concurrently with eBC, NO_x, and PNSD at AURN site in the Leicester city (UK), where air quality is mainly influenced by traffic emissions owing to the high vehicle density across the city.

5.2.1 Monitoring site

In the JOAQUIN project, a range of air quality parameters (including PNSD, eBC, NO_x, LDSA, PM₁₀) were measured in six cities in North West Europe; Amsterdam and Wijk an Zee (The Netherlands), Antwerp (Belgium), Leicester and London (United Kingdom), Lille (France) (Cordell et al., 2016). Data collection started in April 2013 (Amsterdam, Antwerp), November 2013 (Leicester) and April 2014 (London). To check the stability and comparability of the air quality monitors, a mobile monitoring unit performed measurements adjacent to each of the permanent air quality monitoring stations. The PNSD and eBC monitors and PM₁₀ sampler were identical to for the permanent JOAQUIN stations. The detail of the project and information about sites and instrumentation can be found in Joaquin (2015a).

Measurements were carried out at two sites in Leicester as part of the JOAQUIN project. The main and permanent site represents an urban background and is part of the UK government operated AURN. The site was located at the University of Leicester campus (https://uk-air.defra.gov.uk/networks/site-info?site_id=LECU&view=View), as shown in Figure 5.1.

For contrast, a temporary site at Brookfield (see Figure 5.1) was developed with a mobile monitoring station in a large and frequently-used car park. The Brookfield site also represents urban background (Figure 5.1), and was located at a distance of approximately 1.2 km east of the AURN site.

At the AURN site the nearest road is University Road (20 m North-West) with very little traffic and the nearest main road is Welford Road (140 m South-South West). According to traffic counts by the Department for Transport (UK government), the traffic intensity of Welford Road was about 22,600 vehicles/day in 2014 (<http://www.dft.gov.uk/traffic-counts>, count point 36549). At temporary site, the nearest roads are Ashfield Road (90 m in the North) and Holmfield Road (90 m South) and the nearest main road is London Road, at 190 m west. According to traffic counts by the Department for Transport, the traffic intensity on London Road was approximately 20,550 vehicles/day in 2014 (<http://www.dft.gov.uk/traffic-counts>, count point 56147).



Figure 5.1: AURN and Brookfield sites at Leicester University campus, sampling locations.

5.2.2 Instrumentation

Table 5.1 gives a summary of the instruments used in this study at both sites. In the AURN station in Leicester, lung deposited surface area (LDSA) was measured by a Nanoparticle Surface Area Monitors (NSAM, TSI 3550) originally developed by Fissan et al. (2007). The NSAM operational principle is based on diffusion charging of particles followed by detection of the charged aerosol using an electrometer. The instrument can be switched between two sampling modes: the tracheobronchial and alveolar fractions of the total particle. The NSAM monitor was designed to report the surface area of particles only deposited in the alveolar and tracheobronchial regions when the ion trap voltage is set to 200 V and 100 V, respectively (Asbach et al., 2009). In this study the NSAM was set to measure the alveolar lung-deposited particle surface area (reported as $\mu\text{m}^2 \text{cm}^{-3}$). It was operating at 1 minute time resolution during the whole study period (November 2013-May 2015) with a data coverage of 99%. The inlet flow rate is 2.5 L/min, of which 1.5 L/min is used as aerosol flow. The NSAM detects particles size range approximately from 10 to 1000 nm, however, it measures only up to 400 nm with high precision (Asbach et al., 2009). According to Asbach et al. (2009), particle hygroscopicity may cause significant changes in the lung deposition curves, which is a factor that cannot be measured by this instrument.

Table 5.1: Instruments and monitors used in this study (for details, see experimental).

Station	Location	Meteorological Parameters	NSAM	W- CPC	SMPS	NO _x	MAAP
AURN	UoL	-	x	x	-	x	x
Trailer (Mobile Campaign)	UoL and BF	x	-	x	x	-	x

The particle number size distributions were measured by a Mobility particle size spectrometer (type Grimm SMPS+C 5420 with L-DMA). The size spectrometer consists of a Neutralizer (^{85}Kr source, 185 MBq, obtained from Eckert & Ziegler) and a Differential Mobility Analyzer (Vienna type L-DMA, ~ 50 cm long), connected to a butanol-based Grimm-type condensation particle counter (CPC). The flow rate of the CPC is 0.3 L/min. To measure a 10-1100 nm range, the sheath air flow rate is 3 L/min. A complete scan of the particle number size distribution with 45 size bins was done in 10 min. The software corrects for internal diffusion losses and the bipolar charge distribution (Wiedensohler, 1988). Aerosol was kept at low relative humidity (RH) with a Nafion dryer in the inlet system. However, such a drying system leads also to extra losses of the small particles (< 70 nm). Although in Joaquin project these losses were calculated and corrected for, the losses might have been higher, as could be derived from field tests (Joaquin, 2015a; Wiedensohler et al., 2012).

The total particle number concentration (N_{TOTAL}) was measured by a Water-Based Condensation Particle Counter (W-CPC, TSI Environmental Particle Counter (EPC) model 3783 <http://www.tsi.com/environmental-particle-counter-3783>) from November 2013 to May 2015.

The TSI instruments (W-CPC and NSAM) are connected to environmental sampling system (TSI 3031200). The components of the TSI 3031200 are a PM_{10} inlet, sharp cut PM_1 cyclone, flow splitter and Nafion dryer (reduces humidity to less than 50% RH).

The mass concentration of equivalent black carbon (eBC) was measured by a Multi-angle Absorption Photometer (MAAP Thermo Scientific model 5012) for the whole period (Petzold et al., 2013). The MAAP determines particle light absorption due to the light transmission and backscattering at two angles of particles collected on the filter tape (glass fibre type GF10). The eBC mass concentration is calculated using a constant mass absorption cross section of 6.6 g/m^2 . Further information on the principle of the MAAP is given by Petzold et al. (2002). Nitrogen oxides were also measured by a Thermo 42i $\text{NO}-\text{NO}_2-\text{NO}_x$ monitor. This monitor uses chemiluminescence technology to measure the concentration of nitrogen oxides in the air. It has a single chamber, single photomultiplier tube design that cycles between the NO and NO_x mode.

Meteorological data (wind speed and direction) were provided for the whole period by the Air Quality Group from the Leicester City Council. The station is located 4.9 km away from the AURN urban background monitoring site. Moreover, a mobile laboratory van also measured meteorological parameters (temperature, relative humidity, and wind speed and direction) during the three months of mobile monitoring.

5.3 Results and Discussion

5.3.1 The annual behaviour of LDSA, eBC and NO_x concentrations

The data were split into three time periods consisting of the cold period (November to April), the warm period (May to October) as well as the whole period. Statistics for LDSA, eBC, and NO_x concentrations are shown in Table 5.2. During this study, the annual average LDSA concentrations in Leicester was $29.5 \mu\text{m}^2 \text{cm}^{-3}$, and the maximum, median, minimum and standard deviation annual values were, 282.8, 22.3, 0.1, $24.8 \mu\text{m}^2 \text{cm}^{-3}$ respectively. The statistics are based on 30-min data.

Table 5.2: Statistics of LDSA ($\mu\text{m}^2 \text{cm}^{-3}$), eBC ($\mu\text{g m}^{-3}$), and NO_x ($\mu\text{g m}^{-3}$) measured at AURN site from November 2013 to May 2015.

Parameters		Average	Max	Median	Min	St. Dev.
LDSA	Annual	29.5	282.8	22.3	0.1	24.8
eBC		1.4	13	1.07	0.06	1.3
NO _x		36.8	596.7	27.6	0.43	35.2
LDSA	Cold Period	38	282.8	28.2	0.55	33
eBC		1.84	13.5	1.26	0.85	1.8
NO _x		47.9	596.7	34.1	2.06	46.8
LDSA	Warm Period	23	146	20.2	0.1	13.7
eBC		1.25	13	1.02	0.06	0.96
NO _x		29	231.8	24.6	0.43	20.6

The mean LDSA concentration measured at Leicester AURN site was observed to be similar to that found at traffic sites in Zurich, Switzerland ($28\text{--}40 \mu\text{m}^2 \text{cm}^{-3}$) (Fierz et al., 2011). Previous LDSA measurements are summarised in Table 5.3.

Table 5.3: Summary of average and standard deviations of LDSA (Alveolar region) concentrations ($\mu\text{m}^2 \text{cm}^{-3}$) measured in previous studies and this study in urban area.

Site	LDSA($\mu\text{m}^2 \text{cm}^{-3}$)	St .Dev.	Study
Urban background site (Los Angeles) retirement community (outdoor)	68.9	38.7	Ntziachristos et al. (2007)
Urban background site (Los Angeles)	53	27.5	
Freeway 1 (Los Angeles)	105.8	48.3	
Freeway 2 (Los Angeles)	153.4	55.2	
Highway (Zurich)	40		Fierz et al. (2011)
Busy city road-1 (Zurich)	63		
Busy city road-2 (Zurich)	63		
Urban background site, inner city, little traffic (Zurich)	19		
Average city road (Zurich)	28		
Urban background site, no traffic (Zurich)	11		
Urban background site (Cassino)	164		Buonanno et al. (2012)
Rural background site (Cassino)	69		
Urban background site (Lisbon)	35-89		Gomes et al. (2012)
Urban background site with traffic influence (Barcelona)	37	26	Reche et al. (2015)
Park area and traffic site (Helsinki)	12-94		Kuuluvainen et al. (2016)
Urban background site with traffic influence (Leicester)	29.9	24.85	This Study

Monthly variation of LDSA concentrations, with other air quality parameters, such as eBC and NO_x is shown in Figure 5.2. A clear seasonal variation was observed for the LDSA, eBC and NO_x concentrations. The high concentrations of LDSA observed in the cold period in Leicester (November-April) with a 30 min average range between 37-38.5 $\mu\text{m}^2 \text{cm}^{-3}$. The seasonal enhancement might be related to the increase of wood burning for domestic heating, as well as reduced dispersion of local sources and low mixing height in the winter time (Cordell et al., 2016). The lowest LDSA concentrations were observed in summer (July and August) when the average values ranged between 19-21 $\mu\text{m}^2 \text{cm}^{-3}$. The summer minima are likely related to the meteorological conditions that have greater impact, particularly the effective dilution of particles owing to stronger turbulent mixing. The dilution effects are caused by meteorological conditions, for instance wind direction and speed, which control horizontal dilution, and the mixing layer height, which controls the vertical extent. The impact of meteorology on LDSA are discussed in detail in section 3.4. The lower LDSA levels in summer might also be due to loss of semi-volatile particle material during the warm period. Similar patterns were observed for eBC and NO_x concentration in comparison to LDSA (see Figure 5.2). The similarity is likely due to LDSA and other parameters (eBC and NO_x) being influenced by the same factors such as traffic emissions, vertical dilution conditions and meteorological conditions (mixing height, and temperature). The uncertainty bars shown in Figure 5.2 represent the standard deviations based on the 30 minute values of LDSA, eBC, and NO_x concentrations. Higher standard deviations are observed during the cold period and this could be related to the contrast of different weather systems that in cold season is stronger than in warm season. It may be also linked to the inversion conditions, suspension of aerosol particles for longer, lower wind speed and build-up of LDSA as well as other parameters under favorable inversion conditions.

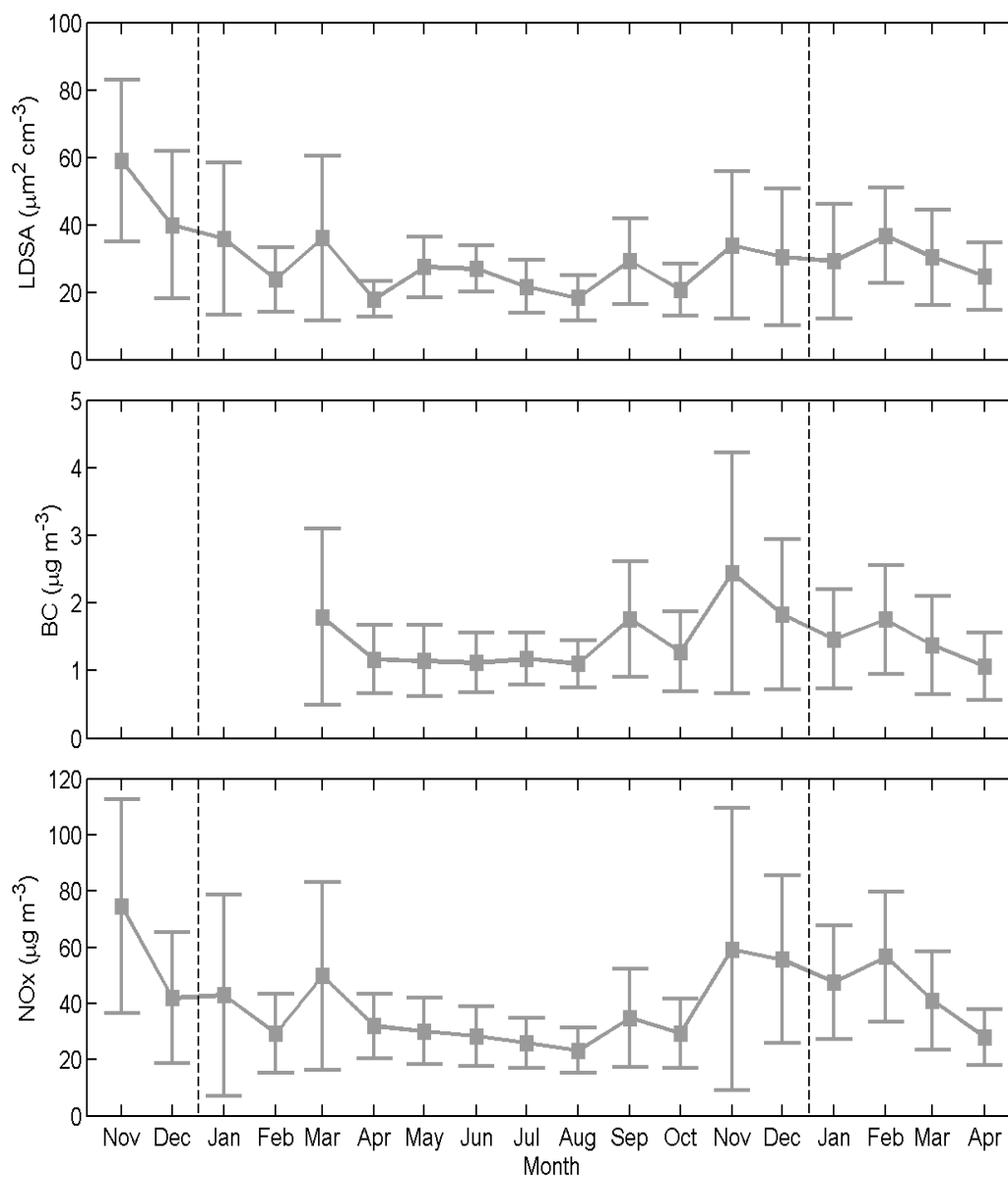


Figure 5.2: Monthly variations of LDSA, eBC, and NOX concentrations (error bars represent the standard deviation) at AURN site.

5.3.2 Diurnal and Weekly variations of LDSA, eBC, and NO_x

The average weekly variations of the LDSA, eBC and NO_x concentrations is shown in Figure 5.3. The diurnal variation of the three parameters is mainly determined by the emission pattern of the dominant sources and the evolution of the mixing layer. The average diurnal patterns of LDSA, eBC, and NO_x based on half-hour means are quite similar in shape. The main sources of eBC in urban atmosphere are diesel vehicles and domestic heating while NO_x is mainly from traffic emissions (Carslaw, 2011; Viana et al., 2012). During the cold period the impact of traffic was obvious on workdays (Monday-Friday) when the highest LDSA concentration was measured during morning and evening rush hours, between 6:00 - 9:00 LT and 18:00-21:00 LT respectively. This is seemingly associated to the result of the high motor vehicle emissions combined with a lower mixing layer height and lower temperature (Reche et al., 2015). Peaks of LDSA concentrations were also observed on workday morning rush hour during the warm period, but with lower absolute values than in the cold period. A similar profile was observed for eBC and NO_x concentrations when compared with LDSA. The similar patterns suggest that LDSA is influenced by mainly the traffic emissions in Leicester urban area. The LDSA evening rush hour peaks in summer months were usually lower than the morning rush hour peaks likely related to the stronger turbulent mixing and higher mixed layer depths, also higher wind speed. It can be concluded that the late afternoon peak is more influenced by local meteorology conditions than by vehicular exhaust emissions. Interestingly, the LDSA pattern shows an additional peak in the afternoon during the warm months. This phenomena might be related to the NPF (see Section 5.3.5). The diurnal variations of the eBC, and NO_x concentrations observed in this work are in line with those observed in other studies for traffic pollutant dominated locations (Gomišček et al., 2004; Harrison et al., 1997; Jones and Harrison, 2005; Laxen et al., 2010).

There is other evidence that contains the relationship between LDSA concentration and traffic emissions. During the weekends, the diurnal variations for LDSA, eBC and NO_x are similar, but differ from those on weekdays. Without traffic rush hours, lower concentrations were observed in the early morning. Moreover, the LDSA evening peak

on weekends in the cold period shows higher than that observed during the warm period. This observation might be related to the increasing traffic activity owing to that people are going out for restaurants or shopping at late afternoon, and also may impact of higher emissions from cooking and domestic heating when people staying at home during weekends (Allan et al., 2010). Additional weekend contributions to LDSA stem from events such as barbeques and late night activities on Saturdays, which result in a peak occurring later in the day and lasting for longer.

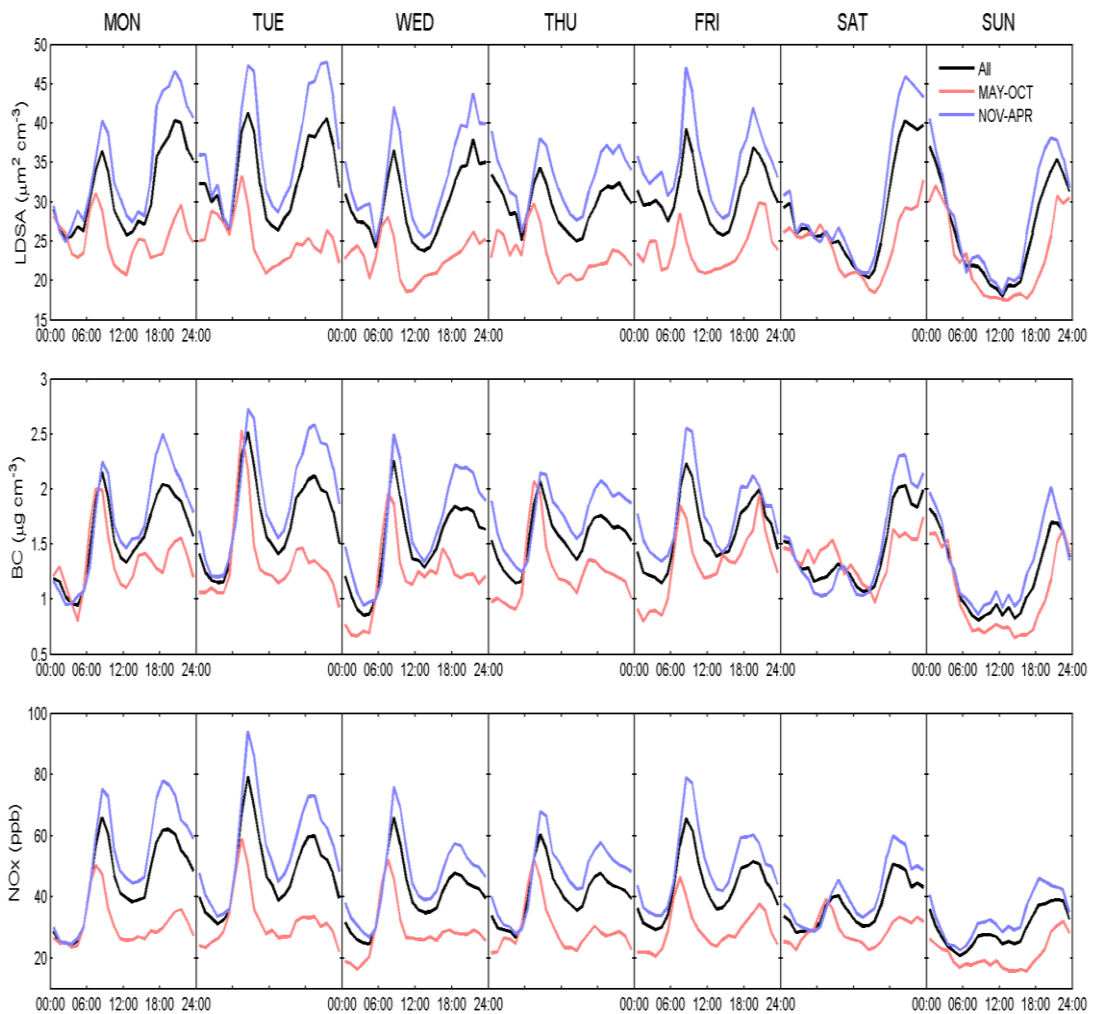


Figure 5.3: The diurnal and weekly variations of LDSA, eBC, and NOx concentrations at AURN site.

5.3.3 Correlation between LDSA and other pollutants (eBC, NO_x and N_{TOTAL})

To assess the relation of LDSA with more commonly monitored pollutants, half-hourly LDSA were plotted against half-hourly eBC, NO_x and N_{TOTAL}. The scatter plots between LDSA and the other parameters from November 2013 to April 2015 at the AURN site are presented in Figure 5.4a-c. The R² for LDSA with eBC, NO_x and N_{TOTAL}, were 0.52, 0.36, and 0.60 (Figure 5.4a-c), and Pearson's correlation coefficients were 0.81, 0.77, and 0.80 (p<0.05), respectively. These results are similar to results from Barcelona (Reche et al., 2015).

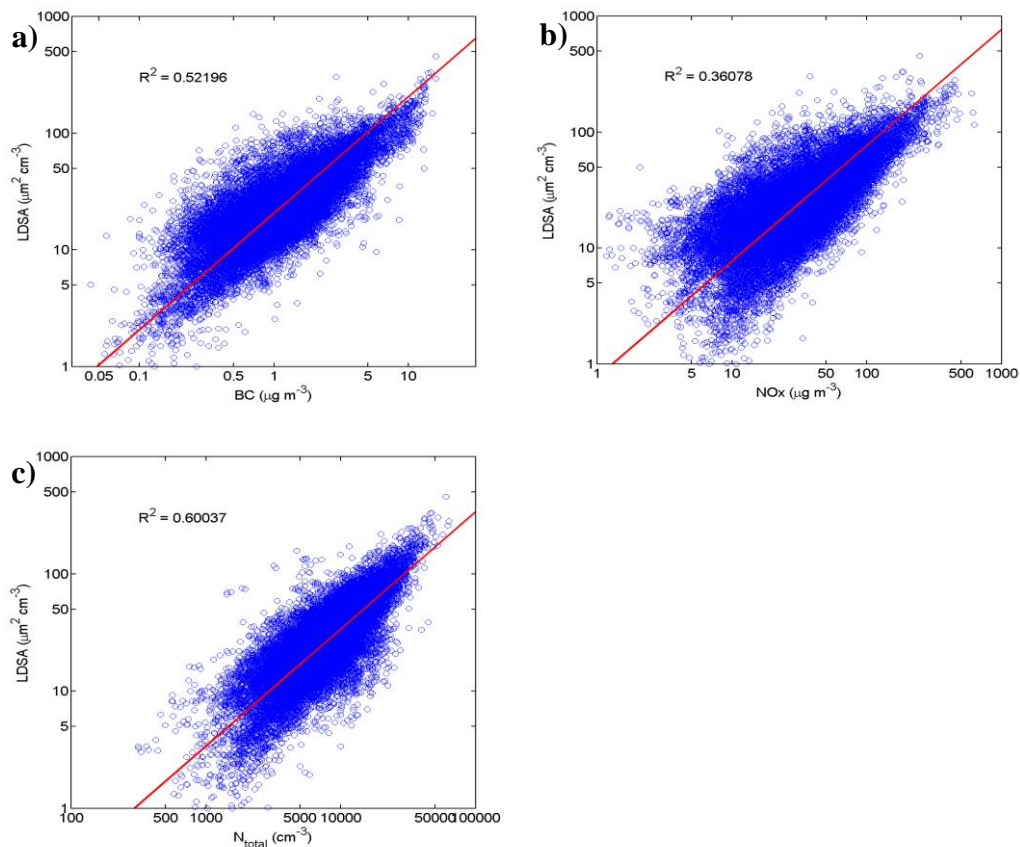


Figure 5.4: : Correlations between LDSA concentrations and (a) Black Carbon (eBC), (b) NO_x, (c) Total Particle Number concentration (N_{TOTAL}) at AURN site from Nov-2013 to Apr-2015.

In addition, seasonal correlation between LDSA and the other pollutants were also observed (Figure 5.5a-c). The correlation considerably increased when only using the cold period (Autumn and Winter) data. The highest correlation ($R^2 = 0.59-0.71$) in the cold season was found between the LDSA and the eBC and NO_x as compared with the summer months. The higher correlation indicates that LDSA in cold season is more dominated by anthropogenic emission such as traffic and heating. The weaker correlation was observed between LDSA and the eBC in summer and with NO_x in spring and summer ($R^2 = 0.34-0.35$), suggesting that the LDSA in spring and summer might be affected by photochemical new particle formation. The LDSA and N_{TOTAL} concentrations in all seasons were relatively well correlated ($R^2 = 0.51-0.7$); Overall, it can be concluded that these correlations between LDSA with other parameters support the annual behavior and diurnal variations of LDSA (discussed in section 5.3.1 and 5.3.2) in that the LDSA concentrations in Leicester urban area are mainly dominated by road transport emissions.

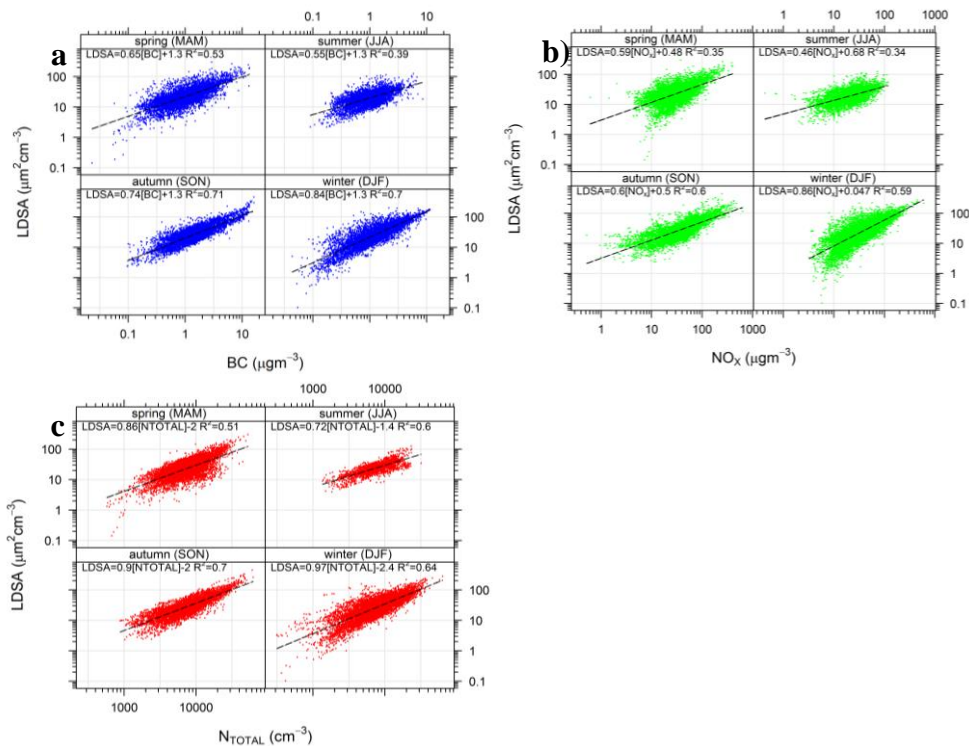


Figure 5.5: Seasonal correlations between LDSA concentrations and (a) Black Carbon (eBC), (b) NO_x , (c) Total Particle Number concentration (N_{TOTAL}) at AURN site from Nov-2013 to Apr-2015.

The correlation between LDSA and different size range of particle number concentrations measured by SMPS (not shown) agreed with the results found in the previous study by Reche et al. (2015). The results showed that the highest correlation between LDSA and particle number size in the range 50-200 nm. However, low correlation was observed between LDSA and particle number concentrations in the size range 10-30 nm, as these particles are outside the NSAM size range (20-400 nm). In addition, a proxy LDSA was calculated from SMPS particle size distributions for the entire period by the method described in Reche et al. (2015). The highest correlation ($R^2=0.89$) between the measured LDSA (from NSAM) and calculated LDSA from PNSD encompassed the range 20-400 nm (see Figure 5.6a-d).

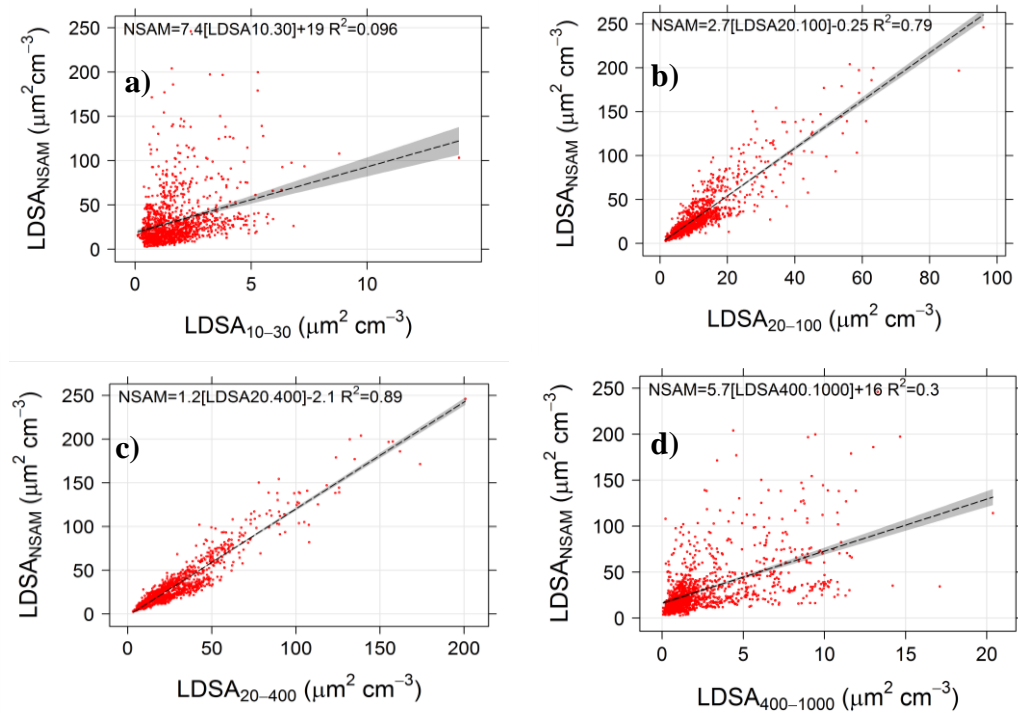


Figure 5.6: : Linear relationship between direct LDSA (from NSAM) and calculated LDSA (from PNSD) concentrations for different particle size ranges, a) 10-30 nm b) 20-100 nm, c) 20-400 nm, d) 400-1000 nm size ranges at AURN site.

In addition, the correlation between calculated LDSA (30-200 nm) and eBC are shown in Figure 5.7. The limited size range of calculated LDSA (30-200 nm) is selected to cover the main size range for eBC (Petzold et al., 2013; Pósfai et al., 2004; Schwarz et al., 2006). Figure 5.7a shows a good correlation ($R^2= 0.6-0.75$, $r=0.82$) between the calculated LDSA and eBC, as well as similar diurnal profile for the calculated LDSA and eBC (Figure 5.7b). The level of agreement between eBC and the calculated LDSA indicates that eBC might be a good indicator, measure or estimate of health impacts in relation to LDSA.

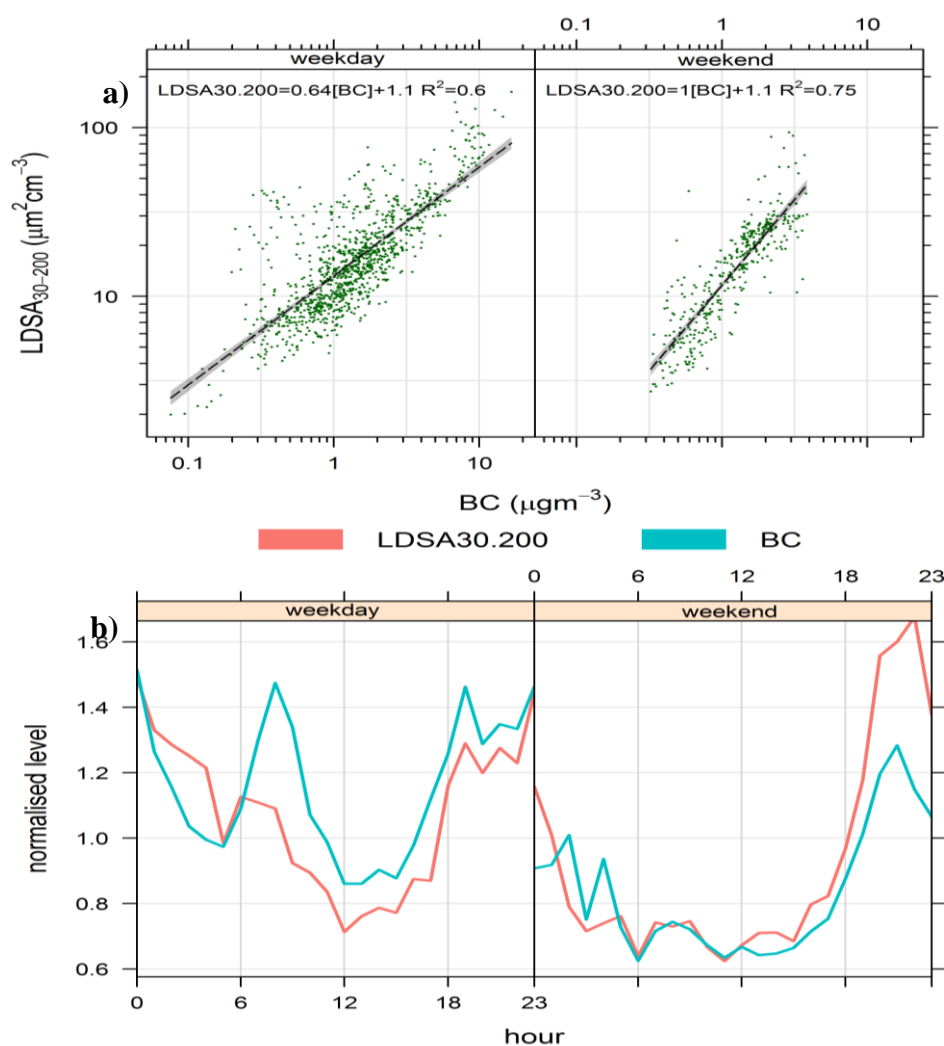


Figure 5.7: Linear relationships between the calculated LDSA and eBC: (a) scatterplots for weekdays and weekends, (b) diurnal variation of the calculated LDSA and eBC at AURN site.

5.3.4 Variation with wind speed and direction

Meteorological parameters play significant roles in determining the concentration levels of air pollutants in urban areas. Previous studies have shown that among the meteorological parameters, wind speed is a significant factor governing the eBC and NO_x concentrations (Carslaw et al., 2006; Xu et al., 2011). In order to investigate the impact of wind speed and direction on LDSA, as well as eBC and NO_x concentrations, wind map plots were generated to show the impact of wind conditions on these parameters (see Figure 5.8). Figure 5.8a-c shows the wind dependence of the LDSA, eBC, and NO_x concentrations generated using the half-hourly data from Nov 2013 to May 2015. A polar coordinate system was used dependent on wind speed and direction (Ma et al., 2011; Xu et al., 2011). For LDSA, the maximum concentration (Figure 5.8a) occurs with calm winds (wind speed $< 2 \text{ m s}^{-1}$, the red and yellow areas in the center of the plots), independent of wind direction. This again reflects a combination of sources i.e. local emissions such as, traffic and domestic heating and particulate size. What is clear from the polar plots is that the contribution of emissions from the surrounding regions is weak. It can be observed the highest average LDSA (dash-dot line) is from the south and north westerly wind direction, affected by the transport of aerosols from both directions. The major roads, the East Midlands airport and Radcliffe upon Soar power station (both of which are around 16.03 miles far from AURN station) are situated in the South and North Westerly regions. For eBC, a similar feature was observed, the maximum eBC (Figure 5.8b) occurring when wind speed below 2 m s^{-1} . In the NW and SW directions, eBC concentrations were higher for wind speed higher than 4 m s^{-1} . The reason being that eBC is being transported from regions lying in those directions. For NO_x, similar patterns to LDSA and eBC are observed with high NO_x (Figure 5.8c) levels found under low wind speeds ($< 2 \text{ m s}^{-1}$). It can be supposed that NO_x is mainly dominated by local sources and emissions. Under such an assumption, levels of NO_x, should display a simple decreasing trend with increasing wind speed to a background level. Such a relationship between NO_x and wind speed was found as well as modelled in previous studies (Aldrin and Haff, 2005; Carslaw et al., 2006). The wind rose data support the supposition that LDSA is dominated

by local emissions, including traffic and domestic heating emissions. Figure 5.8d shows a wind rose for the whole sampling period.

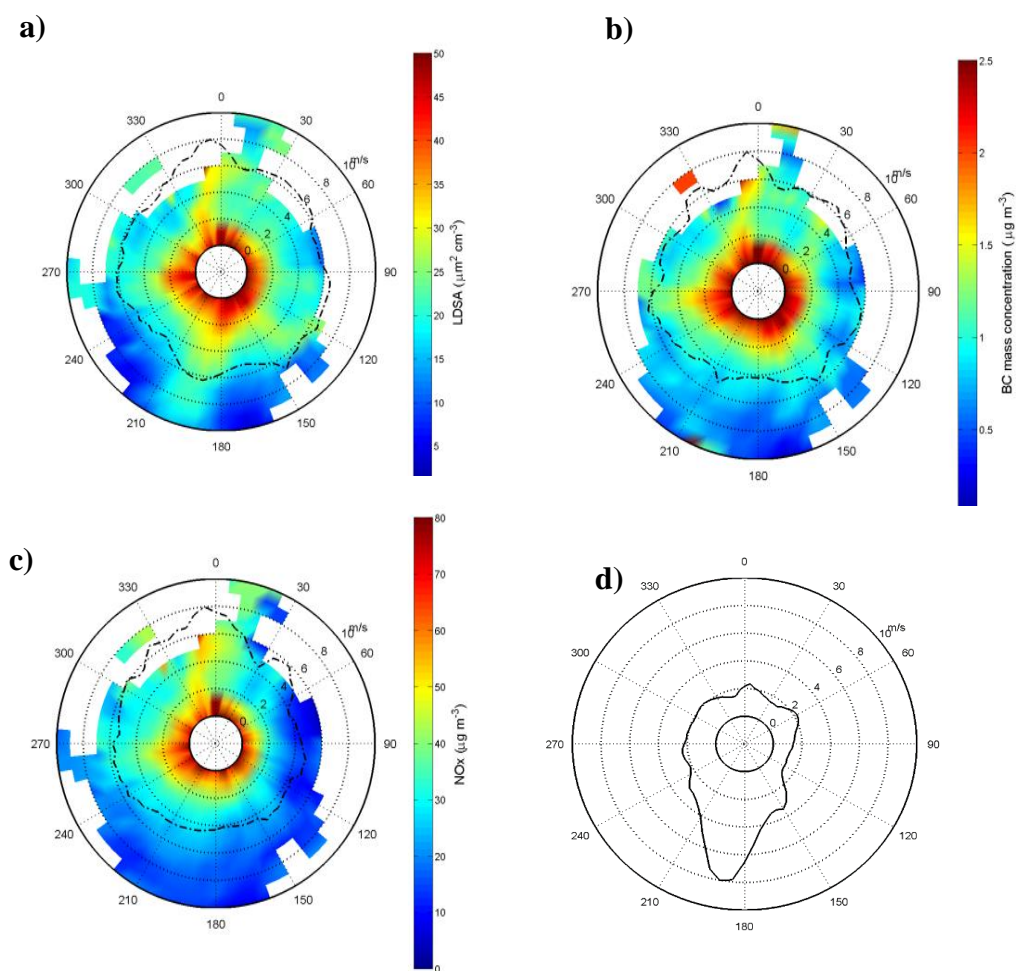


Figure 5.8: Wind speed and direction dependence map of a) LDSA ($\mu\text{g}^2/\text{cm}^3$), b) eBC ($\mu\text{g}/\text{m}^3$), c) NO_x ($\mu\text{g}/\text{m}^3$) at AURN site, d) wind frequency rose for the whole period. In each figure, the shaded contour indicates the average of variables for varying wind speeds (radial direction) and wind direction (transverse direction). The dash-dot lines stand for the relative mean values for each wind direction at AURN site.

5.3.5 Contribution of new particle formation on LDSA: a case study

A recent study in Barcelona identified that NPF events affect LDSA concentration in an urban area (Reche et al., 2015). Within northern Europe, in Birmingham and Helsinki nucleation events in urban atmosphere have been previously observed during noon hours with a maximum during the spring season (Alam et al., 2003; Hussein et al., 2008).

Over the period of our work 14 NPF event days were observed, a typical one was the nucleation event with particle growth was observed on May 3rd, 2014 as shown in Figure 5.9. During the event the peak wind speed observed was 2.3 ms^{-1} , a SE wind dominated in the morning and a SW wind dominated in the afternoon, and the relative humidity remained low at 30-40%. To explore the significance of nucleation events on the LDSA concentration, particle number size distribution (10-1000nm) were studied. The nucleation events characterised by a clear growth in particle size over a long period of time result in the classical “banana” shape (Heintzenberg et al., 2007; Kulmala and Kerminen, 2008). A clear example of “banana-like” nucleation event is shown in Figure 5.9. The nucleation mode particles are observed in the morning, and start to grow in size at around 10:00, indicated as the increase of 10–20 nm particle number concentrations. Moreover, during the event particle number concentrations increased from 4837 particles cm^{-3} at 10:00 and reached the highest number 12060 particles cm^{-3} around 13:30. Total particle volume concentrations were calculated by integrating the number size distributions of size-resolved particles assuming spherical particles as shown in the lowest panel of Figure 5.9. During the NPF event (from 10:00-18:00) the volume concentration has not been significantly increased. The reason is that new particles are small (10-20 nm), and therefore their contribution to the particle volume is insignificant (Wehner and Wiedensohler, 2003). However, between 18:00-20:00, the volume concentration shows a peak, this probably owing to the influence of traffic emissions which coincides with evening rush hours. The particle number size distributions showed a clear ‘banana’ shape, lasting from 10:00 up to 18:00, indicated as high levels of 20–50 nm particle number concentrations owing to the growth of newly formed particles to larger particle sizes. During the NPF event LDSA concentrations increased

nearly doubly (from $15.5 \mu\text{m}^2 \text{cm}^{-3}$ to $35.5 \mu\text{m}^2 \text{cm}^{-3}$) which is comparable to results from a previous study in urban Barcelona (Reche et al., 2015) where an LDSA increase was observed during such an event. In addition, the LDSA continues to increase after 18:00 until 22:00. This is probably being linked to the anthropogenic emissions (such as traffic and domestic heating emissions) and also may effect of NPF on LDSA concentration. Significant increase of eBC concentrations during the event are not observed, but a slight increase is observed after 15:00 that might be related to the traffic emissions; the average black carbon concentration was $0.58 \mu\text{g m}^{-3}$, lower than before and after the event at $1.59 \mu\text{g m}^{-3}$ and $1.53 \mu\text{g m}^{-3}$, respectively. Previous studies in the urban atmosphere of Singapore (Betha et al., 2013) and Barcelona (Reche et al., 2011) showed similar trends in the diurnal variation of black carbon during the NPF events.

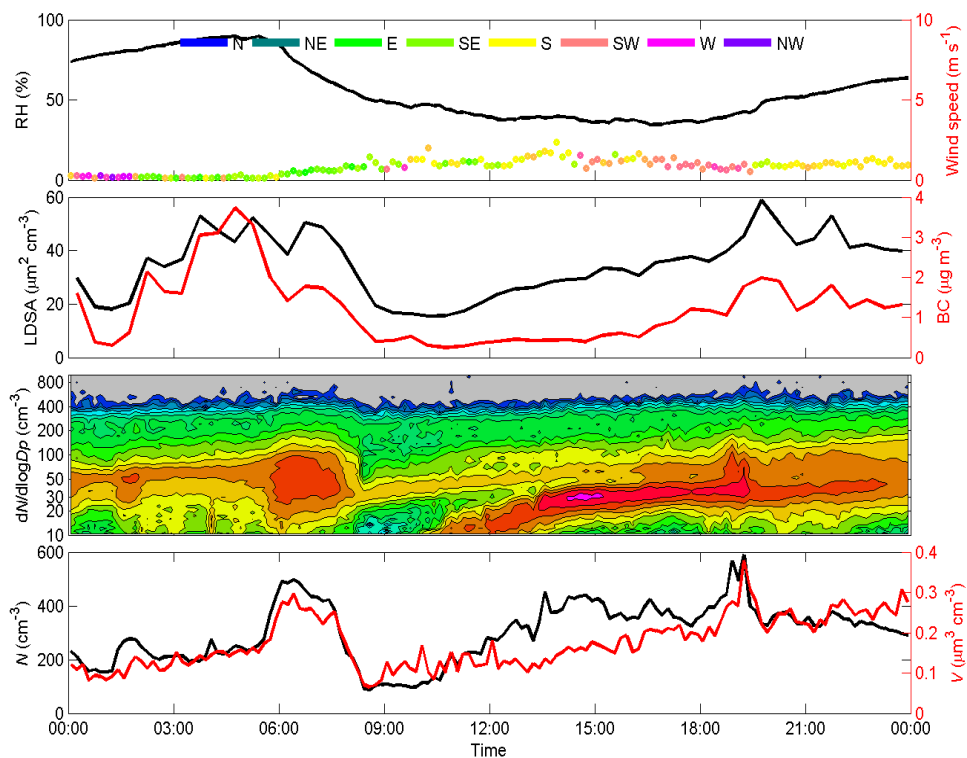


Figure 5.9: Contour plot of particle size distribution observed on 3rd May 2014 (BF site). From bottom to top, the parameters are: (i) total Particle number and volume concentrations, (ii) contour plot of particle size distributions, (iii) LDSA and eBC concentrations (iv) wind speed and relative humidity.

To explore further the overall impact and extent of NPF on LDSA, the diurnal variation of PNSD and LDSA for the NPF and non-NPF event days were averaged as shown in Figure 5.10a, and b. Figure 5.10a clearly shows the LDSA peak follows NPF peak while NO_x does not. Figure 5.10b shows the diurnal variation of non-NPF event days, it can be seen there is no peak for the nucleation mode particles and also LDSA has similar profile as nucleation mode particles. There seems to be a generalisable phenomenon that the NPF events can contribute to an increase in LDSA.

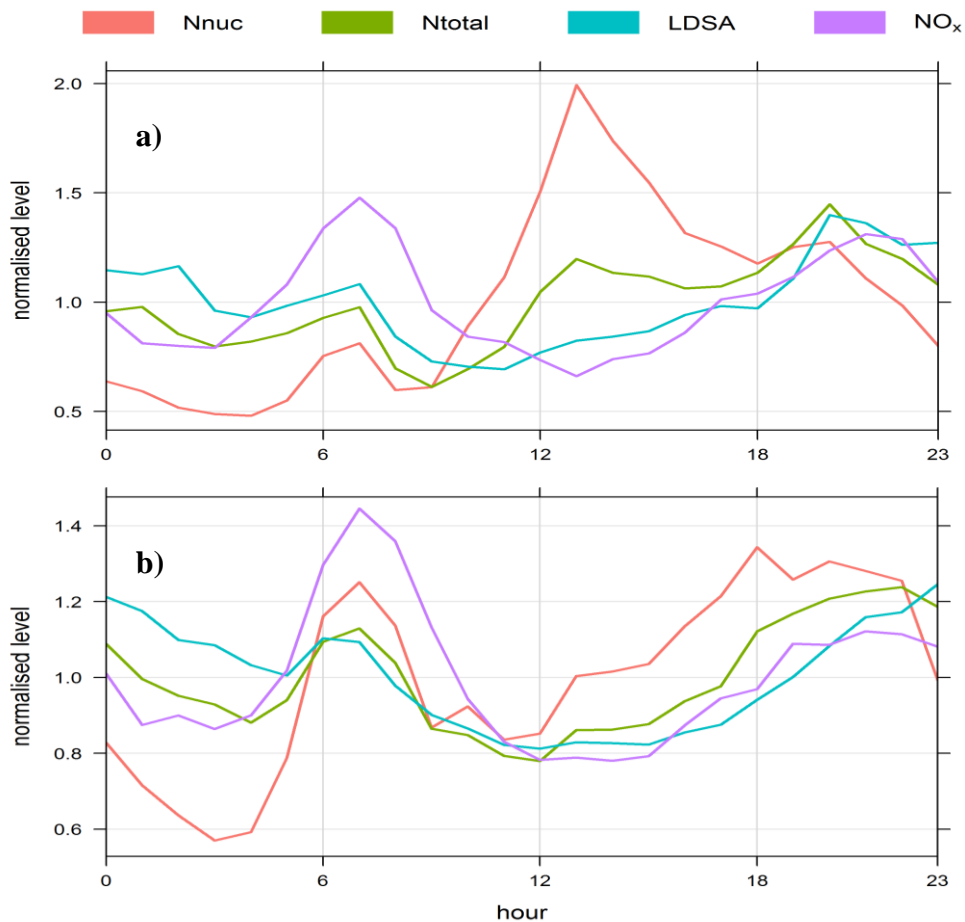


Figure 5.10: Diurnal variation of PNSD, LDSA, and NO_x for a) NPF event days (n=14), and b) Non-NPF event days (n= 72). Nnuc is the particle number concentrations when diameter 10 -25 nm and Ntotal= Particle number concentrations with diameter =10 -1000 nm, at AURN and BF sites.

5.4 Conclusions

In this study, LDSA concentrations and PNSD have been measured in the Leicester urban atmosphere along with observations of eBC, and NO_x concentrations. The annual average LDSA concentration during this study was $29.5 \mu\text{m}^2 \text{cm}^{-3}$, which was lower than previously measured at most other urban backgrounds with the exception of Zurich where the urban background was very low. Strong seasonal values of LDSA, as well as eBC, and NO_x, were measured owing to the influence of meteorological parameters and dilution effects. Furthermore, the diurnal variation of LDSA concentrations observed can be rationalised in terms of the influence of traffic emissions and the dilution effect.

An additional peak was also observed in the afternoon, during the warm season, which could be attributed to NPF events, owing to its occurrence at a time when high traffic emissions are not normally observed. The existence of an NPF event was confirmed by the gradual increase in LDSA concentration during the event to approximately double its initial value. Increases in LDSA occurred whilst eBC concentrations were low, suggesting that the LDSA did not originate from a fossil fuel combustion source, which NPF may another source of LDSA during warm months in Leicester.

Overall it can be concluded that vehicle emissions and biomass burning, particular domestic heating in cold season, in an urban area such as Leicester are the main sources of increased LDSA, eBC and also particle number concentrations.

Chapter Six

Chemical composition and source identification of PM₁₀ in Five North Western European Cities

This Chapter is currently under review in Atmospheric Research.

What are the chemical composition, seasonal variability and spatial distribution of PM₁₀ in North West European cities?

Particulate matter (PM) is a complex, heterogeneous mixture that changes in time and space. It has many different chemical constituents, several of which have been identified as potential contributors to toxicity, and varying physical characteristics. Identifying and quantifying the effects of specific components or source-related combinations on human health, particularly when particles interact with other co-pollutants, therefore represents one of the most challenging areas of environmental health research. Owing to the importance of PM₁₀ chemical composition in understanding particulate pollution sources, PM₁₀ samples were simultaneously collected at five sites (four urban background sites located in Amsterdam (AD), Antwerp (AP), Leicester (LE) and Lille (LL), and one industrial site at Wijk aan Zee (WZ)) across North-West Europe, and chemical species and sources of PM₁₀ were investigated. To facilitate the development of health-relevant air quality policies in the north-western part of Europe a better understanding of sources and composition of PM is required. A number of studies have reported sources and composition of PM in NW Europe (AQEG, 2012; Crilley et al., 2017; Mooibroek et al., 2011; Vercauteren et al., 2011; Waked et al., 2014; Weijers et al., 2011). However, no studies to date have reported a comparative analysis of PM₁₀ chemical composition at five cities across north-west Europe. In this context, the aim of this study is to compare chemical composition, seasonal and spatial variability, chemical characteristics of ambient PM₁₀ concentrations at four urban 108 background sites, and one industrial site located in NW Europe, using a harmonized approach 1 for aerosol sampling and laboratory analyses.

6.1 Introduction

Although air quality in Europe has improved significantly over the past decades, air pollution is still the single largest environmental health risk in Europe with recent studies suggesting that the disease burden resulting from air pollution is significant (EEA, 2016). Ambient particulate matter (PM) is a heterogeneous mixture of organic and inorganic constituents produced from a large variety of mechanisms linked with both natural and anthropogenic sources. Numerous studies have showed that PM exposure is strongly linked with the increase risk of mortality, respiratory, and heart diseases (de Kok et al., 2006; Dockery and Stone, 2007; Meister et al., 2012; Pope and Dockery, 2006; Taiwo et al., 2014a). PM can also impact the climate, ecosystem, and visibility by various important atmospheric processes (IPCC, 2008; Monks et al., 2009; Taiwo et al., 2014a). Nowadays, most studies focus on chemical characteristics of PM and toxicological studies in an effort to find and identify the PM properties (e.g. particle number, size, surface, chemical composition) that have the most significant impact on health and environment. There is great scientific interest in the chemical composition of ambient PM, which depends on a variety of factors including the time of year, the sources of PM and the weather conditions (Röösli et al., 2001). Numerous chemical constituents of atmospheric PM, including organic compounds, heavy metals, trace elements, ions, etc., have the potential to adversely affect human health.

The European Union has established ambient air quality limits for some toxic elements, such as lead, arsenic, nickel, mercury, cadmium, and polycyclic aromatic hydrocarbons (EC, 2004). The north-western part of Europe is considered as a hot spot zone for air pollution with high outdoor concentrations of, amongst others, particulate matter and nitrogen oxides (EEA, 2014). Particulate matter is a complex mixture resulting from several natural and anthropogenic sources including sea salt, suspended dust, pollen, volcanic ash, combustion processes, industrial activities, vehicle tyre, brake and road surface wear. Epidemiological studies attribute the most significant health impacts of air pollution to PM (WHO, 2005), although currently it is still unclear which specific properties (such as size or chemical composition) or sources of aerosol particles are most relevant to health effects (Kelly and Fussell, 2012). Ambient PM concentrations vary substantially between and within regions, as indicated by routine air quality monitoring networks. In urban areas, in addition to background PM concentrations, often imported,

traffic-related emissions and domestic heating can significantly contribute to ambient PM levels (EEA, 2014).

Current monitoring efforts generally focus on the mass concentration of PM₁₀ and PM_{2.5} in line with current air quality legislation (2008/20/EC), but these data generally do not allow the assessment of differing sources. To facilitate the development of health-relevant air quality policies in the north-western part of Europe a better understanding of sources and composition of PM is required. A number of studies have reported sources and composition of PM in NW Europe (AQEG, 2012; Crilley et al., 2017; Mooibroek et al., 2011; Vercauteren et al., 2011; Waked et al., 2014; Weijers et al., 2011). However, no studies to date have reported a comparative analysis of PM₁₀ chemical composition at five cities across north-west Europe. In this context, the main aim of this study is to compare chemical composition, seasonal and spatial variability, chemical characteristics of ambient PM₁₀ concentrations at four urban background sites, and one industrial site located in NW Europe, using a harmonized approach for aerosol sampling and laboratory analyses. Moreover, a mass closure model was applied to daily PM₁₀ samples to test whether the gravimetrically determined mass can be reconstructed by the chemically determined components at the five sampling sites.

The study was carried out between April 2013 and May 2014 over which time aerosol samples were collected daily (24 hour exposure) at fixed sites in Amsterdam (AD), Antwerp (AP), Leicester (LE), Lille (LL) and Wijk aan Zee (WZ). This study was carried out as part of the JOint Air QUality INitiative (JOAQUIN, www.joaquin.eu), an INTERREG IVB NWE funded European project, aimed at supporting health-oriented air quality policies in Europe (Cordell et al., 2016; Hama et al., 2017a, 2017b, and 2017c; Hofman et al., 2016; Joaquin, 2015b)

6.2 Experimental

6.2.1 Sampling sites

Aerosol samples were collected at five sites in NW Europe: Amsterdam (AD; The Netherlands), Wijk aan Zee (WZ; The Netherlands), Antwerp (AP; Belgium), Leicester (LE; United Kingdom) and Lille (LL; France) (Figure 6.1). The detailed site descriptions are summarised in Table 6.1. Site WZ is an industrial monitoring site about 30 km from Amsterdam. The four other sites are considered to be urban background sites for PM₁₀ monitoring. Details about the characteristics and locations of the sampling sites can be found in Cordell et al. (2016). For a detailed overview of the sampling sites and the JOAQUIN project, the reader is referred to the final report (Joaquin, 2015b).

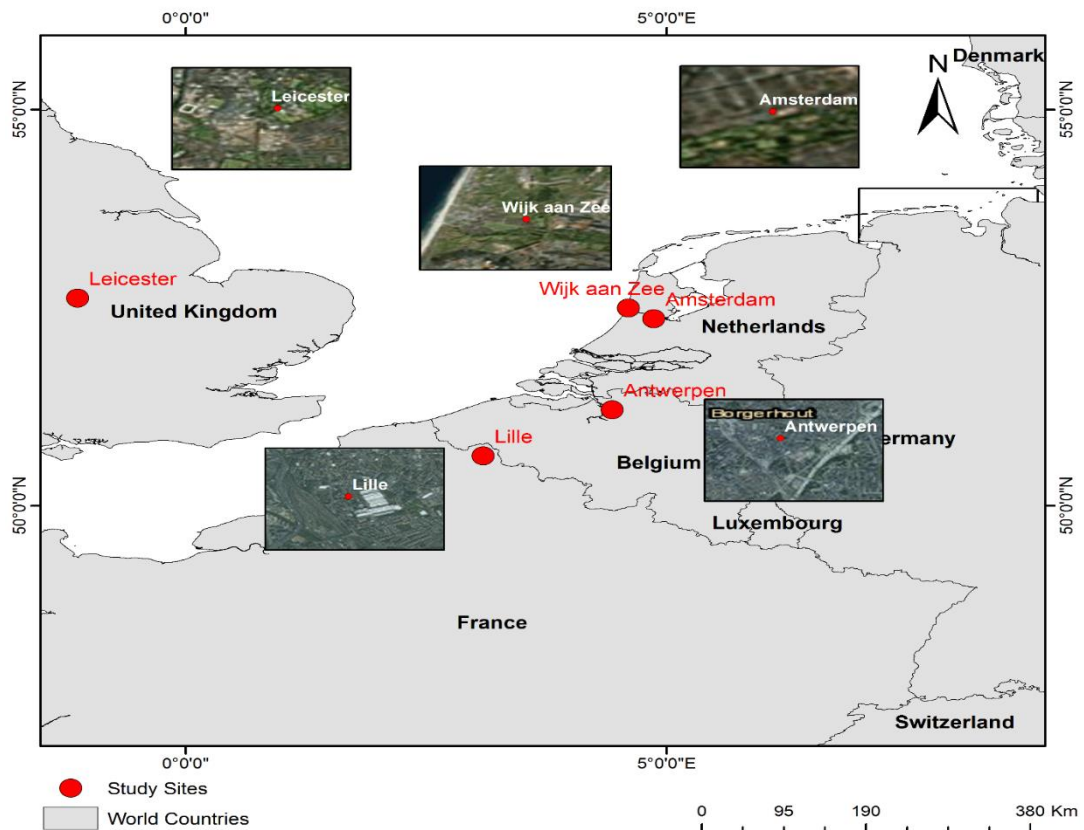


Figure 6.1: Map of the locations of all monitoring sites.

Table 6.1: Location and characteristics of the five PM₁₀ sampling sites.

City	Site name	Latitude	Longitude	Distance to main street (m)	Traffic Intensity (Vehicles/day)
Amsterdam (AD)	Vondelpark	52° 21' 35" N	4° 51' 59" E	64	17000
Antwerp (AP)	Borgerhout	51° 12' 35" N	4° 25' 55" E	30	29500
Leicester (LE)	University of Leicester	52° 37' 12" N	1° 07' 38" W	140	22500
Lille (LL)	Lille Fives	50° 37' 41" N	3° 05' 25" E	35	NA
Wijk aan Zee (WZ)	Wijk aan Zee	52° 49' 40" N	4° 60' 23" E	70	NA

6.2.2 PM₁₀ sampling

Sampling was carried out for 14 months (426 days) from 1 April 2013 to 31 May 2014, except for LL where the measurements started 2 months later (5 June 2013 to 31 May 2014). The samples were collected daily (24 hour exposure) onto 47 mm quartz filters (Pall Tissuquartz™ filters, 2500 QAT-UP) using a sequential sampler (Derenda PNS16 at AD and WZ and Leckel SEQ47/50 at AP, LE and LL) with a PM₁₀ inlet running at 2.3 m³ h⁻¹ for 24 h per filter. Filter samples collected every 6th day for the period were analysed for water-soluble ions, elemental and organic carbon, metals, and monosaccharide anhydrides. Flows were checked every 14 days when changing the filter compartments. Filters were weighed before and after sampling in order to determine total PM₁₀ collection. For pre- and post-sampling weighing filters were conditioned at 20 ± 1°C and 50 ± 5% relative humidity for 48 h, weighed, left for a further 24 h and re-weighed. More details about the PM₁₀ sampling and the instrumentation can be found in Joaquin (2015b).

6.2.3 Chemical analysis and Analytical techniques

Potassium (K^+), calcium (Ca^{2+}), magnesium (Mg^{2+}), and sodium (Na^+) were analysed by inductively coupled plasma optical emission spectroscopy (ICP-OES), and ammonium (NH_4^+), chloride (Cl^-), nitrate (NO_3^-) and sulphate (SO_4^{2-}) were analysed using ion chromatography with conductivity detection (IC-CD) (eluent: methane sulfonic acid (MSA) for NH_4^+ and NaOH for the anions). More details about sample preparation can be found in Joaquin (2015b). The EC/OC analysis was performed according to Technical Report CEN/TR16243 “Ambient air quality - guide for the measurement of elemental carbon (EC) and organic carbon (OC) deposited on filters”. The analysis was done with a laboratory organic/elemental carbon aerosol analyser (Sunset Laboratory Inc, Tigard (OR), USA). The NIOSH protocol, which is most suitable for the traffic influenced PM_{10} samples of the Joaquin project, was selected for the analysis. Calcium (Ca), iron (Fe), potassium (K) and zinc (Zn) were analysed by ICP-OES. Aluminium (Al), titanium (Ti), vanadium (V), chromium (Cr), manganese (Mn), nickel (Ni), copper (Cu), arsenic (As), molybdenum (Mo), cadmium (Cd), antimony (Sb), barium (Ba) and lead (Pb) were analysed by inductively coupled plasma mass spectrometry (ICP-MS). Levoglucosan (Lev), mannosan (Man) and galactosan (Gal) were quantified using a validated gas chromatography-mass spectrometry (GC-MS) method described in detail by Cordell et al. (2014). An improved gas chromatography-mass spectrometry method to quantify atmospheric levels of monosaccharides (MAs) was developed and, for the first-time, fully validated. The method used an optimised, low-volume methanol extraction, derivatisation by trimethylsilylation and analysis with high-throughput GC-MS. Descriptions on chemical analysis (and analytical techniques) and quality assurance and quality control (QA/QC) were described in the final report (Joaquin, 2015b).

6.2.4 The coefficients of divergence

The correlation coefficient is a standard method used to assess the linear relationship between two data sets. Spearman rank correlation coefficients (r) were used to find the spatial variability between sampling sites. To evaluate intra-urban spatial variation coefficients of divergence (COD) were used ((Contini et al., 2012a; Jeong et al., 2010; Krudysz et al., 2009; Turner and Allen, 2008; Wilson et al., 2005):

$$\text{COD}_{ab} = \sqrt{\frac{1}{n} \sum_{i=1}^n \left[\frac{(C_{ia} - C_{ib})}{(C_{ia} + C_{ib})} \right]^2} \quad (6.1)$$

where C_{ia} and C_{ib} are PM_{10} concentrations in day i at sites a and b , respectively, and n is the number of observations (Krudysz et al., 2009; Wongphatarakul et al., 1998). The COD provided information about the degree of uniformity between sampling sites. A COD value equal to zero means the concentrations are nearly identical at both sites while a value of one shows concentrations are highly different. COD values greater than about 0.20 show somewhat heterogeneous spatial distributions (Cesari et al., 2016a; Pinto et al., 2004; Wilson et al., 2005).

6.2.5 Reconstruction of PM_{10}

In order to understand the contributions of each constituent in PM_{10} , PM_{10} at the four urban areas and one industrial site were reconstructed by chemical mass closure. The chemical components were divided into seven categories: mineral dust (MD), organic matter (OM), elemental carbon (EC), trace elements (TE), sea salt (SS), secondary inorganic aerosol (SIA), and monosaccharides (MSS).

MD is the sum of Al, Ca, Fe, and Ti multiplied by various factors (Eq. 2) to convert them to their common oxides (Al_2O_3 , Fe_2O_3 , CaO, MgO, K_2O , TiO_2) (Harrison et al., 2003; Nava et al., 2012; Rodriguez et al., 2004; Terzi et al., 2010):

$$\text{MD} = 2.2 \text{ Al} + 1.16 \text{ Mg} + 0.6 \text{ Fe} + 1.63 \text{ Ca} + 2.42 \text{ Fe} + 1.94 \text{ Ti} \quad (6.2)$$

The chemical structure of OM in the ambient PM is rather complex. When reconstructing OM, it is generally expressed as a certain factor multiplied by the measured concentrations of OC. Previous studies have suggested 1.4 is a suitable factor for organic aerosol in urban area (Harrison et al., 2003; Turpin and Lim, 2001; Vecchi et al., 2008; Viana et al., 2007) and that value is used in this work. EC is measured by direct measurements. TE (As, Ba, Cd, Cr, Cu, Mn, Mo, Ni, Pb, Sb, V, and Zn) were also added to the analysis. TE represent a small percentage of the PM₁₀ total mass concentrations, however, they have a significant impact on health (McNeilly et al., 2004; Moreno et al., 2004) and environment owing to their toxicity and anthropogenic origin (Rees et al., 2004). The marine contribution was found, assuming that soluble Na⁺ in PM₁₀ aerosol samples comes solely from sea salt, the SS was calculated (Eq. 3) by sum of Na⁺ concentrations and fractions of the concentrations other water soluble ions (Cl⁻, Mg²⁺, K⁺, Ca²⁺, SO₄²⁻) based on a standard sea water composition (Seinfeld and Pandis, 2006).

$$SS = [Na^+] + [ssCl^-] + [ssMg^{2+}] + [ssK^+] + [ssCa^{2+}] + [ssSO_4^{2-}] \quad (6.3)$$

where ss-Cl⁻ is calculated as total [Na⁺] multiplied by 1.8, ss-Mg²⁺ as total [Na⁺] multiplied by 0.12, ss-K⁺ as total [Na⁺] multiplied by 0.036, ss-Ca²⁺ as total [Na⁺] multiplied by 0.038, and ssSO₄²⁻ as total [Na⁺] multiplied by 0.252. SIA was calculated as the sum of concentrations of nss-SO₄²⁻ (non-sea salt, obtaining by subtracting ss-SO₄²⁻ from total concentration of SO₄²⁻), NO₃⁻, and NH₄⁺ (Terzi et al., 2010). Finally, MSS is obtained by sum of the monosaccharides (Lev, Gal, and Man). MSS only presents a small percentage of the PM₁₀ mass but were added to the analysis owing to their importance as biomass burning markers (Cordell et al., 2016; Fuller et al., 2014).

6.2.6 Principal component analysis

Principal component analysis (PCA) has widely been used as a statistical factor analysis method capable of identifying and separating chemical components of PM according to their sources in urban areas (Ciaparra et al., 2009; Cusack et al., 2013; Lawrence et al., 2013; Mari et al., 2010; Shi et al., 2011). PCA was undertaken using the software XLSTAT 2016. The orthogonal transformation method with varimax rotation was employed, retaining principal components with eigenvalues greater than one. The PCA method can be used to factorise the input data of different concentration of species assuming a linear relationship between total PM mass and the component concentrations of various species (Bongiovanni et al., 2000; Hopke, 2000). The multivariate mathematical approach contains several steps to group the elemental data. In the first step, the concentrations of species are standardised:

$$X_{is} = \frac{C_{is} - C_i}{d_i} \quad (6.4)$$

where C_{is} is the concentration of the variable i in the sample s , and C_i and d_i are the mean and standard deviation of the variable i for all samples involved in the method analyses. The PCA model is expressed as:

$$X_{is} = \sum_{j=1}^N L_{ij} S_{js} + E_{is} \quad (6.5)$$

where L_{ij} is the factor loading of the variable i in the source j with n number of sources, S_{js} is the factor score of the source j for sample s and E_{is} is the residual of variable i in the sample s which not accounted by j sources (factors). In this statistical analysis a set of multiple inter-correlated variables is substituted by smaller independent variables by orthogonal transformations. A varimax normalized rotation is applied to maximize (or minimize) the values of the factor loadings of each species measured in relation to each rotated principal component.

6.3 Results and Discussion

6.3.1 PM₁₀ Mass concentrations and spatial comparison

Monthly variations of PM₁₀ mass concentrations at the five sites are shown in Figure 6.2. Clear seasonal variations of PM₁₀ concentrations are observed at all the sampling sites throughout the year. It should be noted that the observed seasonal pattern of PM₁₀ at each sampling site shows a high level of similarity (Figure 6.2) indicative of a regional characteristic for PM₁₀ in the north-west Europe region. The data were split into three time periods for analysis: the cold period (November to April), the warm period (May to October), and the entire year. The arithmetic mean and standard deviation of PM₁₀ for the samples collected at the five locations are given in Table 6.2. High concentrations of PM₁₀ in the cold period are probably attributable to the higher frequency of temperature inversion and the relatively stable atmospheric conditions which are not conducive to the dilution or advection of air pollutants, as well as the impacts of reduced mixing height along with increased energy-based emissions including wood burning (Cordell et al., 2016). Lower concentrations of PM₁₀ in summer might be linked to higher mixing layer heights, and reduced (heating) emissions.

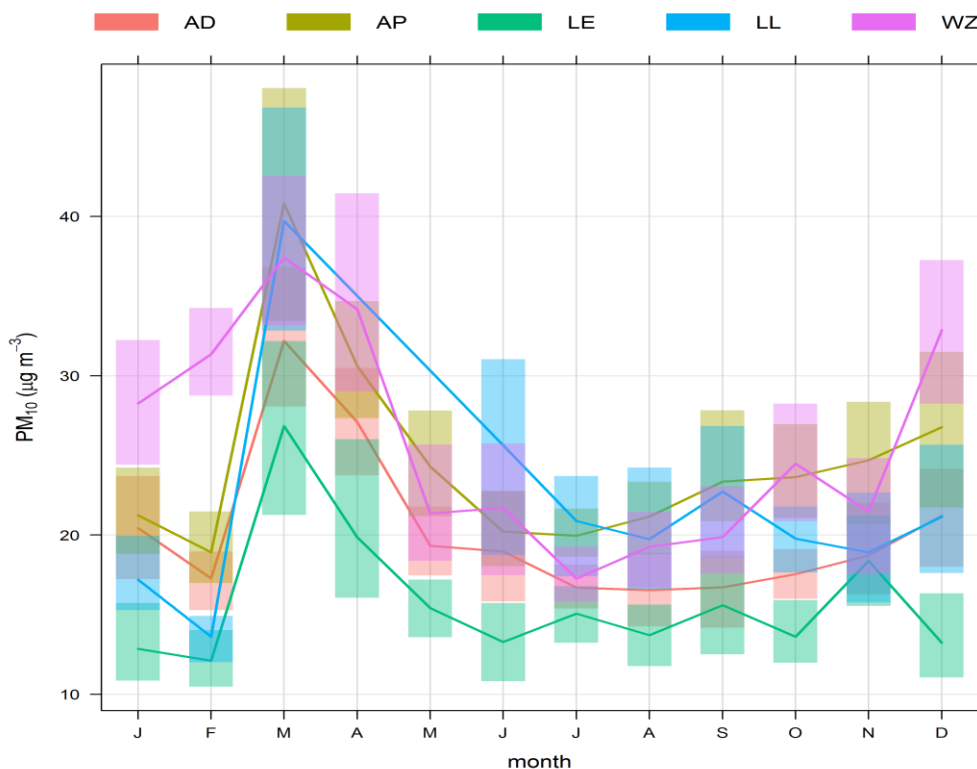


Figure 6.2: Monthly variations of PM₁₀ concentrations at the sampling sites.

Table 6.2: PM₁₀ mass concentration ($\mu\text{g m}^{-3}$) at the five sites.

	AD			AP			LE		
	Annual	Cold Period	Warm Period	Annual	Cold Period	Warm Period	Annual	Cold Period	Warm Period
Average	20.71	24.24	17.65	24.92	28.11	22.1	16.16	18.33	14.45
Max	84.9	84.9	54.62	100.06	100.06	62.43	76.61	76.61	44.96
Median	18.2	20.81	16.23	21.25	24.32	19.92	13.47	14.96	13
Min	6.28	6.28	7.72	7.16	7.16	9.65	2.27	4.42	5.15
St. dev.	10.61	12.81	6.51	12.13	14.59	8.45	9.6	12.09	6.51
	LL			WZ					
Average	22.4	23.23	21.66	25.6	31.2	20.52			
Max	98	98	63.49	81.4	89.22	52.19			
Median	18.39	18.47	18.47	23.77	28.88	18.27			
Min	4.14	6.25	4.14	4.34	4.34	6.05			
St. dev.	13.32	15.3	10.7	12.68	14.35	8.85			

For the experimental period (June 2013-May 2014), the PM₁₀ concentrations vary from 16.1 to 25.6 $\mu\text{g m}^{-3}$ at all sites. The highest annual average concentrations of PM₁₀ were measured in AP (24.9 $\mu\text{g m}^{-3}$), and WZ (25.6 $\mu\text{g m}^{-3}$), which might be related to industrial activities near these sites. The lowest PM₁₀ levels were observed in LE (16.2 $\mu\text{g m}^{-3}$). The annual mean concentrations were 20.7 and 22.4 $\mu\text{g m}^{-3}$ in AD and LL, respectively (Table 6.2). The number of exceedances of the EU day limit value for PM₁₀ (50 $\mu\text{g m}^{-3}$) was highest at AP (20 days/year) and WZ (16), moderate at LL (12) and lowest at AD (8) and LE (6). Exceedances of the day limit value mainly occurred in March and April.

To address the spatial distribution of PM₁₀ the COD values have been calculated between all sites and is shown in Table 6.3. According to previous studies (Cesari et al., 2016a; Contini et al., 2012a; Wilson et al., 2005), the threshold value was set to 0.2 for the comparison of COD values of PM₁₀ between all sites. Most COD values were higher than this threshold, except for the site pairs AD - AP (COD = 0.162; Table 6.3), AD - WZ (0.192), and AP - LL (0.155), indicating those sites had more similar regional PM₁₀ pollution characteristics.

Table 6.3: COD of the daily PM₁₀ ($\mu\text{g m}^{-3}$) between the monitoring sites.

COD					
	AD	AP	LE	LL	WZ
AD	0	0.162	0.24	0.204	0.192
AP		0	0.294	0.155	0.231
LE			0	0.277	0.342
LL				0	0.301
WZ					0

6.3.2 Characteristic of chemical species in PM₁₀

6.3.2.1 The water soluble ions (WSIs) analysis

The annual, cold period and warm period concentrations of WSIs (NO_3^- , SO_4^{2-} , Cl^- , NH_4^+ , Na^+ , K^+ , Mg^{2+} , and Ca^{2+}) for the five sites are given in Table S6.1. At all sites the major contributor to anions was NO_3^- followed by SO_4^{2-} while the dominant cations were NH_4^+ , and Na^+ . In this study, secondary ions NO_3^- , SO_4^{2-} , and NH_4^+ were the major WSIs in PM₁₀, which accounted for 37, 35, 33, 37, and 33% of the PM₁₀ concentrations (Table S6.2) and 79, 82, 72, 82, and 69% of the total WSIs in PM₁₀ for the sites AD, AP, LE, LL, and WZ, respectively. On the contrary, the concentrations of primary ions such as Cl^- , Na^+ , K^+ , Mg^{2+} , and Ca^{2+} were relatively low, which indicated that the secondary particles were the main pollutants in this region. In terms of annual concentrations, the three major secondary ions in all sites followed the order of $\text{NO}_3^- > \text{SO}_4^{2-} > \text{NH}_4^+$.

Similar seasonal variations of the WSIs were observed at all sites, showing higher levels in the cold period (except for SO_4^{2-}) and lower concentrations in the warm period (Table S6.1). These patterns can be ascribed to increased domestic heating in winter (Cordell et al., 2016), leading to high concentrations of precursors, the meteorological conditions as well as regional transportation and secondary reactions. In addition, the higher concentrations of NO_3^- and Cl^- in the cold season could be due to a larger contribution of marine aerosol or lower overall concentrations in the warm period. The autumn and early winter are the seasons with the most storms at sea, generating and transporting sea salt to the continent. Furthermore, there might be an influence of road salting during the winter. These two components react with NH_4^+ to form ammonium salt, and these salts can dissociate to gaseous compounds in the warm period caused to decrease concentrations of NO_3^- and Cl^- in summer. Because of higher storm activity there might be more fresh sea salt during winter compared to the summer. However, relatively higher concentrations of SO_4^{2-} were found during the warm period at AD, AP, and LE sites (Table S6.2), indicating photochemical formation of sulphates at these sites (Hama et al., 2017a, and 2017b; Hofman et al., 2016). Note that the concentrations of Cl^- , Na^+ , and Mg^{2+} were clearly higher in WZ than at the other sites, owing to its close proximity to the North Sea. NO_3^- concentrations at LE site were significantly lower than at the other sites, likely due to the fact that LE site is situated in more residential area, with less traffic and lower industrial/agricultural emissions. High seasonal variation was also observed for K^+ with higher levels in the cold seasons, suggesting impact of biomass combustion sources in this region (Cordell et al., 2016).

It is interesting to note that the ratio of $\text{NO}_3^-/\text{PM}_{10}$ was high in the cold period and low in the warm period, while the $\text{SO}_4^{2-}/\text{PM}_{10}$ ratio was high in summer and low in the cold season consistently for the five sites (Table 6.4). This might be linked to relatively high levels of OH and O_3 , high temperature and solar radiation in summer months, which are conducive for the decomposition of NO_3^- and generation of SO_4^{2-} from SO_2 . Additionally, the ratio $\text{SO}_4^{2-}/\text{NO}_3^-$ in warm months is significantly higher than in other months (Table 6.4), which is probably attributable to the dissociation of nitrate in PM_{10} . WSIs concentrations in this region are comparable to those previously found in other urban sites in Europe and Asia (Takahashi et al., 2008; Terzi et al., 2010; Viana et al., 2007).

Table 6.4: The ratios of $\text{NO}_3^-/\text{PM}_{10}$, $\text{SO}_4^{2-}/\text{PM}_{10}$, and $\text{SO}_4^{2-}/\text{NO}_3^-$ in PM_{10} at five sampling sites during different periods.

	AD			AP			LE		
	Annual	Cold Period	Warm Period	Annual	Cold Period	Warm Period	Annual	Cold Period	Warm Period
$\text{NO}_3^-/\text{PM}_{10}$	0.20	0.233	0.14	0.205	0.237	0.15	0.177	0.21	0.118
$\text{SO}_4^{2-}/\text{PM}_{10}$	0.09	0.075	0.12	0.083	0.067	0.10	0.095	0.07	0.1244
$\text{SO}_4^{2-}/\text{NO}_3^-$	0.45	0.324	0.83	0.403	0.285	0.69	0.538	0.36	1.055
	LL			WZ					
$\text{NO}_3^-/\text{PM}_{10}$	0.22	0.26	0.11	0.172	0.189	0.12			
$\text{SO}_4^{2-}/\text{PM}_{10}$	0.08	0.075	0.09	0.096	0.084	0.12			
$\text{SO}_4^{2-}/\text{NO}_3^-$	0.36	0.290	0.81	0.560	0.443	0.99			

The correlation between the WSIs during different seasons is shown in Figure S6.1. The correlation between NO_3^- and NH_4^+ are $r=0.91-0.98$ (in winter), and $0.78-0.93$ (in summer). The correlation between SO_4^{2-} and NH_4^+ ($r=0.78-0.98$, in winter) shows a similar tendency with that between NO_3^- and NH_4^+ during different seasons at all sampling sites (Figure S6.1), indicating the secondary origin. Higher correlations between NO_3^- and NH_4^+ and between SO_4^{2-} and NH_4^+ were observed at all monitoring sites. However, lower correlations were found between NH_4^+ and Cl^- , suggesting that ammonium nitrate, ammonium sulphate, and ammonium hydrogen sulphate might be major source of NH_4^+ in these cities (Figure S6.1). In addition, the correlation between Cl^- and Na^+ , and Cl^- and Mg^{2+} was significant across seasons and sampling sites. This observation could be related to the presence of marine aerosol and crustal matter for Mg^{2+} .

6.3.2.2 Carbonaceous material analysis

The mean concentrations of OC, EC for the annual, cold, and warm periods are given in Table S6.3. The annual average concentrations of OC and EC are 3.02, and 0.58 $\mu\text{g m}^{-3}$, accounting for 12.7%, and 2.5% of PM_{10} , 4.40, and 1.56 $\mu\text{g m}^{-3}$, accounting for 14.43%, and 5.12% of PM_{10} , 3.39, and 0.95 $\mu\text{g m}^{-3}$, accounting for 17.54%, and 4.94% of PM_{10} , 4.47, and 1.19 $\mu\text{g m}^{-3}$, accounting for 15.0%, and 3.99% of PM_{10} , 2.81, and 0.81 $\mu\text{g m}^{-3}$, accounting for 9.68%, and 2.79% of PM_{10} (Table S6.3) at AD, AP, LE, LL, and WZ sites, respectively. The concentrations of OC and EC are higher in the cold period and lower in the warm months. The mean OC concentration was highest in AP and LL, and lowest in WZ. The average EC concentration was highest in AP, followed by LL, and lowest in AD (Table S6.3). Total carbonaceous aerosol (TCA) was calculated by summing EC and OM (multiplying the concentrations of OC by 1.4) (Turpin and Lim, 2001). The annual levels of TCA are 4.8 $\mu\text{g m}^{-3}$ (20.4% of PM_{10}), 7.7 $\mu\text{g m}^{-3}$ (25.3% of PM_{10}), 5.7 $\mu\text{g m}^{-3}$ (30% of PM_{10}), 7.5 $\mu\text{g m}^{-3}$ (25.0% of PM_{10}), and 4.8 $\mu\text{g m}^{-3}$ (16.4% of PM_{10}) at AD, AP, LE, LL, and WZ sites, respectively (Table S6.3). Higher TCA concentrations were observed in the cold period with the same seasonal variation of OC at all sites. The mean TCA concentration was highest in AP and LL, and lowest in WZ (Table S6.3). Several studies state that the ratios of OC/EC from biomass burning and coal combustion are relatively higher, while that of traffic emissions are relatively lower (Safai et al., 2014; Schauer et al., 2002). The concentration ratio of OC/EC can be used to identify primary and secondary aerosol sources. EC is a component that is related to the combustion of fossil fuels and of (diesel) traffic in particular (primary aerosol sources), while OC exists in both primary and secondary organic aerosol (SOA) sources produced in complex photochemical reactions (Chen et al., 2016; Gray and Cass, 1986; Ho et al., 2002). The highest annual ratio of OC/EC was observed in AD (5.15), while lowest value was found in AP (2.81) (Table S6.3) as a result of moderate secondary organic carbon combined with low EC levels compared to the other sites. The ratio of OC/EC have been found in the range 1-4 in the previous studies for PM_{10} at urban sites (Wang et al., 2005, and references therein).

If the ratio of OC/EC is greater than 2.0, it can be considered that OC is contributed by both primary and secondary sources, and higher the ratio indicating higher contribution of SOA (Cao et al., 2009). In this paper, the OC/EC ratios at the five sites were in the

range of 2.81-5.15, showing a clear prevalence of organic carbonaceous species over EC which indicates potential SOA formation.

The scatter plots of OC and EC concentrations at the five sites are shown in Figure 6.3. The correlations between the OC and EC were stronger in cold months (winter and autumn) at the AP, LE, LL, and WZ sites ($R^2 = 0.52-0.87$ (Figure 6.3), $r = 0.61-0.93$ (Figure 6S.2), suggesting that OC and EC might be influenced by the same sources to some extent in the cold period at these sites. However, the correlations between OC and EC were relatively weaker at the AD site ($R^2 = 0.12$ (Figure 6.3), $r = 0.34-0.41$ (Figure S6.2)). Furthermore, very weak correlations ($R^2 = 0.07-0.3$ (Figure 6.3), $r = 0.08-0.55$ (Figure S6.2)) were observed during the warm period, especially in summer at the five sites. This might be associated to the OC and EC were affected by different emission sources at the sampling sites in summer.

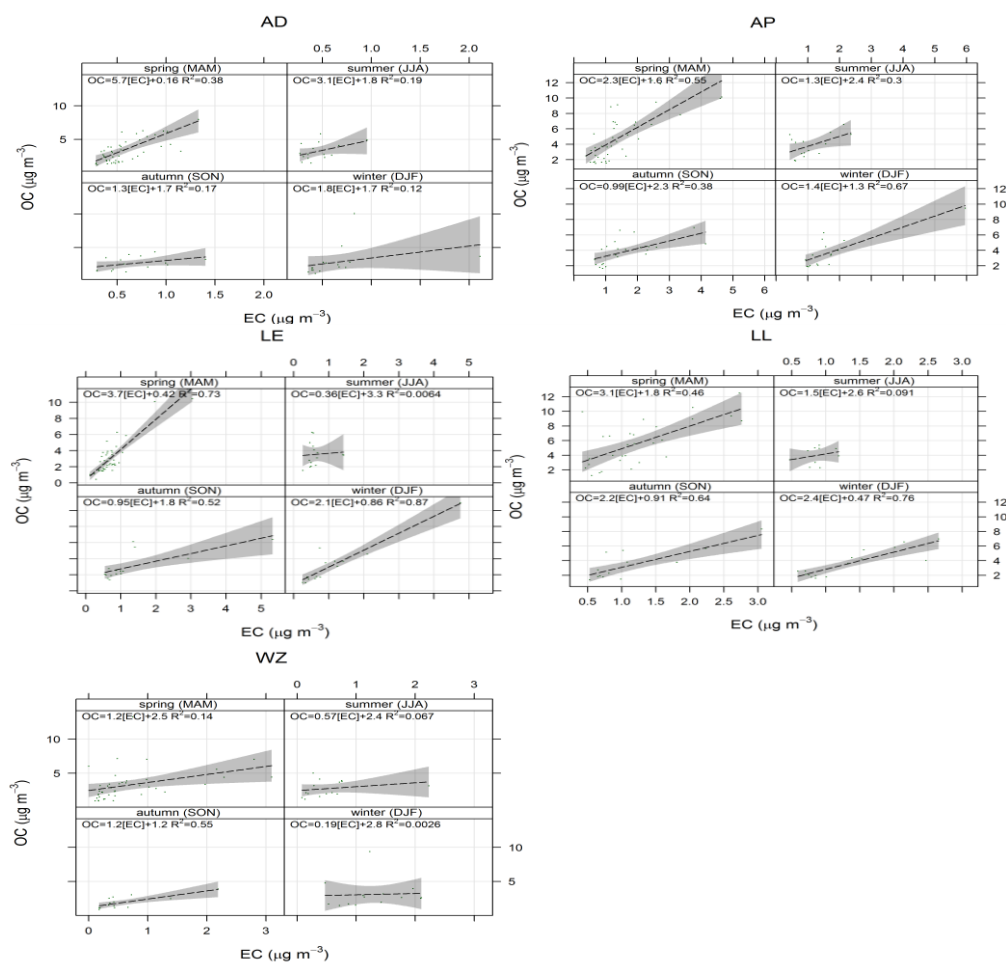


Figure 6.3: Correlations between OC and EC during different seasons at all sampling sites.

6.3.2.3 Minerals and trace elements analysis

The average concentrations (annual, cold, and warm periods) of the seventeen detected elements (Al, As, Ba, Ca, Cd, Cr, Cu, Fe, K, Mn, Mo, Ni, Pb, Sb, Ti, V, and Zn) in PM₁₀ have been quantified at the five sampling sites (Table S6.4). The annual percentages of total detected minerals (excluding K) in PM₁₀ were 4.5, 6.1, 5.3, 6.0, and 9.1% at AD, AP, LE, LL, and WZ, respectively. The average levels of the various elements are highly differentiated. Crustal elements (Al, Ba, Ca, Fe, Mn, and Ti) dominate the identified elements of PM₁₀, accounting for 91.3, 90.8, 91.7, 92.2%, and 94.5% of the total detected minerals at AD, AP, LE, LL, and WZ, respectively. The concentrations of the crustal metals were higher during the cold period and lower in the warm period (Table S6.4), which was consistent with the seasonal variation of PM₁₀ mass concentration. The higher concentration of the crustal elements (94.5%) at WZ might be attributable to the larger industrial activities near this site, for example major steel industry in this area (Joaquin, 2015b). In addition, trace elements (As, Ba, Cd, Cr, Cu, Mo, Ni, Pb, Sb, V and Zn) accounted for 8.7, 9.2, 8.3, 7.8, and 5.5% of the total detected minerals at AD, AP, LE, LL, and WZ, respectively. The levels of the trace elements were relatively higher at AD, AP, and LE sites, suggesting higher influence of traffic emissions.

To show the impacts of anthropogenic emissions on the concentrations of particle associated elements, an enrichment factor (EF) analysis has been employed in previous studies (Adamo et al., 2011; Almeida et al., 2017; Kim et al., 2002; Liu et al., 2017; Samiksha et al., 2017). In this work, Al was used as a reference element (Lin et al., 2015; Samiksha et al., 2017). The EF was calculated as:

$$EF_X = \frac{(C_X|C_R)_{\text{aerosol}}}{(C_X|C_R)_{\text{crust}}} \quad (6.6)$$

where C_X and C_R are the concentrations of the focus and reference element in the aerosol and upper continental crust, respectively (Wedepohl, 1995). The EF analysis provides only qualitative information, owing to the wide variation of the elemental concentrations of the upper crust at various locations. The EF was not carried out for K as almost all of the samples were below the limits of detection, (Joaquin, 2015b). The EF values of the elements in PM₁₀ at the five sampling sites are shown in Figure 6.4. The EF values for Fe, Mn, Ti, Ba, and Ca were all close to 10 at the sampling sites (except WZ), suggesting

that these elements are mostly derived from the crustal sources. It should be noted that the EF values for Fe (EF = 20.3), and Mn (EF = 37.0) at WZ site were higher than the other sites, indicating that these elements were mainly from industrial activities such as the major steel industry in this area (Joaquin, 2015b). The EF values for V, Cr, at all sampling sites, and Fe and Mn at the WZ site were in the range of 10-100, suggesting both natural and anthropogenic sources (such as traffic emissions and industry). Of the other elements, PM₁₀ was highly enriched (EF>100) in As, Cd, Cu, Mo, Ni, Pb, Sn, and Zn at all sampling sites, indicating that these elements are related with human activities, such as vehicular traffic, industrial sources and so on. Notably, amongst all elements in PM₁₀ at all sites, Cd and Sb were highly enriched. Cd was highest at AP and WZ, followed by LL. For AP this is likely due to industrial activities at Umicore (Hoboken) and for WZ likely due to Tata Steel (Joaquin, 2015b). In addition, previous studies have suggested that the high EF values of Sb, Zn, and Cu might be related to brake wear (Amato et al., 2016). Mechanical abrasion of brake wear and tires are possible sources of Cu, Zn, and S accounting for their higher enrichment in PM₁₀ (Amato et al., 2009). The enriched minerals in PM₁₀, particularly Sb, Cu, and Zn, are known to be used in some materials, such as additives to vehicle lubricants as anti-oxidants and anti-corrosives and in in brake linings (Thorpe and Harrison, 2008). Finally, it can be concluded that the anthropogenic sources (vehicular traffic emissions, industrial activities, and brake wear) all contribute to the abundance of these elements.

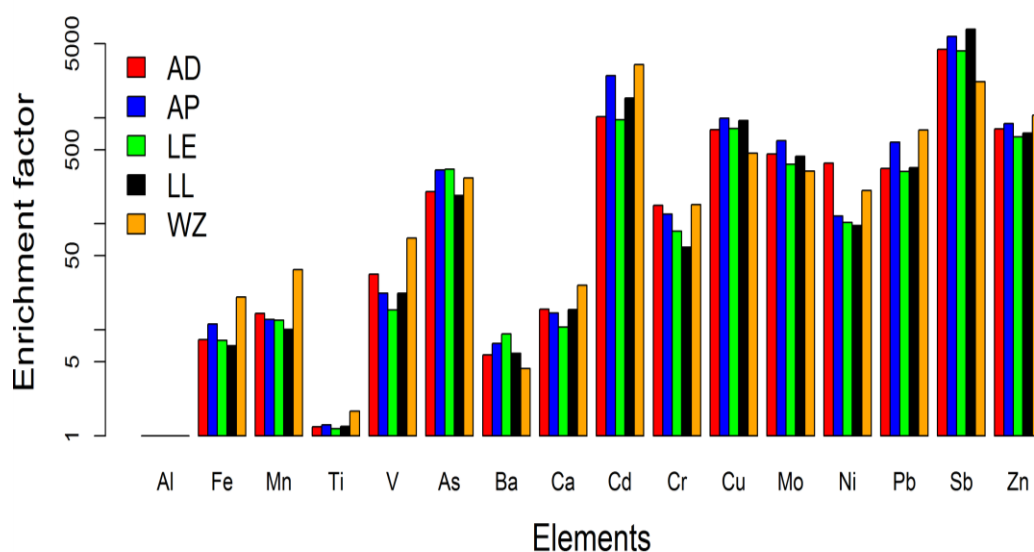


Figure 6.4: Crustal enrichment factor (EF) for the different elements in all cities.

6.3.2.4 Monosaccharide anhydrides (MAs) analysis

Monosaccharide anhydrides (MAs) such as levoglucosan (Lev), Mannosan (Man) and Galactosan (Gal) have been considered as candidate tracers for residential wood combustion (Simoneit et al., 1999). Lev, Man, and Gal were detected in all PM₁₀ aerosol samples at the sampling sites. The annual atmospheric concentrations of Lev, Man, and Gal were 49.9, 12.59, and 4.41 ng m⁻³, 99.69, 26.55, and 12.03 ng m⁻³, 52.83, 16.01, and 5.93 ng m⁻³, 157.7, 35.39, and 12.97 ng m⁻³, 33.5, 10.01, and 5.08 ng m⁻³ at AD, AP, LE, LL, and WZ, respectively, details are given in Table S6.5. The concentrations of MAs in the cold period were on average 5.05, 3.52, 3.49, 7.27, and 4.95 times higher than those in the warm period for AD, AP, LE, LL, and WZ, respectively. The MAs (particularly Lev) concentrations at LL were clearly higher than at the other sites, indicating more biomass/wood burning in LL compared to other regions in the study (Waked et al., 2014). The seasonal variation of MAs (high levels in the cold period, low in summer) can be related to the impact of increased biomass burning from residential heating in winter, and also may be linked to different meteorological condition (wind speed, temperature, and mixing layer height) in cold and warm periods in the north-west European area. Additionally, low concentrations of MAs (especially Lev) or degradation of Lev in summer may be linked to present high OH radicals in atmosphere (Hoffman et al., 2010). However, whilst this might have significant effects in tropical regions it is likely to have little impact in NW Europe (Cordell et al., 2016). Lev, used as a marker of biomass combustion and was the most abundant MA measured during all periods in this study, while Gal was found in the lowest concentrations in all seasons (Table S6.5). The correlation between the MAs and PM₁₀ are shown in Figure S6.3. The highest correlation ($r=0.77-0.89$, see Figure S6.3) between the MAs and PM₁₀ concentrations were observed in the cold period at all sampling sites, suggesting a greater contributions of MAs (particularly Lev) to PM₁₀ in this period. Low and even negative correlations ($r= -0.33-0.41$, see Figure S6.3) were found in summer, indicating that PM₁₀ mass was influenced by other sources than biomass burning in summer. The similar correlation can be found between the Lev and the other MAs (Man and Gal) which are high in the cold period and low in the summer (see Figure S6.3). More information about MAs in this region can be found in a recent study (Cordell et al., 2016).

6.3.3 Chemical Mass closure of PM₁₀

The results of the chemical mass closure (CMC) for PM₁₀ at the five sites are shown in Table 6.5 and Figure 6.5. For the purpose of chemical mass closure the chemical components of PM₁₀ were divided into seven classes as discussed in section 2.5. The relative contributions reflect differences in processes and emission sources governing PM₁₀ aerosol composition (Putaud et al., 2004). MD, OM, SS, and SIA were the main contributors to PM₁₀ mass concentrations at all sites. SIA dominated the PM₁₀ profiles at all sites, accounting for 35.9, 34.5, 32.3, 36.4, and 31.6% at AD, AP, LE, LL, and WZ, respectively (see Figure 6.5). Organic matter was also a major components of PM₁₀ at all sites (except WZ), accounting for 17.8, 20.2, 24.6, 21.0, and 13.5% for AD, AP, LE, LL, and WZ sites, respectively (Figure 6.5). High contributions of mineral dust were also found in AP and WZ, accounting for 12.4 and 19.2%, respectively. This contribution may be attributed to emissions from industrial activities at these sites as already mentioned (Joaquin, 2015b). Notably, sea salt constituted a significant fraction of PM₁₀ at LE, and WZ, accounting for 15.14 and 15.7%, respectively (see Figure 6.5). This might be linked to the photochemical formation of sulphates at LE as shown in previous studies (Hama et al., 2017a, and 2017b; Hofman et al., 2016), and owing to the close distance to the North Sea (for WZ site). Furthermore, unknown fractions were also observed at all sites (see Figure 6.5). UNK is generally attributed to the water content of PM which is related with the estimation of the composition of crustal minerals and organic matter (Tsyro, 2005). This might also be associated with the other source contributions that showed in the PM₁₀ concentrations in this region in the previous report (Joaquin, 2015b).

The average concentrations of main contributors (SS, and SIA) to PM₁₀ are higher in the cold period and lower in the warm period (Table 6.5), which is consistent with the PM₁₀ seasonal pattern. However, there are different seasonal contributions to PM₁₀ at between the sites.

Table 6.5: PM₁₀ mass closure results ($\mu\text{g m}^{-3}$) at sampling sites.

	AD			AP			LE		
	Annual	Cold Period	Warm Period	Annual	Cold Period	Warm Period	Annual	Cold Period	Warm Period
MD	2.26	2.19	2.21	3.79	4.77	3.09	2.05	2.20	1.88
OM	4.22	4.46	3.95	6.15	6.99	5.26	4.75	5.07	4.38
EC	0.58	0.65	0.51	1.56	1.81	1.29	0.95	1.16	0.72
TE	0.12	0.11	0.12	0.19	0.23	0.17	0.10	0.098	0.10
SS	2.80	3.18	2.37	2.51	3.09	1.9	2.93	3.84	1.89
SIA	8.52	11.1	5.61	10.52	13.6	7.28	6.23	8.01	4.23
MSS	0.066	0.11	0.021	0.13	0.20	0.06	0.074	0.11	0.032
UNK	5.13	6.85	3.08	5.58	5.8	5.02	2.23	2.26	2.2
	LL			WZ					
MD	3.38	4.2	2.57	5.58	6.7	3.94			
OM	6.26	6.95	5.33	3.94	4.33	3.4			
EC	1.19	1.31	1.02	0.81	1.02	0.53			
TE	0.16	0.17	0.15	0.18	0.19	0.17			
SS	2.3	2.6	1.76	4.57	5.33	3.52			
SIA	10.85	13.44	6.07	9.16	11.84	5.5			
MSS	0.2	0.34	0.04	0.064	0.097	0.019			
UNK	5.43	3.66	7.39	4.73	6.56	2.36			

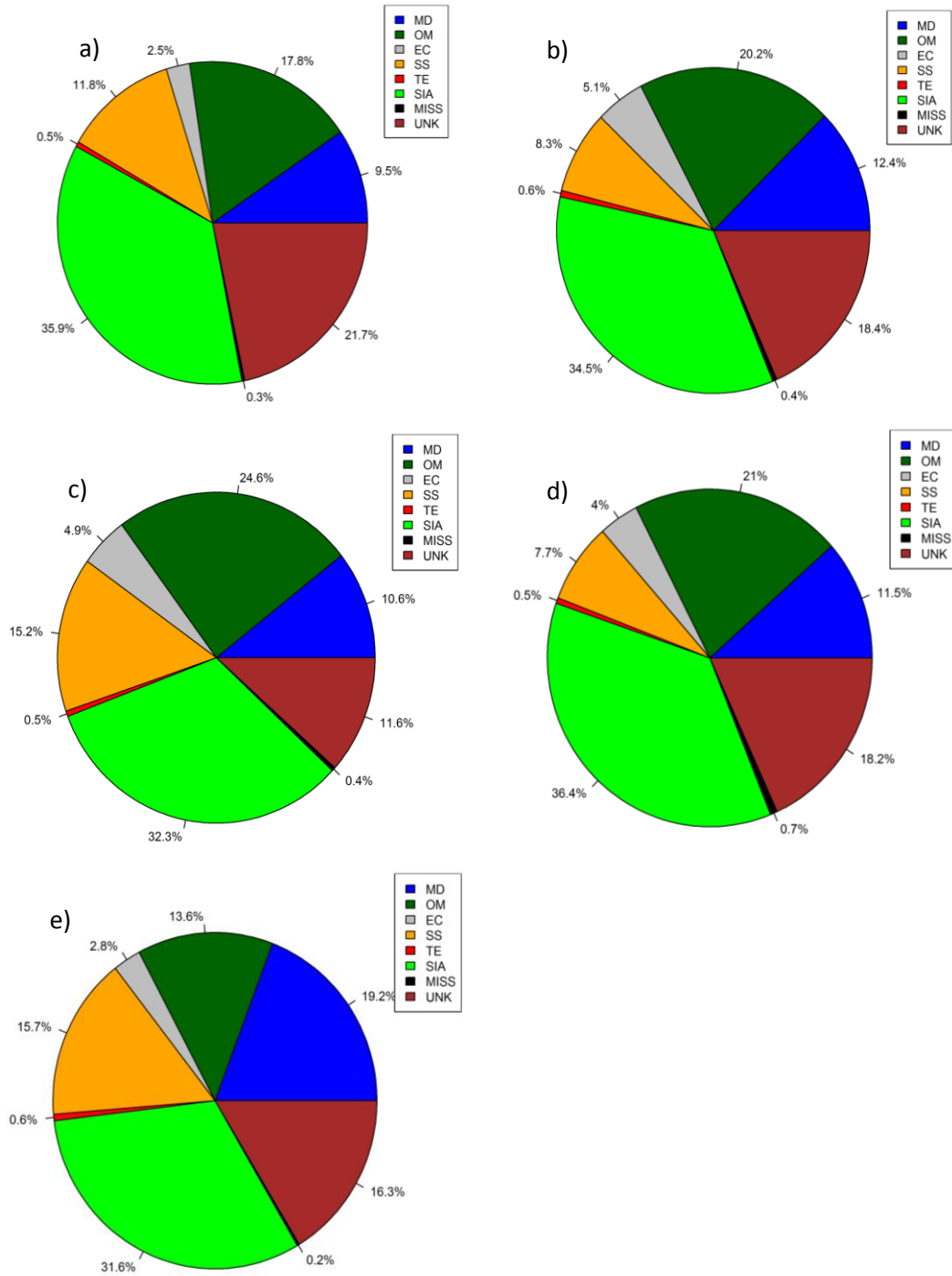


Figure 6.5: Average annual mass closure of PM₁₀ for a) AD, b) AP, c) LE, d) LL, and e) WZ sites.

For example, higher percentages of MD in PM₁₀ were observed in winter and autumn at AD, LE, LL, and WZ sites (see Figure 6.6). In the case of organic matter, OM was higher in the summer at all sites, except LL (relatively higher in winter), and lower in the cold season, suggesting possible photochemical formation of secondary organic aerosol in the north-west European area (Hama et al., 2017b; Hofman et al., 2016; Seinfeld and Pandis, 2006). EC is mostly emitted as primary soot from combustion sources; therefore it has higher levels in the cold period (winter and autumn) and lower levels in summer at all sites (Figure 6.6). This could be related to the heating period (increased wood burning during cold period) across north-west Europe. Moreover, SS showed a higher contribution to PM₁₀ in winter and autumn months at all sites (see Figure 6.6). This is consistent with a previous study (Alastuey et al., 2016). The average concentrations of SS in the cold period is relatively higher at LE (28%), and WZ (23%) than at the other monitoring sites. Higher percentage of SS at LE site can be associated to the passage of clean continental marine air through the monitoring site (Taiwo et al., 2014c). Neutralisation of hydrochloric acid (HCl) vapour (produced from incinerator and power plants) by ammonia may also be responsible for chloride formation in PM₁₀ (Harrison and Yin, 2000). Furthermore, SIA showed a higher percentage contribution in the spring, and a lower one in summer (see Figure 6.6). A combination of meteorological conditions and various emission sources led to highly elevated SIA concentrations in this region in spring, mainly due to high ammonium nitrate concentrations. This is likely related to increased emissions of NH₃ when manure is spread on agricultural lands, and the subsequent increase in the formation of NH₄NO₃. In addition, the high contribution by SIA at LE site is a reflection of the east to west gradient in secondary nitrate and sulphate found all over the United Kingdom (AQEG, 2012; Taiwo et al., 2014b).

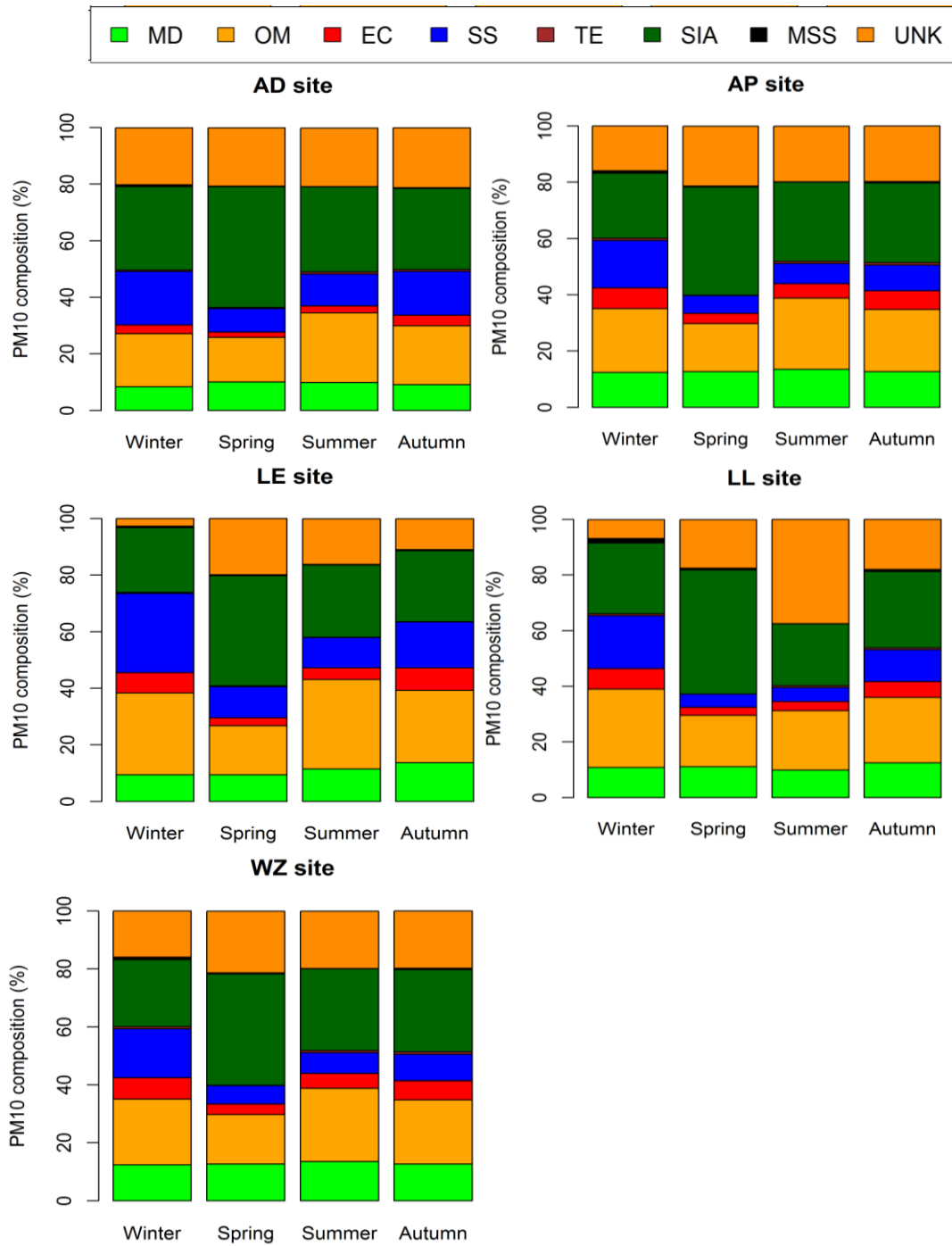


Figure 6.6: Chemical mass closure of PM₁₀ at different season at five sampling sites.

Finally, the correlation between gravimetric and calculated PM_{10} mass are shown in Figure 6.7. It can be seen that there is a strong correlation between gravimetric and chemically determined PM_{10} mass at all the sampling sites ($R^2=0.88-0.96$, see Figure 6.7). This result supports the validity of the mass closure approach with the measured species accounting for the majority of PM_{10} mass.

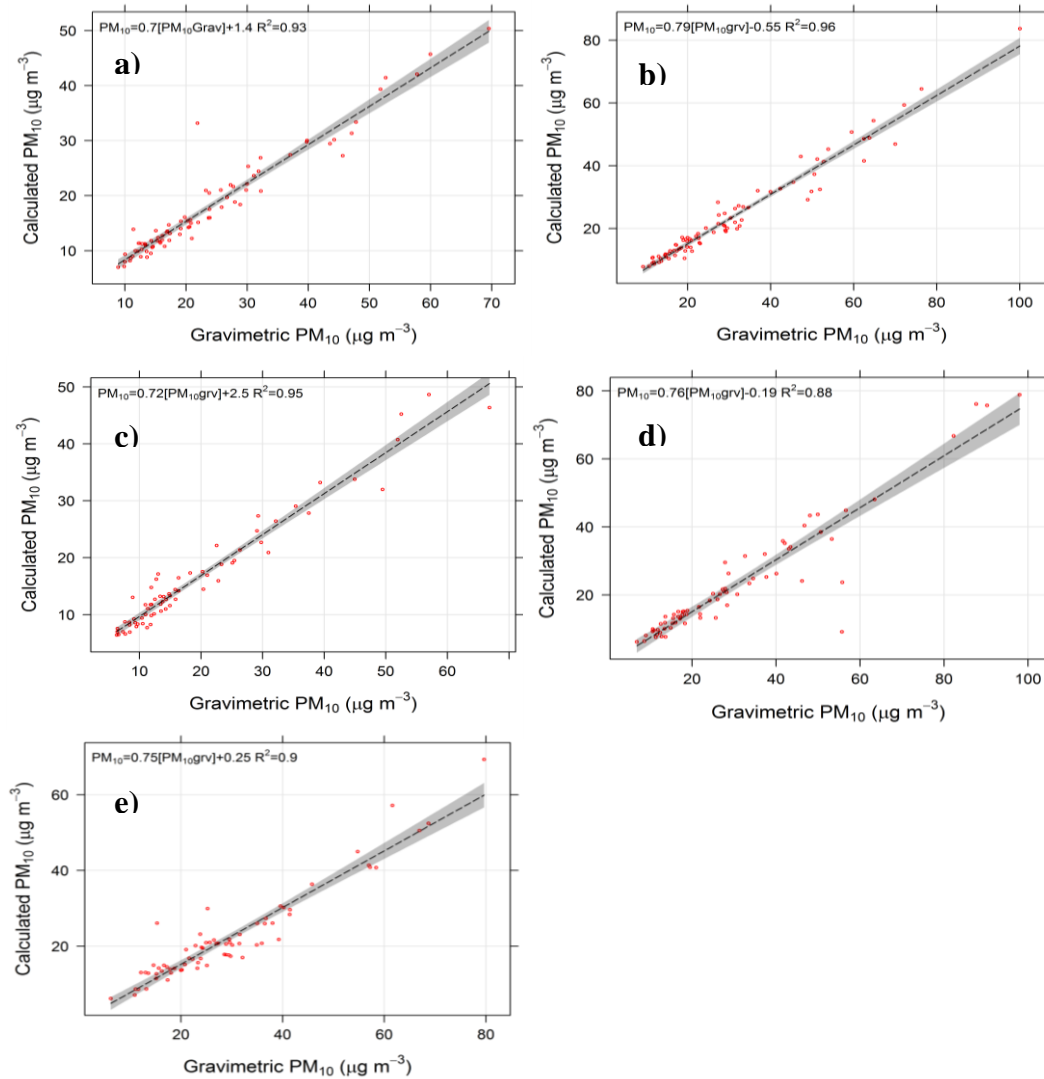


Figure 6.7: Correlation between the calculated and the gravimetric measured PM_{10} mass concentrations at a) AD, b) AP, c) LE, d) LL, and e) WZ sites.

6.3.4 Identification of emission source by PCA

The principal component analysis (PCA) builds on the variability of the PM components at the receptor site and tends to identify species that have a similar correlation in time and space and combines these species. The combination of these species can be used to link them to known sources. In this statistical method a set of multiple inter-correlated variables is replaced by smaller independent variables by orthogonal transformations. A varimax normalized rotation was applied to maximize/minimize the values of the factor loadings of each species measured in relation to each rotated principal component. The eigenvalue for extracted factors was more than 1.0. The number of factors was detected so that they explain the highest maximum total variance of the data. In the literature, it is recommended to use 50–200 samples subject to variable ratios (STV) of 3–20 (de Winter et al., 2009). In this study, statistical analyses are obtained using XLSTAT 2016. Factor analysis was applied to a population with the following data: $N = \text{minimum } 93$, $p = 29$ and $STV > 3.2$. The considered components (p) were: Al, As, Ba, Cd, Fe, Cr, Cu, Fe, Mn, Mo, Ni, Pb, Sb, Ti, V, Zn, Cl^- , NO_3^- , SO_4^{2-} , Na^+ , NH_4^+ , K^+ , Mg^{2+} , Ca^{2+} , OC, EC, Gal, Man, and Lev.

Five factors were extracted as principal components (eigenvalue > 1) that explained 67.4, 80.3, 76.4, and 73.7% of the variance of the data at AD, AP, LL and WZ respectively. In addition, four factors were extracted for LE site explaining 71.3% of the variance (Table 6.6). The first factor (PC1) is responsible for 10.7, 14.2, 22.4 12.6 and 16.1% of the total variance at AD, AP, LL, WZ and LE, respectively. PC1 is designated as crustal origin by the observation of the major contribution of Ca^{2+} , Ba, Zn and Ti. LL site had a greater dispersion of the variables, in fact the first principal component was influenced by anthropogenic elements, such as As, Cd, Cr, Cu; thus describing a possible industrial emission contribution (Querol et al., 2007). The second factor (PC2) is responsible for 13.2, 14.6, 18.1, 12.6, and 12.9% of the total variance at AD, AP, LL, WZ and LE, respectively. PC2 is loaded with NH_4^+ , NO_3^- , SO_4^{2-} and to a smaller extent V; it represents secondary inorganic aerosol (SIA) (Hama et al., 2017b; Hofman et al., 2016). The presence of V in PC2 could indicate a contribution of anthropogenic emissions (possible sources of V and SO_2). These sources are likely linked to emissions from ships (for both AD and AP sites) and the emissions from power plants, located in the large industrial areas (AD, AP, and LL sites). The third factor (PC3) is responsible for 11.9, 10.9, 11.4, 12.6, and 11.2% of the total variance at AD, AP, LL, WZ and LE, respectively.

PC3 is characterized by Na^+ and Cl^- and K^+ for AP, LL, WZ and LE, while for AD site, Na^+ and Cl^- was correlated with Mg^{2+} . All the previous components were identified as part of marine aerosol (see Table 6.6). The fourth component (PC4) is responsible for 21.6, 12.9, 16.9, 16.3, and 31.1% of the total variance at AD, AP, LL, WZ and LE, respectively. The source is associated with biomass burning. In AD, LL, WZ and LE sites the source is characterized by Lev, Man, and Gal. Furthermore, in AD and LE the sites, the presence of metals (i.e. As, Cd, and Pb) associated with K^+ and OC (Bernardoni et al., 2011) confirms even more the hypothesis of biomass burning (Cordell et al., 2016), most likely, from power plants (Maenhaut et al., 2016). However, at the LE site the source is also influenced by vehicle emissions (i.e. EC, Cu, Cr, Mo and Sb) (Table 6.6). The fifth component (PC5) is responsible for 10.6, 27.7, 7.5, and 20.5% of the total variance in AD, AP, LL, WZ sites, respectively. AD site is influenced by Cu, Ni, and V. Furthermore, V/Ni ratio is approximately 0.6; this ratio is associated to diesel fuel combustion (Cesari et al., 2014), confirming the hypothesis of the association with petrol combustion and traffic emissions. AP site is characterized by EC, Al, Cu, Cr, As, Mo, and to a minor extent Cd, Mn, Pb and OC. These elements highlight many anthropogenic sources, in particular metal industries and vehicle emissions (diesel combustion and brakes). LL site is characterized by the presence of Cu and Sb, usually used brake pads wears (Furuta et al., 2005; Muránszky et al., 2011). In addition, also WZ site is correlated with vehicle emissions (Joaquin, 2015b), in fact the signature elements were Pb, Mn, Cu and EC.

Table 6.6: Factor loadings for PM₁₀ at AD, AP, LL, WZ, and LE sites.

Variable	AD					AP				
	PC1	PC2	PC3	PC4	PC5	PC1	PC2	PC3	PC4	PC5
NO ₃ ⁻	0.031	0.745	0.032	0.035	0.003	0.038	0.658	0.023	0.077	0.04
Cl ⁻	0.006	0.005	0.834	0.002	0.027	0.017	0.005	0.907	0.004	0.00
SO ₄ ²⁻	0.04	0.302	0.098	0.185	0.014	0.068	0.66	0.023	0.004	0.03
Na ⁺	0.001	0.043	0.852	0.015	0.024	0.028	0.027	0.913	0.000	0.001
NH ₄ ⁺	0.007	0.736	0.066	0.07	0.006	0.017	0.73	0.035	0.07	0.025
K ⁺	0.006	0.007	0.057	0.791	0.000	0.005	0.005	0.947	0.006	0.005
Mg ²⁺	0.007	0.02	0.751	0.013	0.000	0.817	0.014	0.002	0.000	0.034
Al	0.633	0.196	0.032	0.000	0.196	0.003	0.112	0.011	0.073	0.518
As	0.000	0.184	0.012	0.563	0.059	0.057	0.018	0.000	0.055	0.614
Ba	0.643	0.055	0.025	0.014	0.003	0.867	0.043	0.001	0.002	0.01
Ca	0.788	0.000	0.016	0.003	0.001	0.001	0.054	0.016	0.111	0.241
Cd	0.001	0.133	0.000	0.691	0.003	0.163	0.029	0.002	0.033	0.315
Cr	0.121	0.007	0.169	0.001	0.065	0.042	0.009	0.008	0.052	0.798
Cu	0.000	0.026	0.009	0.01	0.653	0.115	0.029	0.001	0.075	0.708
Fe	0.003	0.463	0.001	0.033	0.172	0.100	0.122	0.001	0.217	0.234
Mn	0.001	0.011	0.000	0.003	0.05	0.176	0.084	0.001	0.023	0.548
Mo	0.013	0.165	0.019	0.011	0.227	0.03	0.09	0.001	0.04	0.673
Ni	0.002	0.000	0.01	0.001	0.643	0.045	0.263	0.001	0.092	0.238
Pb	0.000	0.026	0.019	0.165	0.002	0.000	0.164	0.007	0.087	0.427
Sb	0.002	0.01	0.008	0.004	0.043	0.003	0.194	0.000	0.028	0.457
Ti	0.596	0.061	0.046	0.000	0.283	0.825	0.021	0.006	0.000	0.048
V	0.009	0.451	0.004	0.003	0.549	0.09	0.424	0.001	0.04	0.086
Zn	0.318	0.000	0.108	0.001	0.151	0.377	0.1	0.048	0.046	0.003
Gal	0.004	0.004	0.000	0.910	0.002	0.000	0.022	0.000	0.704	0.23
Man	0.000	0.003	0.007	0.922	0.001	0.021	0.032	0.001	0.743	0.158
Lev	0.001	0.011	0.005	0.857	0.000	0.005	0.011	0.001	0.721	0.202
OC	0.014	0.123	0.103	0.631	0.058	0.068	0.164	0.094	0.181	0.360
EC	0.000	0.316	0.033	0.11	0.03	0.002	0.003	0.001	0.114	0.746

Table 6.6: continued.

Variable	LL					WZ				
	PC1	PC2	PC3	PC4	PC5	PC1	PC2	PC3	PC4	PC5
NO ₃ ⁻	0.028	0.79	0.031	0.068	0.028	0.01	0.819	0.018	0.022	0.001
Cl ⁻	0.048	0.002	0.862	0.001	0.048	0.016	0.051	0.761	0.00	0.061
SO ₄ ²⁻	0.097	0.675	0.053	0.000	0.097	0.053	0.471	0.034	0.129	0.039
Na ⁺	0.053	0.042	0.857	0.001	0.053	0.014	0.09	0.743	0.01	0.031
NH ₄ ⁺	0.018	0.829	0.036	0.045	0.018	0.001	0.796	0.042	0.068	0.002
K ⁺	0.004	0.02	0.857	0.007	0.004	0.000	0.06	0.662	0.035	0.116
Mg ²⁺	0.567	0.054	0.009	0.004	0.567	0.506	0.04	0.093	0.005	0.011
Al	0.098	0.438	0.029	0.14	0.098	0.001	0.092	0.07	0.259	0.123
As	0.358	0.048	0.013	0.164	0.358	0.294	0.032	0.000	0.007	0.004
Ba	0.637	0.144	0.041	0.001	0.637	0.793	0.000	0.000	0.001	0.003
Ca	0.008	0.003	0.002	0.001	0.008	0.036	0.006	0.005	0.02	0.611
Cd	0.562	0.000	0.01	0.023	0.562	0.002	0.003	0.001	0.059	0.194
Cr	0.430	0.000	0.005	0.255	0.43	0.018	0.058	0.205	0.000	0.065
Cu	0.588	0.057	0.005	0.102	0.588	0.022	0.003	0.000	0.087	0.758
Fe	0.739	0.229	0.106	0.183	0.239	0.045	0.001	0.041	0.253	0.457
Mn	0.623	0.021	0.014	0.000	0.223	0.031	0.001	0.005	0.003	0.789
Mo	0.239	0.215	0.000	0.086	0.239	0.116	0.227	0.049	0.003	0.367
Ni	0.264	0.136	0.004	0.000	0.264	0.039	0.004	0.037	0.135	0.043
Pb	0.121	0.438	0.038	0.134	0.121	0.008	0.005	0.002	0.022	0.789
Sb	0.023	0.001	0.004	0.044	0.023	0.001	0.02	0.231	0.164	0.037
Ti	0.669	0.094	0.039	0.02	0.669	0.539	0.022	0.038	0.021	0.15
V	0.18	0.392	0.003	0.000	0.180	0.100	0.221	0.007	0.094	0.214
Zn	0.459	0.08	0.101	0.000	0.459	0.564	0.013	0.003	0.001	0.144
Gal	0.032	0.023	0.000	0.842	0.032	0.005	0.015	0.000	0.695	0.001
Man	0.003	0.057	0.002	0.816	0.003	0.000	0.009	0.012	0.855	0.014
Lev	0.002	0.022	0.000	0.887	0.002	0.001	0.014	0.004	0.863	0.024
OC	0.179	0.255	0.076	0.339	0.179	0.012	0.171	0.156	0.526	0.03
EC	0.148	0.003	0.000	0.576	0.148	0.001	0.055	0.000	0.013	0.655

Table 6.6: continued.

Variable	LE			
	PC1	PC2	PC3	PC4
NO ₃ ⁻	0.00	0.748	0.014	0.116
Cl ⁻	0.015	0.012	0.915	0.006
SO ₄ ²⁻	0.056	0.737	0.004	0.002
Na ⁺	0.022	0.019	0.934	0.003
NH ₄ ⁺	0.000	0.803	0.024	0.086
K ⁺	0.005	0.007	0.948	0.002
Mg ²⁺	0.577	0.029	0.001	0.096
Al	0.015	0.056	0.001	0.481
As	0.168	0.015	0.000	0.544
Ba	0.651	0.021	0.000	0.001
Ca	0.072	0.046	0.01	0.232
Cd	0.228	0.061	0.008	0.039
Cr	0.182	0.06	0.008	0.532
Cu	0.205	0.000	0.027	0.517
Fe	0.147	0.048	0.093	0.29
Mn	0.093	0.018	0.000	0.136
Mo	0.236	0.001	0.015	0.396
Ni	0.091	0.000	0.000	0.018
Pb	0.001	0.043	0.006	0.266
Sb	0.014	0.012	0.009	0.741
Ti	0.709	0.076	0.033	0.002
V	0.142	0.444	0.002	0.013
Zn	0.666	0.061	0.028	0.000
Gal	0.000	0.065	0.000	0.785
Man	0.001	0.037	0.001	0.811
Lev	0.000	0.045	0.000	0.809
OC	0.092	0.137	0.031	0.597
EC	0.031	0.022	0.007	0.779

6.4 Conclusions

The concentration and the chemical composition of PM₁₀ in five cities within NW Europe showed significant spatial and seasonal variations. PM₁₀ mass concentrations were higher at AP and the industrial sites than at the other urban sites. The concentration of SO₄²⁻, NO₃⁻ and NH₄⁺ was 68-81% of total WSIs, and around 32-37% of total PM₁₀ concentration, indicating predominantly secondary sources of pollution. In addition, SO₄²⁻ was highest in summer suggesting photochemical formation. The seasonal variation of OC and EC in PM₁₀ was similar in the five cities. The highest annual ratio of OC/EC was observed in AD (5.15), while the lowest value was found in AP (2.81). Crustal elements (Al, Ba, Ca, Fe, Mn, and Ti) dominated the identified elements of PM₁₀. EF values for Fe, Mn, Ti, Ba, and Ca are all less than 10 at the sampling sites (except WZ), suggesting that these elements are commonly derived from the crustal sources in this study. PM₁₀ was highly enriched (EF>100) in As, Cd, Cu, Mo, Ni, Pb, Sn, and Zn at all sampling sites, indicating that these elements are associated with human activities (anthropogenic sources). The clear seasonal variations of MAs can be linked to the impact of biomass burning within residential heating (increased in winter), and also might be associated to different meteorological conditions. Mass closure allows for source understanding, quality assurance, health and environment effects. A large part of PM₁₀ (31-36%) was attributed to secondary inorganic aerosol, and in particular to the nitrate-rich aerosol source profile, followed by OM and MD at four urban sites, and the major components of PM₁₀ were SIA, followed by MD and SS at WZ site. UNK is generally attributed to the water content of PM which is associated with the estimation of the composition of crustal minerals and organic matter. PCA suggested the following sources: SIA, traffic emissions, marine aerosol, biomass burning, and industrial sources. The total sources explained 67.4, 80.3, 76.4, 73.7, and 71.3% of the variance of the data at AD, AP, LL, WZ and LE sites, respectively. It can be concluded that the results in this study increase our understanding of the composition and sources of PM across NW Europe, which can enable the development of health-related air quality policies.

Chapter Seven

7. Conclusions and Future work

7.1 Conclusions

The aim of this chapter is to bring together the main conclusions from the previous six chapters and to give an overall perspective on the results. This thesis introduces significant new long-term measurements of UFP both in the context of UK urban Leicester as well as across five cities in North West Europe as part of the JOAQUIN project. The current measurements have been put into the context of previous UFP measurements that have been made using a variety of instrumental techniques in other European cities.

Aerosols can have significant adverse effects on the health of people and climate in urban areas. Understanding the physical and chemical dynamics and transformations of atmospheric aerosols helps us to recognise and mitigate their effects on human health and the environment. This study has contributed significantly to scientific knowledge on the dynamics and transformation of urban aerosol particles.

This PhD project was part of a major project called JOAQUIN, which sought to determine the effect of the exposure to airborne UFPs emitted from combustion sources (such as vehicle exhausts) on the health of people in the NW Europe region. This project aimed at obtaining novel time series of simultaneous UFP measurements in four NW European cities (Amsterdam, Antwerp, Leicester and London), both in terms of total and size-resolved particle number concentrations. From this explorative dataset, collected by this continuous UFP monitoring network, the objective was to investigate the temporal variation in UFP number concentration and size distribution, to assess the added value of UFP data in addition to more common parameters such as NO_x and eBC and to evaluate the feasibility of long-term UFP measurements within air quality monitoring networks. Air quality parameters were measured with a focus on UFPs in each city. Data collected from the W-CPC, SMPS and UFP TSI 3031 (see Chapter 2) comprised the main portion of data analysed. All the measurements were conducted in urban background sites. Original and interesting insights on the dynamics and transformation of urban UFPs were obtained.

The intra-urban spatial variation of UFP and eBC was assessed using the trailer measurements conducted within the scope of JOAQUIN Action 3. Although the temporal variation of eBC and UFP at the two intra-urban monitoring sites is well correlated ($R^2=0.69$ to 0.89 for eBC and $r=0.59$ to 0.85), the absolute variance evaluated by the COD can be considerable. This intra-urban variation is influenced by the proximity of UFP sources.

This implies that the location of the UFP monitoring station is of primordial importance in order to evaluate the citizen's exposure to UFPs in urban environments.

Quality assured measurements of UFP and of highly size-resolved TNC in urban environment is still a challenge. However, within JOAQUIN the measuring routine was improved considerably. The JOAQUIN cities showed comparable UFP size distributions with similar proportional contributions of the individual particle size classes ($100-200 < 70-100 < 50-70 < 20-30 < 30-50 < 10-20$ nm (Joaquin, 2015a)). Moreover, the quantified UFP size distributions showed to be fairly stable in time. Nevertheless, quantification of the separate UFP size classes enabled us to identify different contributing emission sources on differing spatial scales. Comparing the UFP size distribution between the monitoring sites, a better link was attained between the large UFP size classes. Larger particles, therefore, seem to be more identical in space, which confirms the regional nature of these aerosols. It can be concluded that all applied UFP monitors performed fairly well and reliably. The experimental intra-urban spatial variation and influence of individual UFP sources proposed that one urban background measuring site will not be representative for an entire city. However, the urban temporal UFP variation appears to be reflected sufficiently by a single urban monitoring site. Determination of the TNC by particle counters (such as W-CPC) could be an alternative for the elaborate size-resolved TNC measurements. However, only PNSD data enable in-depth analysis, particularly for identifying UFP sources.

Following the comparative air quality analysis at the JOAQUIN monitoring sites, it revealed that UFP/TNC depends more on the special location of the measurement site (surrounding houses, traffic intensity, distance to the road, dominant wind direction). This would be considered if choosing the suitable monitoring site for UFP/TNC measurements, especially for long-term studies.

JOAQUIN was one of the first multi-site study investigating the effects of UFP on human health including cities from NW Europe since most UFP studies were so far focused on

Eastern European countries. In addition, this project was the first study on UFP using harmonised UFP-measurements in all sites across NW Europe. It is still not possible to draw confident conclusions on adverse health effects of UFP and exposure to UFP in urban areas despite a growing scientific research and literature. Further multi-site UFP studies such as JOAQUIN are required preferably investigating several years in order to find reasonable results of UFP's health effects.

The overall aim of this study was to examine the physical/chemical dynamics and transformation of UFPs in urban environments. First, this study investigated the spatial variation of PNSD in microscale environments and impact of NPF on TNC. Second, the contributions of primary and secondary aerosol particle sources to the TNC were identified using the eBC concentration as a tracer for primary particles. Third, seasonal variation of LDSA were showed and its impact of NPF on LDSA is also investigated. Finally, this study also provided an improved understanding of PM₁₀ chemical composition, and monthly variation across NW Europe by PCA.

Concerning UFPs, measurements of PNSD were performed in the Leicester urban area as a part of JOAQUIN project (see Chapter 3 and 4). Four SMPS short-term measurements were deployed at two urban background monitoring sites: the AURN site, and the BF site. Measurement size ranges for all monitoring sites were harmonised, with particle sizes between 10 nm and 1093 nm.

- ❖ The highest N_{nuc} and N_{Aitken} were observed during workdays, and the lowest concentrations observed during weekends, especially Sundays.
- ❖ The total particle number was dominated by the nucleation and Aitken modes, with both consisting of 77%, and 81% of total number concentrations at AURN and BF sites, respectively.
- ❖ The temporal variation of N_{accu} was not significant. The diurnal variation of the N_{total} , eBC, and NO_x concentrations demonstrated very similar behaviour at both sites, with the maximum concentrations occurring during morning and late evening hours and the lowest variation during the afternoon hours. This behaviour could be attributed to primary emissions of ultrafine particles (e.g. traffic) and the temporal evolution of mixing layer.
- ❖ The degree of correlation between UFP and other traffic-related pollutants shows that traffic is a significant, but not exclusive, UFP source at all the sites investigated.

- ❖ The PNSD measured display different characteristic modal: at the AURN site shows bimodal distribution at ~22 nm with a minor peak at ~70 nm. The size distribution at BF site, however, exhibits unimodal distribution at ~35 nm.
- ❖ NPF events during spring (under high solar radiation conditions) is occurred in Leicester and contributes to increase TNC. This behaviour points out the very dynamic nature of UFPs, particularly of the smaller size of UFP, and how meteorological conditions impact their evolution in the atmosphere.
- ❖ Photochemical nucleation events are one of the sources of UFP in atmosphere which effect the climate and environment.
- ❖ The contributions of primary and secondary particle sources to the TNC were identified using the eBC concentration as a tracer for primary particles.
- ❖ The majority of particles were expected to be of secondary origin in Leicester urban atmosphere.
- ❖ The highest N1 (49%) was found during the morning rush hours (07:00-09:00 h), when maximum NO_x levels were measured.
- ❖ The maximum contribution of N2 to TNC was observed around midday (11:00-14:00), where it was about 62%, when low eBC and high O₃ levels were measured.
- ❖ The impact of wind speed and direction on primary and secondary aerosol particles have also investigated.
- ❖ Atmospheric and meteorological conditions play a significant role in the evolution of ultrafine particles.
- ❖ According to the bivariate polar plots, high secondary particle concentrations were found around noon. This could be related to NPF effects.

Regarding Lung Deposited Surface Area (LDSA) (see Chapter 5), Owing to increased concern about LDSA and identified as a potential metric for the correlation of a physical aerosol particle property with health outcomes, LDSA and associated measurements were carried out at AURN site in Leicester.

- ❖ The annual average LDSA concentration during this study was lower than previously measured at most other European urban backgrounds.
- ❖ Clear seasonal variation of LDSA, was observed owing to the influence of meteorological parameters and dilution effects.

- ❖ Interestingly, high LDSA levels have been found during the warm season, which could be attributed to NPF events. The existence of an NPF event was confirmed by the gradual increase in LDSA concentration during the event to approximately double its initial value.
- ❖ The effect of wind speed and direction on the LDSA was explored. Moreover, higher LDSA concentrations are observed at low wind speeds, owing to local traffic emissions.
- ❖ Vehicle emissions and biomass burning, particular domestic heating in cold season, and NPF during warm period are the main sources of increased LDSA in urban areas.

With respect to particulate mass (PM_{10}), the concentration and the chemical composition of PM_{10} in five cities within NW Europe that have been measured during JOAQUIN project (see Chapter 6).

- ❖ The concentration and the chemical composition of PM_{10} within NW Europe showed significant spatial and seasonal variations.
- ❖ Chemical characterisation of PM_{10} is more expensive and time-consuming than monitoring of the PM mass concentration, but provides valuable information on the breakdown of PM_{10} sources in urban areas.
- ❖ The clear seasonal variations of MAs can be linked to impact of biomass burning within residential heating (increased in winter), and also might be associated to different meteorological condition.
- ❖ A large part of PM_{10} (31-36%) was attributed to secondary inorganic aerosol, and in particular to the nitrate-rich aerosol source profile.
- ❖ The PCA analysis solution contained 5 factors at AD, AP, LL and WZ: secondary inorganic aerosol, traffic emissions, marine aerosol, biomass burning, and industrial sources.
- ❖ PCA and CMC suggested the following main sources: SIA, and OM at the four urban sites, and SIA, and SS at an industrial site. Overall, SIA dominated the PM_{10} profiles at all sites, accounting for 36, 35, 32, 36, and 32% at AD, AP, LE, LL, and WZ, respectively.

In summary, the results demonstrated that TNC in the Leicester urban area depends strongly on different factors such as the activity of sources whereby the everyday life of people plays a significant role, meteorological conditions. The sources include different

combustion processes such as from vehicle exhaust emissions, domestic heating, fireworks, bonfires or barbecues. Therefore, a reduction of TNC is possible through lower-emission vehicles, less traffic, better air circulation in the city, less biomass burning (cold period) and less bonfires/barbecues (warm period).

Overall UFPs covariate fairly well in time at different sites within the city. However, proportional differences in TNC are found between the individual intra-urban sites, influenced by their proximity to urban UFP sources. This suggests that the location of the UFP monitoring station is of primary importance when assessing the resident's exposure to UFP in urban environments.

7.2 Limitations and Future work

The work presented in this thesis will contribute to and further the understanding of the UFPs and the chemical composition of urban aerosols and their behaviour. This work also contributes to the current state of scientific knowledge on size-resolved particle properties, variability (temporal and spatial), and sources. In addition, the work in this thesis presents the first long-term particle number concentrations and chemical composition of particulate matter measurements from an urban environment using novel techniques such as the NSAM and UFP monitors. The findings make a considerable contribution to further the understanding of the sources and components of urban aerosols, their behaviour, and contributions to total particle number concentrations in urban environments. However, one limitation of the work is that the analysis of size distributions is limited to those within the range of the UFP and SMPS monitors. A consideration of the limitation of the presented work is required to further advance our knowledge on aerosol characteristics and related health effects in urban areas. Understanding NPF in urban environments is vital to accurately estimate ultrafine particle and related exposure. Recently, new instruments have been developed to measure these particles down to 1 nm, but their detailed chemical composition still remains unknown. In general, future measurement campaigns should employ a number of instruments to enable a comprehensive characterisation of the chemical properties and behaviour of aerosol particles in urban areas. Several studies have investigated the chemical composition of particulate matter in urban areas to separate into the different constituents to find sources as well as to examine the chemical, spatial and temporal behaviour of ambient pollution. However, there are still substantial uncertainties in the sources,

formation, and evolution of UFPs in urban environments, which is in part owing to the techniques employed. Furthermore, more measurements of a similar nature are necessary to further constrain source profiles and thus precisely apportion the chemical compositions, the implications from this research highlight the need to target emissions, particularly from anthropogenic sources and during winter. Finally, the essential to collaborate with countries in relatively close proximity to the UK in order to reduce the levels of pollution as well as the frequency and severity of pollution events in cities. This work therefore provides a substantial contribution towards bridging the gap between identifying and understanding the primary and secondary of ultrafine particles in the urban environment.

Appendix

Supplemental Materials

Table S3.1: Minimum and maximum sizes used for calculate GR, J

Site	Event date	Start size (nm)	End size(nm)	GR (nm/h)	J_{10-25} ($\text{cm}^{-3} \text{s}^{-1}$)
AURN	07/03/2014	10	30	8.33	1.1
	15/03/2014	10	18.1	8.1	1.4
	16/03/2014	10	20	6.6	1.82
	24/03/2014	10	20	6.66	0.89
BF	08/04/2014	10	16.5	5.4	1.27
	11/04/2014	10	16.4	4.9	1.46
	27/04/2014	10	15.4	4.7	1.4
	02/05/2014	10	15.4	1.74	0.7
	03/05/2014	10	23.5	5.6	0.41
	07/05/2014	10	19.4	4.27	0.83
	09/05/2014	10	16.4	5.8	0.89
	10/05/2014	10	19.4	7.23	1.7
	14/05/2014	10	21.4	8.77	1.45
	17/05/2014	10	24.4	4.1	1.62

Table S3.2: Calculated CS for size bin (10.25).

CS for N ₁₀₋₂₅₀						
10.25	N1	Kn	7.24878049			
		1+Kn	8.24878049		β_m	0.099182575
			2.44283902	83.1676378		
			9.66504065			
			70.0597581		CS _{10.25}	1.7974E-05

Table S4.1: Range (1st quartile, mean, median, 3rd quartile and maximum) of the half-hourly PM_{2.5} ($\mu\text{g m}^{-3}$), NO_x ($\mu\text{g m}^{-3}$), O₃ ($\mu\text{g m}^{-3}$), eBC ($\mu\text{g m}^{-3}$), CO, (mg m^{-3}), total (TNC) and size-resolved (N) particle number concentrations ($\# \text{ cm}^{-3}$), measured at the AURN site

2014	Mean	1st Quartile	Median	3rd Quartile	St. Dev	Max	Data capture
PM _{2.5}	13.3	6.6	9.9	16.2	11	181	96.1
NO _x	37.47	16.56	28.06	45.08	36.30	629.62	92.5
NO ₂	26.42	14.21	22.91	34.99	16.10	99.86	92.5
NO	11.33	1.68	4.72	10.53	25.17	572.87	92.5
O ₃	40.46	24.81	41.99	55.50	22.02	155.52	92.5
eBC	1.45	0.651	1.09	1.73	1.39	16.05	87.1
TNC	8022	4652	6870.7	9978	5514	63481	83.5
PNC _{20-30nm}	1457	728	1173	1876	1082	13795	98.1
PNC _{30-50nm}	1704	889	1369	2114	1270.9	16461	98.1
PNC _{50-70nm}	1193	602	942	1452	985.8	14614	98.1
PNC _{70-100nm}	1059	510	815	1281	952.7	17444	98.1
PNC _{100-200nm}	980	461	739	1186	912.7	19702	98.1
2015							
PM _{2.5}	12.07	6.4	9.2	14.2	9.4	85.5	97.2
NO _x	36.73	16.94	28.47	45.76	30.71	426.65	97.1
NO ₂	27.15	14.21	22.87	36.22	17.24	103.77	97.1
NO	9.63	1.90	4.80	10.16	16.98	354.06	97.1
CO	0.17	0.0712	0.146	0.214	0.18	2.96	96.7
O ₃	38.89	24.26	39.57	53.19	20.65	161.63	98.8
eBC	1.28	0.59	0.975	1.58	1.16	15.05	91.8
TNC	8364	4883	7370	10698	4936	57558	79.5

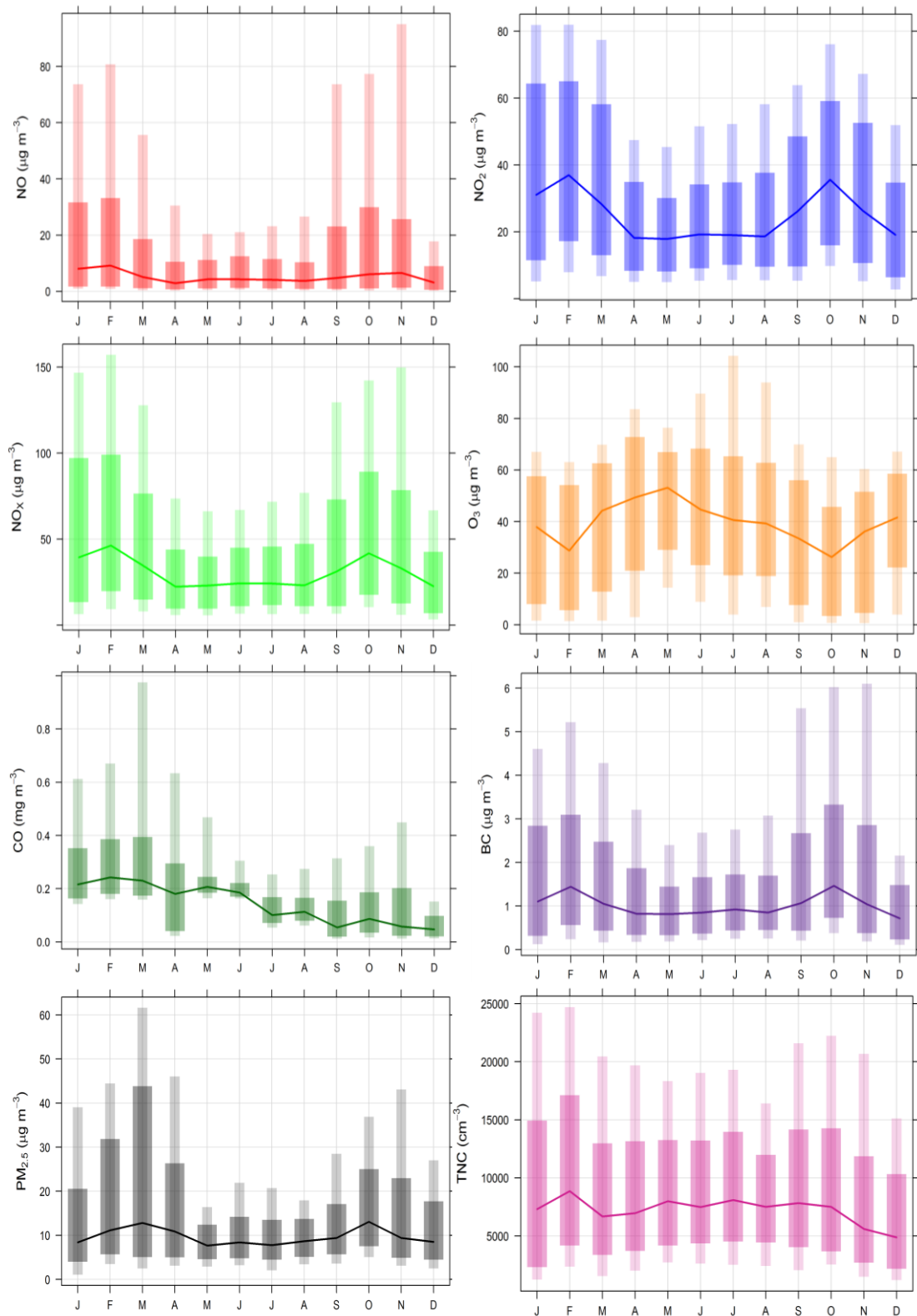


Figure S4.1: Monthly variations in the median, 25/75th and 5/95th quantile values for the gaseous pollutants (NO, NO₂, NO_x, O₃ and CO), eBC, PM_{2.5} and TNC for 2015 at AURN site.

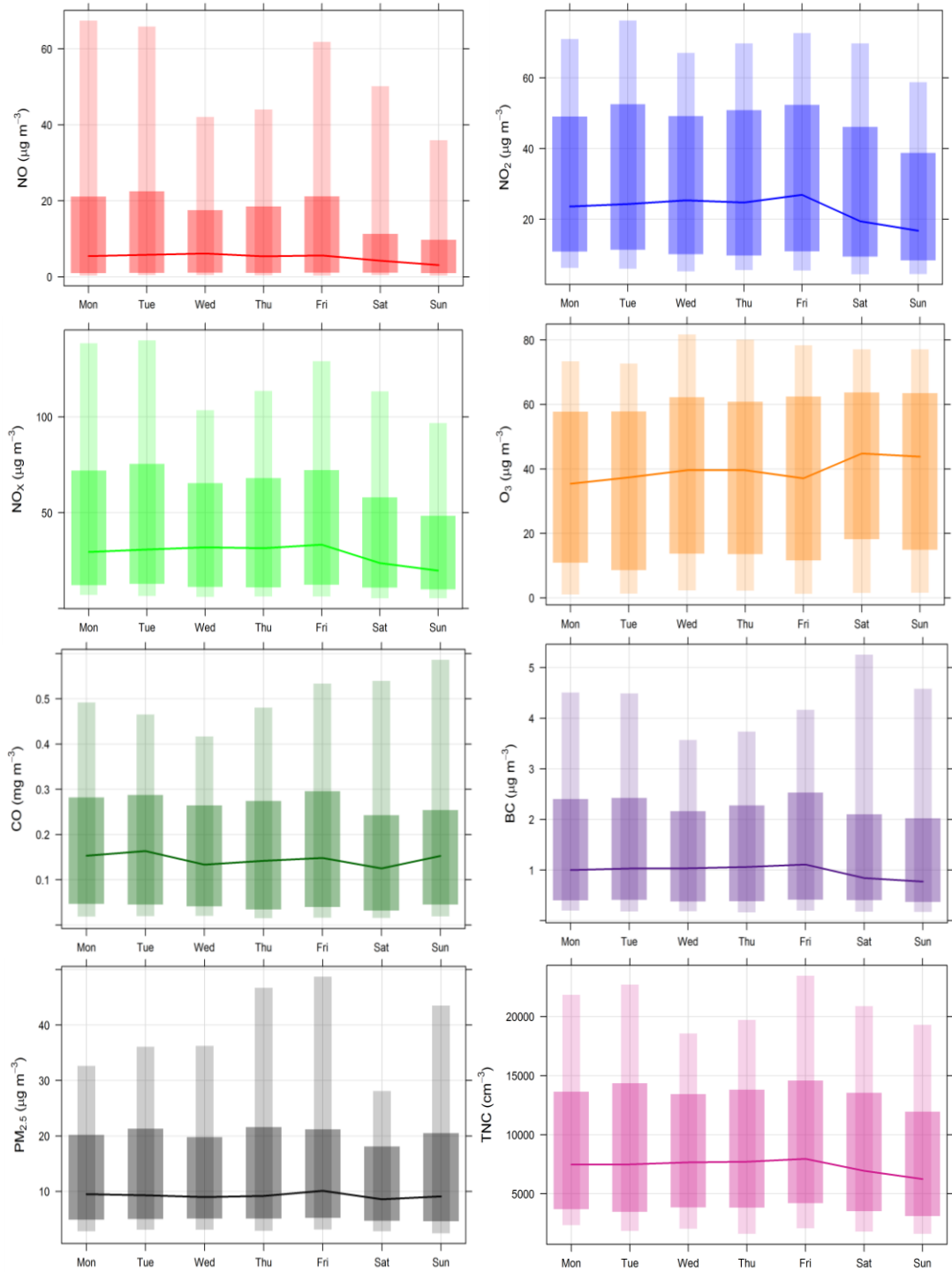


Figure S4.2: Daily variations in the median, 25/75th and 5/95th quantile values for the gaseous pollutants (NO, NO₂, NO_x, O₃ and CO), eBC, PM_{2.5}, and TNC for 2015 at AURN site.

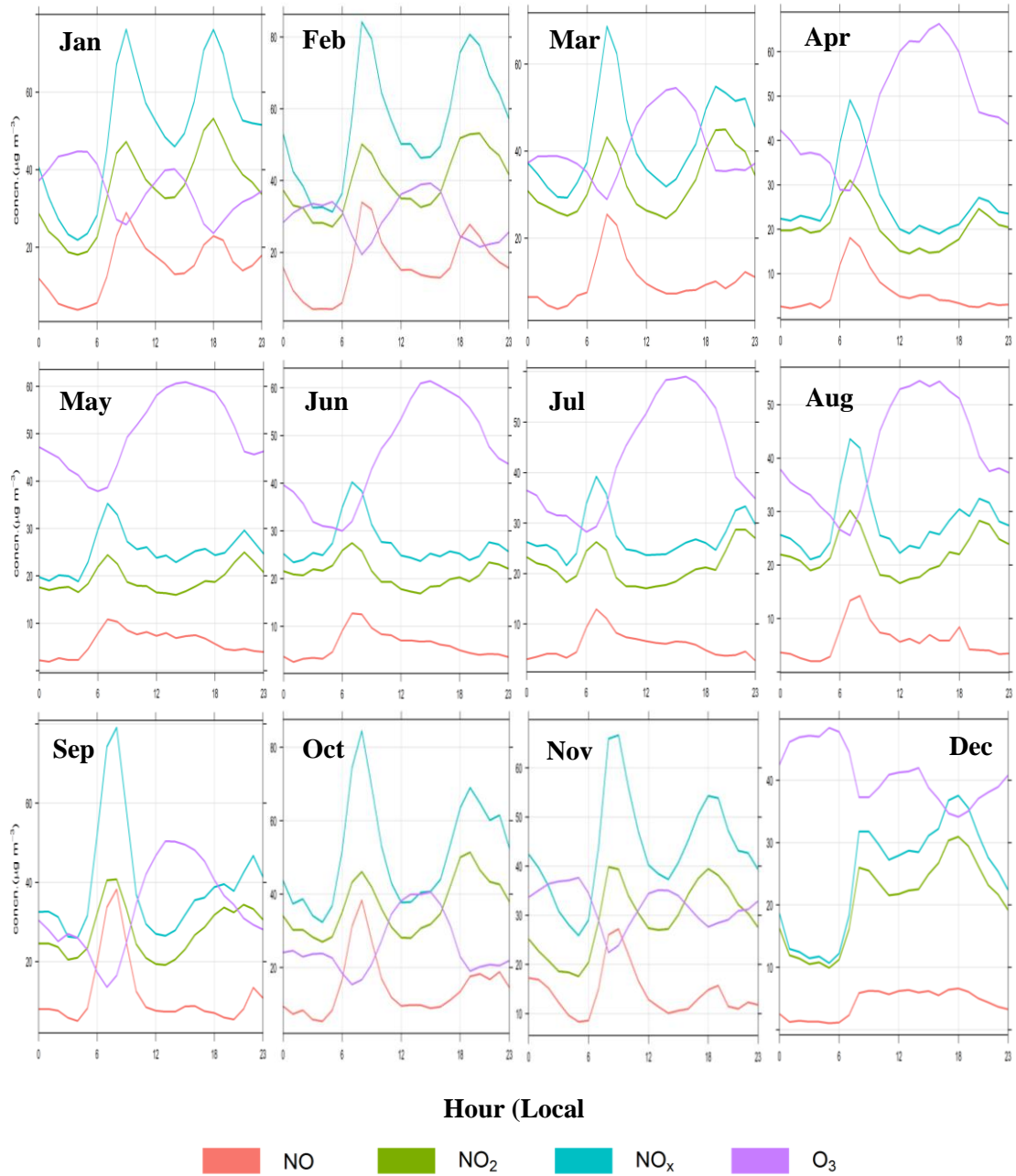


Figure S4.3: Diurnal variations of NO, NO₂, NO_x, and O₃ concentrations for each month in 2015 at AURN site.

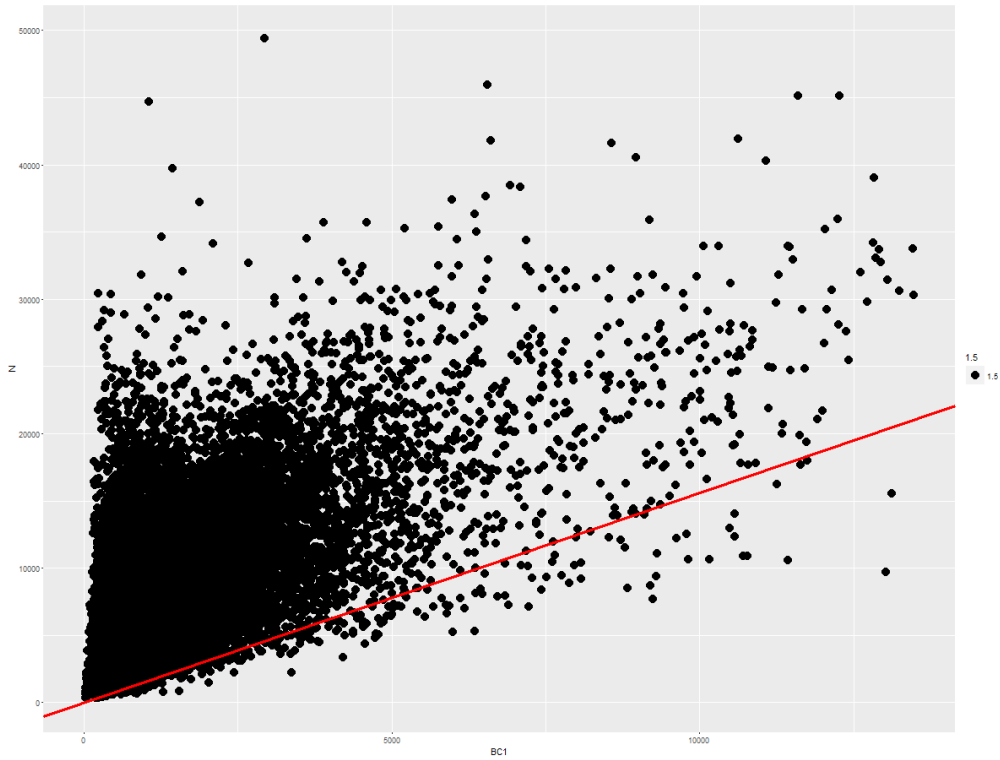


Figure S4.4: determined S1 value by specific regression in R programming.

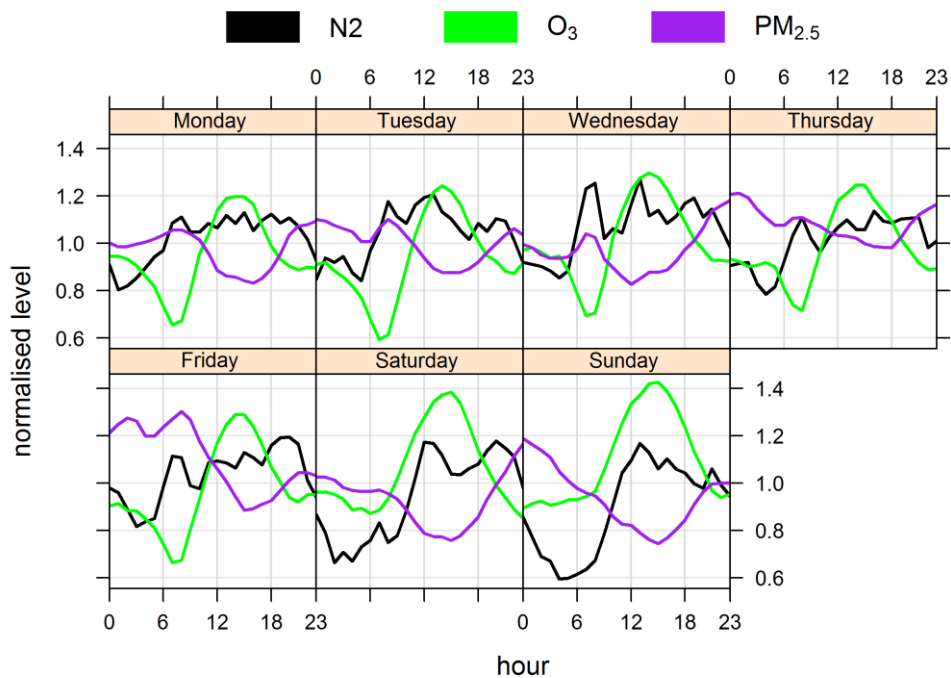


Figure S4.5: Half-hourly mean values of N₂, O₃, and PM_{2.5} concentrations for every day of the week at AURN site.

Table S6.1: The average concentrations ($\mu\text{g m}^{-3}$) of the water-soluble ions in PM_{10} at all sampling sites.

	AD			AP			LE		
	Annual	Cold	Warm	Annual	Cold	Warm	Annual	Cold	Warm Period
NO_3^-	4.79	6.68	2.65	6.24	8.66	3.7	3.43	4.86	1.82
Cl^-	0.98	1.30	0.61	0.85	1.21	0.47	1.08	1.65	0.44
SO_4^{2-}	2.2	2.16	2.21	2.52	2.46	2.57	1.845	1.77	1.92
Na^+	0.86	0.98	0.73	0.77	0.95	0.586	0.90	1.18	0.58
NH_4^+	1.75	2.50	0.93	1.95	2.71	1.148	1.18	1.67	0.63
K^+	0.104	0.124	0.08	0.14	0.17	0.097	0.118	0.14	0.091
Mg^{2+}	0.134	0.133	0.13	0.12	0.13	0.105	0.128	0.15	0.095
Ca^{2+}	0.267	0.248	0.28	0.52	0.60	0.45	0.260	0.10	0.263
	LL			WZ					
NO_3^-	6.57	8.49	2.90	5.0	6.83	2.525			
Cl^-	0.874	1.08	0.50	1.99	2.64	1.107			
SO_4^{2-}	2.41	2.46	2.35	2.80	3.02	2.51			
Na^+	0.710	0.80	0.54	1.40	1.64	1.085			
NH_4^+	2.05	2.69	0.95	1.70	2.4	0.74			
K^+	0.14	0.160	0.10	0.16	0.20	0.106			
Mg^{2+}	0.111	0.118	0.09	0.21	0.23	0.183			
Ca^{2+}	0.67	0.651	0.55	0.53	0.60	0.430			

Table S6.2: Fraction (%) of the WSIs in PM₁₀ at all sampling sites.

	AD			AP			LE		
	Annual	Cold Period	Warm	Annual	Cold	Warm Period	Annual	Cold	Warm Period
NO ₃ ⁻	20.27	23.3	14.8	20.50	23.7	15.39	17.76	21.3	11.79
Cl ⁻	4.13	4.53	3.41	2.80	3.32	1.978	5.59	7.25	2.85
SO ₄ ²⁻	9.26	7.56	12.3	8.27	6.75	10.69	9.55	7.81	12.44
Na ⁺	3.64	3.41	4.06	2.54	2.61	2.43	4.66	5.20	3.77
NH ₄ ⁺	7.43	8.69	5.16	6.40	7.43	4.767	6.11	7.33	4.09
K ⁺	0.44	0.43	0.45	0.45	0.48	0.403	0.61	0.62	0.59
Mg ²⁺	0.56	0.46	0.75	0.399	0.37	0.438	0.66	0.69	0.613
Ca ²⁺	1.13	0.86	1.61	1.73	1.64	1.87	1.35	1.13	1.70
	LL			WZ					
NO ₃ ⁻	22.05	25.98	11.9	17.24	18.9	12.98			
Cl ⁻	2.93	3.32	2.09	6.85	7.31	5.69			
SO ₄ ²⁻	8.10	7.54	9.68	9.66	8.38	12.92			
Na ⁺	2.35	2.45	2.22	4.84	4.55	5.58			
NH ₄ ⁺	6.87	8.23	3.9	5.85	6.66	3.80			
K ⁺	0.467	0.49	0.43	0.564	0.57	0.548			
Mg ²⁺	0.375	0.36	0.40	0.735	0.65	0.944			
Ca ²⁺	2.24	1.99	2.26	1.83	1.69	2.21			

Table S6.3: The averaged concentrations of OC, EC ($\mu\text{g m}^{-3}$), fraction of OC and EC (%) in PM_{10} , and the ratio of OC/EC at all sampling sites. + explain TCA

	AD			AP			LE		
	Annual	Cold Period	Warm	Annual	Cold	Warm Period	Annual	Cold	Warm Period
OC	3.02	3.18	2.83	4.40	4.99	3.76	3.39	3.62	3.13
EC	0.58	0.65	0.51	1.56	1.81	1.29	0.95	1.16	0.72
TCA	4.81	5.11	4.47	7.71	8.81	6.56	5.70	6.23	5.10
OC/ PM_{10}	12.77	11.12	15.7	14.43	13.6	15.61	17.54	15.9	20.26
EC/ PM_{10}	2.47	2.27	2.84	5.12	4.97	5.36	4.94	5.11	4.64
TCA/ PM_{10}	20.36	17.84	24.9	25.32	24.1	27.23	29.5	27.4	33.01
OC/EC	5.15	4.89	5.53	2.81	2.75	2.91	3.55	3.11	4.36
	LL			WZ					
OC	4.47	4.97	3.18	2.81	3.09	2.42			
EC	1.19	1.31	1.02	0.81	1.02	0.53			
TCA	7.45	8.27	6.36	4.75	5.35	3.92			
OC/ PM_{10}	15.01	15.2	15.6	9.68	8.58	12.47			
EC/ PM_{10}	3.99	4.02	4.21	2.79	2.82	2.72			
TCA/ PM_{10}	25.01	25.30	26.1	16.35	14.8	20.18			
OC/EC	3.75	3.78	3.71	3.46	3.03	4.58			

Table S6.4: Mean elemental concentrations (ng m⁻³) in PM₁₀ in annual, cold period, and warm period at the all sampling sites.

	AD			AP		
	Annual	Cold Period	Warm Period	Annual	Cold Period	Warm Period
Al	96.9	113	88.77	134.07	198.8	100.70
As	0.53	0.6	0.405	1.37	1.59	1.11
Ba	5.3	4.8	5.75	10.35	12.26	8.34
Ca	623.9	516	700.63	801.91	1088	654.03
Cd	0.135	0.17	0.093	0.55	0.700	0.403
Cr	7.4	8	6.42	9.25	9.568	8.92
Cu	15.5	14	16.55	30.41	32.11	28.62
Fe	336	378	288.43	720.01	841.6	592.31
K	-	-	-	-	-	-
Mn	9.7	11.6	7.51	13.69	14.62	12.70
Mo	0.9	0.91	0.866	1.82	2.074	1.549
Ni	10.1	7.9	12.68	4.68	5.610	3.708
Pb	6.7	7.6	5.82	19.88	23.81	15.754
Sb	1.9	1.5	2.27	3.89	4.624	3.131
Ti	5.1	5.4	4.77	7.69	9.634	6.693
V	2.45	2.3	2.74	2.41	2.390	2.444
Zn	56.5	54.5	57.60	97.23	120.5	85.21

Table S6. 4: continued.

	LE			LL		
	Annual	Cold Period	Warm Period	Annual	Cold Period	Warm Period
Al	96.9	113	88.77	134.07	198.8	100.70
As	0.53	0.6	0.405	1.37	1.59	1.11
Ba	5.3	4.8	5.75	10.35	12.26	8.34
Ca	623.9	516	700.63	801.91	1088	654.03
Cd	0.135	0.17	0.093	0.55	0.700	0.403
Cr	7.4	8	6.42	9.25	9.568	8.92
Cu	15.5	14	16.55	30.41	32.11	28.62
Fe	336	378	288.43	720.01	841.6	592.31
K	-	-	-	-	-	-
Mn	9.7	11.6	7.51	13.69	14.62	12.70
Mo	0.9	0.91	0.866	1.82	2.074	1.549
Ni	10.1	7.9	12.68	4.68	5.610	3.708
Pb	6.7	7.6	5.82	19.88	23.81	15.754
Sb	1.9	1.5	2.27	3.89	4.624	3.131
Ti	5.1	5.4	4.77	7.69	9.634	6.693
V	2.45	2.3	2.74	2.41	2.390	2.444
Zn	56.5	54.5	57.60	97.23	120.5	85.21

Table S6. 4: continued.

	WZ		
	Annual	Cold Period	Warm Period
Al	117.94	114.3	120.3
As	0.877	1.06	0.630
Ba	4.71	4.65	4.79
Ca	1272.3	1166	1343
Cd	0.563	0.800	0.238
Cr	8.916	9.513	8.10
Cu	10.94	7.57	15.53
Fe	1069.7	1495	488
K	-	-	-
Mn	34.043	42.72	22.18
Mo	0.711	0.803	0.587
Ni	6.29	4.07	9.32
Pb	20.68	26.40	12.86
Sb	0.945	1.04	0.819
Ti	8.482	10.06	7.43
V	6.24	6.69	5.62
Zn	90.13	88.42	91.271

Table S6.5: Mean concentrations of MAs (ng m⁻³) in PM₁₀ at all sampling sites.

	AD			AP			LE		
	Annual	Cold Period	Warm Period	Annual	Cold	Warm Period	Annual	Cold Period	Warm Period
Lev	49.39	79.88	14.8	99.69	154.	42.14	52.83	80.78	21.38
Man	12.59	19.51	4.77	26.55	39.7	12.73	16.01	22.43	8.79
Gal	4.41	7.07	1.39	7.94	12.0	3.65	5.93	9.36	2.08
	LL			WZ					
	Annual	Cold Period	Warm Period	Annual	Cold	Warm Period			
Lev	157.7	263	33.5	46.47	70.6	13.39			
Man	35.39	57.18	10.0	12.85	18.6	4.98			
Gal	12.97	20.71	3.23	5.08	7.88	1.25			

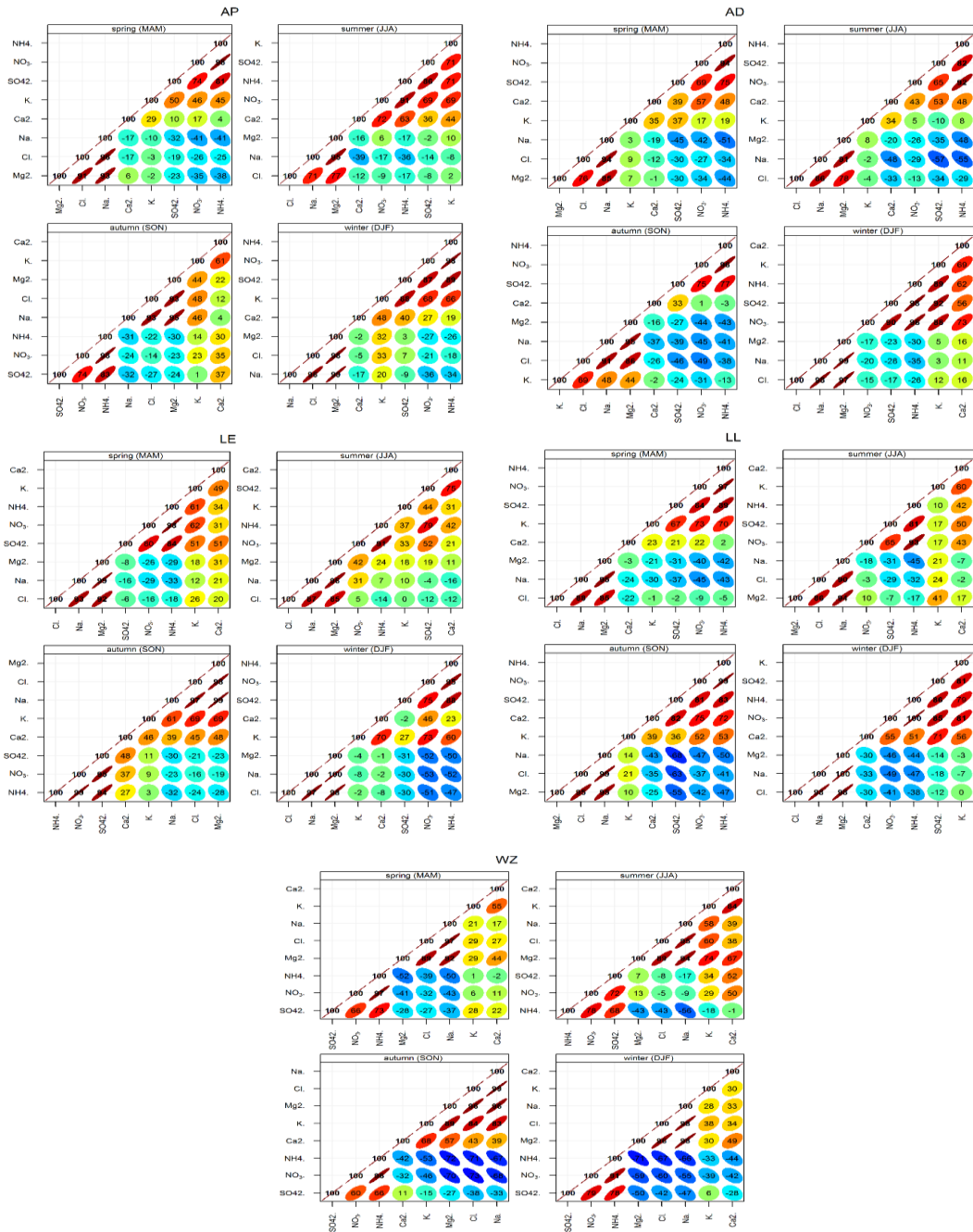


Figure S6.1: Correlation matrix showing the relationships between water soluble ions at all sites. The plot displays the Pearson correlation coefficients expressed as 0 to 100 (no correlation to perfect correlation). Hierarchical cluster analysis has also been applied to the correlation coefficients such that pollutants that are next to each other behave most similarly e.g. SO₄²⁻ and NO₃⁻.

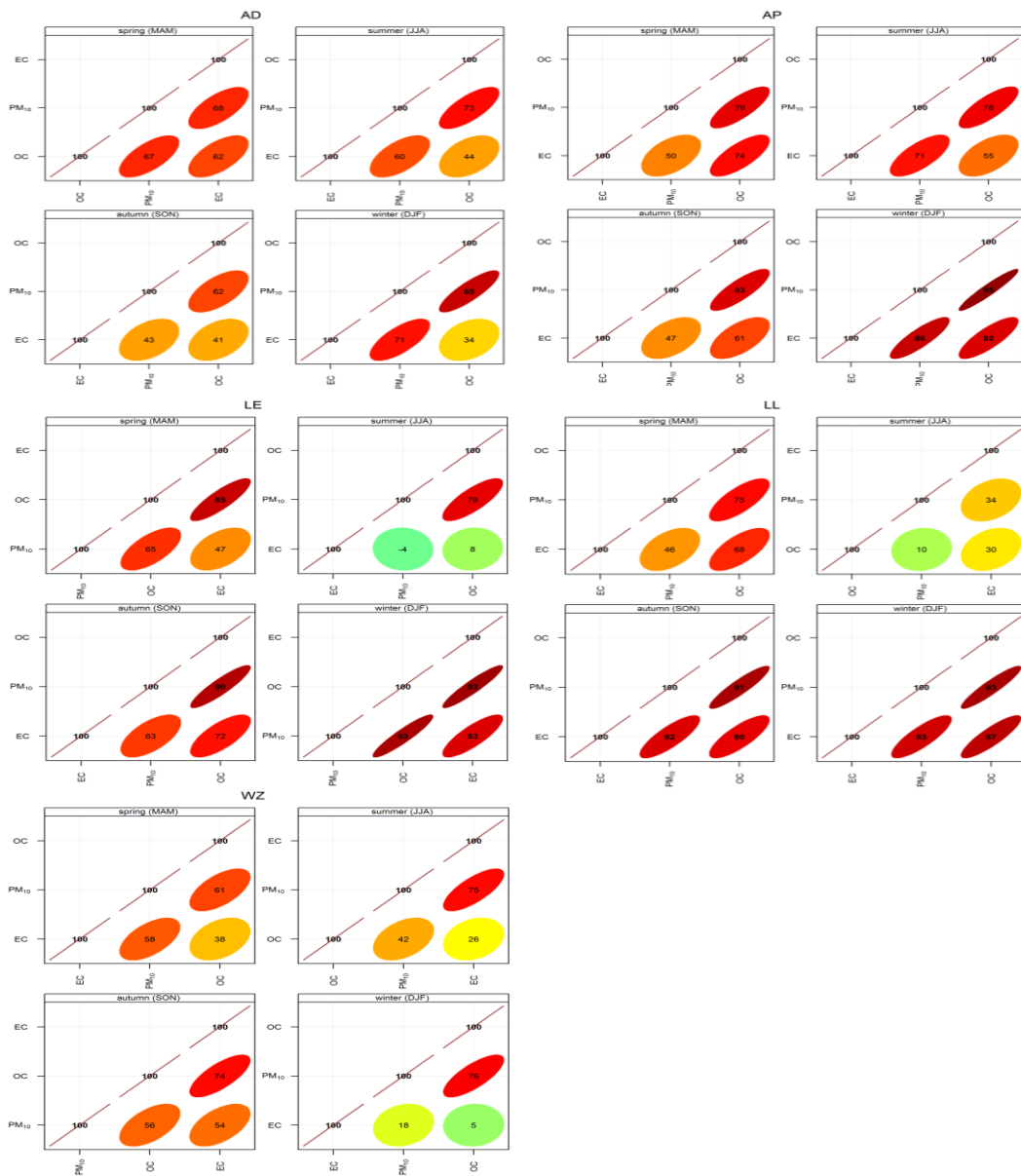


Figure S6.2: Correlation matrix showing the relationships between OC and EC with PM₁₀ at all sites

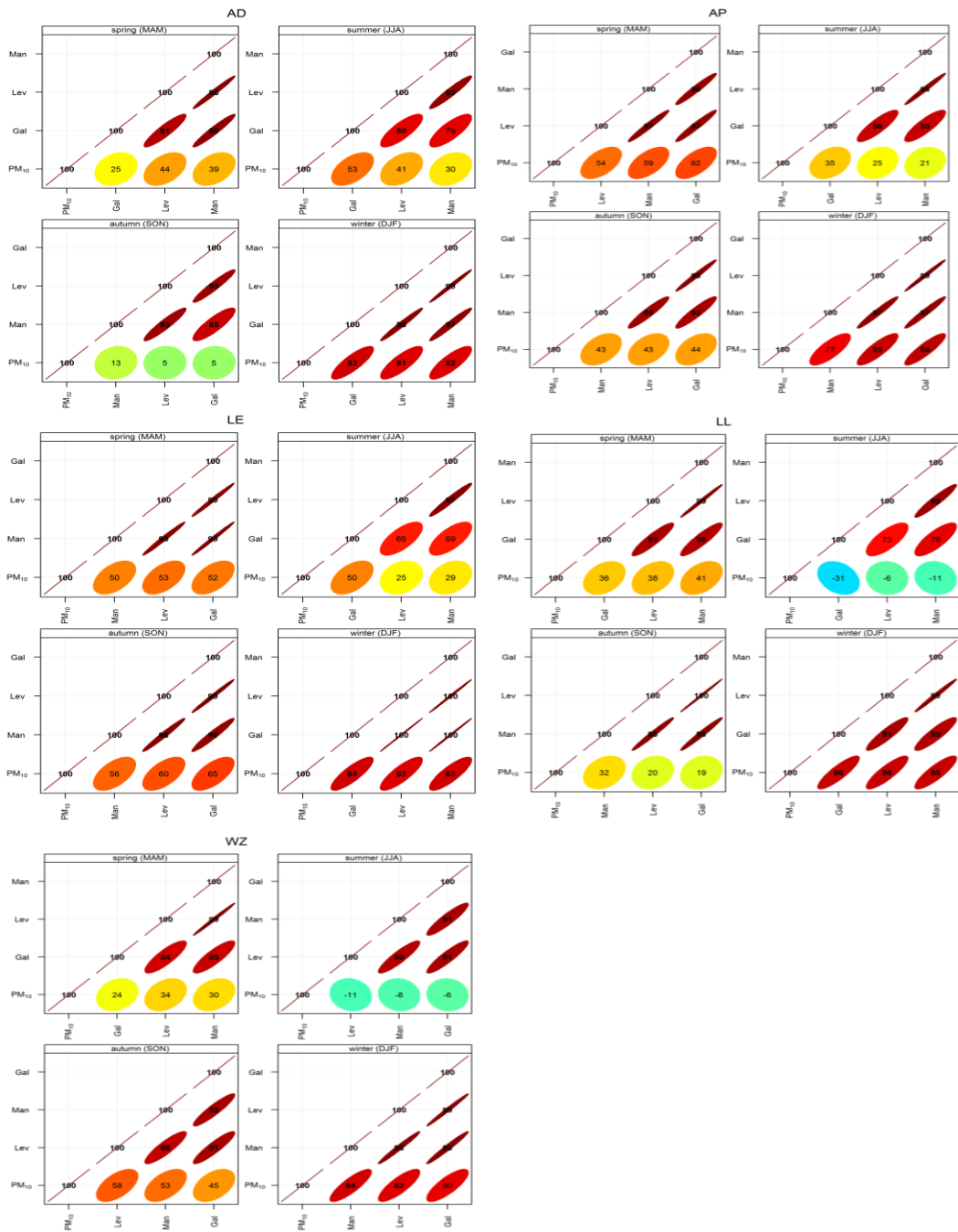


Figure S6.3: Correlation matrix showing the relationships between the MAs at all sites.

Bibliography

Aalto, P.P., Hämeri, K., Paatero, P., Kulmala, M., Bellander, T., Berglind, N., Bouso, L., Castaño-Vinyals, G., Sunyer, J., Cattani, G., Marconi, A., Cyrus, J., Klot, S., Peters, A., Zetzsche, K., Lanki, T., Pekkanen, J., Nyberg, F., Sjövall, B., Forastiere, F., 2005. Aerosol Particle Number Concentration Measurements in Five European Cities Using TSI-3022 Condensation Particle Counter over a Three-Year Period during Health Effects of Air Pollution on Susceptible Subpopulations. *Journal of the Air & Waste Management Association* 55, 1064-1076.

Adamo, P., Giordano, S., Sforza, A., Bargagli, R., 2011. Implementation of airborne trace element monitoring with devitalised transplants of *Hypnum cupressiforme* Hedw.: assessment of temporal trends and element contribution by vehicular traffic in Naples city. *Environ Pollut* 159, 1620-1628.

Agus, E.L., Young, D.T., Lingard, J.J., Smalley, R.J., Tate, J.E., Goodman, P.S., Tomlin, A.S., 2007. Factors influencing particle number concentrations, size distributions and modal parameters at a roof-level and roadside site in Leicester, UK. *The Science of the total environment* 386, 65-82.

Alam, A., Shi, J.P., Harrison, R.M., 2003. Observations of new particle formation in urban air. *Journal of Geophysical Research: Atmospheres* 108, 1-14.

Alastuey, A., Querol, X., Aas, W., Lucarelli, F., Pérez, N., Moreno, T., Cavalli, F., Areskou, H., Balan, V., Catrambone, M., Ceburnis, D., Cerro, J.C., Conil, S., Gevorgyan, L., Hueglin, C., Imre, K., Jaffrezo, J.-L., Leeson, S.R., Mihalopoulos, N., Mitosinkova, M., apos, Dowd, C.D., Pey, J., Putaud, J.-P., Riffault, V., Ripoll, A., Sciare, J., Sellegri, K., Spindler, G., Yttri, K.E., 2016. Geochemistry of PM₁₀ over Europe during the EMEP intensive measurement periods in summer 2012 and winter 2013. *Atmospheric Chemistry and Physics* 16, 6107-6129.

Albuquerque, P.C., Gomes, J.F., Bordado, J.C., 2012. Assessment of exposure to airborne ultrafine particles in the urban environment of Lisbon, Portugal. *Journal of the Air & Waste Management Association* 62, 373-380.

Aldrin, M., Haff, I., 2005. Generalised additive modelling of air pollution, traffic volume and meteorology. *Atmospheric Environment* 39, 2145-2155.

- Allan, J.D., Alfarra, M.R., Bower, K.N., Coe, H., Jayne, J.T., Worsnop, D.R., Aalto, P.P., Kulmala, M., Hyotylainen, T., Cavalli, F., and Laaksonen, A., 2010a. Size and composition measurements of background aerosol and new particle growth in a Finnish forest during QUEST 2 using an Aerodyne Aerosol Mass Spectrometer. *Atmos. Chem. Phys.* 6, 315-327.
- Allan, J.D., Williams, P.I., Morgan, W.T., Martin, C.L., Flynn, M.J., Lee, J., Nemitz, E., Phillips, G.J., Gallagher, M.W., Coe, H., 2010b. Contributions from transport, solid fuel burning and cooking to primary organic aerosols in two UK cities. *Atmos. Chem. Phys.* 10, 647-668.
- Allan, J.D., Williams, P.I., Morgan, W.T., Martin, C.L., Flynn, M.J., Lee, J., Nemitz, E., Phillips, G.J., Gallagher, M.W.a.C., H., 2010c. Contributions from transport, solid fuel burning and cooking to primary organic aerosols in two UK cities. *Atmospheric Chemistry and Physics* 10, 647-668.
- Almeida, T.S., Sant Ana, M.O., Cruz, J.M., Tormen, L., Frescura Bascunan, V.L.A., Azevedo, P.A., Garcia, C.A.B., Alves, J., Araujo, R.G.O., 2017. Characterisation and source identification of the total airborne particulate matter collected in an urban area of Aracaju, Northeast, Brazil. *Environ Pollut* 226, 444-451.
- Amato, F., Favez, O., Pandolfi, M., Alastuey, A., Querol, X., Moukhtar, S., Bruge, B., Verlhac, S., Orza, J.A.G., Bonnaire, N., Le Priol, T., Petit, J.F., Sciare, J., 2016. Traffic induced particle resuspension in Paris: Emission factors and source contributions. *Atmospheric Environment* 129, 114-124.
- Amato, F., Pandolfi, M., Escrig, A., Querol, X., Alastuey, A., Pey, J., Perez, N., Hopke, P.K., 2009. Quantifying road dust resuspension in urban environment by Multilinear Engine: A comparison with PMF2. *Atmospheric Environment* 43, 2770-2780.
- Annual Report for the UK Black Carbon Network, 2014. 2014 Annual Report for the UK Black Carbon Network, National Physical Laboratory, Hampton Road, Teddington, Middlesex, TW11 0LW.
- AQEG, 2012. Fine Particulate Matter (PM_{2.5}) in the United Kingdom, .
- Araujo, J.A., Barajas, B., Kleinman, M., Wang, X., Bennett, B.J., Gong, K.W., Navab, M., Harkema, J., Sioutas, C., Lusic, A.J., Nel, A.E., 2008. Ambient particulate pollutants

in the ultrafine range promote early atherosclerosis and systemic oxidative stress. *Circulation research* 102, 589-596.

Arnold, F., Pirjola, L., Aufmhoff, H., Schuck, T., Lahde, T., Hameri, K., 2006. First gaseous sulfuric acid measurements in automobile exhaust: Implications for volatile nanoparticle formation. *Atmospheric Environment* 40, 7097-7105.

Asbach, C., Fissan, H., Stahlmecke, B., Kuhlbusch, T.A.J., Pui, D.Y.H., 2009. Conceptual limitations and extensions of lung-deposited Nanoparticle Surface Area Monitor (NSAM). *Journal of Nanoparticle Research* 11, 101-109.

Asmi, E., Kivekäs, N., Kerminen, V.M., Komppula, M., Hyvärinen, A.P., Hatakka, J., Viisanen, Y., Lihavainen, H., 2011. Secondary new particle formation in Northern Finland Pallas site between the years 2000 and 2010. *Atmospheric Chemistry and Physics* 11, 12959-12972.

Atkinson, R.W., Fuller, G.W., Anderson, H.R., Harrison, R.M., Armstrong, B., 2010. Urban ambient particle metrics and health: a time-series analysis. *Epidemiology* 21, 501-511.

Atkinson, R.W., Kang, S., Anderson, H.R., Mills, I.C., Walton, H.A., 2014. Epidemiological time series studies of PM_{2.5} and daily mortality and hospital admissions: a systematic review and meta-analysis. *Thorax* 69, 660-665.

Avino, P., Casciardi, S., Fanizza, C., Manigrasso, M., 2011. Deep Investigation of Ultrafine Particles in Urban Air. *Aerosol and Air Quality Research* 11, 654-663.

Bakand, S., Hayes, A., Dechsakulthorn, F., 2012. Nanoparticles: a review of particle toxicology following inhalation exposure. *Inhal Toxicol* 24, 125-135.

Baltensperger, U., Weingartner, E., and Burtscher, H., et al., 2001. Dynamic mass and surface area measurements., in: Baron, P., Willeke, K. (Eds.), *Aerosol measurements: principles, techniques, and applications*. John Wiley & Sons., New York, pp. 387-418.

Barmpadimos, I., Keller, J., Oderbolz, D., Hueglin, C., Prévôt, A.S.H., 2012. One decade of parallel fine (PM_{2.5}) and coarse (PM₁₀-PM_{2.5}) particulate matter measurements in Europe: trends and variability. *Atmospheric Chemistry and Physics* 12, 3189-3203.

- Bau, S., Witschger, O., Gensdarmes, F., Thomas, D., 2012. Evaluating three direct-reading instruments based on diffusion charging to measure surface area concentrations in polydisperse nanoaerosols in molecular and transition regimes. *Journal of Nanoparticle Research* 14.
- Bernardoni, V., Vecchi, R., Valli, G., Piazzalunga, A., Fermo, P., 2011. PM10 source apportionment in Milan (Italy) using time-resolved data. *Sci Total Environ* 409, 4788-4795.
- Betha, R., Spracklen, D.V., Balasubramanian, R., 2013. Observations of new aerosol particle formation in a tropical urban atmosphere. *Atmospheric Environment* 71, 340-351.
- Bigi, A., Harrison, R.M., 2010. Analysis of the air pollution climate at a central urban background site. *Atmospheric Environment* 44, 2004-2012.
- Birmili, W., Beereshheim, H., Plass-Dulmer, C., Elste, T., Gige, S., Wiedensohler, A., Uhrner, U., 2003. The Hohenpeissenberg aerosol formation experiment (HAFEX): a long-term study including size-resolved aerosol, H₂SO₄, OH, and monoterpenes measurements. *Atmos. Chem. Phys.* 3, 361-376.
- Birmili, W., Tomsche, L., Sonntag, A., Opelt, C., Weinhold, K., Nordmann, S., Schmidt, W., 2013. Variability of aerosol particles in the urban atmosphere of Dresden (Germany): Effects of spatial scale and particle size. *Meteorologische Zeitschrift* 22, 195-211.
- Birmili, W., Wiedensohler, A., 2000. New particle formation in the continental boundary layer: Meteorological and gas phase parameter influence. *Geophysical Research Letters* 27, 3325-3328.
- Bond, T.C., Doherty, S.J., Fahey, D.W., Forster, P.M., Berntsen, T., DeAngelo, B.J., Flanner, M.G., Ghan, S., Kärcher, B., Koch, D., Kinne, S., Kondo, Y., Quinn, P.K., Sarofim, M.C., Schultz, M.G., Schulz, M., Venkataraman, C., Zhang, H., Zhang, S., Bellouin, N., Guttikunda, S.K., Hopke, P.K., Jacobson, M.Z., Kaiser, J.W., Klimont, Z., Lohmann, U., Schwarz, J.P., Shindell, D., Storelvmo, T., Warren, S.G., Zender, C.S., 2013. Bounding the role of black carbon in the climate system: A scientific assessment. *Journal of Geophysical Research: Atmospheres* 118, 5380-5552.

- Bongiovanni, S.F., Prati, P., Zucchiatti, A., Lucarelli, F., Mando, P.A., Ariola, V., Bertone, C., 2000. Study of the aerosol composition in the town of La Spezia with continuous sampling and PIXE analysis. *Nuclear Instruments and Methods in Physics Research B* 161-163, 786-791.
- Boogaard, H., Kos, G.P.A., Weijers, E.P., Janssen, N.A.H., Fischer, P.H., van der Zee, S.C., de Hartog, J.J., Hoek, G., 2011. Contrast in air pollution components between major streets and background locations: Particulate matter mass, black carbon, elemental composition, nitrogen oxide and ultrafine particle number. *Atmospheric Environment* 45, 650-658.
- Borsos, T., Rimnacova, D., Zdimal, V., Smolik, J., Wagner, Z., Weidinger, T., Burkart, J., Steiner, G., Reischl, G., Hitzenberger, R., Schwarz, J., Salma, I., 2012. Comparison of particulate number concentrations in three Central European capital cities. *Sci Total Environ* 433, 418-426.
- Boulon, J., Sellegri, K., Hervo, M., Picard, D., Pichon, J.M., Fréville, P., Laj, P., 2011. Investigation of nucleation events vertical extent: a long term study at two different altitude sites. *Atmospheric Chemistry and Physics* 11, 5625-5639.
- Boy, M.a., Kulmala, M., 2002. Nucleation events in the continental boundary layer: Influence of physical and meteorological parameters. *Atmos. Chem. Phys.* 2, 1-16.
- Breitner, S., Liu, L., Cyrus, J., Bruske, I., Franck, U., Schlink, U., Leitte, A.M., Herbarth, O., Wiedensohler, A., Wehner, B., Hu, M., Pan, X.C., Wichmann, H.E., Peters, A., 2011. Sub-micrometer particulate air pollution and cardiovascular mortality in Beijing, China. *Sci Total Environ* 409, 5196-5204.
- Breitner, S., Stolzel, M., Cyrus, J., Pitz, M., Wolke, G., Kreyling, W., Kuchenhoff, H., Heinrich, J., Wichmann, H.E., Peters, A., 2009. Short-term mortality rates during a decade of improved air quality in Erfurt, Germany. *Environ Health Perspect* 117, 448-454.
- Brines, M., Dall'Osto, M., Beddows, D.C.S., Harrison, R.M., Gómez-Moreno, F., Núñez, L., Artñano, B., Costabile, F., Gobbi, G.P., Salimi, F., Morawska, L., Sioutas, C., Querol, X., 2015. Traffic and nucleation events as main sources of ultrafine particles in high-insolation developed world cities. *Atmospheric Chemistry and Physics* 15, 5929-5945.

Brines, M., Dall'Osto, M., Beddows, D.C.S., Harrison, R.M., Querol, X., 2014. Simplifying aerosol size distributions modes simultaneously detected at four monitoring sites during SAPUSS. *Atmospheric Chemistry and Physics* 14, 2973-2986.

Brock, C.A., Washenfelder, R.A., Trainer, M., Ryerson, T.B., Wilson, J.C., Reeves, J.M., Huey, L.G., Holloway, J.S., Parrish, D.D., Hubler, G., and Fehsenfeld, Fred C. , 2002. Particle growth in the plumes of coal-fired power plants. *Journal of Geophysical Research* 107.

Brown, D.M., Wilson, M.R., MacNee, W., Stone, V., Donaldson, K., 2001. Size-dependent proinflammatory effects of ultrafine polystyrene particles: a role for surface area and oxidative stress in the enhanced activity of ultrafines. *Toxicology and applied pharmacology* 175, 191-199.

Brown, L.M., Collings, N., Harrison, R.M., Maynard, A.D., Maynard, R.L., 2000. Ultrafine Particles in the Atmosphere, *Phil. Trans. R. Soc. Lond. A. The Royal Society, London*, pp. 2563–2565.

Bukowiecki, N., Dommen, J., Prevot, A.S.H., Weingartner, E.a., Baltensperger, U., 2003. Fine and ultrafine particles in the Zurich (Switzerland) area measured with a mobile laboratory. An assessment of the seasonal and regional variation throughout a year. *Atmos. Chem. Phys. Discuss* 3, 2739-2782.

Buonanno, G., Marini, S., Morawska, L., Fuoco, F.C., 2012. Individual dose and exposure of Italian children to ultrafine particles. *The Science of the total environment* 438, 271-277.

Buonanno, G., Morawska, L., Stabile, L., Viola, A., 2010. Exposure to particle number, surface area and PM concentrations in pizzerias. *Atmospheric Environment* 44, 3963-3969.

Burtscher, H., 2005. Physical characterization of particulate emissions from diesel engines: a review. *Journal of Aerosol Science* 36, 896-932.

Butt, E.W., Rap, A., Schmidt, A., Scott, C.E., Pringle, K.J., Reddington, C.L., Richards, N.A.D., Woodhouse, M.T., Ramirez-Villegas, J., Yang, H., Vakkari, V., Stone, E.A., Rupakheti, M., S. Praveen, P., G. van Zyl, P., P. Beukes, J., Josipovic, M., Mitchell, E.J.S., Sallu, S.M., Forster, P.M., Spracklen, D.V., 2016. The impact of residential

combustion emissions on atmospheric aerosol, human health, and climate. *Atmospheric Chemistry and Physics* 16, 873-905.

Butterfield, D., Beccaceci, S., Quincey, P., Sweeney, B., Lilley, A., Bradshaw, C., Fuller, G., Green, D., Font Font, A., 2015. 2014 Annual Report for the UK Black Carbon Network. National Physical Laboratory. Hampton Road, Teddington, Middlesex, TW11 0LW, Queen's Printer and Controller of HMSO,.

Cao, J., Shen, Z., Chow, J.C., Qi, G., Watson, J.G., 2009. Seasonal variations and sources of mass and chemical composition for PM10 aerosol in Hangzhou, China. *Particuology* 7, 161-168.

Carslaw, D., Beevers, S., Westmoreland, E., Williams, M., Tate, J., Murrells, T., Stedman, J., Li, Y., Grice, S., Kent, A., and Tsagatakis, I., 2011. Trends in NO_x and NO₂ emissions and ambient measurements in the UK. Defra report.

Carslaw, D.C., 2015a. The openair manual — open-source tools for analysing air pollution data. King's College London.

Carslaw, D.C., 2015b. The openair manual — open-source tools for analysing air pollution data., Manual for version 1.5-9, King's College London.

Carslaw, D.C., Beevers, S., Ropkins, K., Bell, M., 2006a. Detecting and quantifying aircraft and other on-airport contributions to ambient nitrogen oxides in the vicinity of a large international airport. *Atmospheric Environment* 40, 5424-5434.

Carslaw, D.C., Beevers, S.D., Ropkins, K., Bell, M.C., 2006b. Detecting and quantifying the contribution made by aircraft emissions to ambient concentrations of nitrogen oxides in the vicinity of a large international airport. *Atmospheric Environment* 40, 5424-5434.

Carslaw, D.C., Ropkins, K., 2012a. openair — An R package for air quality data analysis. *Environmental Modelling & Software*. 27-28, 52-61.

Carslaw, D.C., Ropkins, K., 2012b. openair — An R package for air quality data analysis. *Environmental Modelling & Software* 27-28, 52-61.

Carslaw, K.S., Lee, L.A., Reddington, C.L., Pringle, K.J., Rap, A., Forster, P.M., Mann, G.W., Spracklen, D.V., Woodhouse, M.T., Regayre, L.A., Pierce, J.R., 2013. Large contribution of natural aerosols to uncertainty in indirect forcing. *Nature* 503, 67-71.

- Casati, R., Scheer, V., Vogt, R., Benter, T., 2007. Measurement of nucleation and soot mode particle emission from a diesel passenger car in real world and laboratory in situ dilution. *Atmospheric Environment* 41, 2125-2135.
- Cesari, D., Donato, A., Conte, M., Merico, E., Giangreco, A., Giangreco, F., Contini, D., 2016a. An inter-comparison of PM_{2.5} at urban and urban background sites: Chemical characterization and source apportionment. *Atmospheric Research* 174-175, 106-119.
- Cesari, D., Genga, A., Ielpo, P., Siciliano, M., Mascolo, G., Grasso, F.M., Contini, D., 2014. Source apportionment of PM(2.5) in the harbour-industrial area of Brindisi (Italy): identification and estimation of the contribution of in-port ship emissions. *Sci Total Environ* 497-498, 392-400.
- Charron, A., Birmili, W., Harrison, R.M., 2007. Factors influencing new particle formation at the rural site, Harwell, United Kingdom. *Journal of Geophysical Research* 112.
- Charron, A., Harrison, R.M., 2003. Primary particle formation from vehicle emissions during exhaust dilution in the roadside atmosphere. *Atmospheric Environment* 37, 4109-4119.
- Chen, R., Hu, B., Liu, Y., Xu, J., Yang, G., Xu, D., Chen, C., 2016a. Beyond PM_{2.5}: The role of ultrafine particles on adverse health effects of air pollution. *Biochim Biophys Acta* 1860, 2844-2855.
- Chen, Y., Schleicher, N., Fricker, M., Cen, K., Liu, X.L., Kaminski, U., Yu, Y., Wu, X.F., Norra, S., 2016b. Long-term variation of black carbon and PM_{2.5} in Beijing, China with respect to meteorological conditions and governmental measures. *Environ Pollut* 212, 269-278.
- Cheung, H.C., Morawska, L., Ristovski, Z.D., 2011. Observation of new particle formation in subtropical urban environment. *Atmospheric Chemistry and Physics* 11, 3823-3833.
- Ciaparra, D., Aries, E., Booth, M.-J., Anderson, D.R., Almeida, S.M., Harrad, S., 2009. Characterisation of volatile organic compounds and polycyclic aromatic hydrocarbons in the ambient air of steelworks. *Atmospheric Environment* 43, 2070-2079.

COMEAP, 2010. The Mortality Effects of Long-Term Exposure to Particulate Air Pollution in the United Kingdom, the Health Protection Agency for the Committee on the Medical Effects of Air Pollutants.UK.

Contini, D., Donato, A., Elefante, C., Grasso, F.M., 2012a. Analysis of particles and carbon dioxide concentrations and fluxes in an urban area: Correlation with traffic rate and local micrometeorology. *Atmospheric Environment* 46, 25-35.

Cordell, R.L., Mazet, M., Dechoux, C., Hama, S.M.L., Staelens, J., Hofman, J., Stroobants, C., Roekens, E., Kos, G.P.A., Weijers, E.P., Frumau, K.F.A., Panteliadis, P., Delaunay, T., Wyche, K.P., Monks, P.S., 2016. Evaluation of biomass burning across North West Europe and its impact on air quality. *Atmospheric Environment* 141, 276-286.

Cordell, R.L., White, I.R., Monks, P.S., 2014. Validation of an assay for the determination of levoglucosan and associated monosaccharide anhydrides for the quantification of wood smoke in atmospheric aerosol. *Anal Bioanal Chem* 406, 5283-5292.

COST 633 Report, 2009. Particulate Matter – Properties Related to Health Effects, in: Regina Hitzenberger, Janja Tursic (Eds.).

Crilley, L.R., Lucarelli, F., Bloss, W.J., Harrison, R.M., Beddows, D.C., Calzolari, G., Nava, S., Valli, G., Bernardoni, V., Vecchi, R., 2017. Source apportionment of fine and coarse particles at a roadside and urban background site in London during the 2012 summer ClearLo campaign. *Environ Pollut* 220, 766-778.

Crumeyrolle, S., Manninen, H.E., Sellegri, K., Roberts, G., Gomes, L., Kulmala, M., Weigel, R., Laj, P., Schwarzenboeck, A., 2010. New particle formation events measured on board the ATR-42 aircraft during the EUCAARI campaign. *Atmospheric Chemistry and Physics* 10, 6721-6735.

Cusack, M., Pérez, N., Pey, J., Alastuey, A., Querol, X., 2013. Source apportionment of fine PM and sub-micron particle number concentrations at a regional background site in the western Mediterranean: a 2.5 year study. *Atmospheric Chemistry and Physics* 13, 5173-5187.

Dal Maso, M., Kulmala, M., Lehtinen, K.E., Makela, J.M., Aalto, P.P., O'Dowd, C., 2002. Condensation and coagulation sinks and formation of nucleation mode particles in coastal and boreal forest boundary layers. *GEOPHYSICAL RESEARCH* 107, 1-10.

Dal Maso, M., Kulmala, M., Riipinen, I., Wagner, R., Hussein, T., Aalto, P.P., Lehtinen, K.E.J., 2005a. Formation and growth of fresh atmospheric aerosols: eight years of aerosol size distribution data from SMEAR II, Hyytiälä, Finland. *Boreal Env. Res.* 10, 323-336.

Dal Maso, M., Kulmala, M., Riipinen, I., Wagner, R., Hussein, T., Aalto, P.P.a.L., Kari E. J. , 2005b. Formation and growth of fresh atmospheric aerosols: eight years of aerosol size distribution data from SMEAR II, Hyytiälä, Finland. *BOREAL ENVIRONMENT RESEARCH* 10, 323-336.

Dal Maso, M., Sogacheva, L., Aalto, P.P., Riipinen, I., Komppula, M., Tunved, P., Korhonen, L., Suur-Uski, V., Hirsikko, A., Kurten, T., Kerminen, V.-M., Lihavainen, H., Viisanen, Y., Hansson, H.-C., and Kulmala, M., 2007. Aerosol size distribution measurements at four Nordic field stations: identification, analysis and trajectory analysis of new particle formation bursts. *Tellus* 59B, 350-361.

Dall'Osto, M., Querol, X., Alastuey, A., O'Dowd, C., Harrison, R.M., Wenger, J., Gómez-Moreno, F.J., 2013. On the spatial distribution and evolution of ultrafine particles in Barcelona. *Atmospheric Chemistry and Physics* 13, 741-759.

Dall'Osto, M., Querol, X., Alastuey, A., O'Dowd, C., Harrison, R.M., Wenger, J., Gómez-Moreno, F.J., 2013a. On the spatial distribution and evolution of ultrafine particles in Barcelona. *Atmospheric Chemistry and Physics* 13, 741-759.

de España, D.C., Wonaschütz, A., Steiner, G., Rosati, B., Demattio, A., Schuh, H., Hitzemberger, R., 2017. Long-term quantitative field study of New Particle Formation (NPF) events as a source of Cloud Condensation Nuclei (CCN) in the urban background of Vienna. *Atmospheric Environment* 164, 289-298.

de Kok, T.M., Driessens, H.A., Hogervorst, J.G., Briede, J.J., 2006. Toxicological assessment of ambient and traffic-related particulate matter: a review of recent studies. *Mutat Res* 613, 103-122.

de Winter, J.C., Dodou, D., Wieringa, P.A., 2009. Exploratory Factor Analysis With Small Sample Sizes. *Multivariate Behav Res* 44, 147-181.

DEFRA, 2011a. Air Quality Plans for the achievement of EU air quality limit values for nitrogen dioxide (NO₂) in the UK, .

Dockery, D.W.a., Stone, P.H., 2007. Cardiovascular Risks from Fine Particulate Air Pollution. *The New England Journal of Medicine* 356(5), 511-513.

Dunn, M.J., Jiménez, J.-L., Baumgardner, D., Castro, T., McMurry, P.H., Smith, J.N., 2004. Measurements of Mexico City nanoparticle size distributions: Observations of new particle formation and growth. *Geophysical Research Letters* 31, n/a-n/a.

EC, 2004. Council Directive 2004/107/EC relating to arsenic, cadmium, mercury, nickel and polycyclic aromatic hydrocarbons in ambient air., pp. 3-16.

EC Directive, 2008. EC. Directive on ambient air quality and cleaner air for Europe (Directive 2008/50/EC). <http://eur-lex.europa.eu/LexUriServ/LexUriServ.do?uri=OJ:L:2008:152:0001:0044:EN:PDF>

EEA, 2013. Air quality in Europe — 2013 report, Luxembourg: Publications Office of the European Union, 2013.

EEA, 2014. Air quality in Europe European Environment Agency, Luxembourg.

EEA, 2016a. Air quality in Europe, European Environment Agency, Luxembourg.

EEA, 2016b. Air quality in Europe — 2016 report, Luxembourg: Publications Office of the European Union, 2016.

Eeftens, M., Phuleria, H.C., Meier, R., Aguilera, I., Corradi, E., Davey, M., Ducret-Stich, R., Fierz, M., Gehrig, R., Ineichen, A., Keidel, D., Probst-Hensch, N., Ragettli, M.S., Schindler, C., Künzli, N., Tsai, M.-Y., 2015. Spatial and temporal variability of ultrafine particles, NO₂, PM_{2.5}, PM_{2.5} absorbance, PM₁₀ and PM_{coarse} in Swiss study areas. *Atmospheric Environment* 111, 60-70.

Ehn, M., Thornton, J.A., Kleist, E., Sipila, M., Junninen, H., Pullinen, I., Springer, M., Rubach, F., Tillmann, R., Lee, B., Lopez-Hilfiker, F., Andres, S., Acir, I.H., Rissanen, M., Jokinen, T., Schobesberger, S., Kangasluoma, J., Kontkanen, J., Nieminen, T., Kurten, T., Nielsen, L.B., Jorgensen, S., Kjaergaard, H.G., Canagaratna, M., Maso, M.D.,

Berndt, T., Petaja, T., Wahner, A., Kerminen, V.M., Kulmala, M., Worsnop, D.R., Wildt, J., Mentel, T.F., 2014. A large source of low-volatility secondary organic aerosol. *Nature* 506, 476-479.

Elder, A., Gelein, R., Silva, V., Feikert, T., Opanashuk, L., Carter, J., Potter, R., Maynard, A., Ito, Y., Finkelstein, J., Oberdörster, G., 2006. Translocation of Inhaled Ultrafine Manganese Oxide Particles to the Central Nervous System. *Environmental Health Perspectives* 114, 1172-1178.

Elder, A., Oberdörster, G., 2006. Translocation and effects of ultrafine particles outside of the lung. *Clin Occup Environ Med.* 4, 785-796.

Evan, D., 2011a. Leicester City's Air Quality Action Plan 2011-2016. <https://www.leicester.gov.uk/media/178152/air-quality-action-plan-2011-2016.pdf>.

Evan, D., 2011b. Leicester City's Air Quality Action Plan 2011-2016. <https://www.leicester.gov.uk/media/178152/air-quality-action-plan-2011-2016.pdf>

Fernández-Camacho, R., Rodríguez, S., de la Rosa, J., Sánchez de la Campa, A.M., Viana, M., Alastuey, A., Querol, X., 2010. Ultrafine particle formation in the inland sea breeze airflow in Southwest Europe. *Atmospheric Chemistry and Physics* 10, 9615-9630.

Fierz, M., Houle, C., Steigmeier, P., Burtscher, H., 2011. Design, Calibration, and Field Performance of a Miniature Diffusion Size Classifier. *Aerosol Science and Technology* 45, 1-10.

Fissan, H., Neumann, S., Trampe, A., Pui, D.Y.H., and, Shin, W.G., 2007a. Rationale and principle of an instrument measuring lung deposited nanoparticle surface area. *J. Nanoparticle Res* 9, 53-59.

Fissan, H., Neumann, S., Trampe, A., Pui, D.Y.H., Shin, W.G., 2007b. Rationale and principle of an instrument measuring lung deposited nanoparticle surface area. *Journal of Nanoparticle Research* 9, 53-59.

Fruin, S., Westerdahl, D., Sax, T., Sioutas, C., Fine, P.M., 2008. Measurements and predictors of on-road ultrafine particle concentrations and associated pollutants in Los Angeles. *Atmospheric Environment* 42, 207-219.

- Fuller, G.W., Tremper, A.H., Baker, T.D., Yttri, K.E., Butterfield, D., 2014. Contribution of wood burning to PM10 in London. *Atmospheric Environment* 87, 87-94.
- Furuta, N., Iijima, A., Kambe, A., Sakai, K., Sato, K., 2005. Concentrations, enrichment and predominant sources of Sb and other trace elements in size classified airborne particulate matter collected in Tokyo from 1995 to 2004. *J Environ Monit* 7, 1155-1161.
- Fuzzi, S., Andreae, M. O. , Huebert, B.J., Kulmala, M., Bond, T.C., Boy, M., Doherty, S.J., Guenther, A., Kanakidou, M., Kawamura, K., Kerminen, V.-M., Lohmann, U., Russell, L.M.a., Pöschl, U., 2006. Critical assessment of the current state of scientific knowledge, terminology, and research needs concerning the role of organic aerosols in the atmosphere, climate, and global change. *Atmos. Chem. Phys.* 6, 2017-2038.
- Geiss, O., Bianchi, I., Barrero-Moreno, J., 2016. Lung-deposited surface area concentration measurements in selected occupational and non-occupational environments. *Journal of Aerosol Science* 96, 24-37.
- Godri, K.J., Harrison, R.M., Evans, T., Baker, T., Dunster, C., Mudway, I.S., Kelly, F.J., 2011. Increased oxidative burden associated with traffic component of ambient particulate matter at roadside and urban background schools sites in London. *PLoS One* 6, 1-11.
- Gomes, J.F., Bordado, J.C., Albuquerque, P.C., 2012. On the assessment of exposure to airborne ultrafine particles in urban environments. *Journal of toxicology and environmental health. Part A* 75, 1316-1329.
- Gómez-Moreno, F.J., Pujadas, M., Plaza, J., Rodríguez-Maroto, J.J., Martínez-Lozano, P., Artíñano, B., 2011. Influence of seasonal factors on the atmospheric particle number concentration and size distribution in Madrid. *Atmospheric Environment* 45, 3169-3180.
- Gomišček, B., Hauck, H., Stopper, S., Preining, O., 2004. Spatial and temporal variations of PM1, PM2.5, PM10 and particle number concentration during the AUPHEP—project. *Atmospheric Environment* 38, 3917-3934.
- González, Y., 2012. Levels and origin of reactive gases and their relationship with aerosols in the proximity of the emission sources and in the free troposphere at Tenerife. University of La Laguna.

González, Y., Rodríguez, S., 2013. A comparative study on the ultrafine particle episodes induced by vehicle exhaust: A crude oil refinery and ship emissions. *Atmospheric Research* 120-121, 43-54.

González, Y., Rodríguez, S., Guerra García, J.C., Trujillo, J.L., García, R., 2011. Ultrafine particles pollution in urban coastal air due to ship emissions. *Atmospheric Environment* 45, 4907-4914.

Gray, H.A.a., Cass, G.R., 1986. Characteristics of Atmospheric Organic and Elemental Carbon Particle Concentrations in Los Angeles. *Environ. Sci. Technol.* 20, 580-589.

Größ, J., Hamed, A., Sonntag, A., Spindler, G., Manninen, H.E., Nieminen, T., Kulmala, M., Hörrak, U., Plass-Dülmer, C., Wiedensohler, A., Birmili, W., 2018. Atmospheric new particle formation at the research station Melpitz, Germany: connection with gaseous precursors and meteorological parameters. *Atmospheric Chemistry and Physics* 18, 1835-1861.

Hama, S.M.L., Cordell, R.L., Kos, G.P.A., Weijers, E.P., Monks, P.S., 2017b. Sub-micron particle number size distribution characteristics at two urban locations in Leicester. *Atmospheric Research* 194, 1-16.

Hama, S.M.L., Cordell, R.L., Monks, P.S., 2017c. Quantifying primary and secondary source contributions to ultrafine particles in the UK urban background. *Atmospheric Environment* 166, 62-78.

Hama, S.M.L., Ma, N., Cordell, R.L., Kos, G.P.A., Wiedensohler, A., Monks, P.S., 2017a. Lung deposited surface area in Leicester urban background site/UK: Sources and contribution of new particle formation. *Atmospheric Environment* 151, 94-107.

Hamed, A., Joutsensaari, S., Mikkonen, L., Sogacheva, M., Dal Maso, M., Kulmala, F., Cavalli, S., Fuzzi, M. C. Facchini, S., Decesari, M., Mircea, K. E. J. Lehtinen, a.A.L., 2007. Nucleation and growth of new particles in Po Valley, Italy. *Atmos. Chem. Phys.* 7, 355-376.

Harris, S.J., Maricq, M.M., 2001. Signature size distributions for diesel and gasoline engine exhaust particulate matter. *Aerosol Science* 32, 749-764.

Harrison, R.M., Deacon, A.R., Jones, M.R., and, Appleby, R.S., 1997. Sources and processes affecting concentrations of PM₁₀ and PM_{2.5} particulate matter in Birmingham. *Atmospheric Environment* 31, 4103-4117.

Harrison, R.M., Jones, A.M., 2005a. Multisite Study of Particle Number Concentrations in Urban Air. *Environ. Sci. Technol.* 39, 6063-6070.

Harrison, R.M., Jones, A.M., 2005b. Multisite Study of Particle Number Concentrations in Urban Air. *Environ. Sci. Technol* 39, 6063-6070.

Harrison, R.M., Jones, A.M., Lawrence, R.G., 2003. A pragmatic mass closure model for airborne particulate matter at urban background and roadside sites. *Atmospheric Environment* 37, 4927-4933.

Harrison, R.M., Jones, A.M., Lawrence, R.G., 2004. Major component composition of PM₁₀ and PM_{2.5} from roadside and urban background sites. *Atmospheric Environment* 38, 4531-4538.

Harrison, R.M., Jones, M., Collins, G., 1999. Measurements of the physical properties of particles in the urban atmosphere. *Atmospheric Environment* 33, 309-321.

Harrison, R.M., Laxen, D., Moorcroft, S., Laxen, K., 2012. Processes affecting concentrations of fine particulate matter (PM_{2.5}) in the UK atmosphere. *Atmospheric Environment* 46, 115-124.

Harrison, R.M., Shi, J.P., Xi, S., Khan, A., Mark, D., Kinnersley, R.a., Yin, J., 2000. Measurement of number, mass and size distribution of particles in the atmosphere. *Phil. Trans. R. Soc. Lond. A* 358, 2567-2580.

Harrison, R.M., Yin, J., 2000. Particulate matter in the atmosphere: which particle properties are important for its effects on health? *The Science of the Total Environment* 249, 85-101.

Heal, M.R., Kumar, P., Harrison, R.M., 2012. Particles, air quality, policy and health. *Chem Soc Rev* 41, 6606-6630.

HEI, 2013a. HEI Review Panel on Ultrafine Particles. 2013. Understanding the Health Effects of Ambient Ultrafine Particles., HEI Perspectives 3, Health Effects Institute, Boston, MA.

- HEI, 2013b. HEI Review Panel on Ultrafine Particles. Understanding the Health Effects of Ambient Ultrafine Particles, HEI Perspectives 3., Health Effects Institute, Boston, MA.
- Heintzenberg, J., Wehner, B., Birmili, W., 2007. How to find bananas in the atmospheric aerosol?: new approach for analyzing atmospheric nucleation and growth events. *Tellus B* 59, 273-282.
- Herrmann, E., Ding, A.J., Kerminen, V.M., Petäjä, T., Yang, X.Q., Sun, J.N., Qi, X.M., Manninen, H., Hakala, J., Nieminen, T., Aalto, P.P., Kulmala, M., Fu, C.B., 2014. Aerosols and nucleation in eastern China: first insights from the new SORPES-NJU station. *Atmospheric Chemistry and Physics* 14, 2169-2183.
- Hinds, W.C., 1999. *Aerosol Technology: Properties, Behavior, and Measurement of Airborne Particles* 2nd ed, JOHN WILEY & SONS, INC., Canada.
- Ho, K.F., Lee, S.C., Yu, J.C., Zou, S.C., Fung, K., 2002. Carbonaceous characteristics of atmospheric particulate matter in Hong Kong. *The Science of the Total Environment* 300, 59-67.
- Hoffman, D., Tilgner, A., Iinuma, Y., Herrmann, H., 2010. Atmospheric stability of levoglucosan: a detailed laboratory and modeling study. *Environ. Sci. Technol.* 44, 694-699.
- Hofman, J., Staelens, J., Cordell, R., Stroobants, C., Zikova, N., Hama, S.M.L., Wyche, K.P., Kos, G.P.A., Van Der Zee, S., Smallbone, K.L., Weijers, E.P., Monks, P.S., Roekens, E., 2016. Ultrafine particles in four European urban environments: Results from a new continuous long-term monitoring network. *Atmospheric Environment* 136, 68-81.
- Holmes, N.S., 2007. A review of particle formation events and growth in the atmosphere in the various environments and discussion of mechanistic implications. *Atmospheric Environment* 41, 2183-2201.
- Hopke, P.K., 2000. *A guide to positive matrix factorization*, U.S. Environmental Protection Agency, Research Triangle Park, NC 27711, USA.
- Hussein, T., Junninen, P., Tunved, A., Kristensson, M., Dal Maso, I., Riipinen, P. P., Aalto, H.-C., Hansson, E., Swietlicki, a.M.K., 2009. Time span and spatial scale of regional new particle formation events over Finland and Southern Sweden. *Atmos. Chem. Phys.* 9, 4699-4716.

- Hussein, T., Hameri, K., Aalto, P., Paatero, P., Kulmala, M., 2005. Modal structure and spatial-temporal variations of urban and suburban aerosols in Helsinki, Finland. *Atmospheric Environment*.
- Hussein, T., Martikainen, J., Junninen, H., Sogacheva, L., Wagner, R., Dal Maso, M., Riipinen, I., Aalto, P.P., Kulmala, M., 2008. Observation of regional new particle formation in the urban atmosphere. *Tellus B* 60, 509-521.
- Hussein, T., Puustinen, A., Aalto, P.P., Makkela, J.M., Hameri, K., Kulmala, M., 2004. Urban aerosol number size distributions. *Atmos. Chem. Phys.* 4, 391-411.
- ICRP, 1994a. Human Respiratory Tract Model for Radiological Protection. . ICRP 66, 1-3.
- ICRP, 1994b. Human Respiratory Tract Model for Radiological Protection., ICRP Publication pp. 1-3.
- Imhof, D., Weingartner, E., Vogt, U., Dreiseidler, A., Rosenbohm, E., Scheer, V., Vogt, R., Nielsen, O.J., Kurtenbach, R., Corsmeier, U., Kohler, M., Baltensperger, U., 2005. Vertical distribution of aerosol particles and NO_x close to a motorway. *Atmospheric Environment* 39, 5710-5721.
- Ingrid Sundvor, N.C.B., Mar Viana, Xavier Querol, Cristina Reche, Fulvio Amato, Giorgos Mellios, Cristina Guerreiro, 2012. Road traffic's contribution to air quality in European cities. The European Topic Centre on Air Pollution and Climate Change Mitigation
- Invernizzi, G., Ruprecht, A., Mazza, R., De Marco, C., Močnik, G., Sioutas, C., Westerdahl, D., 2011. Measurement of black carbon concentration as an indicator of air quality benefits of traffic restriction policies within the ecopass zone in Milan, Italy. *Atmospheric Environment* 45, 3522-3527.
- IPCC, 2007. The Physical Science Basis. Contribution of Working Group I to the Fourth Assessment Report of the Intergovernmental Panel on Climate Change, in: Solomon, S., D. , Qin, M., Manning, Z., Chen, M., Marquis, K.B., Averyt, M., and, T., Miller, H.L. (Eds.), Cambridge, United Kingdom and New York, NY, USA.
- IPCC, 2008. Climate Change 2007 Synthesis Report.

Jeong, C.-H., Hopke, P.K., Chalupa, D., Utell, M., 2004. Characteristics of Nucleation and Growth Events of Ultrafine Particles Measured in Rochester, NY. *Environmental science & technology* 38, 1933-1940.

Jeong, C.H., Evans, G.J., McGuire, M.L., Chang, R.Y.W., Abbatt, J.P.D., Zeromskiene, K., Mozurkewich, M., Li, S.M., Leitch, W.R., 2010. Particle formation and growth at five rural and urban sites. *Atmospheric Chemistry and Physics* 10, 7979-7995.

Joaquin, 2015a. Monitoring of ultrafine particles and black carbon. Joint Air Quality Initiative, Work Package 1 Action 1 and 3, Flanders Environment Agency, Aalst. Available at <http://www.joaquin.eu>.

Joaquin, 2015b. Composition and source apportionment of PM10. Joint Air Quality Initiative, Work Package 1 Action 2 and 3., Flanders Environment Agency, Aalst. Available at <http://www.joaquin.eu>.

Johnston, C.J., Finkelstein, J.N., Mercer, P., Corson, N., Gelein, R., Oberdorster, G., 2000. Pulmonary effects induced by ultrafine PTFE particles. *Toxicology and applied pharmacology* 168, 208-215.

Jones, A.M., Harrison, R.M., 2005. Interpretation of particulate elemental and organic carbon concentrations at rural, urban and kerbside sites. *Atmospheric Environment* 39, 7114-7126.

Joutsensaari, J., Ozon, M., Nieminen, T., Mikkonen, S., Lähivaara, T., Decesari, S., Facchini, M.C., Laaksonen, A., Lehtinen, K.E.J., 2018. Identification of new particle formation events with deep learning. *Atmospheric Chemistry and Physics Discussions*, 1-28.

Karlsson, H.L., Gustafsson, J., Cronholm, P., Moller, L., 2009. Size-dependent toxicity of metal oxide particles--a comparison between nano- and micrometer size. *Toxicol Lett* 188, 112-118.

Kelly, F.J., Fussell, J.C., 2012. Size, source and chemical composition as determinants of toxicity attributable to ambient particulate matter. *Atmospheric Environment* 60, 504-526.

Kerminen, V.M., Paramonov, M., Anttila, T., Riipinen, I., Fountoukis, C., Korhonen, H., Asmi, E., Laakso, L., Lihavainen, H., Swietlicki, E., Svenningsson, B., Asmi, A., Pandis,

S.N., Kulmala, M., Petäjä, T., 2012. Cloud condensation nuclei production associated with atmospheric nucleation: a synthesis based on existing literature and new results. *Atmospheric Chemistry and Physics* 12, 12037-12059.

Ketzel, M., Wahlin, P., Kristensson, A., Swietlicki, E., Berkowicz, R., Nielsen, O.J., Palmgren, F., 2004. Particle size distribution and particle mass measurements at urban, near-city and rural level in the Copenhagen area and Southern Sweden. *Atmos. Chem. Phys.* 4, 281-292.

Keuken, M.P., Moerman, M., Zandveld, P., Henzing, J.S., Hoek, G., 2015. Total and size-resolved particle number and black carbon concentrations in urban areas near Schiphol airport (the Netherlands). *Atmospheric Environment* 104, 132-142.

Kim, K.-H., Lee, J.-H., Jang, M.-S., 2002. Metals in airborne particulate matter from the first and second industrial complex area of Taejon city, Korea. *Environ Pollut* 118, 41-51.

Kirkby, J., Curtius, J., Almeida, J., Dunne, E., Duplissy, J., Ehrhart, S., Franchin, A., Gagne, S., Ickes, L., Kurten, A., Kupc, A., Metzger, A., Riccobono, F., Rondo, L., Schobesberger, S., Tsagkogeorgas, G., Wimmer, D., Amorim, A., Bianchi, F., Breitenlechner, M., David, A., Dommen, J., Downard, A., Ehn, M., Flagan, R.C., Haider, S., Hansel, A., Hauser, D., Jud, W., Junninen, H., Kreissl, F., Kvashin, A., Laaksonen, A., Lehtipalo, K., Lima, J., Lovejoy, E.R., Makhmutov, V., Mathot, S., Mikkila, J., Minginette, P., Mogo, S., Nieminen, T., Onnela, A., Pereira, P., Petaja, T., Schnitzhofer, R., Seinfeld, J.H., Sipila, M., Stozhkov, Y., Stratmann, F., Tome, A., Vanhanen, J., Viisanen, Y., Vrtala, A., Wagner, P.E., Walther, H., Weingartner, E., Wex, H., Winkler, P.M., Carslaw, K.S., Worsnop, D.R., Baltensperger, U., Kulmala, M., 2011. Role of sulphuric acid, ammonia and galactic cosmic rays in atmospheric aerosol nucleation. *Nature* 476, 429-433.

Kittelson, D.B., 1998. ENGINES AND NANOPARTICLES: A REVIEW. *J. Aerosol Sci.* 29, 575-588.

Kittelson, D.B., Watts, W.F., Johnson, J.P., 2004. Nanoparticle emissions on Minnesota highways. *Atmospheric Environment* 38, 9-19.

Kittelson, D.B., Watts, W.F., Johnson, J.P., 2006. On-road and laboratory evaluation of combustion aerosols—Part1: Summary of diesel engine results. *Journal of Aerosol Science* 37, 913-930.

Kreyling, W.G., Semmler-Behnke, M., Möller, W., 2006. Health implications of nanoparticles. *Journal of Nanoparticle Research* 8, 543-562.

Kristensson, A., Dal Maso, M., Swietlicki, E., Hussein, T., Zhou, J., Kerminen, V.M., Kulmala, M., 2017. Characterization of new particle formation events at a background site in Southern Sweden: relation to air mass history. *Tellus B: Chemical and Physical Meteorology* 60, 330-344.

Krudysz, M., Moore, K., Geller, M., Sioutas, C., Froines, J., 2009a. Intra-community spatial variability of particulate matter size distributions in Southern California/Los Angeles. *Atmos. Chem. Phys.* 9, 1061-1075.

Krudysz, M., Moore, K., Geller, M., Sioutas, C., Froines, J., 2009b. Intra-community spatial variability of particulate matter size distributions in Southern California/Los Angeles. *Atmos. Chem. Phys.* 9, 1061-1075.

Kulkarni, P., Baron, P.A., Willeke, K., 2011. *Aerosol Measurement: Principles, Techniques, and Applications.*, 3rd ed, John Wiley & Sons.

Kulmala, M., 2003. How Particles Nucleate and Grow. *Science* 302, 1000-1001.

Kulmala, M., Dal Maso, M., Mekela, J., M., Pirjola, L., Vekeva, M., Aalto, P.P., Miikkulainen, P., Hamer, K., O'Dowd, C., 2001a. On the formation, growth and composition of nucleation mode particles. *Tellus B* 53, 479-490.

Kulmala, M., Ilona Riipinen, Mikko Sipilä, Hanna E. Manninen, Tuukka Petäjä, Heikki Junninen, Miikka Dal Maso, Genrik Mordas, Aadu Mirme, Marko Vana, Anne Hirsikko, Lauri Laakso, Roy M. Harrison, Ian Hanson, Carl Leung, Kari E. J. Lehtinen, a.V.-M.K., 2007. Toward Direct Measurement of Atmospheric Nucleation. *Science* 318, 89-92.

Kulmala, M., Jenni Kontkanen, Heikki Junninen, Katrianne Lehtipalo, Hanna E. Manninen, Tuomo Nieminen, Tuukka Petäjä, M.S., Siegfried Schobesberger, Pekka Rantala, Alessandro Franchin, Tuija Jokinen, Emma Järvinen, Mikko Äijälä, Juha Kangasluoma, Jani Hakala, Pasi P. Aalto, Pauli Paasonen, Jyri Mikkilä, Joonas Vanhanen, Juho Aalto, Hannele Hakola, Ulla Makkonen, Taina Ruuskanen, Roy L.

Mauldin III, Jonathan Duplissy, Hanna Vehkamäki, Jaana Bäck, Aki Kortelainen, Ilona Riipinen, Theo Kurtén, Murray V. Johnston, James N. Smith, Mikael Ehn, Thomas F. Mentel, Kari E. J. Lehtinen, Ari Laaksonen, Veli-Matti Kerminen and Douglas R. Worsnop, 2013. Direct Observations of Atmospheric Aerosol Nucleation. *Science* 339, 943-946.

Kulmala, M., Kerminen, V.-M., 2008a. On the formation and growth of atmospheric nanoparticles. *Atmospheric Research* 90, 132-150.

Kulmala, M., Kerminen, V.M., 2008b. On the formation and growth of atmospheric nanoparticles. *Atmospheric Research* 90, 132-150.

Kulmala, M., Lehtinen, K.E.J., Laaksonen, A., 2006. Cluster activation theory as an explanation of the linear dependence between formation rate of 3nm particles and sulphuric acid concentration. *Atmos. Chem. Phys.* 6, 787-793.

Kulmala, M., Luoma, K., Virkkula, A., Petäjä, T., Paasonen, P., Kerminen, V.-M., Nie, W., Qi, X., Shen, Y., Chi, X., Ding, A., 2016. On the mode-segregated aerosol particle number concentration load: contributions of primary and secondary particles in Hyytiälä and Nanjing. *BOREAL ENVIRONMENT RESEARCH* 21, 319-331.

Kulmala, M., Maso, M.D., Mäkelä, J.M., Pirjola, L., Väkevä, M., Aalto, P., Miikkulainen, P., Hämeri, K., O'dowd, C.D., 2001b. On the formation, growth and composition of nucleation mode particles. *Tellus B: Chemical and Physical Meteorology* 53, 479-490.

Kulmala, M., Petäjä, T., Monkkonen, P., Koponen, K., I., Dal Maso, M., Aalto, P., Lehtinen, K.E., Kerminen, V.M., 2005. On the growth of nucleation mode particles: source rates of condensable vapor in polluted and clean environments. *Atmos. Chem. Phys.* 5, 409-416.

Kulmala, M., Petaja, T., Nieminen, T., Sipila, M., Manninen, H.E., Lehtipalo, K., Dal Maso, M., Aalto, P.P., Junninen, H., Paasonen, P., Riipinen, I., Lehtinen, K.E., Laaksonen, A., Kerminen, V.M., 2012. Measurement of the nucleation of atmospheric aerosol particles. *Nat Protoc* 7, 1651-1667.

Kulmala, M., Pirjola, L., kela, J.M.M., 2000. Stable sulphate clusters as a source of new atmospheric particles. *nature* 204, 66-69.

Kulmala, M., Vehkamäki, H., Petäjä, T., Dal Maso, M., Lauri, A., Kerminen, V.M., Birmili, W., McMurry, P.H., 2004. Formation and growth rates of ultrafine atmospheric particles: a review of observations. *Journal of Aerosol Science* 35, 143-176.

Kumar, P., Fennell, P., Britter, R., 2008. Measurements of particles in the 5-1000 nm range close to road level in an urban street canyon. *The Science of the total environment* 390, 437-447.

Kumar, P., Fennell, P.S., Hayhurst, A.N., Britter, R.E., 2009. Street Versus Rooftop Level Concentrations of Fine Particles in a Cambridge Street Canyon. *Boundary-Layer Meteorology* 131, 3-18.

Kumar, P., Morawska, L., Birmili, W., Paasonen, P., Hu, M., Kulmala, M., Harrison, R.M., Norford, L., Britter, R., 2014. Ultrafine particles in cities. *Environment international* 66, 1-10.

Kumar, P., Robins, A., Vardoulakis, S., Britter, R., 2010. A review of the characteristics of nanoparticles in the urban atmosphere and the prospects for developing regulatory controls. *Atmospheric Environment* 44, 5035-5052.

Kuuluvainen, H., Rönkkö, T., Järvinen, A., Saari, S., Karjalainen, P., Lähde, T., Pirjola, L., Niemi, J.V., Hillamo, R., Keskinen, J., 2016. Lung deposited surface area size distributions of particulate matter in different urban areas. *Atmospheric Environment* 136, 105-113.

Larsen, L.C., Austin, J., Dolislager, L., Lashgari, A., McCauley, E., Motallebi, N., Tran, H., 2003. THE OZONE WEEKEND EFFECT IN CALIFORNIA. California Environmental Protection Agency.

Lawrence, S., Sokhi, R., Ravindra, K., Mao, H., Prain, H.D., Bull, I.D., 2013. Source apportionment of traffic emissions of particulate matter using tunnel measurements. *Atmospheric Environment* 77, 548-557.

Laxen, D., Moorcroft, S., Marnier, B., Laxen, K., Boulter, P., Barlow, T., Harrison, R., and, Heal, M., 2010. PM_{2.5} in the UK, Report for SNIFFER, Edinburgh Available at: <http://www.aqconsultants.co.uk/AQC/media/Reports/SNIFFER-PM25-Rept-Final-201210.pdf>.

- LeBlanc, A.J., Moseley, A.M., Chen, B.T., Frazer, D., Castranova, V., Nurkiewicz, T.R., 2010. Nanoparticle inhalation impairs coronary microvascular reactivity via a local reactive oxygen species-dependent mechanism. *Cardiovascular toxicology* 10, 27-36.
- Lee, Y.-G., Lee, H.-W., Kim, M.-S., Choi, C.Y., Kim, J., 2008. Characteristics of particle formation events in the coastal region of Korea in 2005. *Atmospheric Environment* 42, 3729-3739.
- Lehtinen, K.E., Korhonen, H., Dal Maso, M., Kulmala, M., 2003. On the concept of condensation sink diameter. *Boreal Environment Research* 8, 405-411.
- Li, N., Sioutas, C., Cho, A., Schmitz, D., Misra, C., Sempf, J., Wang, M., Oberley, T., Froines, J., Nel, A., 2002. Ultrafine Particulate Pollutants Induce Oxidative Stress and Mitochondrial Damage. *Environmental Health Perspectives* 111, 455-460.
- Lighty, J., Veranth, J., Sarofim, A.F., 2000. Introduction to the Air & Waste Management Association's 30th Annual Critical Review. *J Air Waste Manag Assoc* 50, 1562-1564.
- Lin, W., Xu, X., Ge, B., Liu, X., 2011. Gaseous pollutants in Beijing urban area during the heating period 2007–2008: variability, sources, meteorological, and chemical impacts. *Atmospheric Chemistry and Physics* 11, 8157-8170.
- Lin, W., Xu, X., Zhang, X., Tang, J., 2008. Contributions of pollutants from North China Plain to surface ozone at the Shangdianzi GAW Station. *Atmos. Chem. Phys.* 8, 5889-5898.
- Lin, Y.C., Tsai, C.J., Wu, Y.C., Zhang, R., Chi, K.H., Huang, Y.T., Lin, S.H., Hsu, S.C., 2015. Characteristics of trace metals in traffic-derived particles in Hsuehshan Tunnel, Taiwan: size distribution, potential source, and fingerprinting metal ratio. *Atmospheric Chemistry and Physics* 15, 4117-4130.
- Liu, B., Wu, J., Zhang, J., Wang, L., Yang, J., Liang, D., Dai, Q., Bi, X., Feng, Y., Zhang, Y., Zhang, Q., 2017. Characterization and source apportionment of PM_{2.5} based on error estimation from EPA PMF 5.0 model at a medium city in China. *Environ Pollut* 222, 10-22.
- Lohmann, U., Feichter, J., 2005. Global indirect aerosol effects: a review. *Atmos. Chem. Phys.* 5, 715-737.

Lohmann, U., Feichter, J., 2005. Global indirect aerosol effects: a review. *Atmos. Chem. Phys.* 5, 715–737.

Longley, I.D., Gallagher, M.W., Dorsey, J.R., Flynn, M., Allan, J.D., Alfarra, M.R., Inglis, D., 2003. A case study of aerosol ($4.6\text{nm} < D_p < 10\mu\text{m}$) number and mass size distribution measurements in a busy street canyon in Manchester, UK. *Atmospheric Environment* 37, 1563-1571.

Ma, N., Birmili, W., 2015. Estimating the contribution of photochemical particle formation to ultrafine particle number averages in an urban atmosphere. *Sci Total Environ* 512-513, 154-166.

Ma, N., Zhao, C.S., Nowak, A., Müller, T., Pfeifer, S., Cheng, Y.F., Deng, Z.Z., Liu, P.F., Xu, W.Y., Ran, L., Yan, P., Göbel, T., Hallbauer, E., Mildenberger, K., Henning, S., Yu, J., Chen, L.L., Zhou, X.J., Stratmann, F., Wiedensohler, A., 2011. Aerosol optical properties in the North China Plain during HaChi campaign: an in-situ optical closure study. *Atmospheric Chemistry and Physics* 11, 5959-5973.

Maenhaut, W., Vermeylen, R., Claeys, M., Vercauteren, J., Roekens, E., 2016. Sources of the PM₁₀ aerosol in Flanders, Belgium, and re-assessment of the contribution from wood burning. *Sci Total Environ* 562, 550-560.

Mari, M., Harrison, R.M., Schuhmacher, M., Domingo, J.L., Pongpiachan, S., 2010. Inferences over the sources and processes affecting polycyclic aromatic hydrocarbons in the atmosphere derived from measured data. *Sci Total Environ* 408, 2387-2393.

Massling, A., Stock, M., Wiedensohler, A., 2005. Diurnal, weekly, and seasonal variation of hygroscopic properties of submicrometer urban aerosol particles. *Atmospheric Environment* 39, 3911-3922.

Maynard, A.D., Maynard, R.L., 2002. A derived association between ambient aerosol surface area and excess mortality using historic time series data. *Atmospheric Environment* 36, 5561-5567.

Maynarda, A.D., Maynard, R.L., 2002. A derived association between ambient aerosol surface area and excess mortality using historic time series data. *Atmospheric Environment* 36, 5561-5567.

McNeilly, J.D., Heal, M.R., Beverland, I.J., Howe, A., Gibson, M.D., Hibbs, L.R., MacNee, W., Donaldson, K., 2004. Soluble transition metals cause the pro-inflammatory effects of welding fumes in vitro. *Toxicol Appl Pharmacol* 196, 95-107.

Medved, A., Dorman, F., Kaufman, S.L., Pöcher, A., 2000. A New Corona-based Charger for Aerosol Particles. *Journal of Aerosol Science* 31, 616-617.

Meister, K., Johansson, C., Forsberg, B., 2012. Estimated short-term effects of coarse particles on daily mortality in Stockholm, Sweden. *Environ Health Perspect* 120, 431-436.

Mejia, J.F., Morawska, L., Mengersen, K., 2008. Spatial variation in particle number size distributions in a large metropolitan area. *Atmos. Chem. Phys.* 8, 1127-1138.

Merikanto, J., D. V. Spracklen, G. W. Mann, S. J. Pickering, a.K.S.C., 2009. Impact of nucleation on global CCN. *Atmos. Chem. Phys.* 9, 8601-8616.

Minoura, H., Takekawa, H., 2005. Observation of number concentrations of atmospheric aerosols and analysis of nanoparticle behavior at an urban background area in Japan. *Atmospheric Environment* 39, 5806-5816.

Mishra, V.K., Kumar, P., Van Poppel, M., Bleux, N., Frijns, E., Reggente, M., Berghmans, P., Int Panis, L., Samson, R., 2012. Wintertime spatio-temporal variation of ultrafine particles in a Belgian city. *Sci Total Environ* 431, 307-313.

Mohr, M., Lehmann, U., Rutter, J., 2005. Comparison of Mass-Based and Non-Mass-Based Particle Measurement Systems for Ultra-Low Emissions from Automotive Sources. *Environ. Sci. Technol* 39, 2229-2238.

Monks, P.S., 2000. A review of the observations and origins of the spring ozone maximum. *Atmospheric Environment* 34, 3545-3561.

Monks, P.S., Granier, C., Fuzzi, S., Stohl, A., Williams, M.L., Akimoto, H., Amann, M., Baklanov, A., Baltensperger, U., Bey, I., Blake, N., Blake, R.S., Carslaw, K., Cooper, O.R., Dentener, F., Fowler, D., Fragkou, E., Frost, G.J., Generoso, S., Ginoux, P., Grewe, V., Guenther, A., Hansson, H.C., Henne, S., Hjorth, J., Hofzumahaus, A., Huntrieser, H., Isaksen, I.S.A., Jenkin, M.E., Kaiser, J., Kanakidou, M., Klimont, Z., Kulmala, M., Laj, P., Lawrence, M.G., Lee, J.D., Liousse, C., Maione, M., McFiggans, G., Metzger, A., Mieville, A., Moussiopoulos, N., Orlando, J.J., O'Dowd, C.D., Palmer, P.I., Parrish, D.D.,

- Petzold, A., Platt, U., Pöschl, U., Prévôt, A.S.H., Reeves, C.E., Reimann, S., Rudich, Y., Sellegri, K., Steinbrecher, R., Simpson, D., ten Brink, H., Theloke, J., van der Werf, G.R., Vautard, R., Vestreng, V., Vlachokostas, C., von Glasow, R., 2009. Atmospheric composition change – global and regional air quality. *Atmospheric Environment* 43, 5268-5350.
- Mooibroek, D., Schaap, M., Weijers, E.P., Hoogerbrugge, R., 2011. Source apportionment and spatial variability of PM_{2.5} using measurements at five sites in the Netherlands. *Atmospheric Environment* 45, 4180-4191.
- Moore, K.F., Ning, Z., Ntziachristos, L., Schauer, J.J., Sioutas, C., 2007. Daily variation in the properties of urban ultrafine aerosol—Part I: Physical characterization and volatility. *Atmospheric Environment* 41, 8633-8646.
- Morawska, L., Jayaratne, E.R., Mengersenb, K., Jamriska, M., Thomas, S., 2002. Differences in airborne particle and gaseous concentrations in urban air between weekdays and weekends. *Atmospheric Environment* 36, 4375-4383.
- Morawska, L., Ristovski, Z., Jayaratne, E.R., Keogh, D.U., Ling, X., 2008. Ambient nano and ultrafine particles from motor vehicle emissions: Characteristics, ambient processing and implications on human exposure. *Atmospheric Environment* 42, 8113-8138.
- Moreno, T., Merolla, L., Gibbons, W., Greenwell, L., Jones, T., Richards, R., 2004. Variations in the source, metal content and bioreactivity of technogenic aerosols: a case study from Port Talbot, Wales, UK. *Sci Total Environ* 333, 59-73.
- Moshhammer, H., Neuberger, M., 2003. The active surface of suspended particles as a predictor of lung function and pulmonary symptoms in Austrian school children. *Atmospheric Environment* 37, 1737-1744.
- Muránszky, G., Óvári, M., Virág, I., Csiba, P., Dobai, R., Zárny, G., 2011. Chemical characterization of PM₁₀ fractions of urban aerosol. *Microchemical Journal* 98, 1-10.
- Nava, S., Becagli, S., Calzolari, G., Chiari, M., Lucarelli, F., Prati, P., Traversi, R., Udisti, R., Valli, G., Vecchi, R., 2012. Saharan dust impact in central Italy: An overview on three years elemental data records. *Atmospheric Environment* 60, 444-452.
- Nel, A., 2005. Air pollution-related illness: effects of particles. 308, 804–806.

Nel, A., Xia, T., Mädler, L., and, Li, N., 2006. Toxic Potential of Materials at the Nanolevel. *SCIENCE* 311, 622-627.

Németh, Z., Rosati, B., Zíková, N., Salma, I., Bozó, L., Dameto de España, C., Schwarz, J., Ždímal, V., Wonaschütz, A., 2018. Comparison of atmospheric new particle formation events in three Central European cities. *Atmospheric Environment* 178, 191-197.

Németh, Z., Salma, I., 2014. Spatial extension of nucleating air masses in the Carpathian Basin. *Atmospheric Chemistry and Physics* 14, 8841-8848.

Ntziachristos, L., Polidori, A., Phuleria, H., Geller, M.D., Sioutas, C., 2007. Application of a Diffusion Charger for the Measurement of Particle Surface Concentration in Different Environments. *Aerosol Science and Technology* 41, 571-580.

Nurkiewicz, T.R., Porter, D.W., Hubbs, A.F., Stone, S., Chen, B.T., Frazer, D.G., Boegehold, M.A., Castranova, V., 2009. Pulmonary nanoparticle exposure disrupts systemic microvascular nitric oxide signaling. *Toxicological sciences : an official journal of the Society of Toxicology* 110, 191-203.

Nygaard, U.C., Samuelsen, M., Aase, A., and, Lovik, M., 2004. The capacity of particles to increase allergic sensitization is predicted by particle number and surface area, not by particle mass. *Toxicological sciences : an official journal of the Society of Toxicology* 82, 515-524.

O'Dowd, C.D., Aalto, P., Hämeri, K., Kulmala, M., Hoffmann, T., 2002. Atmospheric particles from organic vapours. *Nature* 416, 497-498.

O'Dowd, C.D., Y. J. Yoon, W. Junkermann, P. Aalto, M. Kulmala, H. Lihavainen, a.Y.V., 2009. Airborne measurements of nucleation mode particles II: boreal forest nucleation events. *Atmos. Chem. Phys.* 9, 937-944.

Oberdörster, G., 2000. Toxicology of ultrafine particles: in vivo studies. *Phil. Trans. R. Soc. Lond. A* 358, 2719-2740.

Oberdörster, G., Maynard, A., Donaldson, K., Castranova, V., Fitzpatrick, J., Ausman, K., Carter, J., Karn, B., Kreyling, W., Lai, D., Olin, S., Monteiro-Riviere, N., Warheit, D., Yang, H., 2005. Principles for characterizing the potential human health effects from exposure to nanomaterials: elements of a screening strategy. *Particle and fibre toxicology* 2, 1-35.

Oberdorster, G., Sharp, Z., Atudorei, V., Elder, A., Gelein, R., Kreyling, W., Cox, C., 2004. Translocation of inhaled ultrafine particles to the brain. *Inhalation toxicology* 16, 437-445.

Oberdorster, G., Sharp, Z., Atudorei, V., Elder, A., Gelein, R., Lunts, A., Kreyling, W., Cox, C., 2002. Extrapulmonary translocation of ultrafine carbon particles following whole-body inhalation exposure of rats. *J Toxicol Environ Health A* 65, 1531-1543.

Ostro, B., Hu, J., Goldberg, D., Reynolds, P., Hertz, A., Bernstein, L., Kleeman, M.J., 2015. Associations of mortality with long-term exposures to fine and ultrafine particles, species and sources: results from the California Teachers Study Cohort. *Environ Health Perspect* 123, 549-556.

Paasonen, P., Kupiainen, K., Klimont, Z., Visschedijk, A., Denier van der Gon, H.A.C., Amann, M., 2016. Continental anthropogenic primary particle number emissions. *Atmospheric Chemistry and Physics* 16, 6823-6840.

Park, K., Kittelson, D.B., Zachariah, M.R., McMurry, P.H., 2004. Measurement of inherent material density of nanoparticle agglomerates. *Journal of Nanoparticle Research* 6, 267-272.

Penttinen, P., Timonen, K.L., Tiittanen, P., Mirme, A., Ruuskanen, J., Pekkanen, J., 2001. Number concentration and size of particles in urban air: effects on spirometric lung function in adult asthmatic subjects. *Environ. Health Perspect* 109, 319-323.

Pérez, N., Pey, J., Cusack, M., Reche, C., Querol, X., Alastuey, A., Viana, M., 2010. Variability of Particle Number, Black Carbon, and PM₁₀, PM_{2.5}, and PM₁ Levels and Speciation: Influence of Road Traffic Emissions on Urban Air Quality. *Aerosol Science and Technology* 44, 487-499.

Petäjä, T., Kerminen, V.M., Dal Maso, M., Junninen, H., Koponen, K., I., Hussein, T., Aalto, P.P., Andronopoulos, S., Robin, D., Hameri, K., Bartzis, J., G., Kulmala, M., 2007. Sub-micron atmospheric aerosols in the surroundings of Marseille and Athens: physical characterization and new particle formation. *Atmos. Chem. Phys.* 7, 2705-2720.

Peters, A., WICHMANN, H.E., TUCH, T., HEINRICH, J., HEYDER, J., 1997a. Respiratory Effects Are Associated with the Number of Ultrafine Particles. *Am J Respir Crit Care Med* 155, 1376-1383.

Peters, A., Wichmann, H.E., Tuch, T., Heinrich, J., Heyder, J., 1997b. Respiratory effects are associated with the number of ultrafine particles. *Am. J. Respir. Crit. Care Med* 155, 1376-1383.

Peters, T.M., Elzey, S., Johnson, R., Park, H., Grassian, V.H., Maher, T., O'Shaughnessy, P., 2009. Airborne monitoring to distinguish engineered nanomaterials from incidental particles for environmental health and safety. *J Occup Environ Hyg* 6, 73-81.

Petzold, A., Kramer, H., Schönlinner, M., 2002a. Continuous measurement of atmospheric black carbon using a Multi-angle absorption photometer. *Environ Sci Pollut Res* 4, 78-82.

Petzold, A., Kramer, H., Schönlinner, M., 2002b. Continuous measurement of atmospheric black carbon using a Multi-angle absorption photometer. *Environ. Sci. Pollut. Res.* 4, 78-82.

Petzold, A., Ogren, J.A., Fiebig, M., Laj, P., Li, S.M., Baltensperger, U., Holzer-Popp, T., Kinne, S., Pappalardo, G., Sugimoto, N., Wehrli, C., Wiedensohler, A., Zhang, X.Y., 2013. Recommendations for reporting "black carbon" measurements. *Atmospheric Chemistry and Physics* 13, 8365-8379.

Pey, J., Rodríguez, S., Querol, X., Alastuey, A., Moreno, T., Putaud, J.P., Van Dingenen, R., 2008. Variations of urban aerosols in the western Mediterranean. *Atmospheric Environment* 42, 9052-9062.

Pinto, J.P., Lefohn, A.S., Shadwick, D.S., 2004. Spatial Variability of PM_{2.5} in Urban Areas in the United States. *Journal of the Air & Waste Management Association* 54, 440-449.

Pirjola, L., Kulmala, M., Wilck, M., Bischoff, A., Stratmann, F., Otto, E., 1999. Formation of Sulphuric Acid 23 Aerosols and Cloud Condensation Nuclei: An Expression for Significant Nucleation and Model 24 Comparison. *J. Aerosol Sci.* 30, 1079-1094.

Pope, C.A., 2000. Review: Epidemiological Basis for Particulate Air Pollution Health Standards. *Aerosol Science and Technology* 32, 4-14.

Pope, C.A., and Dockery, D.W., 2006a. Health Effects of Fine Particulate Air Pollution: Lines that Connect. *Air & Waste Manage. Assoc.* 56, 709-742.

Pope, C.A.I., Dockery, D.W., 2006b. Health Effects of Fine Particulate Air Pollution: Lines that Connect. *J. Air Waste Ma.* 56, 709-742.

Pöschl, U., 2005. Atmospheric aerosols: composition, transformation, climate and health effects. *Angew Chem Int Ed Engl* 44, 7520-7540.

Pöschl, U., Rudich, Y., Ammann, M., 2007. Kinetic model framework for aerosol and cloud surface chemistry and gas-particle interactions – Part 1: General equations, parameters, and terminology. *Atmos. Chem. Phys.* 7, 5989-6023.

Pósfai, M., Gelencsér, A., Simonics, R., Arató, K., Li, J., Hobbs, P.V., Buseck, P.R., 2004. Atmospheric tar balls: Particles from biomass and biofuel burning. *Journal of Geophysical Research: Atmospheres* 109, n/a-n/a.

Putaud, J.-P., Raes, F., Van Dingenen, R., Brüggemann, E., Facchini, M.C., Decesari, S., Fuzzi, S., Gehrig, R., Hüglin, C., Laj, P., Lorbeer, G., Maenhaut, W., Mihalopoulos, N., Müller, K., Querol, X., Rodriguez, S., Schneider, J., Spindler, G., Brink, H.t., Tørseth, K., Wiedensohler, A., 2004a. A European aerosol phenomenology—2: chemical characteristics of particulate matter at kerbside, urban, rural and background sites in Europe. *Atmospheric Environment* 38, 2579-2595.

Putaud, J.P., Raes, F., Van Dingenen, R., Brüggemann, E., Facchini, M.C., Decesari, S., Fuzzi, S., Gehrig, R., Hüglin, C., Laj, P., Lorbeer, G., Maenhaut, W., Mihalopoulos, N., Müller, K., Querol, X., Rodriguez, S., Schneider, J., Spindler, G., Brink, H., Tørseth, K., Wiedensohler, A., 2004b. A European aerosol phenomenology—2: chemical characteristics of particulate matter at kerbside, urban, rural and background sites in Europe. *Atmospheric Environment* 38, 2579-2595.

Querol, X., Minguillón, M.C., Alastuey, A., Monfort, E., Mantilla, E., Sanz, M.J., Sanz, F., Roig, A., Renau, A., Felis, C., Miró, J.V., Artíñano, B., 2007. Impact of the implementation of PM abatement technology on the ambient air levels of metals in a highly industrialised area. *Atmospheric Environment* 41, 1026-1040.

R Core Team, D., 2014. *R: A Language and Environment for Statistical Computing.*, R Foundation for Statistical Computing, Vienna, Austria.

R Core Team, D., 2015. *R: a Language and Environment for Statistical Computing.*, R Foundation for statistical computing, Vienna, Austria.

- Reche, C., Querol, X., Alastuey, A., Viana, M., Pey, J., Moreno, T., Rodríguez, S., González, Y., Fernández-Camacho, R., de la Rosa, J., Dall'Osto, M., Prévôt, A.S.H., Hueglin, C., Harrison, R.M., Quincey, P., 2011. New considerations for PM, Black Carbon and particle number concentration for air quality monitoring across different European cities. *Atmospheric Chemistry and Physics* 11, 6207-6227.
- Reche, C., Viana, M., Brines, M., Perez, N., Beddows, D., Alastuey, A., Querol, X., 2015. Determinants of aerosol lung-deposited surface area variation in an urban environment. *The Science of the total environment* 517, 38-47.
- Rees, S.L., Robinson, A.L., Khlystov, A., Stanier, C.O., Pandis, S.N., 2004. Mass balance closure and the Federal Reference Method for PM_{2.5} in Pittsburgh, Pennsylvania. *Atmospheric Environment* 38, 3305-3318.
- Řimnáčová, D., Ždímal, V., Schwarz, J., Smolík, J., Řimnác, M., 2011. Atmospheric aerosols in suburb of Prague: The dynamics of particle size distributions. *Atmospheric Research* 101, 539-552.
- Ripoll, A., Pey, J., Minguillón, M.C., Pérez, N., Pandolfi, M., Querol, X., Alastuey, A., 2014. Three years of aerosol mass, black carbon and particle number concentrations at Montsec (southern Pyrenees, 1570 m a.s.l.). *Atmospheric Chemistry and Physics* 14, 4279-4295.
- Ristovski, Z.D., Morawska, L., Bofinger, N.D., Hitchins, J., 1998. Submicrometer and Supermicrometer Particulate Emission from Spark Ignition Vehicles. *Environmental science & technology* 32, 3845-3852.
- Rodríguez, S., Cuevas, E., 2007. The contributions of “minimum primary emissions” and “new particle formation enhancements” to the particle number concentration in urban air. *Journal of Aerosol Science* 38, 1207-1219.
- Rodríguez, S., Cuevas, E., González, Y., Ramos, R., Romero, P.M., Pérez, N., Querol, X., Alastuey, A., 2008. Influence of sea breeze circulation and road traffic emissions on the relationship between particle number, black carbon, PM₁, PM_{2.5} and PM_{2.5-10} concentrations in a coastal city. *Atmospheric Environment* 42, 6523-6534.
- Rodríguez, S., Dingenen, R.V., Putaud, J.P., Dell'Acqua, A., Pey, J., Querol, X., Alastuey, A., Chenery, S., Ho, K.-F., Harrison, R.M., Tardivo, R., Scarnato, B., Gemelli,

V., 2007. A study on the relationship between mass concentrations, chemistry and number size distribution of urban fine aerosols in Milan, Barcelona and London. *Atmos. Chem. Phys.* 7, 2217-2232.

Rodriguez, S., Querol, X., Alastuey, A., Viana, M., Alarcon, M., Mantilla, E., Ruiz, C., 2004. Comparative PM₁₀–PM_{2.5} source contribution study at rural, urban and industrial sites during PM episodes in Eastern Spain. *Science of The Total Environment* 328, 95-113.

Röösli, M., Theis, G., Künzli, N., Staehelin, J., Mathys, P., Oglesby, L., Camenzind, M., Braun-Fahrländer, C., 2001. Temporal and spatial variation of the chemical composition of PM₁₀ at urban and rural sites in the Basel area, Switzerland. *Atmospheric Environment* 35, 3701-3713.

Rose, D., Wehner, B., Ketzel, M., Engler, C., Voigtlander, J., Tuch, T., Wiedensohler, A., 2006. Atmospheric number size distributions of soot particles and estimation of emission factors. *Atmos. Chem. Phys.* 6, 1021-1031.

Rückerl, R., Schneider, A., Breitner, S., Cyrus, J., Peters, A., 2011. Health effects of particulate air pollution: A review of epidemiological evidence. *Inhal Toxicol* 23, 555-592.

Safai, P.D., Raju, M.P., Rao, P.S.P., Pandithurai, G., 2014. Characterization of carbonaceous aerosols over the urban tropical location and a new approach to evaluate their climatic importance. *Atmospheric Environment* 92, 493-500.

Sager, T.M., Castranova, V., 2009. Surface area of particle administered versus mass in determining the pulmonary toxicity of ultrafine and fine carbon black: comparison to ultrafine titanium dioxide. *Particle and fibre toxicology* 6, 15.

Salma, I., Borsós, T., Weidinger, T., Aalto, P., Hussein, T., Dal Maso, M., Kulmala, M., 2011. Production, growth and properties of ultrafine atmospheric aerosol particles in an urban environment. *Atmospheric Chemistry and Physics* 11, 1339-1353.

Salma, I., Németh, Z., Kerminen, V.-M., Aalto, P., Nieminen, T., Weidinger, T., Molnár, Á., Imre, K., Kulmala, M., 2016. Regional effect on urban atmospheric nucleation. *Atmospheric Chemistry and Physics* 16, 8715-8728.

Samiksha, S., Sunder Raman, R., Nirmalkar, J., Kumar, S., Sirvaiya, R., 2017. PM10 and PM2.5 chemical source profiles with optical attenuation and health risk indicators of paved and unpaved road dust in Bhopal, India. *Environ Pollut* 222, 477-485.

Schauer, J.J., Kleeman, M.J., Cass, G.R., Simoneit, B.R., 2002. Measurement of Emissions from Air Pollution Sources. 5. C1-C32 Organic Compounds from Gasoline-Powered Motor Vehicles. *Environ. Sci. Technol.* 36, 1169-1180.

Schwartz, S.E., 1996. THE WHITEHOUSE EFFECT--SHORTWAVE RADIATIVE FORCING OF CLIMATE BY ANTHROPOGENIC AEROSOLS: AN OVERVIEW. *J. Aerosol Sci.* 27, 359-382.

Schwarz, J.P., Gao, R.S., Fahey, D.W., Thomson, D.S., Watts, L.A., Wilson, J.C., Reeves, J.M., Darbeheshti, M., Baumgardner, D.G., Kok, G.L., Chung, S.H., Schulz, M., Hendricks, J., Lauer, A., Kärcher, B., Slowik, J.G., Rosenlof, K.H., Thompson, T.L., Langford, A.O., Loewenstein, M., Aikin, K.C., 2006. Single-particle measurements of midlatitude black carbon and light-scattering aerosols from the boundary layer to the lower stratosphere. *Journal of Geophysical Research* 111.

Schwarz, J.P., Gao, R.S., Spackman, J.R., Watts, L.A., Thomson, D.S., Fahey, D.W., Ryerson, T.B., Peischl, J., Holloway, J.S., Trainer, M., Frost, G.J., Baynard, T., Lack, D.A., de Gouw, J.A., Warneke, C., Del Negro, L.A., 2008. Measurement of the mixing state, mass, and optical size of individual black carbon particles in urban and biomass burning emissions. *Geophysical Research Letters* 35.

Seinfeld, J.H., and, Pandis, S.N., 2006a. *Atmospheric Chemistry and Physics: From Air Pollution to Climate Change*, Second ed, John Wiley and Sons. Inc., New York.

Seinfeld, J.H., Pandis, S.N., 1998. *Atmospheric Chemistry and Physics*, John Wiley & Sons, Inc, New York.

Seinfeld, J.H., Pandis, S.N., 2006b. *Atmospheric chemistry and physics: from air pollution to climate change.*, 2nd ed. John Wiley and Sons, Inc., New York.

Shen, L., Mickley, L.J., Murray, L.T., 2017. Influence of 2000–2050 climate change on particulate matter in the United States: results from a new statistical model. *Atmospheric Chemistry and Physics* 17, 4355-4367.

- Shi, G.-L., Zeng, F., Li, X., Feng, Y.-C., Wang, Y.-Q., Liu, G.-X., Zhu, T., 2011. Estimated contributions and uncertainties of PCA/MLR–CMB results: Source apportionment for synthetic and ambient datasets. *Atmospheric Environment* 45, 2811-2819.
- Shi, J.P., Evans, D.E., Khan, A.A., Harrison, R.M., 2001a. Sources and concentration of nanoparticles ((10nm diameter) in the urban atmosphere. *Atmospheric Environment* 35, 1193-1202.
- Shi, J.P., Evans, D.E., Khan, A.A., Harrison, R.M., 2001b. Sources and concentration of nanoparticles (<10nm diameter) in the urban atmosphere. *Atmospheric Environment* 35, 1193-1202.
- Shi, J.P., Khan, A.A., Harrison, R.M., 1999. Measurements of ultrafine particle concentration and size distribution in the urban atmosphere. *The Science of the Total Environment* 235, 51-54.
- Shi, J.P., Mark, D., Harrison, R.M., 2000. Characterization of Particles from a Current Technology Heavy-Duty Diesel Engine. *Environ. Sci. Technol* 34, 748-755.
- Simoneit, B.R.T., Schauer, J.J., Nolte, C.G., Oros, D.R., Elias, V.O., Fraser, M.P., Rogge, W.F., Cass, G.R., 1999. Levoglucosan, a tracer for cellulose in biomass burning and atmospheric particles. *Atmospheric Environment* 33, 173-182.
- Singh, S., Shi, T., Duffin, R., Albrecht, C., van Berlo, D., Hohr, D., Fubini, B., Martra, G., Fenoglio, I., Borm, P.J., Schins, R.P., 2007. Endocytosis, oxidative stress and IL-8 expression in human lung epithelial cells upon treatment with fine and ultrafine TiO₂: role of the specific surface area and of surface methylation of the particles. *Toxicology and applied pharmacology* 222, 141-151.
- Smargiassi, A., Baldwin, M., Pilger, C., Dugandzic, R., Brauer, M., 2005. Small-scale spatial variability of particle concentrations and traffic levels in Montreal: a pilot study. *The Science of the total environment* 338, 243-251.
- Spinazzè, A., Cattaneo, A., Scocca, D.R., Bonzini, M., Cavallo, D.M., 2015. Multi-metric measurement of personal exposure to ultrafine particles in selected urban microenvironments. *Atmospheric Environment* 110, 8-17.

Spracklen, D.V., Carslaw, K.S., Kulmala, M., Kerminen, V.-M., Sihto, S.-L., Riipinen, I., Merikanto, J., Mann, G.W., Chipperfield, M.P., Wiedensohler, A., Birmili, W., Lihavainen, H., 2008. Contribution of particle formation to global cloud condensation nuclei concentrations. *Geophysical Research Letters* 35.

Stanier, C.O., Khlystov, A.Y., Pandis, S.N., 2004. Ambient aerosol size distributions and number concentrations measured during the Pittsburgh Air Quality Study (PAQS). *Atmospheric Environment* 38, 3275-3284.

Stevens, B., Feingold, G., 2009. Untangling aerosol effects on clouds and precipitation in a buffered system. *Nature* 461, 607-613.

Stoeger, T., Reinhard, C., Takenaka, S., Schroepel, A., Karg, E., Ritter, B., Heyder, J., Schulz, H., 2006. Instillation of Six Different Ultrafine Carbon Particles Indicates a Surface Area Threshold Dose for Acute Lung Inflammation in Mice. *Environmental Health Perspectives* 114, 328-333.

Stoeger, T., Schmid, O., Takenaka, S., Schulz, H., 2007. In search of the most relevant parameter for quantifying lung inflammatory response to nanoparticle exposure: particle number, surface area, or what? *Environ Health Perspect* 115, 187-194.

Stoeger, T., Takenaka, S., Frankenberger, B., Ritter, B., Karg, E., Maier, K., Schulz, H., Schmid, O., 2009. Deducing in vivo toxicity of combustion-derived nanoparticles from a cell-free oxidative potency assay and metabolic activation of organic compounds. *Environ Health Perspect* 117, 54-60.

Stölzel, M., Breitner, S., Cyrys, J., Pitz, M., Wolke, G., Kreyling, W., Heinrich, J., Wichmann, H.E., Peters, A., 2007. Daily mortality and particulate matter in different size classes in Erfurt, Germany. *J Expo Sci Environ Epidemiol* 17, 458-467.

Stommel, Y.G., Riebel, U., 2004. A new corona discharge-based aerosol charger for submicron particles with low initial charge. *Journal of Aerosol Science* 35, 1051-1069.

Taiwo, A.M., Beddows, D.C., Calzolari, G., Harrison, R.M., Lucarelli, F., Nava, S., Shi, Z., Valli, G., Vecchi, R., 2014a. Receptor modelling of airborne particulate matter in the vicinity of a major steelworks site. *Sci Total Environ* 490, 488-500.

Taiwo, A.M., Beddows, D.C., Shi, Z., Harrison, R.M., 2014b. Mass and number size distributions of particulate matter components: comparison of an industrial site and an urban background site. *Sci Total Environ* 475, 29-38.

Taiwo, A.M., Harrison, R.M., Beddows, D.C.S., Shi, Z., 2014c. Source apportionment of single particles sampled at the industrially polluted town of Port Talbot, United Kingdom by ATOFMS. *Atmospheric Environment* 97, 155-165.

Takahashi, K., Minoura, H., Sakamoto, K., 2008. Chemical composition of atmospheric aerosols in the general environment and around a trunk road in the Tokyo metropolitan area. *Atmospheric Environment* 42, 113-125.

Terzi, E., Argyropoulos, G., Bougatioti, A., Mihalopoulos, N., Nikolaou, K., Samara, C., 2010. Chemical composition and mass closure of ambient PM10 at urban sites. *Atmospheric Environment* 44, 2231-2239.

Thorpe, A., Harrison, R.M., 2008. Sources and properties of non-exhaust particulate matter from road traffic: a review. *Sci Total Environ* 400, 270-282.

Tran, C.L., Buchanan, D., Cullen, R.T., Searl, A., Jones, A.D., Donaldson, K., 2000. Inhalation of poorly soluble particles. II. Influence Of particle surface area on inflammation and clearance. *Inhal Toxicol* 12, 1113-1126.

Tsyro, S.G., 2005. To what extent can aerosol water explain the discrepancy between model calculated and gravimetric PM10 and PM2.5? *Atmos. Chem. Phys.* 5, 515-532.

Tuch, T.M., Wehner, B., Pitz, M., Cyrys, J., Heinrich, J., Kreyling, W.G., Wichmann, H.E., Wiedensohler, A., 2003. Long-term measurements of size-segregated ambient aerosol in two German cities located 100km apart. *Atmospheric Environment* 37, 4687-4700.

Turner, J.R., and, Allen, D.T., 2008. Transport of Atmospheric Fine Particulate Matter: Part 2—Findings from Recent Field Programs on the Intraurban Variability in Fine Particulate Matter. *Journal of the Air & Waste Management Association* 58, 196-215.

Turpin, B.J., and, Lim, H.-J., 2001. Species Contributions to PM2.5 Mass Concentrations: Revisiting Common Assumptions for Estimating Organic Mass. *Aerosol Science and Technology* 35, 602-610.

Uria-Tellaetxe, I., Carslaw, D.C., 2014. Conditional bivariate probability function for source identification. *Environmental Modelling & Software* 59, 1-9.

Vana, M., 2004. Comparative study of nucleation mode aerosol particles and intermediate air ions formation events at three sites. *Journal of Geophysical Research* 109.

Vecchi, R., Chiari, M., D'Alessandro, A., Fermo, P., Lucarelli, F., Mazzei, F., Nava, S., Piazzalunga, A., Prati, P., Silvani, F., Valli, G., 2008. A mass closure and PMF source apportionment study on the sub-micron sized aerosol fraction at urban sites in Italy. *Atmospheric Environment* 42, 2240-2253.

Vehkamäki, H., M. Dal Maso, T. Hussein, R. Flanagan, A. Hyvärinen, J. Lauros, J. Merikanto, P. Mönkkönen, M. Pihlatie, K. Salminen, L. Sogacheva, T. Thum, T. M. Ruuskanen, P. Keronen, P. P. Aalto, P. Hari, K. E. J. Lehtinen, U. Rannik, a.M.K., 2004. Atmospheric particle formation events at Värriö measurement station in Finnish Lapland 1998–2002. *Atmos. Chem. Phys.* 4, 2015-2023.

Vercauteren, J., Matheussen, C., Wauters, E., Roekens, E., van Grieken, R., Krata, A., Makarowska, Y., Maenhaut, W., Chi, X., Geypens, B., 2011. Chemkar PM10: An extensive look at the local differences in chemical composition of PM10 in Flanders, Belgium. *Atmospheric Environment* 45, 108-116.

Viana, M., Maenhaut, W., Chi, X., Querol, X., Alastuey, A., 2007. Comparative chemical mass closure of fine and coarse aerosols at two sites in south and west Europe: Implications for EU air pollution policies. *Atmospheric Environment* 41, 315-326.

Viana, M., Querol, X., Alastuey, A., Reche, C., Favez, O., Malherbe, L., Ustache, A., Bartonova, A., Liu, H., Guerreiro, C., , 2012. Particle number (PNC) and black carbon (BC) in European urban air quality networks. ETC/ACM Technical Paper.

Voigtländer, J., Tuch, T., Birmili, W., Wiedensohler, A., 2006. Correlation between traffic density and particle size distribution in a street canyon and the dependence on wind direction. *Atmos. Chem. Phys.* 6, 4275-4286.

von Bismarck-Osten, C., Birmili, W., Ketzel, M., Massling, A., Petäjä, T., Weber, S., 2013. Characterization of parameters influencing the spatio-temporal variability of urban particle number size distributions in four European cities. *Atmospheric Environment* 77, 415-429.

von Schneidmesser, E., Monks, P.S., Allan, J.D., Bruhwiler, L., Forster, P., Fowler, D., Lauer, A., Morgan, W.T., Paasonen, P., Righi, M., Sindelarova, K., Sutton, M.A., 2015. Chemistry and the Linkages between Air Quality and Climate Change. *Chem Rev* 115, 3856-3897.

Vu, T.V., Delgado-Saborit, J.M., Harrison, R.M., 2015. Review: Particle number size distributions from seven major sources and implications for source apportionment studies. *Atmospheric Environment* 122, 114-132.

Waked, A., Favez, O., Alleman, L.Y., Piot, C., Petit, J.E., Delaunay, T., Verlinden, E., Golly, B., Besombes, J.L., Jaffrezo, J.L., Leoz-Garziandia, E., 2014. Source apportionment of PM₁₀ in a north-western Europe regional urban background site (Lens, France) using positive matrix factorization and including primary biogenic emissions. *Atmospheric Chemistry and Physics* 14, 3325-3346.

Wang, H., Kawamura, K., Shooter, D., 2005. Carbonaceous and ionic components in wintertime atmospheric aerosols from two New Zealand cities: Implications for solid fuel combustion. *Atmospheric Environment* 39, 5865-5875.

Wang, H., Zhu, B., Shen, L., An, J., Yin, Y., Kang, H., 2014. Number size distribution of aerosols at Mt. Huang and Nanjing in the Yangtze River Delta, China: Effects of air masses and characteristics of new particle formation. *Atmospheric Research* 150, 42-56.

Wang, Z.B., Hu, M., Sun, J.Y., Wu, Z.J., Yue, D.L., Shen, X.J., Zhang, Y.M., Pei, X.Y., Cheng, Y.F., Wiedensohler, A., 2013. Characteristics of regional new particle formation in urban and regional background environments in the North China Plain. *Atmospheric Chemistry and Physics* 13, 12495-12506.

Weber, R.J., K. Moore, V. Kapustin, A. Clarke, R. L. Mauldin, E. Kosciuch, C. Cantrell, F. Eisele, B. Anderson, Thornhill, L., 2001. Nucleation in the equatorial Pacific during PEM-Tropics B: Enhanced boundary layer H₂SO₄ with no particle production. *Geophysical Research* 106, 757-776.

Weber, S., Kordowski, K., Kuttler, W., 2013. Variability of particle number concentration and particle size dynamics in an urban street canyon under different meteorological conditions. *Sci Total Environ* 449, 102-114.

Wedepohl, K.H., 1995. The composition of the continental crust. *Geochimica et Cosmochimica Acta* 59, 1217-1232.

Wehner, B., and , Wiedensohler, A., 2003a. Long term measurements of submicrometer urban aerosols: statistical analysis for correlations with meteorological conditions and trace gases. *Atmos. Chem. Phys* 3, 867-879.

Wehner, B., Birmili, W., Gnauk, T., Wiedensohler, A., 2002. Particle number size distributions in a street canyon and their transformation into the urban-air background: measurements and a simple model study. *Atmospheric Environment* 36, 2215-2223.

Wehner, B., Siebert, H., Stratmann, F., Tuch, T., Wiedensohler, A., Petäjä, T., Dal Maso, M., Kulmala, M., 2007. Horizontal homogeneity and vertical extent of new particle formation events. *Tellus B: Chemical and Physical Meteorology* 59, 362-371.

Wehner, B., Uhrner, U., von Löwis, S., Zallinger, M., Wiedensohler, A., 2009. Aerosol number size distributions within the exhaust plume of a diesel and a gasoline passenger car under on-road conditions and determination of emission factors. *Atmospheric Environment* 43, 1235-1245.

Wehner, B., Wiedensohler, A., 2003b. Long term measurements of submicrometer urban aerosols: statistical analysis for correlations with meteorological conditions and trace gases. *Atmos. Chem. Phys.* 3, 867-879.

Wehner, B., Wiedensohler, A., 2003c. Long term measurements of submicrometer urban aerosols: statistical analysis for correlations with meteorological conditions and trace gases. *Atmos. Chem. Phys.* 3, 867-879.

Weijers, E.P., Schaap, M., Nguyen, L., Matthijsen, J., Denier van der Gon, H.A.C., ten Brink, H.M., Hoogerbrugge, R., 2011. Anthropogenic and natural constituents in particulate matter in the Netherlands. *Atmospheric Chemistry and Physics* 11, 2281-2294.

Westmoreland, E.J., Carslaw, N., Carslaw, D.C., Gillah, A., Bates, E., 2007. Analysis of air quality within a street canyon using statistical and dispersion modelling techniques. *Atmospheric Environment* 41, 9195-9205.

WHO, 2005. Air quality guidelines. Global update 2005. Particulate matter, ozone, nitrogen dioxide and sulfur dioxide., Regional Office for Europe, Copenhagen.

WHO, 2013a. Review of evidence on health aspects of air pollution – REVIHAAP Project. DK-2100 Copenhagen Ø, Denmark, WHO Regional Office for Europe.

Wichmann, H.E., Spix, C., Tuch, T., Wölke, G., Peters, A., Heinrich, J., Kreyling, W.G., Heyder, J., 2000. Daily mortality and fine and ultrafine particles in Erfurt, Germany part I: role of particle number and particle mass. *Res Rep Health Eff Inst.* 98, 87-94.

Wiedensohler, A., 1988. An approximation of the bipolar charge distribution for particles in the submicron size range. *Journal of Aerosol Science* 19, 387-389.

Wiedensohler, A., Birmili, W., Nowak, A., Sonntag, A., Weinhold, K., Merkel, M., Wehner, B., Tuch, T., Pfeifer, S., Fiebig, M., Fjåraa, A.M., Asmi, E., Sellegri, K., Depuy, R., Venzac, H., Villani, P., Laj, P., Aalto, P., Ogren, J.A., Swietlicki, E., Williams, P., Roldin, P., Quincey, P., Hüglin, C., Fierz-Schmidhauser, R., Gysel, M., Weingartner, E., Riccobono, F., Santos, S., Grüning, C., Faloon, K., Beddows, D., Harrison, R., Monahan, C., Jennings, S.G., O'Dowd, C.D., Marinoni, A., Horn, H.G., Keck, L., Jiang, J., Scheckman, J., McMurry, P.H., Deng, Z., Zhao, C.S., Moerman, M., Henzing, B., de Leeuw, G., Löschau, G., Bastian, S., 2012. Mobility particle size spectrometers: harmonization of technical standards and data structure to facilitate high quality long-term observations of atmospheric particle number size distributions. *Atmospheric Measurement Techniques* 5, 657-685.

Willeke, K., 1976. Temperature dependence of particle slip in a gaseous medium. *Journal of Aerosol Science* 7, 381-387.

Wilson, J.G., Kingham, S., Pearce, J., Sturman, A.P., 2005. A review of intraurban variations in particulate air pollution: Implications for epidemiological research. *Atmospheric Environment* 39, 6444-6462.

Wilson, W.E., Stanek, J., Han, H.-S., Johnson, T., Sakurai, H., Pui, D.Y.H., and, J.T., Chen, D.-R., Duthie, S., 2007. Use of the Electrical Aerosol Detector as an Indicator of the Surface Area of Fine Particles Deposited in the Lung. *Journal of the Air & Waste Management Association* 57, 211-220.

Wonaschütz, A., Demattio, A., Wagner, R., Burkart, J., Zíková, N., Vodička, P., Ludwig, W., Steiner, G., Schwarz, J., Hitznerberger, R., 2015. Seasonality of new particle

formation in Vienna, Austria – Influence of air mass origin and aerosol chemical composition. *Atmospheric Environment* 118, 118-126.

Wongphatarakul, V., Friedlander, S.K., Pinto, J.P., 1998. A Comparative Study of PM_{2.5} Ambient Aerosol Chemical Databases. *Environ. Sci. Technol.* 32, 3926-3934.

Woo, K.S., Chen, D.R., Pui, D.Y.H., McMurry, P.H., 2001. Measurement of Atlanta Aerosol Size Distributions: Observations of Ultrafine Particle Events. *Aerosol Science and Technology* 34, 75-87.

Wu, Z., Hu, M., Lin, P., Liu, S., Wehner, B., Wiedensohler, A., 2008. Particle number size distribution in the urban atmosphere of Beijing, China. *Atmospheric Environment* 42, 7967-7980.

Xiao, S., Wang, M.Y., Yao, L., Kulmala, M., Zhou, B., Yang, X., Chen, J.M., Wang, D.F., Fu, Q.Y., Worsnop, D.R., Wang, L., 2015. Strong atmospheric new particle formation in winter in urban Shanghai, China. *Atmospheric Chemistry and Physics* 15, 1769-1781.

Xu, W.Y., Zhao, C.S., Ran, L., Deng, Z.Z., Liu, P.F., Ma, N., Lin, W.L., Xu, X.B., Yan, P., He, X., Yu, J., Liang, W.D., Chen, L.L., 2011. Characteristics of pollutants and their correlation to meteorological conditions at a suburban site in the North China Plain. *Atmospheric Chemistry and Physics* 11, 4353-4369.

Yli-Juuti, T., Nieminen, T., Hirsikko, A., Aalto, P.P., Asmi, E., Hörrak, U., Manninen, H.E., Patokoski, J., Dal Maso, M., Petäjä, T., Rinne, J., Kulmala, M., Riipinen, I., 2011. Growth rates of nucleation mode particles in Hyytiälä during 2003–2009: variation with particle size, season, data analysis method and ambient conditions. *Atmospheric Chemistry and Physics* 11, 12865-12886.

Yoo, J.M., Jeong, M.J., Kim, D., Stockwell, W.R., Yang, J.H., Shin, H.W., Lee, M.I., Song, C.K., Lee, S.D., 2015. Spatiotemporal variations of air pollutants (O₃, NO₂, SO₂, CO, PM₁₀, and VOCs) with land-use types. *Atmospheric Chemistry and Physics* 15, 10857-10885.

Zhang, Q., Jimenez, J.L., Canagaratna, M.R., Allan, J.D., Coe, H., Ulbrich, I., Alfarra, M.R., Takami, A., Middlebrook, A.M., Sun, Y.L., Dzepina, K., Dunlea, E., Docherty, K., DeCarlo, P.F., Salcedo, D., Onasch, T., Jayne, J.T., Miyoshi, T., Shimojo, A.,

Hatakeyama, S., Takegawa, N., Kondo, Y., Schneider, J., Drewnick, F., Borrmann, S., Weimer, S., Demerjian, K., Williams, P., Bower, K., Bahreini, R., Cottrell, L., Griffin, R.J., Rautiainen, J., Sun, J.Y., Zhang, Y.M., Worsnop, D.R., 2007. Ubiquity and dominance of oxygenated species in organic aerosols in anthropogenically-influenced Northern Hemisphere midlatitudes. *Geophysical Research Letters* 34, 1-6.

Zhang, R., Khalizov, A.F., Pagels, J., Zhang, D., Xue, H., McMurry, P.H., 2008. Variability in morphology, hygroscopicity, and optical properties of soot aerosols during atmospheric processing. *Proc Natl Acad Sci U S A* 105, 10291-10296.

Zhu, B., Wang, H., Shen, L., Kang, H., Yu, X., 2013. Aerosol spectra and new particle formation observed in various seasons in Nanjing. *Advances in Atmospheric Sciences* 30, 1632-1644.

Zhu, Y., Hinds, W.C., Kim, S., Sioutas, C., 2002. Concentration and Size Distribution of Ultrafine Particles Near a Major Highway. *Journal of the Air & Waste Management Association* 52, 1032-1042.